DNA-POLYMER CONJUGATES TOWARD SELF-ASSEMBLED POLYMER-ORIGAMI ARCHITECTURES

Dissertation

zur Erlangung des Grades “Doktor der Naturwissenschaften”

im Promotionsfach Chemie

am Fachbereich 09

Chemie, Pharmazie, Geographie und Geowissenschaften

der Johannes-Gutenberg-Universität Mainz

vorgelegt von

Nico Alleva

Geboren in

Itzehoe

Mainz, 2024

MAX PLANCK INSTITUTE
FOR POLYMER RESEARCH

JOHANNES GUTENBERG
UNIVERSITÄT MAINZ

Dekan	Prof. Dr. Eva Rentschler
1. Betreuer	Prof. Dr. Tanja Weil
2. Gutachter	Prof. Dr. Pol Besenius

Datum der mündlichen Prüfung: 18.12.2024

DANKSAGUNG

An dieser Stelle möchte ich mich bei Prof. Dr. Tanja Weil und Dr. David Y. W. Ng für die Möglichkeit bedanken, bei Ihnen meine Promotion durchführen zu können und mir stets bei Projekten mit Visionen und wertvollen Vorschlägen zur Projektentwicklung zur Seite standen. Hervorheben möchte ich hier die großartigen Führungsqualitäten beider und die herzliche, schöne Atmosphäre.

Ein großes Dankeschön möchte ich Dr. Pia Winterwerber und Dr. Colette J. Whitfield für die detaillierte und großartiger Anleitung in dieses spannende Fachgebiet aussprechen. Dadurch konnte die Arbeit erst zu dem werden, was sie geworden ist.

Insbesondere bedanke ich mich bei der gesamten Arbeitsgruppe für die herzliche und spaßige Zeit im Arbeitskreis und in den Kaffeepausen, und die sehr angenehme Arbeitsatmosphäre.

Von ganzem Herzen möchte ich mich bei meiner Familie und vor allem bei meinen Freunden bedanken. Ihr wart immer dar, wenn mal was nicht lief, aber auch wenns lief. Unsere Truppe ist einfach nur der Hammer und ich genieße jeden Augenblick mit euch! Auf viele weitere Jahre des Feierns und der guten Laune! #Elefantenhorde

Mein größter Dank geht an meine Freundin Verena Freya Gaßel, welche mich stets unterstützt hat und für mich da war. Sie gab mir Mut und Kraft auch nach Rückschlägen während der Thesis weiterzumachen. Danke mein Kuschel ♥

ABSTRACT

The advent of DNA nanotechnology inaugurated a new era of defined, highly controllable nanostructures, equipping scientists with the tools to design nanoscale objects at the molecular level. The precise nature of DNA sequences to build architectures unlocked new possibilities and new material classes, particularly suited for demanding applications such as biosensors, nanocarriers, and templates for reaction cascades. The precise assembly of DNA-origami nanostructures offers a unique opportunity to combine them with other materials, such as polymers, in order to create distinct two- and three-dimensional hybrid materials with nanometer precision. Therefore, DNA strands can be modified with polymers, integrating the functionality and stimulus-responsive characteristics of the polymer world with the programmability of DNA, allowing the creation of conjugates with distinctive attributes, including pH and temperature responsiveness, superstructure formation, fluorescence or cell-surface binding.

The main goal of this thesis was the design, preparation and characterization of DNA-polymer conjugates with special focus on their synthesis and purification in order to achieve DNA-origami objects with nanoscale patterned surfaces. Therefore, reversible addition-fragmentation chain-transfer (RAFT) polymerization was performed to create a wide repertoire of water-soluble polymers of three different polymer classes (acrylates, methacrylates and acrylamides) with defined molecular weight. The advantage of RAFT polymerization is the usage of already pre-functionalized chain transfer agents (CTAs) to obtain end-functionalized polymers. Subsequently, a *grafting to* approach was adopted to conjugate DNA with the synthesized polymers, requiring careful solvent selection and reaction optimization to achieve successful coupling and high yields (Chapter III.I). Following the coupling reaction, the reaction mixtures were purified using a newly developed protocol for anion exchange chromatography. This method allows for the purification of larger reaction scales than other purification methods, such as reverse phase HPLC. Additionally, it is suitable for the purification of various DNA-polymer conjugates and those containing different sized blocks copolymers consisting of DNA or polymer segments (Chapter III.II). Notably, this purification method permits the recovery of unreacted DNA sequences for reuse and therefore is resource saving. Furthermore, the obtained DNA-polymer conjugates were employed to create polymer patterns with nanometer resolution on DNA-origami through annealing with complementary DNA strands protruding from the origami surface. This versatile strategy allows the design of functional, diverse surface modifications on a single DNA nanostructure, allowing precise 3-D engineering of complex nanoscale objects (Chapter III.I).

In summary, this study paves the way for obtaining a wide range of DNA-polymer conjugates formed with high yields and excellent accessibility, including an easy-to-use, widely applicable method for purification. This lays the groundwork for future applications. Additionally, the synthesized DNA-polymer conjugates have been demonstrated to be effective in serving as versatile surface coatings of DNA-origami nanostructures, yielding dense and well-defined surface patterns. Furthermore, they offer the capability for multipatterning of different polymer species on a single architecture, thereby expanding their utility and versatility.

ZUSAMMENFASSUNG

Mit der Entwicklung der DNA-Nanotechnologie begann ein neues Zeitalter definierter, hochgradig kontrollierbarer Nanostrukturen, welche der Wissenschaft die Möglichkeit gab, Objekte im Nanomaßstab bis hinunter auf die molekulare Ebene zu konstruieren. Die Präzision der verwendeten DNA-Sequenzen beim Aufbau von Architekturen eröffnete neue Möglichkeiten zur Herstellung hoch definierter Nanomaterialien, die sich besonders für anspruchsvolle Anwendungen wie Biosensoren, Nanotransporter und als Plattform für Reaktionskaskaden eignen. Der präzise Aufbau von DNA-Origami ermöglicht die Herstellung hochdefinierter Architekturen und bietet einzigartige Möglichkeiten der Kombination mit anderen Molekülklassen, wie den Polymeren. Auf diese Weise lassen sich neuartige, definierte DNA-Polymer Hybridmaterialien mit einer einzigartigen Nanostrukturierung herstellen. So können DNA-Stränge mit Polymeren ausgestattet werden, wobei die Funktionalität und die physiko-chemischen Eigenschaften der „Polymerwelt“ mit der Programmierbarkeit der DNA Sequenzen kombiniert werden. Hierdurch lassen sich Funktionsmaterialien herstellen, die interessante Eigenschaften wie eine einstellbare pH- und Temperaturresponsivität, Selbstassemblierung, Fluoreszenz oder präzise Wechselwirkungen z.B. mit Zellmembranen aufweisen.

Im Rahmen dieser Arbeit wurde die Herstellung von DNA-Polymer-Konjugaten eingehend untersucht und im Hinblick auf ihre Synthese und Reinigung optimiert, um ihre Anwendung als nanoskalige Oberflächenfunktionalisierungen auf DNA-Origami zu ermöglichen. Dazu wurde die Reversible Additions-Fragmentierungs-Kettentransfer (RAFT)-Polymerisation verwendet, um ein breites Repertoire an wasserlöslichen Polymeren aus drei verschiedenen Polymerklassen (Acrylate, Methacrylate und Acrylamide) mit definiertem Molekulargewicht zu synthetisieren. Der Vorteil der RAFT-Polymerisation besteht in der Verwendung bereits funktionalisierter Kettenüberträger („chain transfer agents“, CTAs), um endfunktionalisierte Polymere zu erhalten. Anschließend wurde ein *grafting to* Strategie angewandt, um DNA mit den synthetisierten Polymeren zu konjugieren. Um eine erfolgreiche Kopplung und hohe Ausbeuten zu erzielen, war eine breites testen gängiger Lösungsmittel und eine Optimierung der Reaktionsparameter erforderlich, (Kapitel III.I). Nach der Kopplung wurden die Reaktionsgemische mit einem neu entwickelten Protokoll für die Anionenaustauschchromatographie gereinigt, welche nicht nur die Reinigung größerer Mengen an Material im Vergleich zu anderen Reinigungsmethoden wie der Umkehrphasen-HPLC ermöglicht, sondern auch für verschiedene DNA-Polymer-Konjugate sowie für Konjugate mit DNA- oder Polymerblöcken unterschiedlicher Größe geeignet ist (Kapitel III.II).

Insbesondere ermöglicht diese Reinigungsmethode die Rückgewinnung nicht umgesetzter DNA-Sequenzen zur Wiederverwendung und Einsparung von Ressourcen. Darüber hinaus wurden die erhaltenen DNA-Polymer-Konjugate zur Herstellung von Polymermustern mit Nanometerauflösung auf DNA-Origami durch „Annealing“ mit komplementären DNA-Strängen, welche aus der Origami-Oberfläche herausragen, verwendet. Mit dieser vielseitigen Strategie lassen sich funktionelle, vielfältige Oberflächenmodifikationen auf DNA-Architekturen erzeugen, was eine präzise 3-D-Konstruktion von Objekten im Nanometermaßstab ermöglicht (Kapitel III.I)

Zusammenfassend eröffnen diese Studien einen Zugang zu einer breiten Palette von DNA-Polymer-Konjugaten, welche mit hohen Ausbeuten und in größeren Maßstäben synthetisiert werden können. Die nötige Reinheit dieser Konjugate wurde über eine einfach zu handhabende Methode zur Aufreinigung von Reaktionsgemischen gewährleistet, was eine wichtige Grundlage für potenzielle zukünftige Anwendungen schafft. Darüber hinaus zeigen die synthetisierten DNA-Polymer-Konjugate, dass sie als präzise Oberflächenmodifizierungen für DNA-Origami-Strukturen verwendet werden können und dichte, gut definierte Oberflächenstrukturen ergeben. Darüber hinaus bieten sie die Möglichkeit, verschiedene Polymerspezies auf einer einzigen Nanostrukturoberfläche präzise anzuordnen, wodurch sich ihr Anwendungspotential und ihre Vielseitigkeit erweitert.

CONTENTS

GRAPHICAL ABSTRACTS

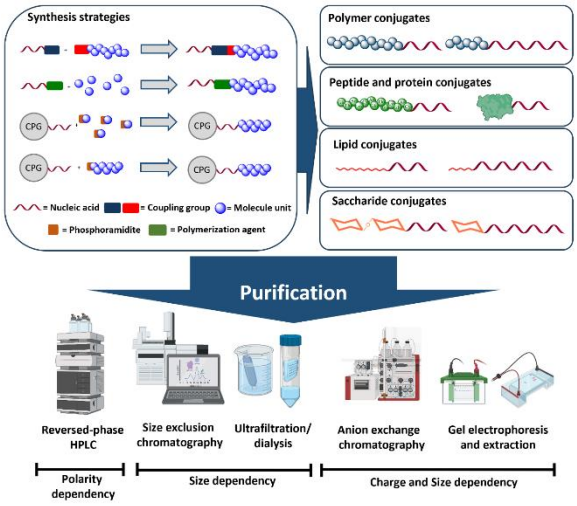

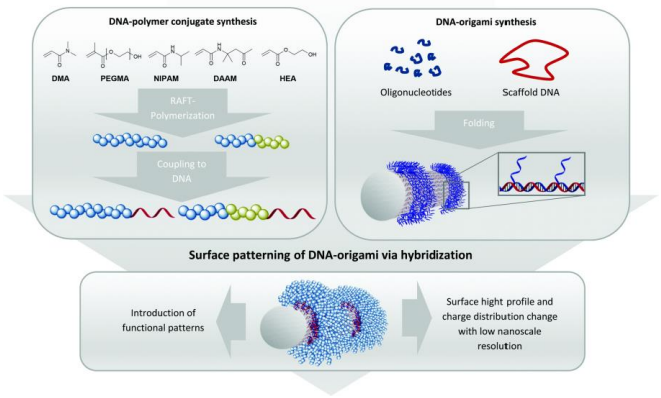

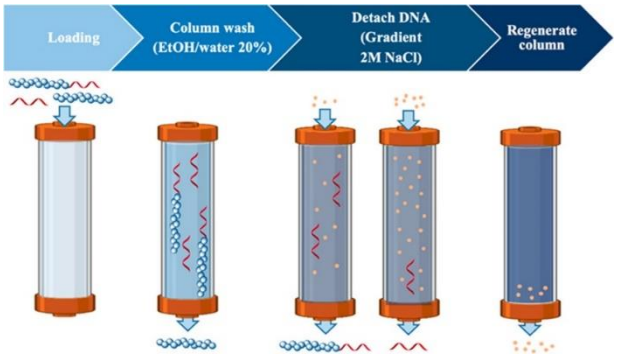

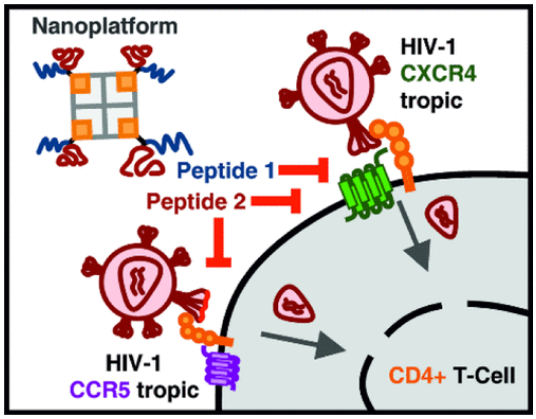

LIST OF ABBREVIATIONS

2D	two-dimensional
3D	three-dimensional
ACN	acetonitrile
AFM	atomic force microscopy
ARGET	activators regenerated by electron transfer
ATRP	atom transfer radical polymerization
bp	base pair
CTA	chain transfer agent
DAAM	diacetone acrylamide
DBCO	dibenzo cyclooctyne
DMA	dimethyl acrylamide
DMF	dimethyl formamide
DMSO	dimethyl sulfoxide
DNA	deoxyribonucleic acid
ds	double stranded
eATRP	electrochemically mediated ATRP
FRET	Förster resonance energy transfer
HEA	hydroxyethyl acrylate
HIV-1	human immunodeficiency virus 1
HPLC	high performance liquid chromatography
ICAR	initiators for continuous activator regeneration
Mg	magnesium
MWD	molecular weight distribution
NHS	*N*-hydroxy succinimide

NIPAM	*N-iso*propylacrylamide
NMP	nitroxide mediated polymerization
OEGMA	oligo ethylene glycol methacrylate
PAGE	polyacrylamide gel electrophoresis
PET	photo-induced electron transfer
photoATRP	photoinitiated ATRP
RAFT	reversible addition-fragmentation chain-transfer
RDRP	reversible-deactivation radical polymerization
sF	spin filtration
ss	single stranded
TAE	TRIS-acetate-EDTA
TEMPO	(2,2,6,6-Tetramethylpiperidin-1-yl)oxyl
t-RNA	transfer-ribonucleic acid
UV	ultraviolet

I. INTRODUCTION AND BASIC CONCEPTS

DNA-polymer nanotechnology is an emerging and rapidly advancing field at the intersection of synthetic biology, polymer chemistry, and nanotechnology. It leverages DNA's unique structural and functional properties, along with the tunable versatility of synthetic polymers. This thesis presents a robust, versatile, and resource-efficient approach for synthesizing and purifying DNA-polymer conjugates with minimal material loss.

To introduce the topic, I begin with the fundamental principles of polymerization, establishing polymers as an essential class of materials for both research and industry. This is followed by a discussion on DNA as a functional material, emphasizing its programmability for constructing complex DNA architectures. The thesis then explores strategies for synthesizing DNA-polymer hybrid materials, highlighting the benefits and limitations associated with different polymer components and synthesis methods. Additionally, I include a comprehensive review (currently under submission) that provides a detailed overview of various purification strategies, assessing their advantages, limitations, and novel opportunities for enhancing the purification process.

RADICAL POLYMERIZATION TECHNIQUES

With the development and understanding of polymers, beginning with Hermann Staudinger in 1920, the then revolutionary polymer chemistry was introduced, playing a decisive role in the development of today's world. Today, polymers, commonly known as plastics, have become an integral part in each aspect of everyday life and their unique properties rendering them irreplaceable. Global plastic production currently exceeds 400 million tons annually, with a rising proportion constituted by bio-based polymers.[1] Among the various techniques employed for polymer synthesis, radical polymerization emerges as a widely utilized approach for the fabrication of common plastics like polyethylene, as well as a diverse array of monomers. This technique requires only a C=C double bond instigating the formation of propagational radicals via initiation with an initiator compound.[2] The polymerization mechanism encompasses initiation, propagation occurring in the growth of the polymer chain and termination of the reaction. However, owing to the high reactivity of radicals they have short lifetimes and can undergo side reactions and terminations. Those side or termination reactions like disproportionation or recombination occur in different polymerization times and therefore a broader molecule weight

dispersity (MWD). Consequently, this variability can influence material properties, presenting challenges in achieving precise architectural configurations and specific material applications within research context. Despite these limitations, radical polymerization exhibits remarkable versatility, accommodating a wide array of solvents, including protic solvents like water, and boasting a broad monomer scope, thereby facilitating extensive polymer formation.[3] In contrast to free radical polymerization, living polymerization offers superior control over molecular weight dispersity, resulting in narrow dispersity and precise polymerization control. An example of these characteristics is the anionic polymerization, wherein highly reactive initiators generate anions to initiate polymerization as simultaneously as possible.[4] However, anionic polymerization is highly susceptible to termination caused by impurities. Contaminants such as oxygen, water, or carbon dioxide can trigger side reactions and premature termination. Consequently, polymerization must be carried out under inert gas and chemicals must be dried and cleaned beforehand. Given its high sensitivity, anionic polymerization is rarely used and is associated with very high costs.[5,6] In response to these challenges, an alternative methodology was sought that could offer robustness while maintaining ease of control. Radical polymerization exhibits excellent properties in terms of monomer versatility and contamination tolerance. Leveraging these attributes, a novel strategy with living characteristics was developed in the mid-1980s.[7] The strategy aimed to undergo fast termination or recombination events by introducing a dynamic equilibrium sufficiently fast to minimize these processes. Thus, Reversible Deactivation Radical Polymerization (RDRP) emerged, revolutionizing polymer chemistry. Through RDRP, radical polymerization was controlled in a highly defined manner, exhibiting typical features of living polymerization without the high sensitivity of the respective methods.[8] This groundbreaking advancement facilitated the synthesis of intricately structured polymers, including cyclic architectures and precisely controlled compositions such as block copolymers, thereby expanding the horizons of polymer science.[9]

To achieve the dynamic equilibrium essential for the controlled radical polymerization, two approaches have been devised: reversible activation/deactivation or the reversible degenerative chain transfer techniques. In the reversible deactivation/activation mechanism, the equilibrium lies on the dormant species side reducing radical concentration and thus termination and recombination. This method is exemplified by reversible-addition-fragmentation chain-transfer (RAFT) and nitroxide mediated polymerization (NMP), both of which employ specialized functional groups to establish dormant species. Conversely, reversible degenerative chain transfer relies on the rapid equilibrium between active and dormant species occurring concurrently with chain growth, without significant reduction in radical concentrations. Atom transfer radical

polymerization (ATRP) represents the strategy and is widely employed in practice. Due to the exceptional controllability, broad monomer scope and modification possibilities, RDRPs are essential for modern polymer research. Moreover, they offer remarkable capabilities for bottom-up architecture construction, thereby advancing the horizon of polymer science.[10]

ATOM TRANSFER RADICAL POLYMERIZATION

The atom transfer radical polymerization technique stands out as one of the most prevalent reversible-deactivation polymerization techniques and emerged as a very interesting technique for research to create nanoparticles as well as hybrid materials. Developed in 1995 by Sawamoto[11] and Matyaszewski[12], this approach demonstrates exceptional controllability and efficacy in polymer synthesis via radical polymerization. In ATRP, an alkyl halide serves as the initiator, while a redox-active metal catalyst, stabilized by a ligand, facilitates the polymerization process. The polymerization mechanism (Figure 1) is based on the cleavage of the carbon-halide bond which is interfered by the metal-ligand complex acting as an activator. The metal-ligand complex is in the lower oxidation state, drawing the halogenide to form the higher oxidative state. This process generates an active radical species capable of initiating monomer polymerization. Notably, this active species can reversibly interact with the halogen-bearing metal complex, leading to the lower oxidative state. The equilibrium between dormant and active species is pivotal in determining polymerization kinetics, with the activation and deactivation rates (k_{act} and k_{deact}) playing key roles for the polymerization speed and can be influenced by the metal complex ligands and the reaction parameters.[13,14] The ratio between active and dormant species as well as the activation and deactivation rates adjuvate the controllability and living character of the ATRP. In pursuit of achieving precise control over polymerization while minimizing termination reactions, it is essential for the equilibrium to favor deactivation, thereby ensuring low radical concentrations. This equilibrium needs to be optimized by the usage of suitable metal-ligand complexes whereby the ligand adjusts the redox potential of the metal complex (Figure 2). The primary role of the ligand is to enhance the solubility of both the metal complex itself and the formation of metal-halide species. Suboptimal solubility may impede metal-halide formation, resulting in less control over polymerization dynamics. The selection of ligands capable of forming more active metal complexes can elevate the concentration of active species, potentially leading to a broader dispersity in the resulting polymer. Typically, the metal center incorporates the copper(I)/copper(II) redox pair, owing to the wide array of nitrogen ligands available for catalysts.[15]

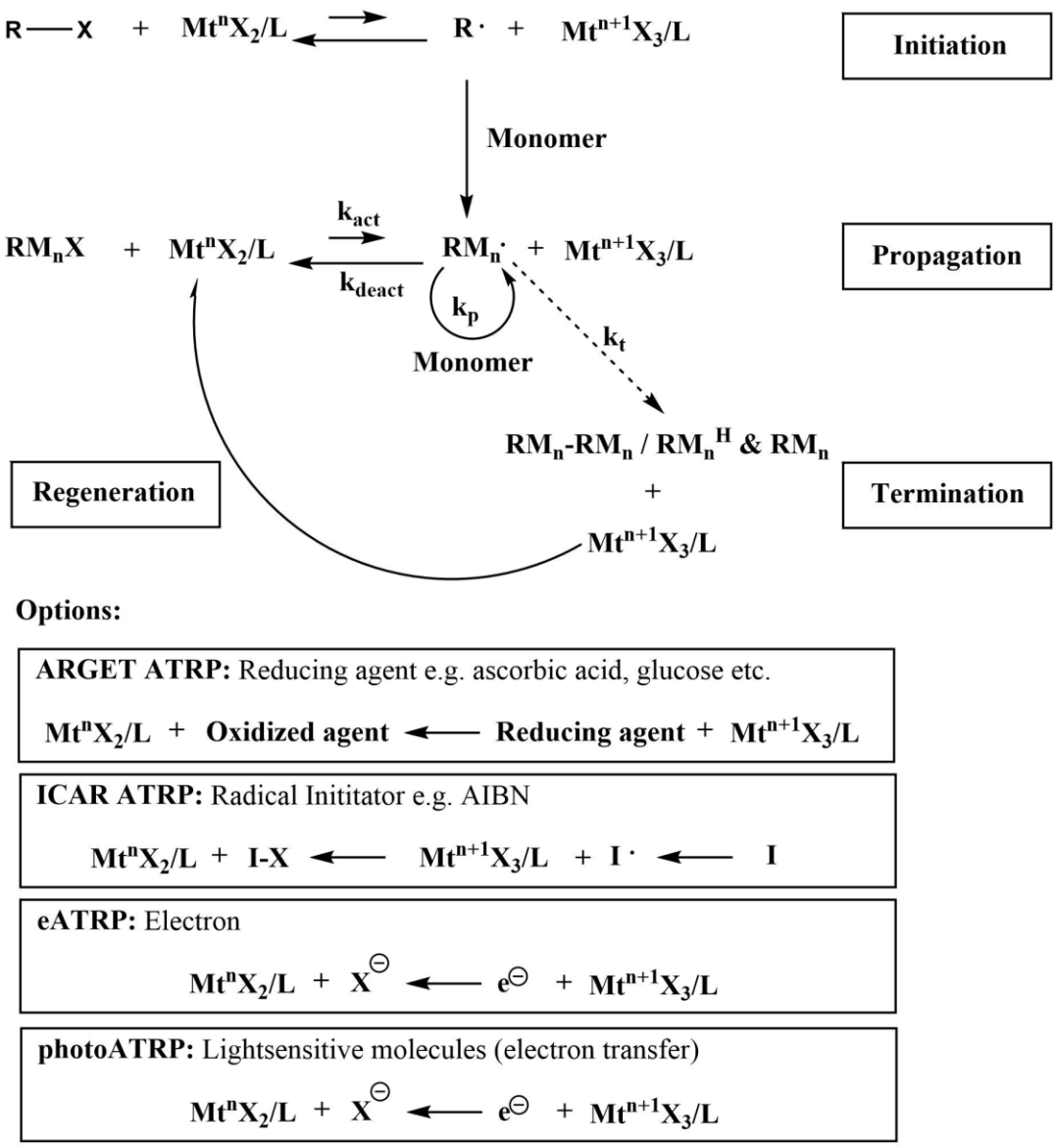

Figure 1: Mechanism of ATRP including initiation, propagation and termination, whereby M represent the monomer, polymer chain length is n and m, X is a halogen atom, L represents the respective ligand. Furthermore, for catalyst regeneration, several options are represented.

Additionally, alternative metals such as ruthenium[16,17], molybdenum[18,19] or iron[20,21] seems promising for ATRP application.

Additionally, several modifications were developed in the last decade, optimizing or introducing new applications for the ATRP technique (Figure 1). To avoid side reactions caused by oxygen, the active transition metal can be formed in situ by using for example ascorbic acid together with the inactive copper(II) complex. Ascorbic acid activates the metal complex by electron transfer and thereby starts the ATRP.[22,23] Other possible reagents are hydrazine[24], phenols or sugars.[25] This

technique is called activators regenerated by electron transfer (ARGET) and is one of various methods of activator regeneration ATRP techniques. Other approaches try to reduce the amount of metal catalyst needed for an optimal polymerization. Here, residual metals are toxic and removal after polymerization is challenging, which sometimes limits its usage for biological applications. Nevertheless, by regenerating the deactivated catalyst, occurring from side reactions for example with radical initiators the amount of catalyst can be reduced to ppm range. These so-called initiators for continuous activator regeneration (ICAR) make ATRP interesting for industrial applications.[26,27] Newer developments like electrochemically mediated (eATRP) as well as photoinduced ATRP (photoATRP) can also decrease the amount of catalyst by regenerating the catalyst.[28,29] The advantage is that the regeneration can be performed *in situ* without external force, occurring in a better reaction control. Furthermore, photo ATRP reveals the potential of performing the ATRP without the usage of metals, leading to a highly interesting approach for applications in or for biological systems. In this technique organic-based photo redox catalysts are used to initiate and control the polymerization.[30,31]

Nowadays, ATRP is an indispensable polymerization method giving access to various polymers and bock copolymer formations with toolbox character. Furthermore, this technique utilizes the formation of a broad range of hybrid materials, like conjugates of polymers with biomolecules or other biomaterials. The ATRP has been very well researched and makes it easy to use due to various standard protocols and guidelines.

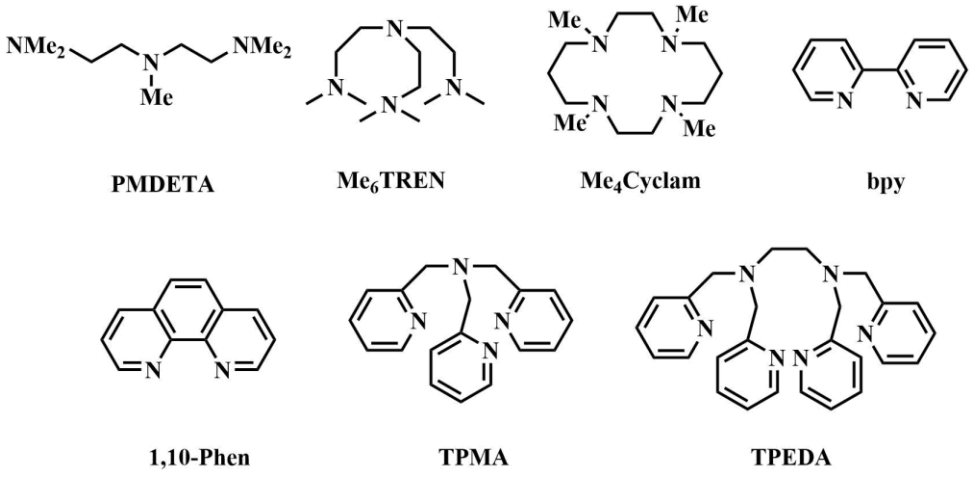

Figure 2: Suitable ligands for the metal complex to perform ATRP; from left to right: Pentamethyldiethylenetriamine (PMDETA), Tris[2-(dimethylamino)ethyl]amin (Me_6TREN), 1,4,8,11-Tetramethyl-1,4,8,11-tetraazacyclotetradecan (Me_4Cyclam), 2,2'-Bipyridine (bpy), 1,10-Phenanthroline (1,10-Phen), Tris(2-pyridylmethyl)amine (TPMA), tetrakis(pyridine-2-ylmethyl)ethane-1,2-diamine (TPEDA).

NITROXIDE-MEDIATED RADICAL POLYMERIZATION

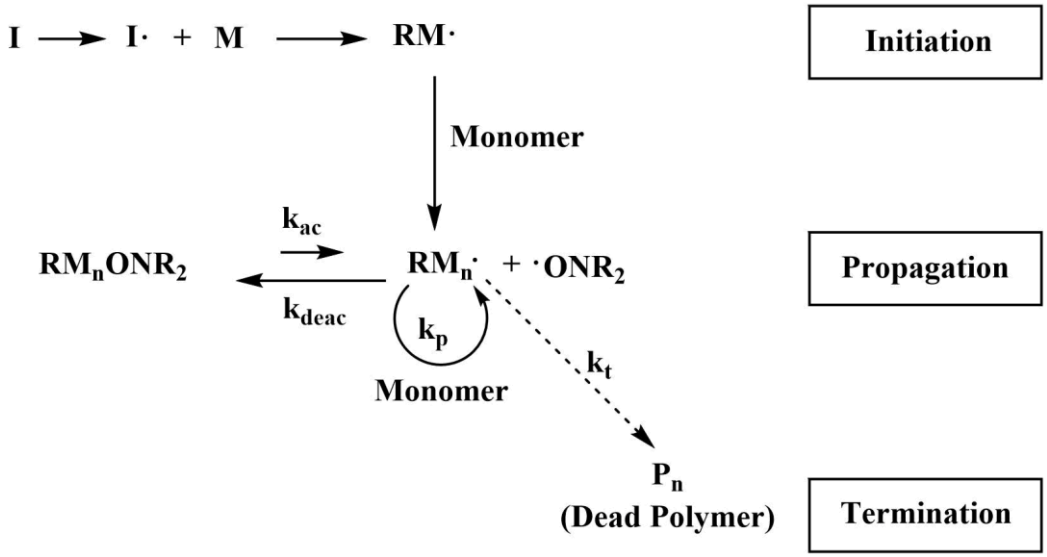

Figure 3: Mechanism of NMP including initiation, propagation and termination, whereby I is the initiator, M represent the monomer, P is polymer, polymer chain length is n and m, ONR_2 represents the nitroxide molecule and k_x are the representative rate constants of propagation (x = p), termination (x = t), deactivation (x = deact.) and activation (x = act.).

The nitroxide-mediated radical polymerization (NMP) is a reversible deactivation chain transfer technique where alkoxyamines are utilized to control the polymerization by a reversible recombination of propagating species with the nitroxide group (Figure 3). Thereby, the radical concentration is held low decreasing irreversible termination reactions. Furthermore, due to the fast formation of the dormant species, the chain growth is equal, forming homologous chain length and polymerization will take place till the monomer is fully consumed. Here, the key molecule is the alkoxyamine, forming the dormant species. The structure of the molecule is usually an N-O group wearing two alkane groups.[32] Those alkane groups are commonly tertiary due to the stabilization effect in the radical state. The alkane groups need to be optimized to allow polymerization for the respective monomer, by forming more reactive or less reactive radicals, thus influencing the equilibrium of the dormant to the active species. In general, a greater steric bulk in the alpha position of the nitroxide group leads to a higher strain, occurring in a more unstable C-O bond of the dormant species. For cyclic nitroxides, due to strain within the ring system including the nitroxide group, the pentagonal rings seem faster at the cleavage.[33,34] A commonly used example is (2,2,6,6-Tetramethylpiperidin-1-yl)oxyl (TEMPO), which wears tertiary alkanes in alpha position and is commonly used for the polymerization of styrene. If less reactive monomers like butyl acrylate are targeted for polymerization, the alpha position of the nitroxide group can be modified, introducing more steric demanding groups. Those groups favor the

homolysis and form the active species faster.[35] Another factor influencing the homolysis is the solvent. To perform the C-O homolysis, polar solvents which cannot bind to the active nitroxide species are the favored polymerization media. The advantage of the NMP is the metal free procedure, which makes the usage for biological applications attractive. Also, NMP is not colored, favored for material forming in an industrial aspect. Limitation of this procedure seems to bethe choice of polymerizable monomers, whereby the nitroxide group needs to be tuned in terms of reactivity to obtain optimal results and controllability.[36] However, the NMP technique is ideal to form block copolymers due to the stability of the dormant species. The polymer can first be purified post polymerization and then reused to create the second block at the polymer end.[37] In current studies NMP is used to modify surfaces of nanoparticles by using initiators protruding from the surface. This can be done, for example on silica surfaces where block copolymers are created at the surface due to NMP.[38,39]

REVERSIBLE ADDITION-FRAGMENTATION CHAIN-TRANSFER POLYMERIZATION

The reversible addition-fragmentation chain-transfer polymerization (RAFT) was developed in 1998 by Rizzardo and since then it has become very important for research in several fields due to the excellent controllability, robustness towards impurities and broad range of monomers. The RAFT polymerization relies on an equilibrium of active and dormant species where the balance lies on the dormant species. As a consequence, the concentration of radicals during polymerization is reduced, resulting in less termination reactions and therefore better dispersity. This can be realized with functional groups like dithio or trithio groups forming the dormant species by introducing an active radical. These molecules can switch from the dormant to the active species, forming a radical and continue the polymerization. Due to this key function, those molecules are called chain transfer agents (CTAs).[40,41] The mechanism of the RAFT polymerization contains initiation, reversible chain transfer, reinitiation, chain equilibrium and termination (Figure 4). For initiation, the initiator forms a radical by decomposing with heat or photo-induced electron transfer (PER) process. The active initiator (I·) starts polymerizing monomer (M) forming a polymer chain with an active end (Pn·). The active polymer end stands in equilibrium with the CTA forming a dormant species which can decompose into either Pn· or a new radical species R·, which can polymerize forming Pm·. Due to the polymerization equilibrium, the polymerization is

continued, while the radical concentration is kept low. Combination and disproportionation are the termination steps of the polymerization.[42]

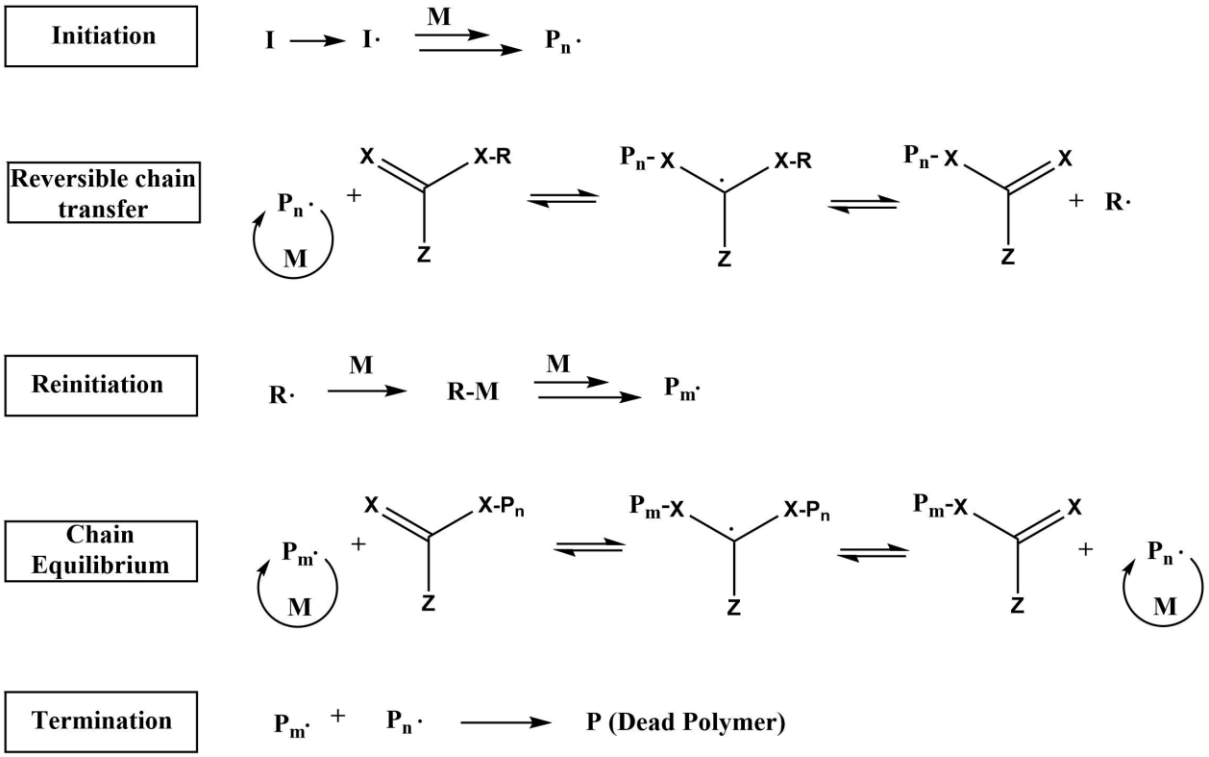

Figure 4: Representative mechanism for RAFT polymerization showing initiation, reversible chain transfer, reinitiation, chain equilibrium and termination, whereby I is the initiator, M represent the monomer, P is polymer, polymer chain length is n and m and the CTA contains X for sulfur and Z and R group.

The key molecule to perform the RAFT polymerization is the CTA. The reactivity of this molecule must be tailored to the specific monomer being utilized (Figure 5). The reactivity of the CTA occurs from the C=S double bond, the Z and the R group. To form the C=S functionality, the dithiol group and the trithio group are commonly used, whereby the trithio group shows higher activity. The Z group controls the reactivity of the C=S double bond and therefore affects the lifetime of the intermediate radical, while the R group serves as the leaving group, triggering polymerization reinitiation in the pre-equilibrium phase. Moreover, the R group contributes to the solubility of the CTA for both polar and nonpolar solvents. For different activities of the monomers, the CTA group is often optimized for the polymerization of interest. The general terms are that the higher the activity of the monomer, the more suitable the dithio CTA is whereas monomers of lesser activity favor the trithio CTA.[43,44]

RAFT polymerization stands out as a highly adaptable technique applicable to a diverse array of monomers. The monomer scope varies from vinylic benzenes to (meth) acrylates to (meth) acrylamides and can also contain sterically demanding sidechains without a loss of

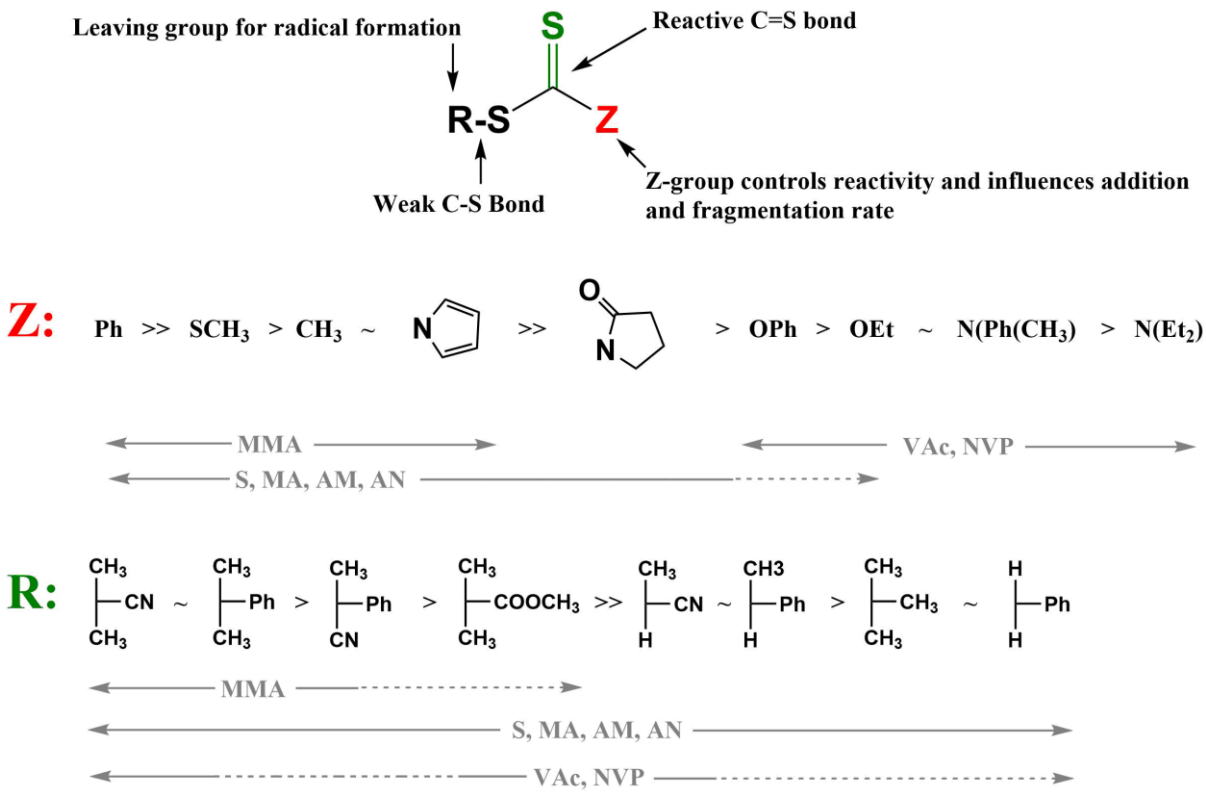

Figure 5: CTA structure with possible R and Z groups which influence the polymerizable monomers, shown with arrows, whereby MMA stands for methyl methacrylate, S for styrene, MA for methacrylate, AM for acrylamide, AN for acrylonitrile, Vac for vinyl acetate and NVP for vinylpyrrolidone.

polymerization performance. It can also perform at higher or lower temperatures without losing controllability or worsen the molecular weight dispersity. Moreover, as it operates without toxic metals like copper, RAFT polymers are less toxic towards biological systems compared to metal mediated polymerization.[45] The RAFT group can be easily eliminated or modified, further mitigating potential toxicity concerns. A recent approach explored RAFT polymerization within living biological systems, enabling the in-situ construction of networks or architectures, paving the way of new dynamic systems in biological behavior.[46]

FUNCTIONALIZATION OF RAFT POLYMERS

The RAFT polymerization methodology offers a broad spectrum for precisely controlled polymer synthesis. Moreover, it facilitates polymer functionalization either prior or following polymerization, thereby enabling the incorporation of reactive groups and modifications suitable for coupling with other molecules such as DNA or for imparting new properties such as fluorescence. Two strategies of introducing functionality can be performed by using a functional CTA intrinsically possessing a target group or by chemically transforming the CTA group (Figure 6). Former functional CTA can contain biomolecules like DNA or peptides or functional groups like NHS or DBCO groups allowing coupling post polymerization. It is crucial that the functionality of the CTA does not impede polymerization. For post-polymerization functionalization, the CTA group can be converted into the desired end functionality, such as thiols. Various strategies have emerged, including cycloaddition or thermolysis methods to introduce new double bonds. Alternatively, some strategies necessitate initial conversion of the CTA group into thiol end groups before subsequent modification with epoxides or Michael acceptors.[47–51]

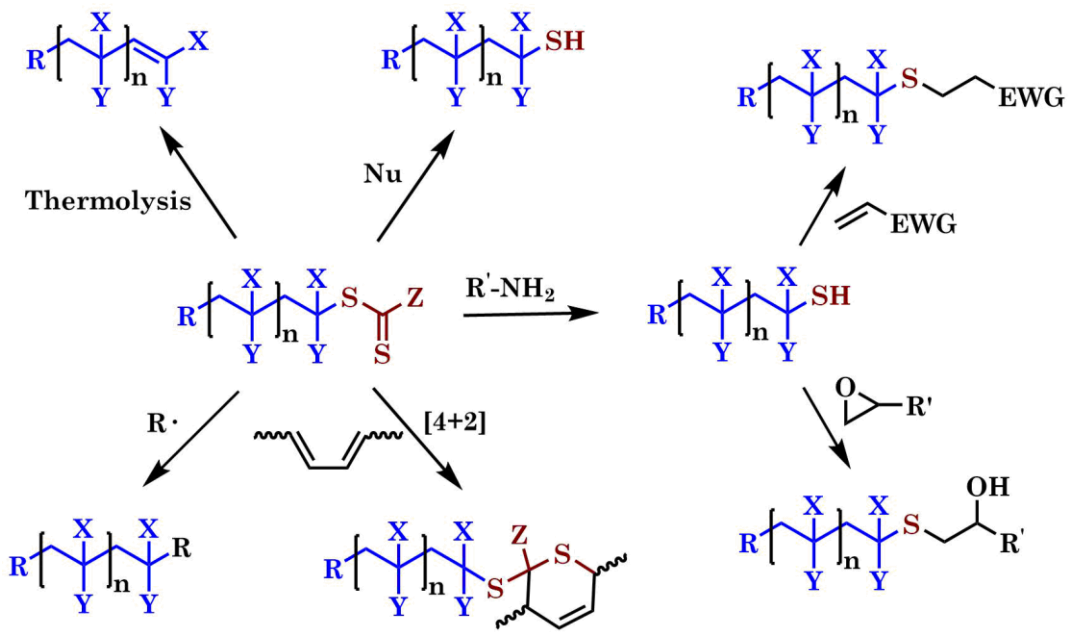

Figure 6: Functionalization options for RAFT polymers post polymerization.

DNA AS A UNIQUE BIOPOLYMER

In biological systems, DNA serves several functions, primarily acting as the repository of genetic information. Nature has evolved the programmability and precision of this molecule over millions of years, making it one of the most exquisitely engineered structures available in the natural world. The architecture of DNA resembles a code, composed of a backbone and four nucleobases—cytosine (C), guanine (G), adenine (A), and thymine (T)—bound to a deoxyribose-phosphate unit, forming a sequence for information storage. These macromolecular nucleic acids assemble into complementary strands, facilitated by hydrogen bonding between specific base pairs (Figure 7). Those so-called base pairing rules gives the DNA a unique structure in a highly controlled way. The pyrimidines T and C pair with purines A and G through two or three hydrogen bonds. The resulting double-stranded DNA molecule adopts a helical structure due to the slight strain imposed by these hydrogen bonds, with the strands winding around each other in opposite directions. This helical configuration was first discovered by Watson and Crick in 1953 using the X-ray based fiber diffraction of DNA provided by Rosalind Franklin and represents one of the most important breakthroughs in medical and biological research.[52] The double helix formation positions the more hydrophobic bases inward, while the sugar-phosphate backbone forms a highly hydrophilic exterior. This arrangement energetically favors water solubility, contributing to the stability of the double-stranded DNA molecule. The interaction of the nucleobases causes the

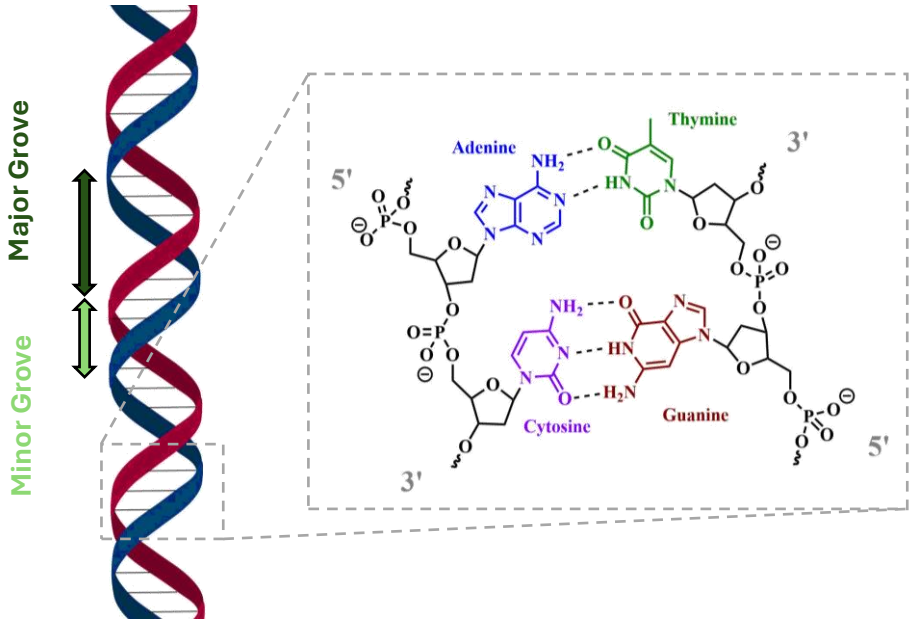

Figure 7: Schematic presentation of the DNA double helical structure, showing the complementary nucleic bases and their hydrogen bonding to stabilize the structure. Owing to the nucleic acid interactions the double helix forms a minor and a major grove with different gap sizes.

double stranded DNA to be less flexible than single stranded DNA.[53,54] However, it is primarily the formation of these interactions that makes DNA very interesting as a material in today's research. Copied from RNA, which exhibits the ability to form complex structures such as t-RNA, DNA nanotechnology aims to leverage these properties to engineer precise material structures. The underlying concept is the formation of architectures due to the interaction of a single strand with the complementary strands and drive the formation into a defined shape, facilitated by interactions such as hydrogen bonds between the strands. This approach has given rise to a novel class of DNA materials characterized by self-assembly and self-organization driven by kinetic processes. The pioneering work of Nadrian Seeman in 1982 marked the initial step into utilizing DNA as a structural material for crafting nanoscale shapes.[55] Seeman proposed employing DNA strands to construct nanoscale objects based on the selective interaction of sequence-based DNA strands. Subsequently, in collaboration with Sung Ha Park in 1998, Seeman demonstrated the fabrication of DNA nanotubes using self-assembling tiles capable of forming tubular structures in solution. Another attempt was to use the already in 1964-predicted Holliday and three-way junctions (Figure 8) to form DNA lattices and architectures.[56] This approach involved

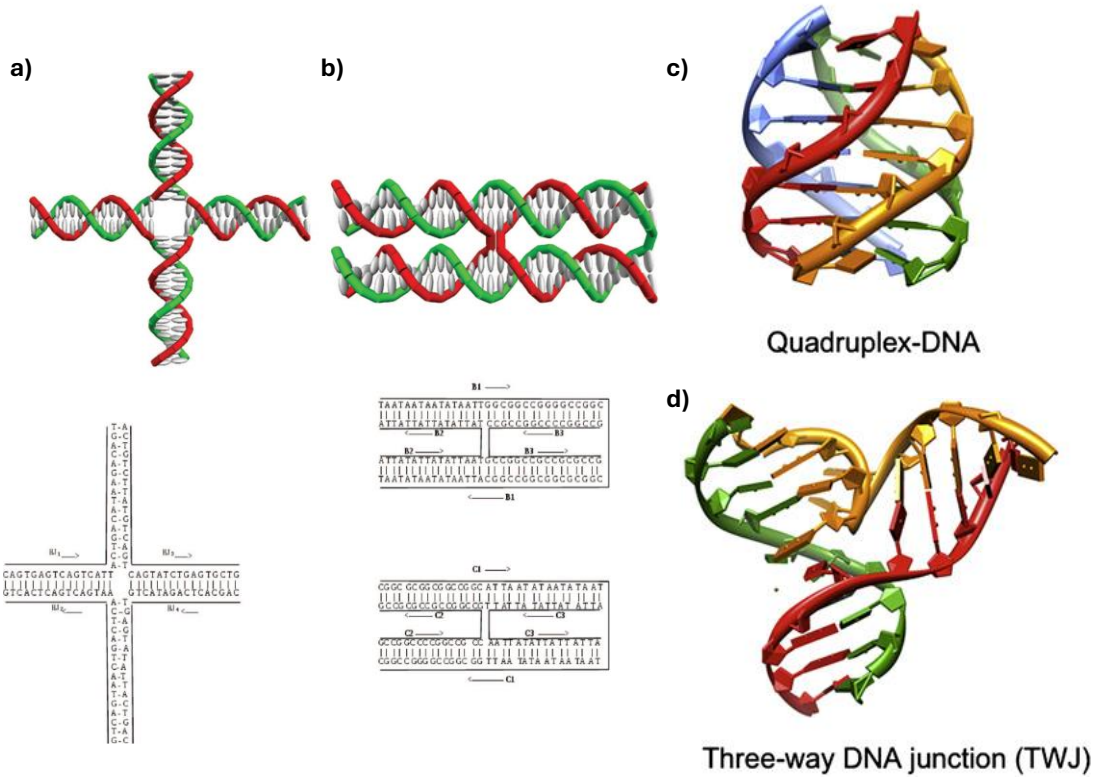

Figure 8: a) Holiday junction with representative nucleic acid sequence. b) Bent Holliday junction with representative nucleic acid sequence. c) schematic representation of the G4-quadruplex DNA structure. d) schematic representation of the Three-way DNA junction. Adapted and reprinted with permission of the authors.[110,111]

designing DNA sequences that fostered interaction crossovers, thereby enabling the formation of secondary and tertiary structures. These interaction points can be used to form new DNA lattices or architectures, with the base sequence programmed precisely to facilitate their formation.[57–60]

DNA-ORIGAMI

DNA-origami offer precise control over the assembly of nanoscale structures with unprecedented accuracy and versatility. Building upon the pioneering work of Nadrian Seeman, Paul Rothemund introduced a method in 2006 utilizing a long single-stranded DNA scaffold and short oligonucleotides, termed staple strands, to enable programmable folding and create DNA architectures.[61] In this technique, staple strands selectively bind to predetermined regions of the scaffold DNA, utilizing crossover motifs to induce folding and shape the structure (Figure 9 a). Using the Watson-Crick base pairing interactions, the staple strands fold and therefore wind around the scaffold DNA, with a rotation of 240 degrees occurring every 7 base pairs. This rotational property enables the creation of interhelical crossovers every 180 degrees, reinforcing the framework and yielding 2D sheets.[62,63] By adjusting the length of the scaffold DNA and the quantity of staple strands, the size of the resulting architecture can be finely controlled.[64] These controlled interactions between scaffold DNA and staple strands allows the computational design of DNA architectures by determining the location of the staple strands to guide the folding into the target structure. This breakthrough has facilitated the creation of a diverse array of shapes ranging from tubes to stars to smileys (Figure 9 c).[65] However, 2D DNA-origami structures, due to their single-layered construction, may exhibit conformational flexibility, which can limit their utility as self-assembling platforms. This flexibility arises from the wireframe design, wherein DNA helices feature vacancies at the vertices.[66]

To address this issue, 3D DNA-origami structures offer a viable solution. By stacking single-layered DNA architectures, it becomes possible to construct multi-layered DNA architectures by using for example honeycomb-shaped lattices in the cross section. Here, every 7 bp the DNA helix is connected to another helix in approximately 120° forming a multidimensional lattice. Each helix is perpendicular to two other helices, enhancing the structural rigidity. Alternatively, a four-helix bundle arrangement can be utilized to achieve a square alignment of each helix, resulting in denser packaging. In this arrangement, the strand transfers every 8 bp, (270°) to the neighbor

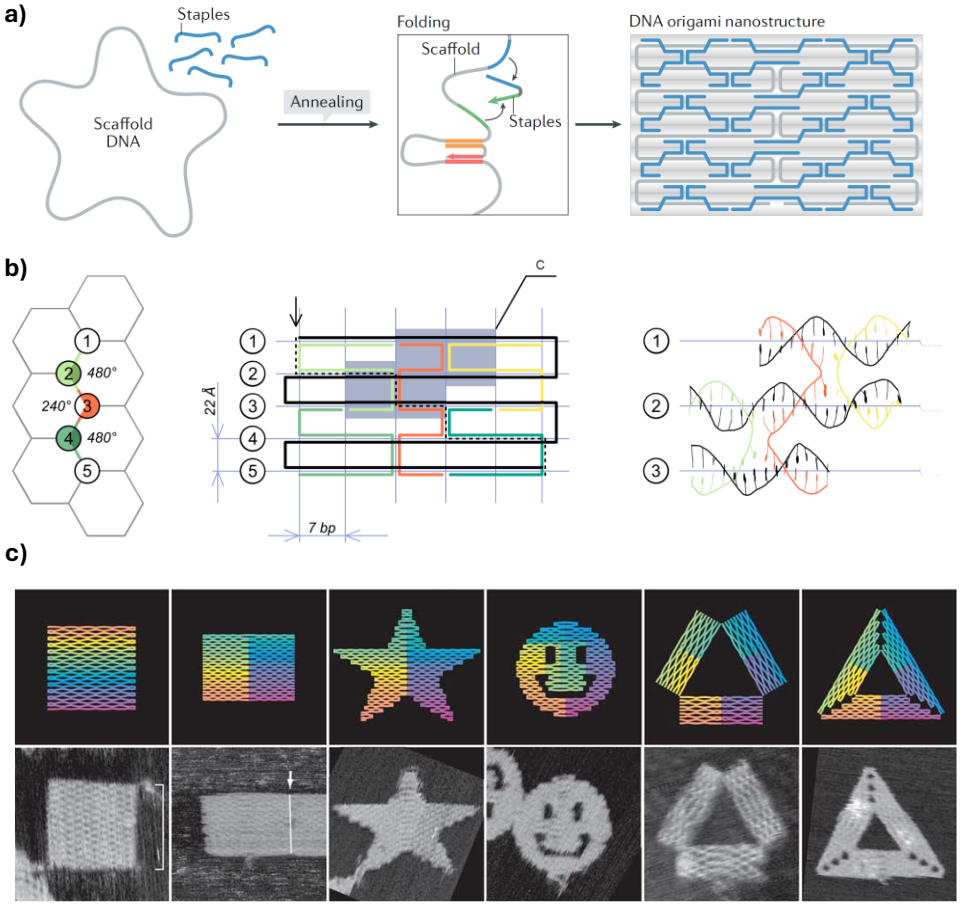

Figure 9: a) Schematic representation of the DNA-origami creation by annealing staple strands to the scaffold DNA to form the architecture. b) Helix to helix neighbor connection to stabilize the architecture. c) Examples for DNA-origami shapes. Adapted and reprinted with permission of the authors.[112–114]

strand stabilizing the architecture.[67–70] These multilayer structures exhibit increased rigidity and typically require higher concentrations of magnesium ions (Mg^{2+}) for stabilization.[67,71] DNA-origami structures produced using these strategies are characterized by dense, solid architectures devoid of pores or gaps. To create hollow DNA-origami structures, a wireframe single-layered design has been developed.[72,73] One method involves employing knot points constructed from four 4-arm junctions that connect the strands, forming a square frame. Multiple units of these structures can assemble into a 2D lattice, capable of forming spheres due to the tension.[74] These spheres can be functionalized with enzymes to facilitate cascade reactions[75] and utilized as capsules[76] for various applications.

DNA-ORIGAMI AS FUNCTIONAL TEMPLATES

DNA origami provides excellent template properties, thanks to their precise construction, rendering them ideal for creating functional architectures. Each staple strand within the DNA scaffold possesses a specific sequence and position. By extending specific staple strands with additional bases, known as sticky sequences, the extended portion protrudes from the surface, creating new sites for functionalization on the DNA-origami surface.[77] This distinct elongation enables the introduction of functionality with nanometer precision, facilitated by the precise positioning of the staple strands. Subsequently, the protruding sequence can be targeted post-origami creation by complementary strands, facilitating the noncovalent attachment of molecules such as polymers[10], fluorophores[78], photo initiators[79] or proteins[80,81]. This functionalization offers a wide variety of applications of DNA-origami for analytical[82] or cell uptake studies [83]. One notable application involves utilizing highly defined DNA-origami structures equipped with fluorophores to conduct Förster Resonance Energy Transfer (FRET). In this technique, photoactive molecules are strategically positioned at defined distances from each other, enabling the observation of FRET occurrence within specific distance ranges.[84,85] This methodology can also be employed to assess the structural integrity of the architecture post-application (Figure 10 a).[86] Additionally, introducing sequences that form secondary structures, such as G4 sequences, allows for the intercalation of functional molecules onto the origami surface. G4 quadruplex sequences create flat areas comprised of four guanines through π-π stacking interactions. These regions serve as anchoring sites for molecules containing π systems, such as photoactive molecules, enabling their immobilization onto the surface (Figure 10 c). Those photo active molecules can be utilized to create polymer formation on the origami surface promoted by visible light. Recently, Winterwerber and colleagues achieved successful local polydopamine and norepinephrine formation using this strategy on DNA-origami surfaces. These coatings serve to stabilize the DNA-origami structures and induce cell uptake.[79,86] Other strategies require the formation of conjugates containing the complementary strand. Here several molecule classes like proteins, peptides, synthetic polymers, lipids or saccharides can be combined with the DNA strand open the possibility to have multi functionality within one architecture. This functionality was demonstrated by the Dietz group to immobilize viruses on DNA-origami architectures to function as virus catchers. The strategy to combine several DNA-origami units to one macro structure expand the array of possibility for new applications. In this approach, several DNA-origami units were combined into a single macrostructure, which was functionalized with antibodies to bind surface proteins of the immobilized virus (Figure 10 d).[87] Additionally, the

negatively charged surface of DNA-origami can be exploited to immobilize positively charged molecules like polylysine onto the architecture. These noncovalent coatings enhance the stability of the origami structures and facilitate cell uptake owing to the interaction with the charged cell membrane.[88,89]

In short, DNA-origami offer due to their unique construction, several functionalization strategies and are ideal scaffolds template various other (macro)molecules. Furthermore, the precise positioning of the functionalization lead to a highly controlled and fully customizable 3-D space at the nanoscale.

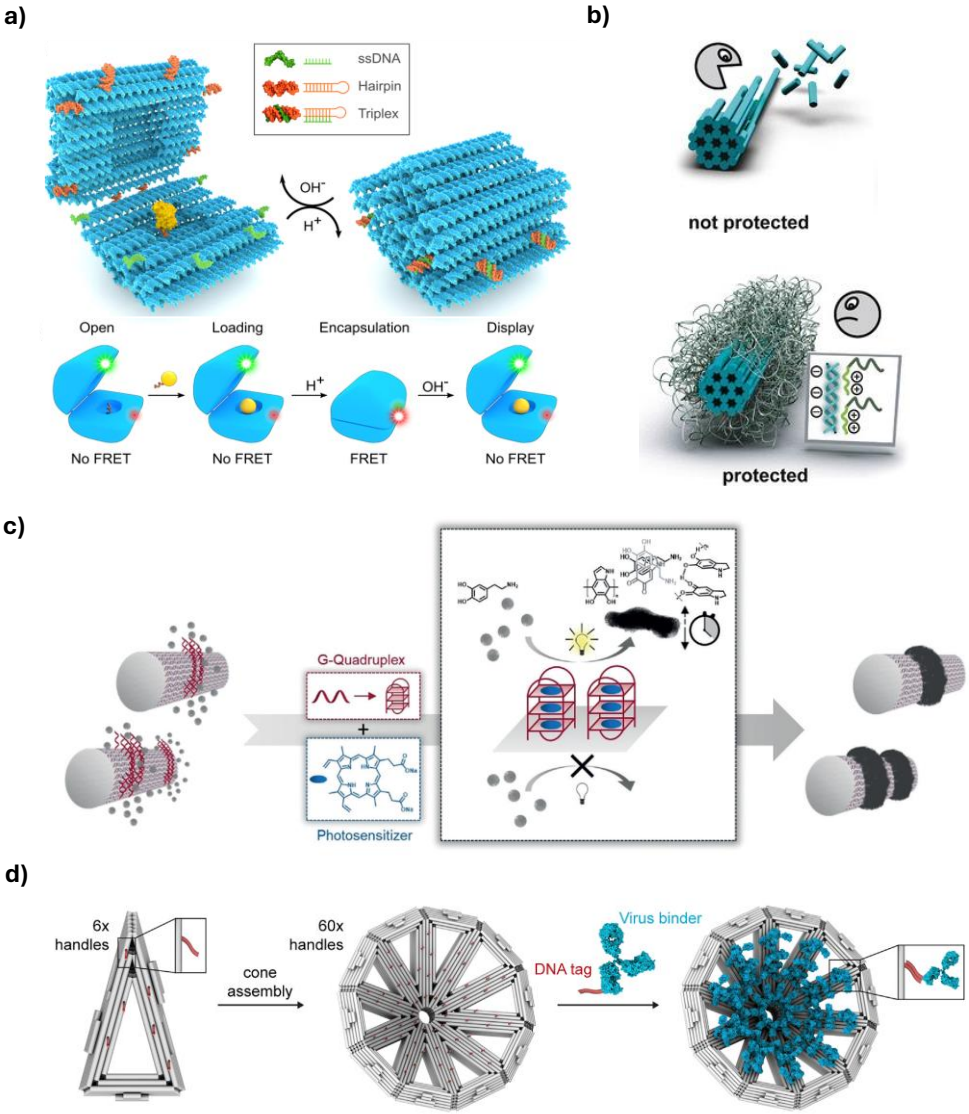

Figure 10: a) DNA-origami architecture as nano capsule equipped with a hinge region to perform FRET. This signal is used to visualize that the architecture is closed. b) DNA-origami surface protected with cationic polymer to protect DNase degradation. c) DNA-origami tubes, equipped with G4 quadruplex structures to intercalate photo initiators on the surface. These can be used to initiate dopamine polymerization. d) DNA-origami triangles can be hybridized to capsules. These capsules can act as virus catchers when equipped with virus binder. Adapted and reprinted with permission of the authors. [79,87,89,115]

FORMATION OF DNA-POLYMER CONJUGATES

Polymers represent a versatile class of materials that can be precisely tailored in terms of size, composition, and dispersity. They give access to diverse properties like thermo[90] or pH responsiveness[91,92] as well as morphologies and architectures like branches[93] or worm-like[94,95] structures resulting from phase separation. By combining different monomers or blocks with distinct properties within a single molecule, a wide range of properties and applications can be achieved. Integration of these polymers with highly defined, polar DNA strands or architectures gives rise to a new class of hybrid materials with applications spanning biosensors[96,97], responsive hydrogels[97–99] or nanocarriers[100,101]. Various strategies are employed to form these hybrid materials, including direct polymerization from DNA architectures[10] or annealing of DNA-polymer conjugates onto the DNA nanostructure[77,102]. Direct polymerization from DNA architectures necessitates initiator or polymerization propagating molecules that are either attached or intercalated onto the DNA scaffold. The former can be done by the usage of DNA strands equipped with polymerization propagating molecules annealed to the DNA architecture protruding from the surface.[10] Subsequently, polymerization can be performed by introducing initiator and monomer to the functionalized DNA architecture, forming the hybrid structure *in situ*. In the case of intercalating initiators, primarily photo initiators, sequences capable of forming small morphologies on the architecture surface are required. G4 quadruplex sequences are commonly employed for this purpose, creating π-π stacking regions where initiators preferentially intercalate. Through precise positioning of G4 structures, spatially defined polymerization can be achieved, leading to the formation of DNA-polymer architectures.[79,86] Another strategy involves utilizing the annealing process to position polymer-conjugates onto DNA architectures, necessitating the synthesis of DNA-polymer conjugates beforehand. Two strategies are available for this purpose (Figure 11). For the *grafting from* procedure a DNA sequence is equipped with an alkyl halogenide[103] or a chain transfer agent at the end. The functionalized DNA strand is mixed with monomer and initiator to conduct controlled radical polymerization *in situ*. It is crucial that the reaction mixture is oxygen free to perform the radical polymerization. Oxygen removal can be achieved through methods such as freeze-pump-thaw cycles or enzymatic treatment using glycose oxidase, which converts oxygen into hydrogen peroxide in the presence of glucose. For the enzymatic removal, only few solvents like water or DMF are compatible to ensure that the enzyme stays active, limiting the monomer choice.[104,105] The simplicity of purification, mainly achieved through spin filtration, is a notable advantage of the *grafting from* method. However, limitations arise from solvent restrictions, consequently restricting monomer choices due to the

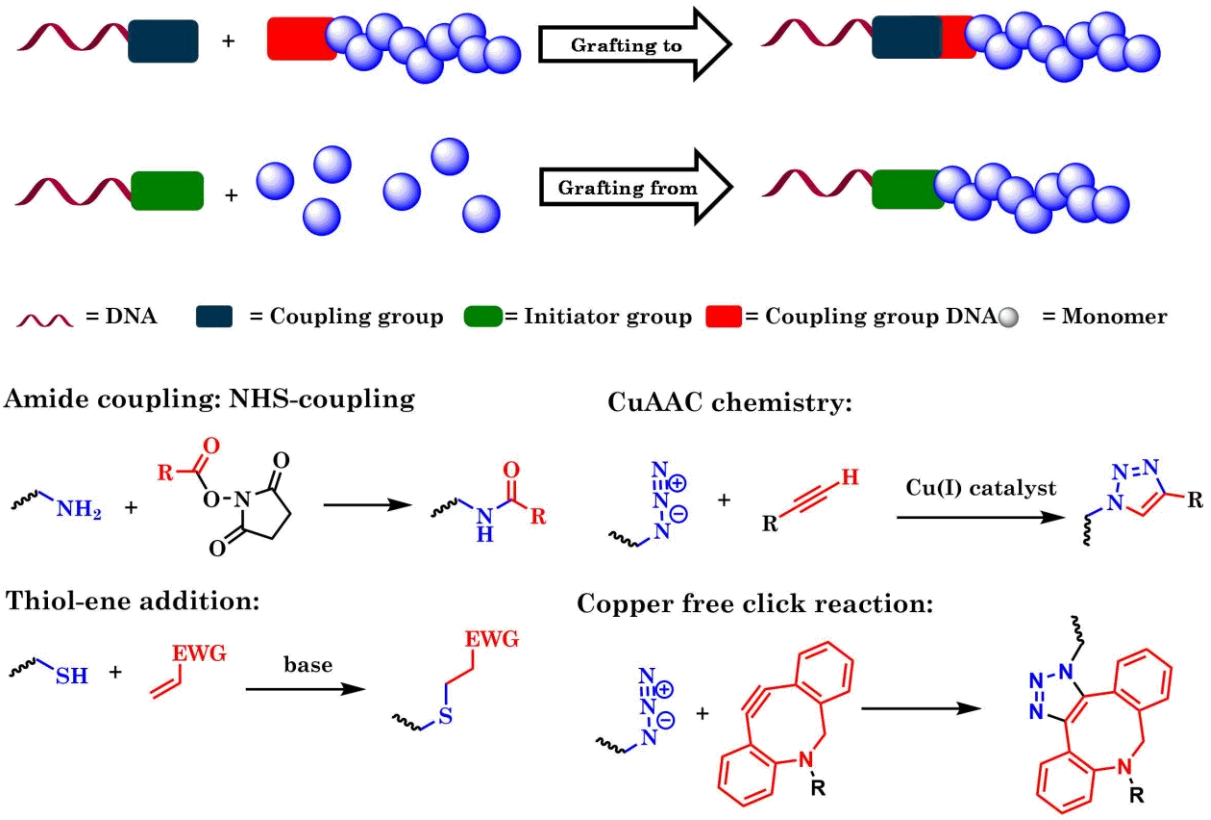

Figure 11: DNA-polymer formation strategies showing the *grafting to* and the *grafting from* strategy. For the *grafting to* strategy the polymer and the DNA block are coupled through reactive groups to each other. Examples for coupling partners are shown below. For the *grafting from* technique the DNA block is equipped with a functional molecule performing polymerization to form the conjugate.

requirement for more protic solvents. Additionally, polymer characteristics such as dispersity and exact polymer length are less controllable due to polymer formation *in situ*.[103,106] In contrast, the *grafting to* strategy involves synthesizing the polymer prior to conjugate synthesis using conventional polymerization methods. Both the polymer as well as the DNA sequence need to be equipped with a functional group which can be coupled to the respective molecule. Those groups are typically NHS/amine or DBCO/azide. Successful coupling requires close proximity of the functional groups, making solvent selection crucial due to steric hindrance and chain collapse. Poor solubility of the polymer or DNA may lead to increased molecular density in solution, hindering the coupling reaction. Therefore, the solvent optimization plays an important role for the successful reaction to achieve high yield. Unlike the *grafting from* technique, the *grafting to* strategy allows the use of cheaper materials in excess to obtain higher yields. Additionally, synthesizing the polymer prior to coupling allows precise control over polymer properties, optimizing them for the desired conjugate. However, the disadvantage of this approach lies in the need for purification of the reaction mixture due to the larger amount of unreacted materials typically used in excess.[107–109]

This underscores the ongoing need for improvement in DNA-polymer conjugate formation. While initial steps have been taken to develop strategies with their respective advantages and disadvantages, further optimization is necessary to broaden their applications and enhance their suitability for simplified production of hybrid nano architectures.

DNA-POLYMER CONJUGATE PURIFICATION

Publication: **"Functionalizing nucleic acids: synthesis and purification strategies for bioconjugates"**

Authors: **Nico Alleva,**[#] Jian Zhang,[#] David Y. W. Ng, Torsten John,* Tanja Weil*

Published: **To be submitted**

Author Contribution:

Nico Alleva	Conceptualization of review structure and outline; writing of the original draft (introduction, general purification strategies, DNA-polymer conjugates); review and editing of the manuscript; design and visualization of figures; project administration.
Jian Zhang	Writing of the original draft (DNA-polymer and DNA-peptide/protein; conjugates); review and editing of the manuscript; visualization of figures.
David Y. W. Ng	Review and editing of the manuscript; supervision; project administration; funding acquisition.
Torsten John	Conceptualization of review structure; writing of the original draft (abstract, introduction, DNA-lipid and DNA-saccharide conjugates); review and editing of the manuscript; visualization of draft figures; supervision; project administration.
Tanja Weil	Conceptualization of review structure; review and editing of the manuscript; supervision; project administration; funding acquisition.

Graphical Abstract:

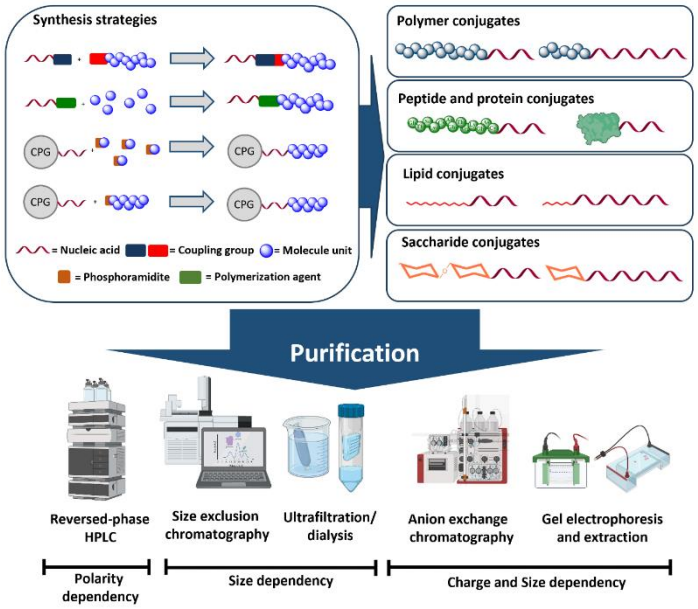

Summary:

DNA-polymer conjugates represent hybrid entities formed by linking DNA molecules with synthetic polymers. These conjugates combine the unique properties of DNA, such as sequence-specific recognition and molecular self-assembly, with the versatility and functionality of polymers. This enables a broad spectrum of applications across diverse fields including biotechnology, materials science, nanotechnology, and medicine. The creation of DNA-polymer conjugates involves various strategies, like *grafting to*, *grafting from* or the solid supported synthesis, each presenting unique challenges in purification. Due to the different properties within the molecule, purification is usually problematic and requires extensive experimentation and optimization. Moreover, the choice of synthesis strategy dictates the purification approach, tailored to address specific side products. In this review, we aim to provide a comprehensive overview of purification methodologies and offer illustrative examples of successful purification strategies employed for various types of DNA-polymer conjugates.

Functionalizing nucleic acids: synthesis and purification strategies for bioconjugates

Nico Alleva,[#] Jian Zhang,[#] David Y. W. Ng, Torsten John,[*] Tanja Weil[*]

Max Planck Institute for Polymer Research, Ackermannweg 10, 55128 Mainz, Germany.

[#] These authors contributed equally.

[*] Corresponding authors: Torsten John (johnt@mpip-mainz.mpg.de), Tanja Weil (weil@mpip-mainz.mpg.de)

Abstract

Nucleic acids are fundamental to life, encoding and storing genetic information, catalyzing biological processes, and directing protein synthesis. The primary classes, DNA and RNA, have become increasingly significant in biomedical applications due to advances in stabilizing these structures against degradation and elucidating their molecular roles. Important applications include the therapeutic use of messenger RNAs (mRNAs) as vaccines and small interfering RNAs (siRNAs) for gene silencing. Nucleic acids fold into diverse structures dictated by their sequences and base-pairing, with the DNA double-helix being the most recognized. The sequence-specific hybridization properties of nucleic acids have driven the rapid development of DNA nanotechnology, which enables the creation of programmed shapes and conformations, using DNA as a three-dimensional biological scaffold with nanoscale precision. Functionalization of RNA and DNA with various molecules through noncovalent or covalent strategies can enhance therapeutic delivery properties or lead to novel functional structures. This review highlights major synthesis approaches, with a particular focus on the challenges and strategies for purification, emphasizing the importance of obtaining highly purified nucleic acid bioconjugates for effective biomedical applications.

Introduction

Nucleic acids are essential building blocks of life, storing genetic information encoded by their sequences and directing cellular processes such as protein synthesis. DNA and RNA fold into characteristic tertiary structures, most famously the double-stranded helix of DNA.[1] The self-assembly of nucleic acids into three-dimensional structures is driven by the hybridization of single-stranded nucleic acids through hydrogen bonding, dictated by the sequence specificity of the four nucleobases. The precise hybridization properties and resulting structural diversity of nucleic acids offer unique versatility for nanoscale functionalization, which can be harnessed to develop nanomaterials tailored for specific applications. The nanoscale addressability of DNA and RNA, along with their complex architectures, make them intriguing scaffolds for materials science. The field known as DNA or RNA nanotechnology involves using nucleic acids to make programmable nanoscale structures used to generate 2D patterns and 3D geometries for potential application as a template or porous host for nanomaterials.[2-4] By coupling molecules such as synthetic polymers, peptides and proteins, lipids, or saccharides to nucleic acids (**Fig. 1**), new functional materials can be created.

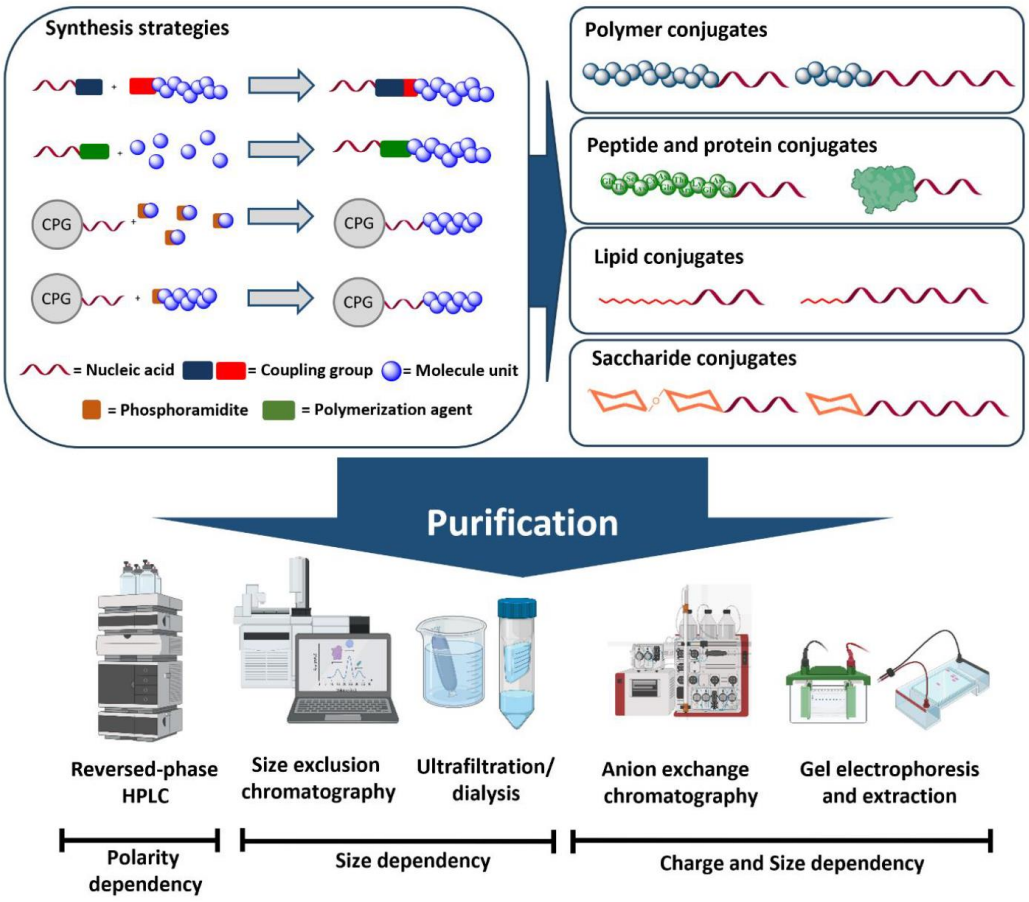

Figure 1. Overview of synthesis and purification strategies of nucleic acid bioconjugates. Focus on conjugates with polymers, peptides and proteins, lipids, and saccharides, along with their synthesis and purification strategies (Figure created with BioRender.com). CPG = controlled pore glass.

These hybrid materials, which combine various physicochemical properties and biological activities within a single molecule, find a wide range of applications as biosensors,[5-7] drug delivery systems,[8-13] self-healing nanogels,[14-16] and defined functional architectures such as micelles or patterned polymers.[17,18] For instance, polymer-nucleic acid conjugates can form hydrogels and nanocarriers.[8-10,14,15] Conjugates with (cationic) cell-penetrating peptides (CPPs) enhance intracellular delivery,[19-21] while therapeutic peptides, such as antigens, can induce immune responses when conjugated to DNA origami.[22] Protein conjugates are used in creating enzyme cascades on DNA origami[23] and antibody-mediated targeted delivery of nucleic acids.[24] Lipid and saccharide conjugates are primarily used to mediate interactions with cell membranes.[25,26]

The synthesis of nucleic acid conjugates can be achieved through various approaches.[27,28] One common method involves synthesizing the building blocks separately and then coupling them in the final step,[29] while another approach forms the respective blocks *in situ*.[17] The coupling of defined building blocks requires specific orthogonal functional groups, which perform bioorthogonal reactions, such as click chemistry, to form the linkage.[30,31] Although nucleic acids can be connected to other macromolecules via non-covalent interactions, such as biotin-streptavidin binding,[32] covalent conjugation methods are more stable and customizable.[33]

For most applications, the purification of target conjugates from their constituents or side products is essential, as impurities can significantly impact results and observations.[34] Given the diverse range of properties of bioconjugates, several challenges can arise during purification, including undesired aggregation or precipitation, separation challenges due to an excess of reactants, or solubility issues.[35,36] Common purification methods are based on differences in size, charge, or polarity between the conjugates and impurities.[37] To ensure stoichiometric functionality and hybridization of nucleic acid conjugates in applications such as DNA origami, it is crucial to remove any unconjugated DNA or RNA before self-assembly. The removal of unconjugated nucleic acids ensures morphological uniformity, therapeutic indices, and biosafety for the application of nanostructures in biomedical contexts, such as for intracellular delivery.[38] For example, antibody-mediated targeted delivery of oligonucleotides requires the removal of unconjugated oligonucleotides to prevent off-target effects *in vivo*, ensuring homogeneous conjugates for stable therapeutic outcomes.[39] Excess unconjugated CPPs, used to enhance uptake and endosomal escape of oligonucleotides, can be toxic to cells.[40] Similarly, nucleic acid conjugates with lipids and saccharides need to be of high purity to ensure recognition and interaction with cell membranes.[25,26]

This review explores purification strategies for nucleic acid conjugates with polymers, peptides and proteins, lipids, and saccharides. While we provide information on synthesis as well, our primary focus is on purification methods. Our goal is to guide researchers seeking effective techniques for their conjugates. Although review articles have been published on the synthesis of bioconjugates[41-43] and the functionalization of DNA origami structures,[44] the purification of nucleic acid bioconjugates has been sparsely covered, and many methods sections in published works lack detailed protocols. In this review, we aim to collate available information, offering a summary and practical guidance for researchers exploring major nucleic acid conjugates with biomacromolecules.

Nucleic acid bioconjugate synthesis and purification

Synthesis and purification strategies

To synthesize nucleic acid conjugates with functional molecules, well-defined reaction conditions and approaches are essential for achieving high yields. Various strategies have emerged in recent years, using both solution-phase and solid-support synthesis, depending on the desired nucleic acid functionalization.[13,27,28,45,46] Direct bioconjugation strategies in solution, often employing click chemistry techniques, are commonly used (**Fig. 1**).[30,31] This method involves coupling pre-synthesized building blocks via accessible reactive end groups, which requires careful reaction and solvent optimization. An excess of the more easily accessible building block is often used to achieve high yields, but this leads to purification challenges due to significant unreacted residues in solution.[29,47,48]

To address these challenges, polymer-nucleic acid conjugates, for instance, can be obtained using the *grafting from* method.[17] In this strategy, the nucleic acid starting material is covalently linked to a polymerization agent, such as chain transfer agents (CTAs), and polymerization is achieved with the monomer in solution, leading to the *in situ* formation of the polymer chain on the nucleic acid. Monomers are the main impurities, which can be removed relatively easily using ultrafiltration.[17,49] However, this approach lacks control over the polymer block in terms of dispersity and size. When these parameters are crucial, conjugates can be obtained using *grafting to* or solid-supported methods, where the pre-synthesized polymer is coupled to the nucleic acid.[28]

For the creation of peptide- or protein-nucleic acid conjugates, the peptide or protein is coupled to the nucleic acid block through reactive end groups. This can be performed in solution[50] or on a solid support.[29] One possible strategy for solid-supported synthesis is to conjugate the peptide or protein directly to the solid-supported nucleic acid.[51] To achieve modifications at any position of the nucleic acid chain, phosphoramidite-modified monomers can be used.[45,52] This approach allows the newly introduced block to be built by iterative solid-phase synthesis, enabling synthesis of complex conjugate structures like brushes. The advantage of solid-phase techniques is the easy removal of unreacted reagents during the washing steps within the synthetic cycle, facilitating post-cleavage purification. This strategy is also used for the formation of conjugates with lipids,[13,53] saccharides[26,54] and challenging synthetic polymers.[55]

The choice of synthesis technique for desired conjugates also determines the most suitable purification approach. Several purification methods are available, mostly based on size or charge separation, including reversed-phase high-performance liquid chromatography (RP-HPLC),[56,57] size exclusion chromatography (SEC),[58] ultrafiltration,[47,59] dialysis,[60] anion exchange chromatography (AEC),[61,62] and gel electrophoresis (**Fig. 2**).[63,64] To determine which method is best suited for nucleic acid conjugates, we briefly present each method.

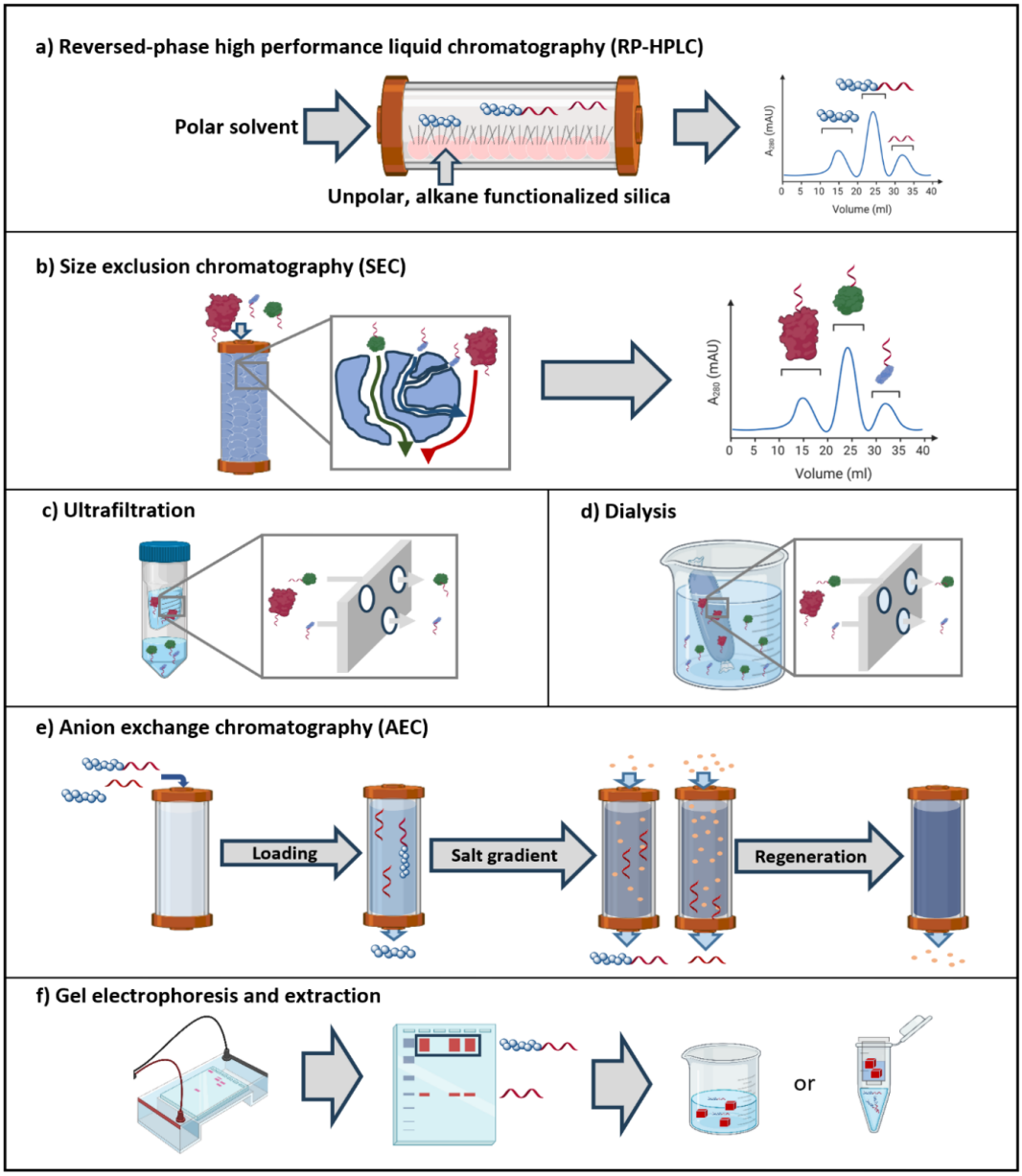

Figure 2. Schematic representation of the purification principles. (a) Reversed-phase high-performance liquid chromatography (RP-HPLC), (b) size exclusion chromatography (SEC), (c) ultrafiltration (spin filtration), (d) dialysis, (e) anion exchange chromatography (AEC), and (f) gel electrophoresis and extraction (Figure created with BioRender.com).

RP-HPLC. RP-HPLC is a commonly used technique to purify nucleic acids (**Fig. 2a**).[57,65] It uses a nonpolar stationary phase and a polar mobile phase, driven by a solvent gradient. Common stationary phase materials include C8 (octylsilane) or C18 (octadecylsilane). Non-polar molecules interact more strongly with the stationary phase, resulting in longer elution times.[56] To successfully purify nucleic acid conjugates by RP-HPLC, the lipophilic-to-hydrophilic ratio should differ from that of the individual building blocks to ensure effective separation. However, separation efficiency and peak sharpness decrease with higher sample loads, limiting the

method when applied to syntheses with high excess of one component.[61] Despite this, RP-HPLC remains an effective and fast method with good sensitivity and resolution. It can be combined with various detection techniques, including ultraviolet (UV), fluorescence and mass spectrometry (MS).

SEC. SEC uses a porous gel matrix to separate molecules based on their size (**Fig. 2b**). The porous structure of the matrix causes small molecules to traverse longer paths through the solid phase, eluting later than larger molecules.[66] The crucial parameter in this process is the hydrodynamic radius of the molecule. Resolution in SEC depends on the molecular weight difference affecting the hydrodynamic radius between molecules and the sample load, with resolution decreasing at higher loads, similar to RP-HPLC. SEC typically does not distort the shape or biological activity of higher-ordered architectures and macromolecules, making it a valuable tool. Additionally, SEC can determine relative molecular weights by comparing elution times with known standards.[58,67,68]

Ultrafiltration. Ultrafiltration (spin filtration) separates molecules based on molecular weight cutoff (MWCO) membranes under centrifugal force (**Fig. 2c**). Small molecules pass through the filter membrane, while larger molecules are retained in the supernatant.[59] Molecules are not separated by their specific properties but only based on their size. Similar to SEC, nanoscale architectures and macromolecules retain their shape and biological function.[47,69] The principle of size-based separation also applies to dialysis, where dissolved molecules are filtered through a membrane (**Fig. 2d**).[70]

AEC. AEC leverages the negatively charged phosphate backbone of nucleic acids to separate them from uncharged or less charged molecules (**Fig. 2e**). An anion-exchange resin is used as the stationary phase, interacting with charged molecules that displace the resin's counter ions.[71] After sample loading, non-charged molecules can be washed away, and a gradient elution with increasing NaCl concentration is applied, with weaker charged molecules eluting first. However, these charged interactions and the use of low/high salt concentrations can cause DNA architectures and higher-order structures like DNA origami or wireframe structures to lose their order and assembly.[61,62,72]

Gel electrophoresis. Purification by gel electrophoresis involves separating nucleic acid-containing molecules based on their charge-to-size ratio via electrophoresis, followed by manual extraction from the gel (**Fig. 2f**). The desired band is excised, and its contents are extracted either mechanically or with chaotropic salts. Available gel extraction kits provide step-by-step instructions for ease of use and optimal yields.[63,64,73]

These purification methods, each with their strengths and limitations (**Tab. 1**), provide a range of options for isolating nucleic acid conjugates depending on the specific requirements of the synthesis and the nature of the impurities.

Table 1. Purification strategies for nucleic acid conjugates. Overview of the main characteristics, advantages, limitations, and suitability of methods for purifying various nucleic acid conjugates. Note that suitability recommendations are made independently of synthesis approaches (e.g., excess of reagents); detailed discussions are provided in the following chapters. Legend: +++ highly suitable, ++ suitable, + suitable in some cases, - unsuitable, N/A no information available (icons from BioRender.com).

		RP-HPLC 	SEC 	Ultrafiltration/ dialysis 	AEC 	Gel electrophoresis and extraction 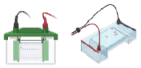
Characteristics		▪ separation through differences in polarity ▪ optimization of eluent gradient	▪ separation through differences in hydrodynamic radius ▪ optimization of pore size and loading of sample	▪ separation through differences in size ▪ optimization of pore size and loading of sample ▪ option to filter solvent	▪ separation through differences in charge ▪ optimization of eluent gradient and resin charge strength	▪ separation through differences in charge and size ▪ optimization of gel material, concentrations, buffer system, voltage, and time used
Advantages		▪ flexibility in column choice (C4, C8, C18)	▪ easy to use ▪ method requires little optimization ▪ architectures remain intact	▪ easy to use ▪ architectures remain intact	▪ easy separation of charged and uncharged components	▪ challenging conjugates possible ▪ gel composition can be easily modified ▪ architectures remain intact
Limitations		▪ chemically equal educts & conjugates causing peak overlap ▪ excess of educt can result in loss of separability of product ▪ method requires optimization (e.g., solvent gradient)	▪ excess of educts can cause separation issues ▪ phase separating components can cause purification issues	▪ morphology-forming conjugates not separated ▪ small loss of conjugate in membranes	▪ components need to be water-soluble ▪ method needs optimization for getting best results	▪ small amounts ▪ time-consuming
X-DNA-conjugates						
Polymer	**uncharged**	+++	++	-	++	+++
	polar	++	+++	++	+++	+++
	charged	-	N/A	N/A	++	++
Polymer	**uncharged**	+++	++	-	+	+++
	polar	++	+++	++	++	+++
	charged	-	N/A	+	++	++
Peptide 		+++	++	++	++	++
Protein 		+	+++	+++	+++	++
Lipid		+++	N/A	-	N/A	++
Saccharide 		+++	N/A	N/A	++	++

7

Polymer-nucleic acid conjugates

Polymer-nucleic acid conjugates have gained significant attention for their potential applications as biosensors,[7] hydrogels,[74] and nanocarriers.[75,76] For instance, by combining highly hydrophilic nucleic acid blocks with orthogonal hydrophobic polymer blocks, new hybrid amphiphilic materials capable of forming micelles,[77] vesicles,[7] or stimuli-responsive gels[78] can be created, while ensuring a defined size, dispersity and thermo-responsiveness. To fabricate polymer-nucleic acid conjugates, various synthetic strategies exist. The *grafting from* method uses single-stranded nucleic acids equipped with a functional molecule like a CTA to perform reversible addition-fragmentation chain-transfer (RAFT) polymerization in solution. This method requires both the DNA-CTA complex and the monomers to be soluble in protic solvents such as water or DMF.[49] *Grafting from* is also applied to controlled radical polymerization strategies such as atom transfer radical polymerization (ATRP).[79] Alternatively, the *grafting to* strategy uses nucleic acid and polymer building blocks with reactive end groups for conjugation.[47]

Another approach, primarily used for amphiphilic conjugates, involves solid-supported couplings with the nucleic acid building block immobilized on a controlled pore glass (CPG) bead, as used in DNA/RNA synthesis, while the polymer block is coupled to the reactive end.[28] Conjugation can be performed in organic solvents, enhancing the yield for lipophilic polymers. The final washing step simplifies purification by removing impurities from the coupling.[51] Another CPG-supported strategy involves creating phosphoramidite-functionalized monomers and coupling these to the solid-supported nucleic acids step-by-step, building a defined sequence of polymeric and nucleic acid units.[80] This technique is crucial for incorporating demanding monomers where conjugate synthesis would otherwise be challenging. Given the various synthesis methods and resulting conjugate properties, purification strategies vary. Relevant purification strategies for nucleic acid conjugates with polymers, ranging from lipophilic to hydrophilic and charged, are outlined below.

Hydrophobic polymers. Linking hydrophobic polymers to nucleic acids yields a material class with unique features such as phase separation and stimuli responsiveness.[81] The emerging amphiphilicity enables modulation of nanoscale morphology by changes in the nucleic acid block from single-stranded to double-stranded, as well as by varying the polymer length. Micelle formation of these materials facilitates the transportation of lipophilic drugs or biomarkers, making them potential nanocarriers.[81-83]

One example of these phase-separating conjugates is polystyrene-DNA (PSt-DNA).[77] Phase separation between the DNA and polymer building blocks can pose challenges during synthesis and purification, as unreacted polymers may be trapped within the condensed phases, rendering ultrafiltration ineffective for purifying the products. To address this challenge, DNA was initially synthesized on solid support and equipped with an alkyne end group. Subsequently, PSt polymer, containing an azide end group, was coupled to the solid-supported DNA strand via copper(I)-catalyzed azide-alkyne cycloaddition (CuAAC) (**Fig. 3a**). The reaction mixture was then washed to remove unreacted polymer, cleaved and purified. Given the differences in charge-to-size ratio of unreacted DNA and the conjugate, gel electrophoresis emerges as an excellent purification method, capable of circumventing solubility issues and maintaining higher-order structures. This is achieved by applying a potential difference to draw the charged molecules or colloidal particles to their respective poles (1% agarose gel), and the conjugate

band can be excised, extracted using a spin column, and desalted using dialysis (6-8 kDa MWCO).[77] Similarly, fluorescent polymer-DNA conjugates were synthesized using poly(9,9-dioctylfluorene-alt-benzothiadiazole) (P(FBT)) as the polymer block, enabling the formation of photoactive, amphiphilic conjugates. Solid-supported alkyne functionalized DNA (4.6 kDa) were coupled to azide P(FBT) (4.3 kDa) via CuAAC, followed by washing to remove unreacted polymer and other impurities. Since polymer removal occurs prior to cleavage, DNA impurities can be easily eliminated using ultrafiltration.[51]

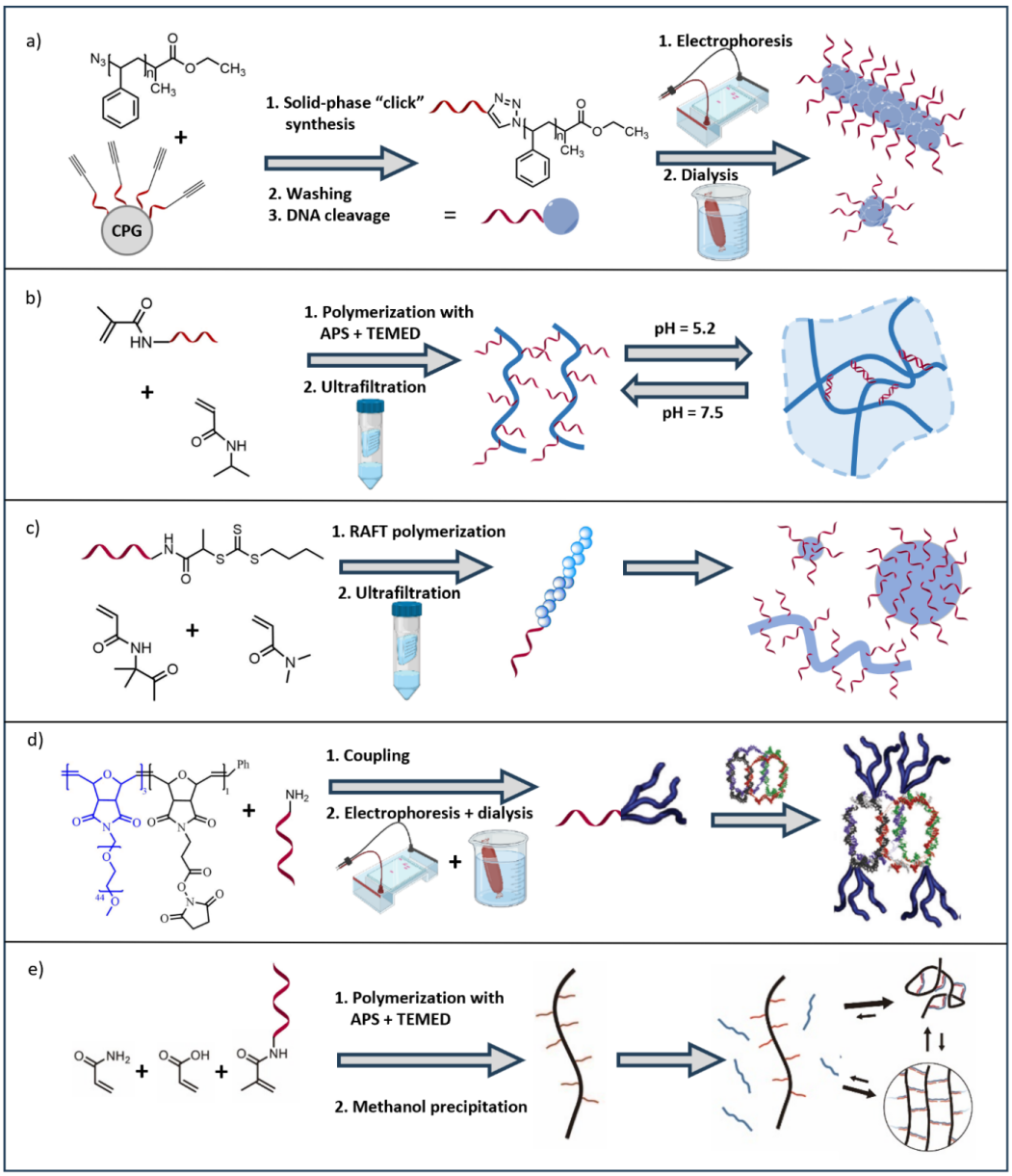

Figure 3. Synthesis and purification strategies of polymer-DNA conjugates. (a) P(St)-DNA synthesis via solid phase coupling and purification using gel electrophoresis and extraction,[77] (b) P(NIPAM)-DNA synthesis via *grafting from* and purification via ultrafiltration,[78] (c) P(DAAM-DMA)-DNA conjugate formation via RAFT polymerization using the *grafting from* method. After spin filtration the pure

conjugate forms various morphologies,[17] (d) Formation of a three-armed PEG-DNA conjugate via NHS coupling. Purification was performed by gel electrophoresis and extraction.[84] Reproduced with permission from American Chemical Society. (e) Ultrahigh MW P(acrylamide-co-acrylic acid)-DNA conjugate synthesis via *grafting from* and purification via methanol precipitation.[85] Reproduced with permission from ref Springer Nature (Figure created with BioRender.com).

Multiblock polymer-DNA conjugates, such as poly(hexaethylene-hexaethylene glycol)-DNA (P(HE-HEG)-DNA), were synthesized via similar approaches, with the polymer block added step by step.[80] Initially, the DNA block (5.8 kDa) was constructed using a DNA synthesizer, with phosphoramidite functionalized polymer monomers sequentially coupled to produce a 12-unit long polymer block. The step-by-step coupling approach ensures precise definition of the sequence and monodispersity. Furthermore, this strategy facilitates easier removal of small impurities due to the washing step after each coupling. At the end of synthesis, the solid supported conjugate (9.4 kDa) underwent washing to remove unreacted monomers, followed by cleavage and ultrafiltration (0.22 µm) to remove solid impurities. RP-HPLC (C18) was performed using an elution gradient of 3–70% acetonitrile (ACN) to isolate the respective conjugate.[80] The same synthesis procedure was used to create poly(9,9-di-n-octylfluorenyl-2,7-diyl)-DNA conjugates (PFO-DNA) as dispersing agents to aid in solubilizing insoluble nanostructures, such as single-walled nanotubes (SWNT).[55] PFO-phosphoramidite was synthesized, and solid-phase synthesis performed to assemble a growing conjugate on the DNA block (DNA: 6.6 kDa, polymer: 5.3 kDa). Following cleavage and deprotection, AEC (HiTrap Q HP) was used to purify the crude conjugate. However, this method is only applicable when the conjugate is water-soluble due to interactions with the charged resin of the column. In this case, a gradient of Tris-HCl buffer and NaCl-Tris buffer was used to elute the conjugate separately from the impurities. Subsequently, desalting of the conjugate was achieved via dialysis (2 kDa MWCO).[55]

Semiconducting polymer-DNA conjugates offer a unique combination of the optoelectronic properties of the conjugated polymer with the programmable molecular recognition capability of DNA. To introduce a semiconductive conjugate capable of size-controllable micelle formation, a poly[3-(2,5,8,11-tetraoxatridecanyl)thiophene]-DNA conjugate (PTOTT-DNA) was synthesized.[86] The high amphiphilicity of the resulting conjugate makes it amenable to solid support synthesis using phosphoramidite monomers. PTOTT-phosphoramidite (6.9 kDa) was coupled to the 5' end of the solid-supported DNA (7.7 kDa). After washing and cleavage, purification was performed by rapidly dissolving the solution in water and centrifuging, exploiting the good water solubility of the unreacted DNA to remain in the aqueous phase while the conjugate precipitated out of solution.[86] Similar synthesis procedures can be performed to obtain polypropylene glycol-DNA conjugates (PPG-DNA). Denaturing polyacrylamide gel electrophoresis (dPAGE) was employed for purification to prevent micellization or precipitation during isolation. Subsequently, the conjugates were filtered and desalted.[87] To produce morphologies of biodegradable conjugates such as micelles, polycaprolactone-DNA (P(CL)-DNA) can be used. PCL is functionalized with multiple azide groups, leading to the formation of brush-like PCL-DNA conjugates through strain-promoted azide-alkyne cycloaddition (SPAAC). Due to the significant size difference between the conjugate and the unreacted DNA, ultrafiltration (50 kDa MWCO) was performed to achieve high purity.[88]

Poly(N-isopropylacrylamide)-DNA conjugates (P(NIPAM)-DNA) are commonly used to introduce stimuli-responsive materials exhibiting thermo-sensitivity, enabling the creation of

materials with switchable morphologies.[89] These conjugates exhibit a lower critical solution temperature (LCST) in the physiological range of 30 °C to 35 °C, making them appealing for biomedical applications. P(NIPAM) solubilizes at temperatures below its LCST and agglomerates above. To manufacture and purify these conjugates, several strategies have been used. One approach involves using CuAAC to couple P(NIPAM) (5.3/10.4/19.8 kDa) to DNA, followed by RP-HPLC (C18, gradient 5–70% ACN in triethylammonium acetate (TEAA)) purification of the reaction mixture.[90] In another study, P(NIPAM) (11.5 kDa) was coupled to solid-supported DNA (5.2 kDa), washed, cleaved and purified by gel electrophoresis and extraction. PAGE was performed and the bands of interest were excised and redissolved to obtain the pure conjugate.[89] To create brush-like conjugates, DNA can be functionalized with dibenzocyclooctyne (DBCO) groups via non-natural nucleotides (DBCO-2´-deoxyuridine-5´-triphosphate, DBCO-dUTP), allowing the grafting of P(NIPAM) using a SPAAC reaction. Given the high molecular weight of the branched conjugate, excess polymer was removed via ultrafiltration (100 kDa MWCO).[91] These brush-like conjugates offer versatility in creating temperature-responsive gels capable of swelling under physiological conditions. Another study demonstrated the creation of P(NIPAM)-DNA conjugates with P(NIPAM) forming the backbone via free radical polymerization of NIPAM with acrydite-functionalized DNA (**Fig. 3b**). Excess monomers were easily removed via ultrafiltration (10 kDa MWCO).[78] An innovative approach to use P(NIPAM)-DNA is within a thrombin-responsive pore, where the pore closes upon DNA hybridization due to a charge shift around the P(NIPAM)-DNA conjugate, leading to polymer aggregation. The pore reopens upon removal of the complementary strand by thrombin. As in other studies, the conjugate is formed through *grafting to* and purified via ultrafiltration.[92] P(NIPAM)-RNA conjugates were obtained using an ATRP initiator attached to a Torula Yeast RNA backbone for photopolymerization. The obtained material was purified using dialysis in ice-cold water to guarantee solubility. This study introduced temperature-responsiveness to RNA-based materials and can also provide degradation resistance to the RNA block.[60]

Poly(diacetone acrylamide-block-dimethylacrylamide)-DNA conjugates (P(DAAM-*b*-DMA)-DNA) can form a variety of self-assembled architectures depending on polymer length and block ratios. Polymerization-induced self-assembly (PISA) was achieving using the *grafting from* strategy through RAFT polymerization with DNA containing a macro initiator (**Fig. 3c**). This technique resulted in only small impurities or unreacted excess, which could easily be removed by ultrafiltration.[17] Another strategy to obtain high yields of P(DAAM-*b*-DMA)-DNA conjugates is the *grafting to* strategy. Here, the polymer is coupled through reactive groups to the DNA block in excess. AEC effectively purified the reaction solution. The reaction mixture was loaded onto a column, where charged molecules interacted with the charged resin, and uncharged molecules were washed away. After this, a gradient of NaCl solution was applied to elute the unreacted oligonucleotide as well as the conjugate from the column and separate them.[61] RNA conjugates can also exhibit high amphiphilicity and undergo micellization when combined with hydrophobic polymers. This was demonstrated for the formation of poly(methacrylate)-RNA (P(MA)-RNA; P(MA): 41 kDa; RNA: 6.3 kDa) by attaching an ATRP initiator to the RNA strand. After polymerization, unreacted small molecules could be removed by dialysis and precipitation in water.[93]

Hydrophilic polymers. The design of increasingly hydrophilic polymer-nucleic acid conjugates is receiving attention for stabilizing or programming self-assembly onto nanoarchitectures such as DNA origami and smaller architectures like multiarm DNA prisms.[47,84,94] In contrast to

amphiphilic conjugates, hydrophilic polymer conjugates do not spontaneously form characteristic morphologies but can effectively stabilize other structures in solution. Additionally, hydrophilic polymer-nucleic acid conjugates play a crucial role in creating self-healing hydrogels, leveraging the complementarity and dynamic nature of DNA strands to facilitate gel reconnection and reassembly after mechanical damage.[16] Moreover, the polymer block of these conjugates may serve to shield against nuclease degradation or enhance biocompatibility.[84]

To facilitate the self-assembly of DNA prisms, poly(hexaethylene) phosphate conjugates with DNA (P(HE)-DNA) were used (5.8 kDa; polymers with 1 to 12 units). Phosphoramidite-modified monomers of hexaethylene phosphate were synthesized and coupled to solid-supported DNA, allowing precise control over the formation and number of monomers constituting the polymer block. After coupling, washing, and cleavage, the mixture underwent purification using PAGE. The separated bands were excised and incubated in sterile water. Additionally, the sample underwent filtration, drying, and desalting by SEC (Sephadex G-25).[94] The same purification strategy was applied to synthesize three-arm polyethylene glycol-DNA (PEG-DNA) conjugates (**Fig. 3d**). The objective was to prepare organized coatings on DNA architectures to stabilize the structure and enhance biocompatibility. A PEG_{44} macromonomer was polymerized (6.7 kDa) using ring-opening metathesis polymerization (ROMP), coupled post-polymerization to DNA (4.3 kDa), and purified following the aforementioned procedure.[84] In another approach, polymers were first synthesized containing phosphoramidite-modified nucleic acids to construct brush-like conjugates, with the oligonucleotides forming the side chains. These conjugates were used to create programmable arbitrary polymer routings on DNA origami, with the potential to form optical wires based on the conjugated properties of the polymer. Poly(2,5-dialkoxy)paraphenylene vinylene-tert-butyldiphenylsilyl conjugates with DNA (P(APPV-TBPDS)-DNA) were synthesized by initially loading the polymer onto 2-deoxythymidine (dT) and conducting solid-phase DNA synthesis. Following cleavage and deprotection, the conjugates underwent purification using SEC (PD-10) and elution with TEAA buffer.[95] In another approach, water-soluble polymer-DNA conjugates were purified using AEC for a variety of conjugates (polymers: P(DMA), 10 kDa, 20 kDa, 48 kDa; P(NIPAM) 20 kDa; P(HEA) 20 kDa; P(DAAM-*b*-DMA) 27 kDa or P(OEGMA) 20 kDa). These conjugates demonstrated annealing capability on DNA origami surfaces to create patterns with nanometer resolution. After loading the reaction mixture onto the chromatography column, unreacted polymer was removed via washing, and a NaCl gradient was introduced to partially dissociate charged molecules from the column. This method facilitated the recovery of unreacted DNA and yielded excellent quantities (60%) of the obtained conjugate.[47,61] Poly hexaethyl acrylate (P(HEA)) was utilized to create RNA conjugates by equipping the RNA strand with an ATRP initiator and conducting photoinduced polymerization. Due to minimal reaction impurities, dialysis was employed for purification.[93] For the creation of polymer-DNA hydrogels, star shaped conjugates can be used. In this method, DNA strands (4.9 kDa) undergo coupling via *N*-hydroxysuccinimide (NHS) chemistry to a 4-arm PEG polymer star (40 kDa). With respect to the size difference between unreacted DNA and the conjugate, SEC (Superdex 200) was used, yielding the pure conjugate.[16]

PEG-RNA conjugates were created by the functionalization of PEG polymers (0.4/1/4 kDa) with phosphoramidite and coupling to solid-supported RNA (1.7 kDa). After coupling, washing, and cleavage, RP-HPLC (C4, gradient: 0.8 to 32% ACN in TEAA) was employed.[96] The same

purification technique was used post-synthesis of thiol-modified PEG and RNA via a sulfhydryl exchange reaction.[97] For constructing brush-like conjugate materials using the *grafting from* technique, a DNA backbone with an ATRP initiator and photoactive group was used. After synthesizing the DNA backbone via solid-phase synthesis, polymerization of oxopentanoate ethyl methacrylate ($OEMA_{500}$) was performed using photopolymerization to form the brush-like conjugate. Utilizing the *grafting from* technique, only small molecule impurities remained, which could be readily removed by ultrafiltration (100 kDa MWCO).[98] This approach was also employed to obtain P($OEMA_{500}$)-RNA conjugates.[79] In another study, P($OEMA_{500}$)-RNA (torula yeast) brush conjugates were formed similarly by attaching an ATRP initiator to the RNA backbone and performing photo-catalyzed polymerization. However, the product was purified using RP-HPLC (C18).[60] Expanding the polymer library, linear P(PEGMA-$OEOMA_{475}$)-RNA, P($OEOMA_{300}$-*co*-MEO_2MA)-RNA, and P($OEOMA_{475}$-*co*-DMAEMA)-RNA conjugates were prepared, where the polymer block acted as a protector against nucleases and facilitated cellular internalization. These polymers, with an average molecular weight of 20 kDa, were synthesized and coupled via CuAAC to short interfering RNA (siRNA) (11.8 kDa). After coupling, ultrafiltration (30 kDa MWCO) was used to remove catalyst and unreacted components.[99]

Charged polymers. Conjugates of nucleic acids with charged polymers, both cationic and anionic, have been explored for a range of applications, including DNA sensors,[100] immune stimulation,[101] intracellular delivery,[102] and supramolecular hydrogels.[85] Charged polymers extend the physicochemical properties of nucleic acid conjugates, introducing pH-responsive polymers with acidic or basic groups.[103] For instance, π-conjugated polymers, widely applied in sensor technologies, face challenges in water solubility, which can be overcome by incorporating charged side chains.[100] The carboxyl groups of anionic polymer scaffolds, similarly to the amino groups of cationic polymers, facilitate the introduction of orthogonal groups for the spatial display of bioactive molecules.[101] High molecular weight poly(acrylamide-co-acrylic acid) demonstrates biocompatibility and responsiveness to methanol, making it suitable for coculture with cells.[85,104] Cationic polymers, with the capacity to cross cell membranes, have been instrumental in delivering therapeutic molecules into cells.[105] Few studies have explored charged polymer conjugates with nucleic acids, all of which were conducted in aqueous solution. This limited study may stem from electrostatic repulsion between anionic nucleic acids and anionic polymers, resulting in low reaction yields.[28] Conversely, cationic polymers are electrostatically attracted,[106-109] which can hinder targeted conjugation of reactive sites in each block, also leading to low yields and challenging purification processes. Moreover, the ratio of cationic polymer to anionic nucleic acids, along with the high density of cationic units within the polymer, may contribute to potential aggregation or precipitation during synthesis and purification.[28,110] Currently, most studies focus on cationic polymers, while the nucleic acids are conjugated non-covalently based on electrostatic interactions. Among the available purification methods, ultrafiltration[100,101] and PEG purification[102] have been the most commonly employed techniques.

As an illustration of anionic polymer-DNA conjugates, poly(p-phenyleneethynylene) (PPE) was used, with the π-conjugated polymer exhibiting amplified fluorescence properties for DNA detection. PPE (MW 13 kDa) was conjugated with two carboxylic acids as end groups to DNA (MW 4.8 kDa) using carbodiimide chemistry at a 5'-end amine group.[100] Sulfonate ions were introduced as side chains to enhance the water solubility of PPE, enabling solution chemistry, and DNA was added in excess to ensure complete reaction of all PPE. The resulting PPE-DNA

conjugate (MW 22 kDa) was purified through ultrafiltration (molecular weight cutoff, MWCO 10 kDa) to selectively remove free DNA. In the aforementioned study, anionic polymer-DNA conjugates were obtained via the *grafting to* method. Conversely, poly(acrylamide-co-acrylic acid)-DNA conjugates (MW 3 MDa) were synthesized as 3D cell-culture matrices by copolymerizing acrylamide, sodium acrylate and acrylamide-functionalized DNA in the presence of ammonium persulfate (APS) and tetramethylethylenediamine (TEMED) as polymerization initiators (**Fig. 3e**).[85] Methanol precipitation was conducted to remove cytotoxic monomers, which could be harmful when incubated with cells.

To prepare a cationic polymer-DNA conjugate, a photocaging strategy was used to facilitate *in situ* ATRP of the photocaged monomer 4-(methacryloyloxytris-(ethoxy)ethylcarba-moyloxypropanyl)-3-nitrobenzoic acid (MCNB) on a DNA origami macroinitiator.[102] MCNB, an anionic monomer with a carboxyl group, can be transformed into 2-aminotris(ethoxy)ethylmethacrylate (AEMA), a cationic monomer with an amine group, under 365 nm UV irradiation. This transformation occurs as the UV-sensitive carbamate cages are cleaved, exposing the basic amine groups. Similarly, anionic p(MCNB), which serves as a *grafting from* DNA origami macroinitiator, can be transformed into cationic p(AEMA). PEG purification was used to remove unreacted monomers as well as other impurities. For the direct conjugation of nucleic acids and cationic polymers, aiming to alleviate issues such as precipitation and aggregation during synthesis and purification, the ratio and density of cationic units present in polymers are crucial for obtaining cationic polymer-nucleic acid conjugates of high purity.[28,110] Specifically, the ratio of cationic polymers to oligonucleotides should be kept as low as possible to ensure successful conjugation and prevent potential precipitation during synthesis. Additionally, the density of cationic units within polymers should be considered, as excessively high density may result in an inseparable mixture of conjugates, oligonucleotides, and cationic polymers that cannot be effectively purified further.

Peptide-nucleic acid conjugates

Peptide-nucleic acid conjugates have been investigated for various applications such as genetic sequencing,[111] self-assembly,[112,113] enhanced cellular uptake by introducing CPPs or cell recognition motifs such as RGD,[19,114] and immune stimulation.[22] While nucleic acids provide unparalleled programmability as a building block,[115] they lack diverse chemical functionalities.[116] Hence, the conjugation of nucleic acids to peptides leverages the programmability of nucleic acids and the chemical functionalities of peptides, playing an important role in biomedical and materials science research. Peptides offer versatile biological functions and chemical diversity.[116,117] However, the disparate physicochemical properties, including molecular weight, charge, polarity, and acidity, induced by the sequence and length of the two building blocks pose challenges in the conjugation and purification of these conjugates,[118] particularly regarding their polarity and charge characteristics.

To obtain purified peptide-nucleic acid conjugates, RP-HPLC stands out as the most common method,[115,117-125] while PAGE gel purification,[120,126] dialysis,[29,112] ultrafiltration,[117,123,125] gravity SEC,[123,127,128] and AEC[35,129] are also used. When using solid-phase supported approaches for conjugate synthesis, impurities can be effectively removed through washing steps with organic solvents.[29,112,113,119] Strategies for synthesizing peptide-nucleic acid conjugates typically involve solid-phase stepwise synthesis and fragment conjugation.[36] In solid-phase stepwise synthesis, akin to the *grafting from* strategy for polymers, nucleic acids and peptides, or vice versa, are sequentially elongated on identical solid support, necessitating specific protecting groups for side chains and constraining the length of nucleic acids and peptides. In contrast, fragment conjugation, akin to the *grafting to* strategy for polymers, involves synthesizing nucleic acids and peptides individually, followed by the conjugation of the two fragments in either solid or liquid phase. This method uses conventional protecting groups and imposes no restrictions on the length of the two building blocks, but necessitates careful consideration of the solubility and charge of the building blocks.[36]

Using solid-phase synthesis, peptide-DNA conjugates were synthesized for therapeutic applications.[130] A branched trifunctional linker was conjugated to PEG-PS resin with an amino group in a reversible way. Subsequently, an insulin-like growth factor 1 (IGF1) D-peptide analogue was synthesized via Fmoc chemistry, starting from the protected amino group of the linker. This was followed by DNA synthesis using phosphoramidite chemistry, starting from the protected OH group. Using mild deprotection conditions, cleavage was conducted in aqueous ammonia. The resultant conjugate underwent purification via RP-HPLC (C18), using a gradient of 4.5–58.5% ACN in TEAA. Peptide-DNA conjugates, containing up to four amino acids (AA) (tetrapeptides),[131] incorporating most natural AAs except arginine and histidine, were synthesized. This involved initiating from 3'-end CPG-supported DNA hexamers and octamers with an amino group terminally protected at their 5'-end via phosphoramidite chemistry. Then, tryptophan and lysine were sequentially elongated at the 5'-end of DNA through Fmoc chemistry. After Fmoc deprotection, RP-HPLC or AEC was used to remove impurities. A series of CPP-DNA conjugates containing two to eight amine and guanidinium moieties were prepared for intercellular delivery of oligonucleotides.[19] Initially, PEG-PS resin-supported peptides with two, four, and eight lysine residues were synthesized employing Boc chemistry. After deprotection, DNA sequences were elongated in a DNA synthesizer. After cleavage from resins, lysine-DNA conjugates underwent filtration, concentration, and desalting via gravity SEC (NAP-10), followed by purification through semipreparative HPLC (DMT-based protocols).

15

Homoarginine-DNA conjugates were obtained by introducing guanidinium groups into lysine-DNA conjugates, followed by desalting using gravity SEC (NAP-5). Additional lysine-lipophilic urea-DNA conjugates were synthesized.

Using the fragment conjugation strategy, peptide-DNA conjugates were synthesized through solid-phase fragment condensation (SPFC).[119] Initially, a 3'-end CPG-supported oligonucleotide fragment with an amino group on its 5'-end was coupled to 1,6-diisocyanatohexane. Following this, washing with ACN was conducted to remove excess diisocyanate, after which partially protected peptide fragments with an amino group were introduced to yield 3'-end CPG-supported peptide-oligonucleotide conjugates. Subsequent steps involved cleavage from the CPG support and deprotection with aqueous ammonia, followed by purification using RP-HPLC with a gradient of 7–70% ACN in TEAA. TEAA buffer served as an ion pairing agent.[118] Oligonucleotide fragments were synthesized using cyanoethylphosphoramidite chemistry, while peptide fragments were prepared using Fmoc chemistry. The SPFC strategy was used to conjugate a 3'-end CPG-supported oligonucleotide fragment with an amino group on its 5'-end to hydrophobic diphenylalanine (FF),[29,112] ditryptophan (WW),[112,113] and the amyloid beta peptide motif (16–21)[112] for self-assembly studies (**Fig. 4a**). Following washing to remove unreacted peptides and other side products, the CPG support and protecting groups were removed using ammonia. Subsequent steps involved dialysis (MWCO 2 kDa)[29,112] against MilliQ water or lyophilization and dissolution[113] in nuclease-free water, followed by filtration through a 0.45 µm membrane[113] to remove non-polar impurities. Cationic peptide-nucleic acid conjugates, owing to the opposite charges of the two building blocks, may precipitate during reaction, posing challenges in purification. For instance, antisense oligonucleotides were conjugated to highly cationic arginine-rich peptides (with a maximum of 9 arginine residues) through on-resin fragment conjugation (a variant of SPFC) (**Fig. 4b**).[129] This method involved binding antisense oligonucleotides with a pyridine sulfenyl-activated thiol group at the 5'-end to an anion exchange resin column through electrostatic interaction. Then, cysteine residue-containing arginine-rich peptides were added, reacting with the absorbed oligonucleotides through the formation of disulfide bonds. Following washing with water to remove unreacted cationic peptides, the absorbed conjugates were eluted. An oligonucleotide purification cartridge was further used for desalting, followed by purification via AEC-HPLC with a 0–80% gradient of 1 M NaCl in water.

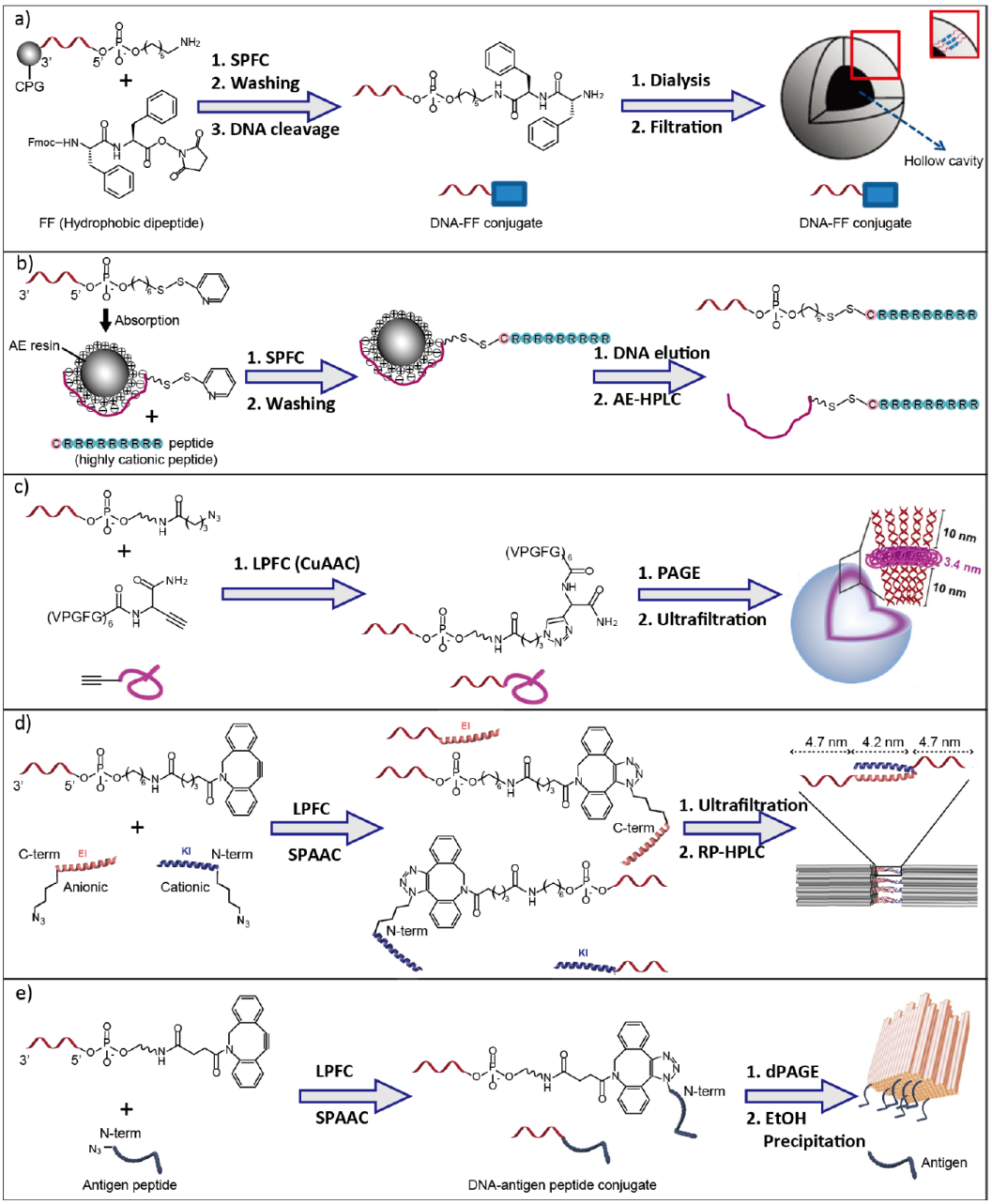

Figure 4. Synthesis and purification strategies of peptide-DNA conjugates. (a) FF-DNA conjugate synthesis employing SPFC, followed by purification using dialysis and membrane filtration.[29] Reproduced with permission from Royal Society of Chemistry. (b) Synthesis of arginine rich peptide-DNA conjugates via SPFC, followed by purification using AEC.[129] Reproduced with permission from American Chemical Society. (c) ELP-DNA conjugate synthesis via LPFC through CuAAC, followed by purification through PAGE and ultrafiltration.[126] Reproduced with permission from Royal Society of Chemistry, (d) Charged peptide-DNA conjugate synthesis via LPFC using SPAAC, followed by purification using ultrafiltration and RP-HPLC.[117] Reproduced with permission from American Chemical Society. (e) Antigen peptide-DNA conjugate synthesis via LPFC using SPAAC, followed by purification using dPAGE and ethanol precipitation.[22] Reproduced with permission from Nature Springer.

Peptide-oligonucleotide conjugates can also be achieved through liquid-phase fragment conjugation (LPFC).[120] For instance, a heterobifunctional linker, succinimidyl-4-(N-maleimidomethyl)cyclohexane-1-carboxylate (SMCC), was used to conjugate DNA with an amino group to cysteine-containing peptides. Initially, the NHS moiety of the SMCC linker was conjugated to the amine-modified DNA, followed by conjugation of the maleimide moiety of the SMCC linker to the thiol group of cysteine-containing peptides. Then, RP-HPLC or PAGE was performed to remove unreacted peptides and other impurities. RP-HPLC purification involved a gradient of 5–100% ACN, while for PAGE purification, target bands were excised, dissolved in gel elution buffer, then passed through a 0.45 µm spin filter. Ethanol precipitation[120] was performed to remove any stains such as SYBR Gold from PAGE purification. Following either RP-HPLC or PAGE purification, a gravity SEC (NAP-10) was used to remove excess salts. Conjugates of DNA with weakly hydrophobic elastin-like polypeptides (ELPs) were prepared through LPFC for self-assembly studies (**Fig. 4c**).[126] In this process, DNA with an azido group on its 5' or 3' end was conjugated to ELPs with an alkyne group through CuAAC reaction. Subsequently, PAGE purification was performed, wherein excised bands were dialyzed against water and concentrated by ultrafiltration (MWCO 3 kDa).

Aptamers with a 5'-end amino group were conjugated to peptide amphiphiles (PAs), which consist of a hydrophobic tail and a peptide sequence with charged residues to ensure solubility in the reaction buffer, through a heterobifunctional linker of dibenzocyclooctyne-sulfo-*N*-hydroxysuccinimidyl ester (DBCO-sulfo-NHS).[123] Initially, the NHS moiety of the DBCO-sulfo-NHS linker was conjugated to the amine-modified aptamer, then the DBCO moiety of the DBCO-sulfo-NHS linker to PAs via SPAAC. Excess PAs were removed through ultrafiltration (MWCO 3 kDa), followed by SEC (NAP-5) purification to desalt. RP-HPLC purification was performed with a gradient of 4.5–90% ACN in TEAA. In another study, DNA of different lengths (19 and 46 bases) with an amino group on its 3' or 5'-end was conjugated to the azidolysine residue of FF dipeptides (Fmoc-FF-$(PEG)_2$-azidolysine-NH_2) through a DBCO-sulfo-NHS linker for morphological studies of self-assembly.[125] $(PEG)_2$ units were inserted into FF dipeptides to increase solubility in the reaction buffer. After the reaction, ultrafiltration (MWCO 3 kDa) was conducted, followed by RP-HPLC (C18) purification. These conjugates can self-assemble into nanofibers and can be further crosslinked in the presence of DNA, making them attractive candidates for the synthesis of engineered synthetic cytoskeletons. The self-assembled nanofibers were applied as the cytoskeleton for the bottom-up construction of artificial cells.[50]

To achieve coiled-coil self-assembly of peptide-DNA conjugates and further application in DNA origami, DNA with an amino group on its 5'-end was coupled to the azidolysine residue on the C-terminus of anionic domain-containing peptides and the N-terminus of cationic domain-containing peptides separately through DBCO-sulfo-NHS (**Fig. 4d**).[117] Initially, the NHS moiety of the DBCO-sulfo-NHS linker was conjugated to the amine-modified DNA, then the DBCO moiety of the DBCO-sulfo-NHS linker to azide-modified peptides via SPAAC. DNA and cationic domain-containing peptides were reacted at a 1:1 ratio to avoid electrostatic aggregation. After the reaction, ultrafiltration (MWCO 3 kDa) was conducted and the conjugate purified through RP-HPLC (C18) with a gradient of 10–100% methanol in TEAA. In another study, a series of cationic peptide-DNA conjugates were synthesized through LPFC by coupling DNA with an amino group on its 5'-end to thiol-modified peptides using the SMCC linker.[128] Cationic peptides, composed of five residues, were variable to the cationic amino acids lysine, ornithine, histidine and arginine, the hydrophobic amino acid tryptophan, and alanine as a spacer.

Conjugates were purified through a NAP-5 column, eluting with water to remove excess peptides. As aforementioned, it is extremely difficult to synthesize and purify highly cationic peptide-nucleic acid conjugates in the liquid phase due to precipitation. Oligonucleotides with a pyridine sulfenyl-activated thiol group at its 5'-end were conjugated to highly cationic peptides with a thiol-containing cysteine residue derived from the HIV-Tat protein via LPFC through the formation of a disulfide bond.[35] To avoid precipitation, high salt concentration of KCl and ACN of up to 40% were used to help solubilization during the coupling reaction. AE-HPLC was performed to remove excess cationic peptides, using a gradient from 20–60% of 0.65 M KCl in 40% (v/v) ACN. Conjugates were precipitated into ethanol to desalt. For the synthesis of conjugates of highly cationic peptides with nucleic acids, denaturing conditions such as salts at high concentration and formamide addition are important.[36] Conjugates with therapeutic peptides like antigens also play an important role for its application in biomedical science. For instance, DNA with an amino group at its 5'-end was conjugated to an azide-modified neoantigen peptide through LPFC via the DBCO-sulfo-NHS linker and incorporated into DNA origami for immune stimulation (**Fig. 4e**). 8% dPAGE and ethanol precipitation were performed for purification.[22]

Protein-nucleic acid conjugates

Protein-nucleic acid conjugates have gained significant attention due to their diverse applications in immune stimulation,[22] as intracellular probes,[132,133] Janus nanoparticle formation,[134] and hierarchical assembly.[135] Proteins, ranging from enzymes to antibodies and other functional proteins, offer vast functional diversity within biological systems. Enzymes catalyze essential biochemical reactions[136-138] and antibodies elicit targeted immune responses by binding to membrane receptors and activating signaling pathways.[139,140] Instances of protein-nucleic acid conjugates occur naturally,[141] such as DNA-topoisomerase 1 (TOP1) crosslinks, and they can also be synthesized chemically, akin to the *grafting to* strategy employed for polymers.[142] However, chemical synthesis often yields side products, including unconjugated nucleic acids and proteins, as well as heterogeneous protein-nucleic acid conjugates with varying numbers of conjugated nucleic acids. These impurities pose challenges for successful hybridization with complementary nucleic acid sequences, essential for intended applications.[34,143] Additionally, unconjugated proteins may influence potential delivery efficiency and self-assembly behavior, underscoring the importance of ensuring the purity of protein-nucleic acid conjugates for their effective utilization.[144]

The yield and purity of protein-nucleic acid conjugates are primarily influenced by factors such as the protein molecular weight (MW), the ratio of nucleic acids to proteins, and the number of solvent-exposed AA residues per protein available for coupling in the reaction. Proteins exhibit a wide range of MWs, spanning from 5 kDa to over 200 kDa, while DNA MWs range from 6–30 kDa for single-stranded DNA (20–100mer) to larger entities like plasmids and DNA origami stuctures.[137,138] The choice of nucleic acid to protein ratio in a coupling reaction is determined by considerations of cost, availability, and the specific requirements of targeted conjugates for their intended applications. In the synthesis of spherical nucleic acids (SNAs), for instance, the ratio of DNA to protein typically ranges from 30:1 to 350:1.[132,133,145,146] SNAs find usage in intracellular delivery and self-assembly studies.[132,133,145,146] Achieving homogenous protein-DNA conjugates with a defined number of DNA strands per protein can be challenging when multiple DNAs are conjugated to numerous reaction sites on a single protein. However,

homogeneity in the number of conjugated DNAs is often unnecessary when a large number of DNA strands are attached, and SEC or ultrafiltration are commonly used purification methods.[23,133,145] Conversely, for the synthesis of protein-DNA conjugates with fewer DNA strands per protein, especially for DNA-antibody conjugates, the ratio of DNA to protein is typically around 1 to 8.[147-149] Given their potential clinical applications, obtaining homogeneous antibody-DNA conjugates with predictable therapeutic indices is crucial, often necessitating the use of AEC for purification.[23]

Methods for synthesizing these conjugates often involve site-selective (residue-specific) coupling, targeting specific AA residues over others, or site-specific coupling, which aims at single occurrences of particular AAs (e.g., non-catalytic cysteine residues).[142] Commonly selected AAs for coupling include lysine and cysteine, chosen based on considerations of abundance and reactivity, as well as methionine, tyrosine, serine, and genetically encoded AAs.[150] Classical synthesis methods, such as site-selective coupling, often result in random DNA labeling of proteins, resulting in heterogeneous products in terms of stoichiometry, which can impede their function and yield.[33,148,151] Despite this limitation, the single-step process and ease of purification make classical methods attractive for researchers. Modern methods aim to produce more homogeneous products, but they too face limitations, such as the requirement for distinct microenvironments for selective modification, such as the existence of metal-binding sites[149] and proximal reactive residues,[142] or the need for multiple-step synthesis in genetic manipulation of proteins, which can lead to low expression levels.[142] Most purification processes for protein-nucleic acid conjugates focus on removing unreacted DNA and proteins from the conjugates. While further separation of conjugates with varying numbers of attached nucleic acids may not always be necessary, it is essential for studies involving antibody-nucleic acid conjugates, where predictable therapeutic effects induced by homogeneous products are crucial for future clinical trials.[147]

Purification of protein-DNA conjugates relies on considerations of size (as influenced by the MW change induced by conjugated DNA), charge densities (resulting from the number of conjugated DNA strands and the distribution of surface-reactive AA residues), and polarity (affected by the number of present conjugated hydrophilic DNAs). Among the available purification methods, ultrafiltration and AEC are the most commonly employed. Size-based purification methods effectively separate protein-nucleic acid conjugates from impurities such as unreacted DNA and proteins. However, they have limitations in isolating heterogeneous conjugate products and are only applicable when there is a detectable difference in MW between the nucleic acid and protein components.[23,132,133,144,145,152,153] Charge-based purification is also frequently used, given the variability in net charge densities among proteins, anionic nucleic acids, and protein-nucleic acid conjugates, allowing for their separation based on charge differences.[23,147,148] In contrast, polarity-based purification of protein-nucleic acid conjugates is less common and is typically reserved for cases where a significant polarity difference exists between the nucleic acid and protein components, such as for insulin. This method is employed when more conventional techniques have proven ineffective.[147]

Enzymes. Enzymes, as globular proteins, possess active sites that catalyze physiologically important functions with exceptional efficiency, with their size varying from less than 100 to over 2000 AA residues.[136] Enzyme-nucleic acid conjugates find applications in designing enzyme cascades on DNA origami structures, leveraging the programmability of nucleic acids.[23] Additionally, they are used in constructing spherical nucleic acids (SNAs) for intracellular

catalysis and self-assembly studies.[132] To purify synthesis mixtures containing enzyme-oligonucleotide conjugates and remove unconjugated oligonucleotides, ultrafiltration[23,132,133,144,145,152,153] is the most commonly used method. The choice of the MWCO for the filter is determined based on the MWs of the proteins and oligonucleotides involved.[133] For example, in the case of β-galactosidase (β-Gal) (MW 446 kDa), which features both solvent-accessible lysine and cysteine residues, and glucose oxidase (GOx) (MW 160 kDa), which has solvent-accessible lysine residues,[133] different DNA strands (MW 10-14 kDa) with a DBCO group at their 5'-end were conjugated to β-Gal and GOx using a NHS-PEG_4-azide heterobifunctional linker through SPAAC and carbodiimide crosslinking chemistry for SNA studies (**Fig. 5a**). The number of DNA strands conjugated per β-Gal is approximately 31 (with a theoretical maximum of 40), while specific information regarding GOx remains unavailable (with a theoretical maximum of 28). Unreacted DNA was removed through ultrafiltration (100 kDa MWCO) or SEC (ENrich SEC column) from β-Gal-SNAs. A MWCO of 100 kDa was used to ensure retention of the conjugate and removal of unconjugated DNA. When coupling proteins with smaller MWs such as HRP (44 kDa), ultrafiltration with a smaller MWCO (e.g. 30 kDa) can be used. Similar procedures were employed for synthesizing i-motif β-Gal-SNAs (with approximately 30 conjugated i-motif per β-Gal) (MW of i-motif 12 kDa) and T-rich GOx-SNAs (with approximately 28 conjugated T-rich DNA per GOx) (MW of T-rich DNA 4 kDa).[145] In these cases, ultrafiltration was performed using filters with MWCOs of 100 kDa for GOx-SNAs and β-Gal-SNAs, respectively. Additionally, a series of β-Gal-SNAs (comprising T-rich DNA with MW 10-14 kDa and G-quadruplex-forming DNA sequences with MW 6-12 kDa) with around 30-37 conjugated DNA per β-Gal were synthesized and purified by ultrafiltration (MWCO 100 kDa).[132]

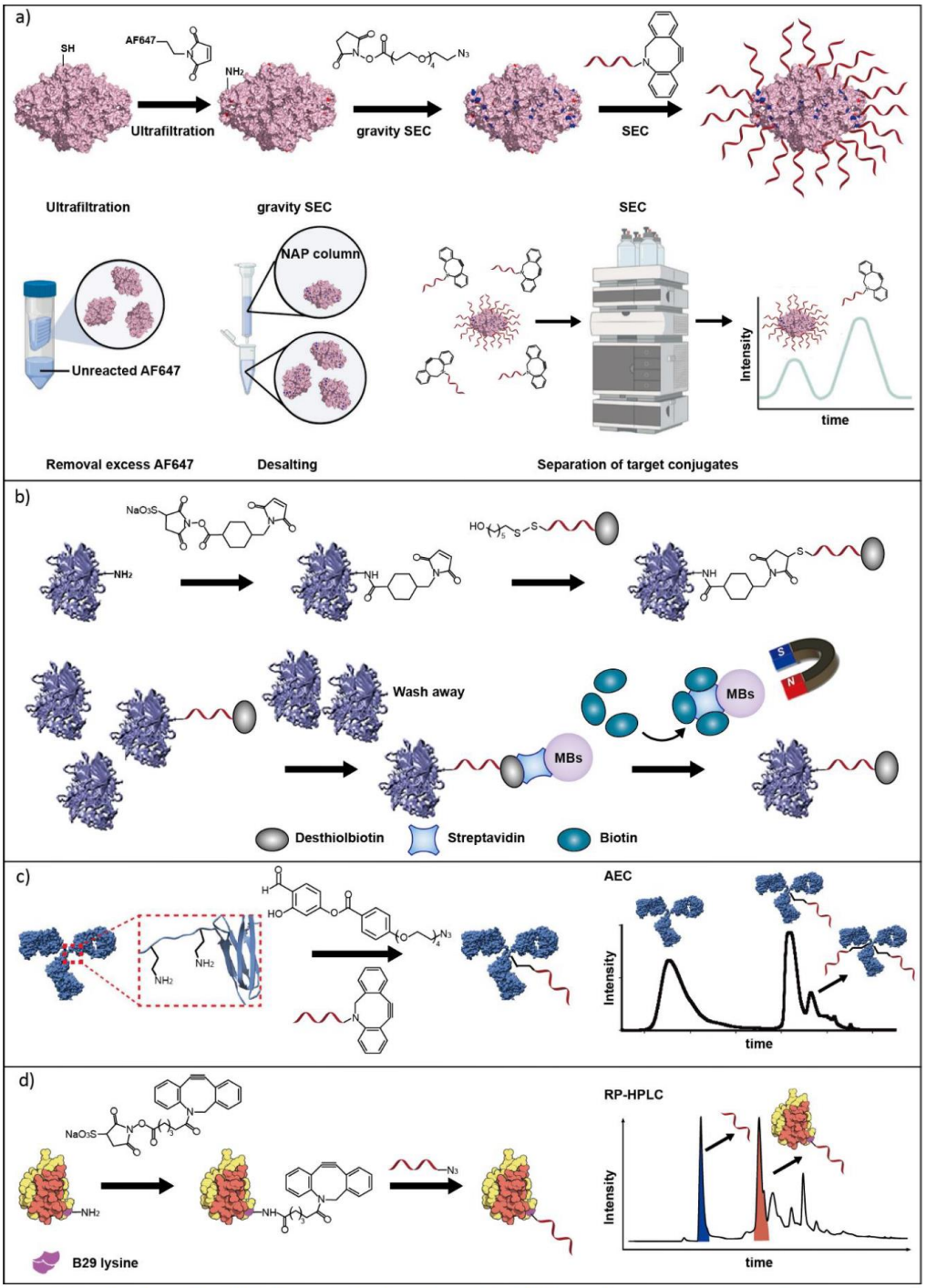

Figure 5. Synthesis and purification strategies of protein-DNA conjugates. (a) Schematic representation of β-Gal-DNA conjugate synthesis via SPAAC and subsequent purification using ultrafiltration, gravity SEC, and SEC separately.[133] Reproduced with permission from Nature Springer. (b) Synthesis of invertase-DNA conjugates through disulfide bond formation and purification using magnetic bead based biotin-displacement.[144] Reproduced with permission from American Chemical Society. (c) Belimumab-DNA conjugate synthesis via SPAAC and purification using AEC.[147] Reproduced with permission from Wiley. (d) Synthesis of insulin-DNA conjugates via SPAAC and purification using RP-HPLC.[154] Reproduced with permission from Nature Springer.

22

In an alternative approach, DNA with a thiol group at its 3'-end was conjugated to amine-containing enzymes, including alcohol dehydrogenase (ADH) (MW 141-151 kDa), horseradish peroxidase (HRP) (MW 44 kDa), and GOx (MW 160 kDa), using a succinimidyl 3-(2-pyridyldithio) propionate (SPDP) heterobifunctional linker, followed by purification via ultrafiltration (MWCO 30 kDa) to remove excess DNA (MW 17 kDa).[153] Similarly, DNA with a thiol group at its 3'-end was linked to amine-containing GOx and HRP using a *N*-[ε-maleimidocaproyloxy] sulfosuccinimide ester (sulfo-EMCS) linker, followed by purification through ultrafiltration (MWCO 30 kDa).[152] While the ultrafiltration method effectively removes excess DNA from conjugates, it does not eliminate unconjugated enzymes, underscoring the importance of ensuring DNA excess and complete enzyme conjugation before purification. To achieve removal of unconjugated enzymes, an on-bead biotin displacement method can used to purify enzyme-DNA conjugates. 3'-end desthiobiotin-modified DNA (MW 11 kDa) with a thiol group at its 5'-end was conjugated to invertase (MW 270 kDa) with amine groups using a sulfo-SMCC linker, followed by ultrafiltration (MWCO 100 kDa) (**Fig. 5b**).[144] Desthiobiotin-labeled conjugates were attached to streptavidin-coated magnetic beads due to the high affinity of desthiobiotin and streptavidin, after which unconjugated invertase was washed away. Upon addition of biotin, with a much higher affinity to streptavidin, desthiobiotin-labeled DNA-invertase conjugates were released from beads, yielding purified conjugates. This method can effectively remove excess DNA and unconjugated enzymes and can be applied to almost all proteins with solvent-accessible amino groups, using the same procedure. However, while ultrafiltration, SEC, and magnetic bead-based methods can remove unconjugated DNA, obtaining enzyme-DNA conjugates with a defined number of conjugated DNA per enzyme may remain challenging.

When it is important to obtain conjugates with a defined number of DNA strands per enzyme, AEC can be used since nucleic acids are highly charged and the method is suitable to separate differently charged species. This approach has been applied to assemble enzyme cascades on DNA origami. DNA bearing a thiol group at its 5'-end was conjugated to amine groups of lysine residues on malic dehydrogenase (MDH) (MW 70 kDa) and glucose-6-phosphate dehydrogenase (G6pDH) (MW 100 kDa) using a SPDP linker.[23] Ultrafiltration (MWCO 30 kDa) was used to remove excess DNA, and washing was conducted with high salt concentration buffer or detergent-containing buffer to remove nonspecifically adsorbed DNA on the enzyme surface, resulting from electrostatic interactions. Despite the presence of multiple lysine residues on the enzyme surface, the enzyme-DNA conjugates remained a mixture with varying numbers of conjugated DNA per enzyme. Subsequent AEC was carried out to separate unconjugated DNA and proteins from the conjugates, as well as to isolate conjugates with 1 to 4 conjugated DNA molecules per enzyme.

In the preceding methodologies, enzymes were initially conjugated to oligonucleotides, which could then be hybridized with large DNA scaffolds like DNA origami. However, further purification is necessary to remove any unhybridized conjugates. Another strategy is to link enzymes directly to DNA origami. For instance, streptavidin-modified alkaline phosphatase (AP) (MW 94 kDa) and HRP were conjugated to biotin-modified DNA origami bearing two hexahistidine affinity tags (His tags), exploiting the biotin-streptavidin interaction.[138] A cobalt-based affinity purification was performed to separate unconjugated enzymes (HRP and AP) from enzyme-conjugated DNA origami via the specific interaction between the His tags and a cobalt-based immobilized metal affinity resin. Unconjugated enzymes were removed by

washing, while enzyme-DNA origami conjugates were later eluted from the resin. Another approach involved the preparation of S-selective NADP+/NADPH-dependent oxidoreductase (GRE2) (MW 38 kDa) variants, including with SNAP-tag (GRE2-Snap), Halo-tag (GRE2-Halo), and streptavidin-binding peptide (SBP) tag (GRE2-SBP), along with the reductase domain BMR of monooxygenase P450 BM3 (MW 64 kDa) with a Halo tag (BMR-Halo), through a genetic fusion strategy.[137] Subsequently, Halo- and Snap-tagged enzymes were conjugated to DNA origami functionalized with suicide ligands (benzylguanine and chlorohexane groups) via interactions with their respective tags. GRE2-SBP was linked to biotin-functionalized DNA origami through biotin-streptavidin interaction. Free-flow electrophoresis (FFE) purification was then performed to separate unconjugated enzymes from enzyme-conjugated DNA origami.

Antibodies. Antibodies (immunoglobulins), typically weighing around 150 kDa and measuring approximately 10 nm in size, are composed of two heavy chains (HC) and two light chains (LC), containing over 80 lysine residues which provide abundant sites for coupling via NHS chemistry.[147] Antibody-nucleic acid conjugates find extensive application in therapeutics, including targeted delivery and enhancing the circulatory half-life of nucleic acids in the bloodstream, as well as in signal amplification for detection purposes.[139] The synthesis of antibody-nucleic acid conjugates via site-directed mutagenesis and labeling yields more homogeneous conjugates with enhanced therapeutic efficacy.[147] These conjugates are commonly purified through methods such as AEC,[147,148,155] PAGE gel purification[149] and immobilized metal-ion affinity chromatography (IMAC) purification.[156]

In one method, a template-facilitated reaction was used to conjugate DNA, featuring an NHS ester group at its 3'-end, to lysine residues of IgG antibodies (Anti-c-Myc, anti-FLAG® M2, anti-EGFR, and anti-ß-tubulin).[149] Typically, guiding DNA, equipped with a tris-nitrilotriacetic acid (NTA) ligand at its 5'-end, non-covalently binds (coordinates) to IgG antibodies possessing a metal-binding region (histidine-rich cluster) on their constant Fc domain, in the presence of $Cu(NO_3)_2$, forming a Cu(II) complex. Subsequently, reactive DNA with an NHS ester group on its 3'-end was added and hybridized with guiding DNA already bound to IgG antibodies, facilitating the reaction between NHS-modified DNA and site-selective lysine residues on IgG antibody surfaces due to their close proximity. Following this, ultrafiltration (MWCO 3 kDa) was performed to concentrate samples, followed by PAGE purification, where targeted bands were excised and extracted by passive diffusion in EPPS buffer. While this templated method is suitable for the site-selective conjugation of DNA to His6-tagged proteins and wild-type metal-binding proteins like transferrin, proteins lacking metal-binding sites are challenging to conjugate using this approach (except through specific tag incorporation via genetic fusion). Building upon the NTA-modified DNA templated method, a peptide-directed template method was developed to conjugate DNA, featuring a benzaldehyde group, to the amino group of lysine residues of IgG antibodies (Rituximab, Trastuzumab, Cetuximab,[155] Panitumumab, and anti-anti-ß-tubulin).[148] Initially, a DNA strand functionalized with FC-III peptide, serving as guiding DNA, non-covalently attached to the Fc domain of IgG antibodies. The FC-III peptide, a cyclic peptide, exhibits specific binding to certain domains of proteins. Subsequently, reactive DNA with a benzaldehyde group hybridized with the complementary guiding DNA, bringing the benzaldehyde group in close proximity to the amino group of lysine residues on the IgG antibody surface, thereby facilitating conjugation between reactive DNA and IgG antibodies. Finally, complementary DNA liberated the reactive DNA strand and AEC removed unconjugated DNA and proteins, as well as dissociated peptide of guiding DNA.

Using site-directed azide group labeling, DNA featuring a DBCO group was conjugated to IgG antibodies (Belimumab) (**Fig. 5c**).[147] A new lysine-directed labeling reagent (LDLR) with an azide group was designed, where the salicylaldehyde group of LDLR can form an iminium ion with lysine residues of IgG antibodies (Belimumab, Cetuximab, Pertuzumab, Trastuzumab, and Rituximab). Adjacent nucleophilic lysines can attack the labile intramolecular ester of LDLR due to proximity, efficiently inserting an azide group into IgG antibodies via stable covalent bond formation, while the salicylaldehyde iminium ion leaving group undergoes hydrolysis. Subsequently, an azide-modified antibody, Belimumab, was conjugated to DBCO-modified DNA using the SPAAC method. Belimumab-DNA conjugates were purified using AEC, with separation achieved between Belimumab with 1 and 2 conjugated DNA strands. The LDLR reagent for site-directed labeling reactions was further used to synthesize anti-HAS antibody-DNA and anti-Human IgG antibody-DNA (Rituximab, Cetuximab, Trastuzumab,[39] and Panitumumab) conjugates,[24] which were purified through AEC. Similarly, using site-specific coupling of DNA to PD-1, DNA with an azide group was conjugated to engineered PD-1 antibodies with a SrtA recognition motif LPETG (sortag) via an amine-DBCO linker.[157] Ultrafiltration (MWCO 30 kDa) was used to remove excess DNA, while unconjugated antibodies and DNA underwent further purification via AEC. In another study, DNA with a thiol group on its 3'- and 5'-ends was conjugated to anti-CD antibodies (CD3, CD19, CD22, CD28, CD33, CD123, and CD137) through a sulfo-SMCC linker, followed by purification using AEC.[140]

Affibodies offer an alternative to antibodies in therapeutic and diagnostic applications.[158] They are small non-immunoglobulin affinity proteins that are engineered through combinatorial protein engineering and selection from numerous variants, identifying those binding to target proteins. To prepare affibody-DNA conjugates, DNA with an amino group on its 5'-end was conjugated to the thiol group of cysteine residues on the HER2 affibody surface using a sulfo-SMCC linker.[156] HER2 affibody is a small protein composed of 58 amino acids (MW 6 kDa).[159] AEC was used to remove excess HER2 affibody. However, due to the low MW of HER2 affibodies, separating DNA (MW 6 kDa) from HER2 affibody-DNA conjugates via AEC is challenging. To address this, a Ni-NTA column was used to remove excess DNA, leveraging the presence of the metal-binding region (histidine-rich residues) on HER2 affibodies, followed by dialysis.

Other functional proteins encompass a wide range of MWs, spanning from less than 10 kDa to over 200 kDa. This includes engineered proteins such as green fluorescent proteins (GFP),[160] and naturally occurring proteins like insulin,[154] Cas9,[146] or ovalbumin (OVA).[22] Conjugating such proteins to nucleic acids has been explored for applications like SNAs and intracellular delivery.[133,146] Common purification methods include AEC[134,160-163] and ultrafiltration,[134,135,164] with RP-HPLC[154] also used at times. For instance, to obtain protein-based DNA-functionalized Janus particles, the orthogonal reactivity of lysine and cysteine residues has been used. DNA with an amine group was linked to a single surface cysteine residue of enhanced green fluorescent protein mutant (mEGFP) using a SPDP linker.[134] Ultrafiltration (MWCO 30 kDa) removed excess DNA, followed by AEC to isolate mEGFP with DNA modifications at the cysteine site from unconjugated mEGFP. Then, the lysine residues of purified mEGFP-DNA conjugates were further modified with an NHS-PEG_4-N_3 linker for reaction with DNA with a DBCO group at its 5'-end to form Janus nanoparticles. Excess DNA was removed by ultrafiltration (MWCO 50 kDa), with SEC then used to obtain purified mEGFP-DNA conjugates, averaging 14 DNA modifications per mEGFP. Although SEC cannot precisely separate

conjugates with different specific numbers of DNA modifications, it was chosen here as it does not interfere with further assembly. Similarly, mEGFP was conjugated to DNA with an amine group for hybridization chain reaction (HCR) studies,[161] followed by IMAC purification to remove excess DNA. AEC was performed to separate mEGFP from mEGFP-DNA conjugates. In a crystallization study, mGFP was conjugated to DNA via a SPDP linker attached to a single surface cysteine residue,[160] and excess DNA was removed through IMAC purification. Subsequently, AEC separated the thiol and disulfide forms of mGFP from mGFP-DNA conjugates.

Mutant selected stable protein 1 (Sp1m) (MW ≈ 300 kDa) has 24 primary amino groups, including surface lysine and N-termini residues axially, and 12 thiol groups containing surface cysteine residues equatorially. Spatially conjugating DNA to Sp1m allows for hierarchical assembly across one to three dimensions. Initially, a maleimide-azide linker was attached to equatorial thiol groups of surface cysteine residues of Sp1m, followed by the conjugation of a methyltetrazine-PEG_5-NHS ester linker to axial amine groups of lysine and N-termini residues. This sequential process installs azide groups equatorially and tetrazine groups axially.[135] Subsequently, trans-cyclooctene (TCO)-DNA and DBCO-DNA were conjugated to Sp1m. Ultrafiltration (MWCO 30 kDa) removed most excess DNA, with SEC purification used to remove any remaining DNA. There were about 10 equatorially conjugated DNA strands and 6 to 8 axially conjugated DNA strands per Sp1m.

CRISPR/Cas9 systems have found broad applications in genome editing. In one study, DNA with a DBCO group was linked to lysine residues of surface Cas9 through an NHS-PEG4-azide linker, followed by the formation of Cas9 SNAs. SEC purification removed excess DNA.[146] There were 14 conjugated DNA strands per Cas9 protein. In another study, DNA with an amino group at its 5'-end was conjugated to the thiol group of cysteine residues of OVA through LPFC via an SMCC linker. This conjugate was incorporated into DNA origami for immune stimulation, with ultrafiltration (MWCO 30 kDa) used to remove excess DNA.[22] Additionally, DNA with an azide group was coupled to the amino group of lysine-29 of the B chain (B29 lysine) residue of insulin (MW 5.8 kDa) via a DBCO-sulfo-NHS linker for hybridization with DNA origami in intracellular studies (**Fig. 5d**).[154] The reaction mixture underwent RP-HPLC purification (C18, gradient: 27–45% ACN in TEAA) to remove excess DNA and unconjugated insulin, followed by concentration through ultrafiltration (MWCO 3 kDa).

Lipid-nucleic acid conjugates

Conjugates of nucleic acids with lipid molecules serve various purposes, including modifying liposomes,[53] mediating vesicle fusion,[165] facilitating drug delivery,[12] influencing membrane properties,[25] and studying structure formation.[166] These applications capitalize on the amphiphilic nature of lipid-nucleic acid conjugates, with lipids introducing larger hydrophobic domains capable of integrating into cell membranes. RP-HPLC is the primary method for purifying such conjugates.[166,167] Two main approaches are used to synthesize lipid-oligonucleotide conjugates: solution-phase (postsynthetic) or stepwise solid-phase (presynthetic).[13] The solid-phase method facilitates purification by allowing the removal of unreacted reagents through simple washing steps.[13] For example, DNA oligonucleotides were functionalized with $(C_{18})_2$ lipids by removing the terminal dimethoxytrityl (DMT) group at the DNA 5′-end during oligonucleotide synthesis, followed by iodination to make the 5′-end electrophilic, reaction with lipid-thiolate, and final deprotection and cleavage from the solid support (**Fig. 6a**).[53,168] Purification involved separating unreacted and iodinated oligonucleotides from the lipid-oligonucleotide conjugates using RP-HPLC (C4 column) with a gradient of 0–60% ACN in TEAA buffer.[53]

In an alternative approach, phosphoramidite chemistry was used to modify DNA oligonucleotides at both the 3′- and 5′-end.[165,169-173] $(C_{18})_2$ lipids were functionalized with phosphoramidite groups and coupled to the DNA oligomer as the last "base" using a DNA synthesizer. RP-HPLC purification was then performed.[165] To modify siRNA with various lipids, phosphoramidite chemistry was again used, followed by RP-HPLC purification (Source 15RPC column) with a 10–70% gradient of ACN in sodium acetate.[174] In another study, a cholesterol modification was introduced at the 3'-end of DNA oligonucleotides using commercial 3'-cholesteryl-TEG (triethylene glycol spacer) CPGs during oligonucleotide synthesis (**Fig. 6b**).[25] The functionalized oligonucleotides were purified using RP-HPLC (C18 column).[25] Similarly, DNA was functionalized at both the 3′- and 5′-end using commercially obtained oligonucleotides with thiol end (**Fig. 6c**).[175] After reducing disulfide bonds in the modified DNA, followed by ultrafiltration (3 kDa MWCO), a maleimide lipid was added and the product was purified by RP-HPLC (C4 column) using a gradient of 10–40% ACN.[175] In some cases, lipid-DNA conjugates, which were incorporated into liposomes, were separated from unconjugated DNA using isopycnic centrifugation in iodixanol gradients,[176] or purified on agarose gel in the presence of Triton X-100 while HPLC or dPAGE could not be used due to micelle formation.[177]

For solution-phase coupling, squalene was coupled to the 3'-end of siRNA via maleimide-sulfhydryl chemistry, and excess squalenoyl maleimide was washed away. Purification was monitored using RP-HPLC.[178] The choice of RP-HPLC protocol depends on lipid polarity, chain length, the eluents used. C18 columns are suitable for highly non-polar samples, while C4 columns offer versatility, especially with high ACN gradients.

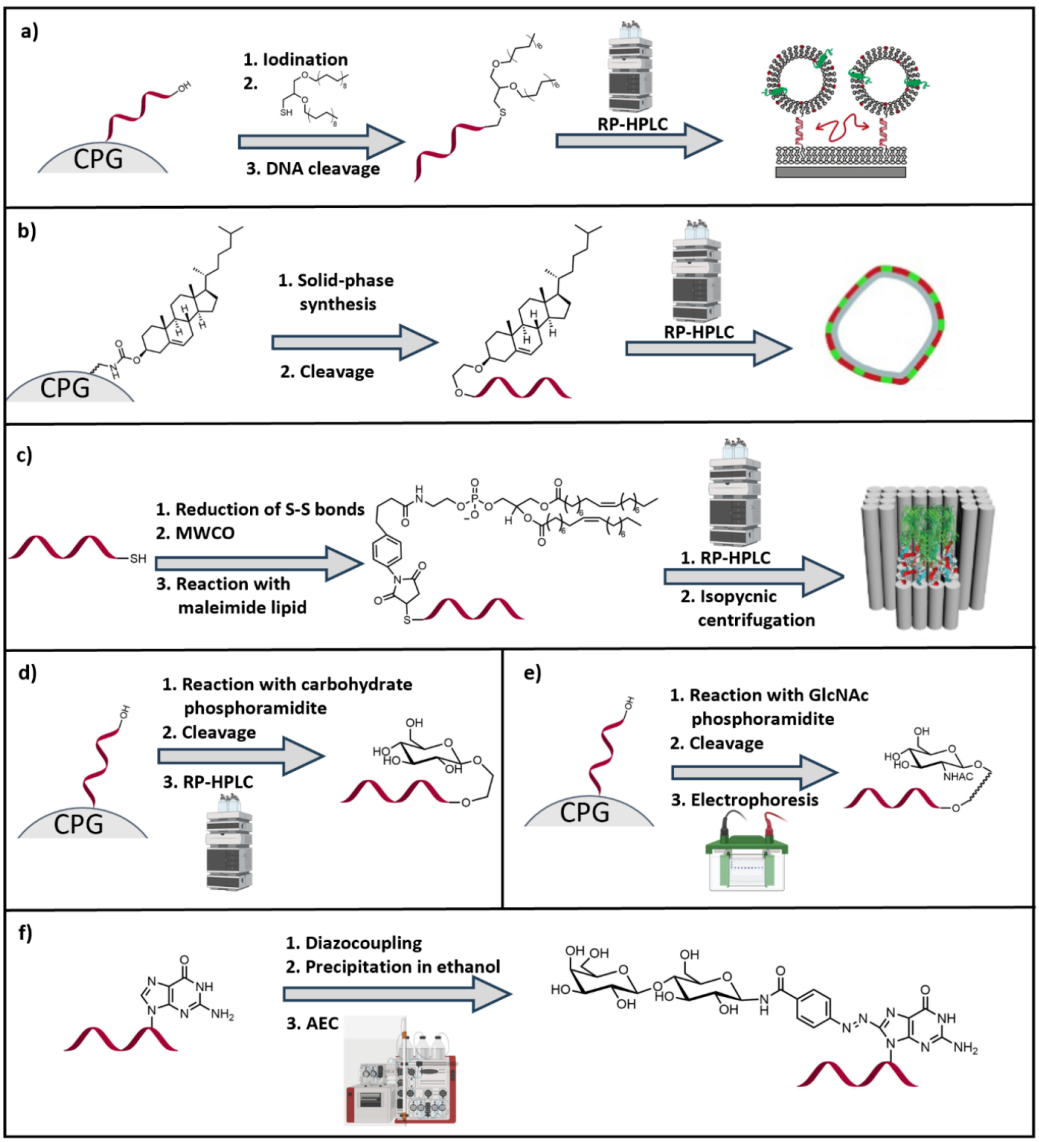

Figure 6. Synthesis and purification strategies of lipid-DNA and saccharide-DNA conjugates. (a) DNA oligonucleotides are functionalized with $(C18)_2$ lipids by iodination of 5′-end, followed by reaction with lipid-thiolate. RP-HPLC was used to remove unreacted and iodinated oligonucleotides.[53] Reproduced with permission from American Chemical Society. (b) A 3'-cholesteryl-TEG CPG was used to introduce a cholesterol modification at the 3'-end of DNA oligonucleotides, which was purified by RP-HPLC.[25] Reproduced with permission from Wiley. (c) DNA oligonucleotides with thiol ends were reduced, followed by MWCO filtration, and functionalized with maleimide lipids. The conjugates were purified by RP-HPLC.[175] Reproduced with permission from Wiley. (d) Carbohydrate-DNA conjugates achieved by phosphoramidite chemistry and purification using RP-HPLC.[26] (e) Synthesis of carbohydrate-DNA conjugates by phosphoramidite chemistry, followed by dPAGE purification.[54] (f) DNA and RNA was functionalized with lactose and cellobiose at the guanine bases by diazo coupling of carbohydrate diazonium salts. The conjugates were precipitated into ethanol, collected by centrifugation and purified by AEC.[179] (Figure created with BioRender.com)

Saccharide-nucleic acid conjugates

Conjugates of nucleic acids with saccharides or carbohydrates offer enhanced stability and cellular uptake of DNA and RNA structures[26,180] due to their recognition by cellular membranes. One approach for synthesizing saccharide-nucleic acid conjugates is using phosphoramidite chemistry, which involves, for instance, functionalizing the DNA 5'-end with saccharides such as glucose, fucose, maltose, and maltotriose in a DNA synthesizer.[26] These saccharide-DNA conjugates were purified using RP-HPLC (C18 column) with a gradient of 5–37.5% ACN (**Fig. 6d**).[26] Similarly, DNA can be functionalized on solid support at both the 3'- and 5'-ends with carbohydrates[181,182] like methyl 4'-deoxy-lactoside,[183] with purification achieved by dPAGE (**Fig. 6e**).[54,183] Oligoribonucleotide conjugates with glucose or galactose at the RNA 5'-end were synthesized using phosphoramidite chemistry and purified by RP-HPLC (C18 column).[184]

In another method, DNA was functionalized at the 5'-end using SPFC.[180] The oligonucleotide was subjected to carbonyldiimidazole (CDI), ethylenediamine and hexamethylene-1,6-disocyanate to yield the isocyanato derivative, which was then reacted with the amino sugars D-glucosamine and D-galactosamine. These saccharide-DNA conjugates were purified using RP-HPLC.[180] DNA oligonucleotides were also functionalized with carbohydrates using 3,4-diethoxy-3-cyclobutene-1,2-dione as a linking reagent between carbohydrates with amino group at the reducing end and DNA with aminoalkyl modification, with purification achieved by RP-HPLC (C18 column).[185] A similar approach was followed to prepare mannosylated oligoribonucleotides.[186] Carbohydrate conjugation to DNA and RNA was also achieved by diazo coupling of carbohydrate diazonium salts to the guanine bases, with purification through precipitation into ethanol followed by centrifugation and AEC (**Fig. 6f**).[179,187] In another method, aldehyde-containing DNA was conjugated to the aminooxy group at the reducing end of a saccharide, followed by RP-HPLC purification.[188] Additionally, carbohydrates with an alkylamine linker were attached to NHS-carboxy-dT phosphoramidite during DNA synthesis, with purification by RP-HPLC (C18 column) with a 6–12% ACN gradient in TEAA buffer.[189] Overall, most saccharide-nucleic acids conjugates were purified by RP-HPLC using a C18 column with a gradient of low amounts of ACN (5-37.5%).

Conclusion and outlook

The synthesis and purification of nucleic acid conjugates is crucial for a wide range of applications in biotechnology, medicine, and nanotechnology. We have comprehensively reviewed various strategies for purifying nucleic acid conjugates, detailing the methodologies, advantages, limitations, and suitability of different techniques. The diverse range of conjugates discussed includes polymer-, peptide- and protein-, lipid-, and saccharide-nucleic acid conjugates, each presenting unique challenges and requiring tailored purification approaches. Each method has its own set of advantages and limitations, making the choice of purification strategy dependent on the specific type of conjugate and its intended application. Polymer-nucleic acid conjugates are vital for creating robust, biocompatible materials for drug delivery, hydrogels, and biosensors. Peptide and protein-nucleic acid conjugates are essential for therapeutic applications and diagnostics. Lipid-nucleic acid conjugates leverage the amphiphilic nature of lipids for drug delivery and membrane studies, predominantly purified by RP-HPLC. Saccharide-nucleic acid conjugates enhance the stability and cellular uptake of nucleic acids through carbohydrate recognition, synthesized using phosphoramidite chemistry and solid-phase synthesis, with RP-HPLC as the primary purification technique.

Future research will focus on improving the efficiency and specificity of conjugation reactions and developing refined purification techniques. Advances in high-throughput synthesis, on-chip technologies, and automated purification systems could significantly enhance the scalability and reproducibility of nucleic acid conjugate production. Innovations in chromatography optimization, new affinity tags, and hybrid purification strategies are expected to achieve higher purity and yield. Overall, the purification of nucleic acid conjugates remains a critical aspect of the synthesis, directly impacting functionality and applicability.

References

1 Watson, J. D. & Crick, F. H. C. Molecular Structure of Nucleic Acids: A Structure for Deoxyribose Nucleic Acid. *Nature* **171**, 737-738, doi:10.1038/171737a0 (1953).
2 Seeman, N. C. Nucleic acid junctions and lattices. *Journal of Theoretical Biology* **99**, 237-247, doi:10.1016/0022-5193(82)90002-9 (1982).
3 Rothemund, P. W. Folding DNA to create nanoscale shapes and patterns. *Nature* **440**, 297-302, doi:10.1038/nature04586 (2006).
4 Seeman, N. C. & Sleiman, H. F. DNA nanotechnology. *Nature Reviews Materials* **3**, 17068, doi:10.1038/natrevmats.2017.68 (2017).
5 Liu, X., Fan, Q. & Huang, W. DNA biosensors based on water-soluble conjugated polymers. *Biosens Bioelectron* **26**, 2154-2164, doi:10.1016/j.bios.2010.09.025 (2011).
6 Sassolas, A., Leca-Bouvier, B. D. & Blum, L. J. DNA Biosensors and Microarrays. *Chemical Reviews* **108**, 109-139, doi:10.1021/cr0684467 (2008).
7 Peterson, A. M. & Heemstra, J. M. Controlling self-assembly of DNA-polymer conjugates for applications in imaging and drug delivery. *Wiley Interdiscip Rev Nanomed Nanobiotechnol* **7**, 282-297, doi:10.1002/wnan.1309 (2015).
8 Kang, H. *et al.* Photoresponsive DNA-cross-linked hydrogels for controllable release and cancer therapy. *Langmuir* **27**, 399-408, doi:10.1021/la1037553 (2011).
9 Kedracki, D., Maroni, P., Schlaad, H. & Vebert-Nardin, C. Polymer–Aptamer Hybrid Emulsion Templating Yields Bioresponsive Nanocapsules. *Advanced Functional Materials* **24**, 1133-1139, doi:10.1002/adfm.201302475 (2013).
10 Rodriguez-Pulido, A. *et al.* Light-triggered sequence-specific cargo release from DNA block copolymer-lipid vesicles. *Angew Chem Int Ed Engl* **52**, 1008-1012, doi:10.1002/anie.201206783 (2013).
11 Pokholenko, O. *et al.* Lipid oligonucleotide conjugates as responsive nanomaterials for drug delivery. *J Mater Chem B* **1**, 5329-5334, doi:10.1039/c3tb20357c (2013).
12 Soutschek, J. *et al.* Therapeutic silencing of an endogenous gene by systemic administration of modified siRNAs. *Nature* **432**, 173-178, doi:10.1038/nature03121 (2004).
13 Raouane, M., Desmaele, D., Urbinati, G., Massaad-Massade, L. & Couvreur, P. Lipid conjugated oligonucleotides: a useful strategy for delivery. *Bioconjug Chem* **23**, 1091-1104, doi:10.1021/bc200422w (2012).
14 Wang, C., Fadeev, M., Vázquez-González, M. & Willner, I. Stimuli-Responsive Donor–Acceptor and DNA-Crosslinked Hydrogels: Application as Shape-Memory and Self-Healing Materials. *Advanced Functional Materials* **28**, doi:10.1002/adfm.201803111 (2018).
15 Tanaka, S. *et al.* Intelligent, Biodegradable, and Self-Healing Hydrogels Utilizing DNA Quadruplexes. *Chem Asian J* **12**, 2388-2392, doi:10.1002/asia.201701066 (2017).
16 Ohira, M. *et al.* Star-Polymer-DNA Gels Showing Highly Predictable and Tunable Mechanical Responses. *Adv Mater* **34**, e2108818, doi:10.1002/adma.202108818 (2022).
17 Luckerath, T. *et al.* DNA-Polymer Nanostructures by RAFT Polymerization and Polymerization-Induced Self-Assembly. *Angew Chem Int Ed Engl* **59**, 15474-15479, doi:10.1002/anie.201916177 (2020).
18 Tokura, Y. *et al.* Bottom-Up Fabrication of Nanopatterned Polymers on DNA Origami by In Situ Atom-Transfer Radical Polymerization. *Angew Chem Int Ed Engl* **55**, 5692-5697, doi:10.1002/anie.201511761 (2016).
19 Grijalvo, S., Terrazas, M., Avino, A. & Eritja, R. Stepwise synthesis of oligonucleotide-peptide conjugates containing guanidinium and lipophilic groups in their 3'-termini. *Bioorg Med Chem Lett* **20**, 2144-2147, doi:10.1016/j.bmcl.2010.02.049 (2010).
20 Lebleu, B. *et al.* Cell penetrating peptide conjugates of steric block oligonucleotides. *Adv Drug Deliv Rev* **60**, 517-529, doi:10.1016/j.addr.2007.09.002 (2008).

21 Chen, L., Fang, S., Xiao, X., Zheng, B. & Zhao, M. Single-Stranded DNA Assisted Cell Penetrating Peptide-DNA Conjugation Strategy for Intracellular Imaging of Nucleases. *Anal Chem* **88**, 11306-11309, doi:10.1021/acs.analchem.6b03743 (2016).

22 Zeng, Y. C. *et al.* Fine tuning of CpG spatial distribution with DNA origami for improved cancer vaccination. *Nat Nanotechnol*, doi:10.1038/s41565-024-01615-3 (2024).

23 Fu, J. *et al.* Multi-enzyme complexes on DNA scaffolds capable of substrate channelling with an artificial swinging arm. *Nat Nanotechnol* **9**, 531-536, doi:10.1038/nnano.2014.100 (2014).

24 Baranda Pellejero, L., Nijenhuis, M. A. D., Ricci, F. & Gothelf, K. V. Protein-Templated Reactions Using DNA-Antibody Conjugates. *Small* **19**, e2200971, doi:10.1002/smll.202200971 (2023).

25 Czogalla, A. *et al.* Amphipathic DNA origami nanoparticles to scaffold and deform lipid membrane vesicles. *Angew Chem Int Ed Engl* **54**, 6501-6505, doi:10.1002/anie.201501173 (2015).

26 Ugarte-Uribe, B. *et al.* Synthesis, Cell-Surface Binding, and Cellular Uptake of Fluorescently Labeled Glucose−DNA Conjugates with Different Carbohydrate Presentation. *Bioconjugate Chemistry* **21**, 1280-1287, doi:10.1021/bc100079n (2010).

27 Niemeyer, C. M. Functional devices from DNA and proteins. *Nano Today* **2**, 42-52, doi:10.1016/s1748-0132(07)70058-0 (2007).

28 Whitfield, C. J. *et al.* Functional DNA-Polymer Conjugates. *Chem Rev* **121**, 11030-11084, doi:10.1021/acs.chemrev.0c01074 (2021).

29 Gour, N., Kedracki, D., Safir, I., Ngo, K. X. & Vebert-Nardin, C. Self-assembling DNA-peptide hybrids: morphological consequences of oligonucleotide grafting to a pathogenic amyloid fibrils forming dipeptide. *Chem Commun (Camb)* **48**, 5440-5442, doi:10.1039/c2cc31458d (2012).

30 El-Sagheer, A. H. & Brown, T. Click chemistry with DNA. *Chem Soc Rev* **39**, 1388-1405, doi:10.1039/b901971p (2010).

31 Fantoni, N. Z., El-Sagheer, A. H. & Brown, T. A Hitchhiker's Guide to Click-Chemistry with Nucleic Acids. *Chem Rev* **121**, 7122-7154, doi:10.1021/acs.chemrev.0c00928 (2021).

32 Weber, P. C., Ohlendorf, D. H., Wendoloski, J. J. & Salemme, F. R. Structural Origins of High-Affinity Biotin Binding to Streptavidin. *Science* **243**, 85-88, doi:10.1126/science.2911722 (1989).

33 Rocha Tapia, A. *et al.* Site-directed Conjugation of Single-Stranded DNA to Affinity Proteins: Quantifying the Importance of Conjugation Strategy. *Chemical Science*, doi:10.1039/d4sc01838a (2024).

34 Franzini, R. M. *et al.* "Cap-and-Catch" Purification for Enhancing the Quality of Libraries of DNA Conjugates. *ACS Comb Sci* **17**, 393-398, doi:10.1021/acscombsci.5b00072 (2015).

35 Vivès, E. & Lebleu, B. Selective coupling of a highly basic peptide to an oligonucleotide. *Tetrahedron Letters* **38**, 1183-1186, doi:10.1016/S0040-4039(97)00059-2 (1997).

36 Venkatesan, N. & Kim, B. H. Peptide Conjugates of Oligonucleotides: Synthesis and Applications. *Chemical Reviews* **106**, 3712-3761, doi:10.1021/cr0502448 (2006).

37 Sapsford, K. E., Tyner, K. M., Dair, B. J., Deschamps, J. R. & Medintz, I. L. Analyzing nanomaterial bioconjugates: a review of current and emerging purification and characterization techniques. *Anal Chem* **83**, 4453-4488, doi:10.1021/ac200853a (2011).

38 Briggs, J. & Panfili, P. R. Quantitation of DNA and protein impurities in biopharmaceuticals. *Analytical Chemistry* **63**, 850-859, doi:10.1021/ac00009a003 (1991).

39 Marcher, A., Nijenhuis, M. A. D. & Gothelf, K. V. A Wireframe DNA Cube: Antibody Conjugate for Targeted Delivery of Multiple Copies of Monomethyl Auristatin E. *Angew Chem Int Ed Engl* **60**, 21691-21696, doi:10.1002/anie.202107221 (2021).

40 Saar, K. *et al.* Cell-penetrating peptides: a comparative membrane toxicity study. *Anal Biochem* **345**, 55-65, doi:10.1016/j.ab.2005.07.033 (2005).

41 Stephanopoulos, N. & Francis, M. B. Choosing an effective protein bioconjugation strategy. *Nat Chem Biol* **7**, 876-884, doi:10.1038/nchembio.720 (2011).

42 Lutz, J.-F. & Börner, H. G. Modern trends in polymer bioconjugates design. *Progress in Polymer Science* **33**, 1-39, doi:10.1016/j.progpolymsci.2007.07.005 (2008).

43 Sunasee, R. & Narain, R. in *Chemistry of Bioconjugates* 1-75 (John Wiley & Sons, Ltd, 2014).

44 Knappe, G. A., Wamhoff, E. C. & Bathe, M. Functionalizing DNA origami to investigate and interact with biological systems. *Nat Rev Mater* **8**, 123-138, doi:10.1038/s41578-022-00517-x (2023).

45 Lönnberg, H. Solid-Phase Synthesis of Oligonucleotide Conjugates Useful for Delivery and Targeting of Potential Nucleic Acid Therapeutics. *Bioconjugate Chemistry* **20**, 1065-1094, doi:10.1021/bc800406a (2009).

46 Liu, K. *et al.* Nucleic acid chemistry in the organic phase: from functionalized oligonucleotides to DNA side chain polymers. *J Am Chem Soc* **136**, 14255-14262, doi:10.1021/ja5080486 (2014).

47 Alleva, N., Winterwerber, P., Whitfield, C. J., Ng, D. Y. W. & Weil, T. Nanoscale patterning of polymers on DNA origami. *J Mater Chem B* **10**, 7512-7517, doi:10.1039/d2tb00812b (2022).

48 Song, Z., Li, R., Yang, X., Zhang, Z. & Luo, X. Functional DNA-peptide conjugates with enhanced antifouling capabilities for electrochemical detection of proteins in complex human serum. *Sensors and Actuators B: Chemical* **367**, doi:10.1016/j.snb.2022.132110 (2022).

49 Lueckerath, T. *et al.* DNA-Polymer Conjugates by Photoinduced RAFT Polymerization. *Biomacromolecules* **20**, 212-221, doi:10.1021/acs.biomac.8b01328 (2019).

50 Daly, M. L. *et al.* Designer peptide-DNA cytoskeletons regulate the function of synthetic cells. *Nat Chem*, doi:10.1038/s41557-024-01509-w (2024).

51 Xiao, F. *et al.* Light-Harvesting Fluorescent Spherical Nucleic Acids Self-Assembled from a DNA-Grafted Conjugated Polymer for Amplified Detection of Nucleic Acids. *Angew Chem Int Ed Engl* **61**, e202115812, doi:10.1002/anie.202115812 (2022).

52 Weisbrod, S. H. & Marx, A. Novel strategies for the site-specific covalent labelling of nucleic acids. *Chem Commun (Camb)*, 5675-5685, doi:10.1039/b809528k (2008).

53 Yoshina-Ishii, C., Miller, G. P., Kraft, M. L., Kool, E. T. & Boxer, S. G. General Method for Modification of Liposomes for Encoded Assembly on Supported Bilayers. *Journal of the American Chemical Society* **127**, 1356-1357, doi:10.1021/ja043299k (2005).

54 Wang, Y. & Sheppard, T. L. Chemoenzymatic Synthesis and Antibody Detection of DNA Glycoconjugates. *Bioconjugate Chemistry* **14**, 1314-1322, doi:10.1021/bc034144p (2003).

55 Kwak, M. *et al.* DNA block copolymer doing it all: from selection to self-assembly of semiconducting carbon nanotubes. *Angew Chem Int Ed Engl* **50**, 3206-3210, doi:10.1002/anie.201007098 (2011).

56 Karger, B. L. & Giese, R. W. Reversed phase liquid chromatography and its application to biochemistry. *Analytical Chemistry* **50**, 1048A-1073A, doi:10.1021/ac50034a001 (1978).

57 Gehrke, C. W., McCune, R. A., Gama-Sosa, M. A., Ehrlich, M. & Kuo, K. C. Quantitative reversed-phase high-performance liquid chromatography of major and modified nucleosides in dna. *Journal of Chromatography A* **301**, 199-219, doi:10.1016/S0021-9673(01)89189-5 (1984).

58 Huang, X., McLean, R. S. & Zheng, M. High-Resolution Length Sorting and Purification of DNA-Wrapped Carbon Nanotubes by Size-Exclusion Chromatography. *Analytical Chemistry* **77**, 6225-6228, doi:10.1021/ac0508954 (2005).

59 Jönsson, A.-S. & Trägårdh, G. Ultrafiltration applications. *Desalination* **77**, 135-179, doi:10.1016/0011-9164(90)85024-5 (1990).

60 Jeong, J. *et al.* RNA-Polymer Hybrids via Direct and Site-Selective Acylation with the ATRP Initiator and Photoinduced Polymerization. *J Am Chem Soc* **145**, 14435-14445, doi:10.1021/jacs.3c03757 (2023).

61 Alleva, N., Eigen, K., Ng, D. Y. W. & Weil, T. A Versatile and Efficient Method to Isolate DNA-Polymer Conjugates. *ACS Macro Lett* **12**, 1257-1263, doi:10.1021/acsmacrolett.3c00371 (2023).

62 Strege, M. A. & Lagu, A. L. Anion-exchange chromatography of DNA restriction fragments. *Journal of Chromatography A* **555**, 109-124, doi:10.1016/S0021-9673(01)87171-5 (1991).

63 Bellot, G., McClintock, M. A., Lin, C. & Shih, W. M. Recovery of intact DNA nanostructures after agarose gel-based separation. *Nat Methods* **8**, 192-194, doi:10.1038/nmeth0311-192 (2011).

64 Langridge, J., Langridge, P. & Bergquist, P. L. Extraction of nucleic acids from agarose gels. *Analytical Biochemistry* **103**, 264-271, doi:10.1016/0003-2697(80)90266-3 (1980).

65 Tamaoka, J. & Komagata, K. Determination of DNA base composition by reversed-phase high-performance liquid chromatography. *FEMS Microbiology Letters* **25**, 125-128, doi:10.1111/j.1574-6968.1984.tb01388.x (1984).

66 Barth, H. G., Boyes, B. E. & Jackson, C. Size Exclusion Chromatography. *Analytical Chemistry* **68**, 445-466, doi:10.1021/a19600193 (1996).

67 Latulippe, D. R. & Zydney, A. L. Size exclusion chromatography of plasmid DNA isoforms. *J Chromatogr A* **1216**, 6295-6302, doi:10.1016/j.chroma.2009.07.009 (2009).

68 Langlois, N. I. & Clark, H. A. Characterization of DNA nanostructure stability by size exclusion chromatography. *Anal Methods* **14**, 1006-1014, doi:10.1039/d1ay02146j (2022).

69 Winterwerber, P., Harvey, S., Ng, D. Y. W. & Weil, T. Photocontrolled Dopamine Polymerization on DNA Origami with Nanometer Resolution. *Angew Chem Int Ed Engl* **59**, 6144-6149, doi:10.1002/anie.201911249 (2020).

70 Schuett, T., Geitner, R., Zechel, S. & Schubert, U. S. Dialysis Diffusion Kinetics in Polymer Purification. *Macromolecules* **54**, 9410-9417, doi:10.1021/acs.macromol.1c01241 (2021).

71 Prazeres, D. M. F., Schluep, T. & Cooney, C. Preparative purification of supercoiled plasmid DNA using anion-exchange chromatography. *Journal of Chromatography A* **806**, 31-45, doi:10.1016/S0021-9673(97)01254-5 (1998).

72 Budelier, K. & Schorr, J. Purification of DNA by anion-exchange chromatography. *Curr Protoc Mol Biol* **Chapter 2**, Unit2 1B, doi:10.1002/0471142727.mb0201bs42 (2001).

73 Jaakola, L., Pirttilä, A. M., Vuosku, J. & Hohtola, A. Method Based on Electrophoresis and Gel Extraction for Obtaining Genomic DNA-free cDNA Without DNase Treatment. *BioTechniques* **37**, 744-748, doi:10.2144/04375BM06 (2004).

74 Li, F., Tang, J., Geng, J., Luo, D. & Yang, D. Polymeric DNA hydrogel: Design, synthesis and applications. *Progress in Polymer Science* **98**, doi:10.1016/j.progpolymsci.2019.101163 (2019).

75 Hamner, K. L. *et al.* Using Temperature-Sensitive Smart Polymers to Regulate DNA-Mediated Nanoassembly and Encoded Nanocarrier Drug Release. *ACS Nano* **7**, 7011-7020, doi:10.1021/nn402214e (2013).

76 Ganta, S., Devalapally, H., Shahiwala, A. & Amiji, M. A review of stimuli-responsive nanocarriers for drug and gene delivery. *J Control Release* **126**, 187-204, doi:10.1016/j.jconrel.2007.12.017 (2008).

77 Jia, F., Lu, X., Tan, X. & Zhang, K. Facile synthesis of nucleic acid-polymer amphiphiles and their self-assembly. *Chem Commun (Camb)* **51**, 7843-7846, doi:10.1039/c5cc01934f (2015).

78 Guo, W. *et al.* Switchable bifunctional stimuli-triggered poly-N-isopropylacrylamide/DNA hydrogels. *Angew Chem Int Ed Engl* **53**, 10134-10138, doi:10.1002/anie.201405692 (2014).

79 Averick, S. E., Dey, S. K., Grahacharya, D., Matyjaszewski, K. & Das, S. R. Solid-phase incorporation of an ATRP initiator for polymer-DNA biohybrids. *Angew Chem Int Ed Engl* **53**, 2739-2744, doi:10.1002/anie.201308686 (2014).

80 Edwardson, T. G., Carneiro, K. M., Serpell, C. J. & Sleiman, H. F. An efficient and modular route to sequence-defined polymers appended to DNA. *Angew Chem Int Ed Engl* **53**, 4567-4571, doi:10.1002/anie.201310937 (2014).

81 Sabir, F. *et al.* DNA Based and Stimuli-Responsive Smart Nanocarrier for Diagnosis and Treatment of Cancer: Applications and Challenges. *Cancers (Basel)* **13**, doi:10.3390/cancers13143396 (2021).

82 Kim, T., Nam, K., Kim, Y. M., Yang, K. & Roh, Y. H. DNA-Assisted Smart Nanocarriers: Progress, Challenges, and Opportunities. *ACS Nano* **15**, 1942-1951, doi:10.1021/acsnano.0c08905 (2021).

83 Kim, J. *et al.* Functional-DNA-Driven Dynamic Nanoconstructs for Biomolecule Capture and Drug Delivery. *Adv Mater* **30**, e1707351, doi:10.1002/adma.201707351 (2018).

84 McLaughlin, C. K. *et al.* Three-dimensional organization of block copolymers on "DNA-minimal" scaffolds. *J Am Chem Soc* **134**, 4280-4286, doi:10.1021/ja210313p (2012).

85 Peng, Y. H. *et al.* Dynamic matrices with DNA-encoded viscoelasticity for cell and organoid culture. *Nat Nanotechnol* **18**, 1463-1473, doi:10.1038/s41565-023-01483-3 (2023).

86 Kamps, A. C., Cativo, M. H. M., Chen, X.-J. & Park, S.-J. Self-Assembly of DNA-Coupled Semiconducting Block Copolymers. *Macromolecules* **47**, 3720-3726, doi:10.1021/ma500509u (2014).

87 Ding, K., Alemdaroglu, F. E., Borsch, M., Berger, R. & Herrmann, A. Engineering the structural properties of DNA block copolymer micelles by molecular recognition. *Angew Chem Int Ed Engl* **46**, 1172-1175, doi:10.1002/anie.200603064 (2007).

88 Zhang, C. *et al.* Biodegradable DNA-Brush Block Copolymer Spherical Nucleic Acids Enable Transfection Agent-Free Intracellular Gene Regulation. *Small* **11**, 5360-5368, doi:10.1002/smll.201501573 (2015).

89 Kim, C. J., Hu, X. & Park, S. J. Multimodal Shape Transformation of Dual-Responsive DNA Block Copolymers. *J Am Chem Soc* **138**, 14941-14947, doi:10.1021/jacs.6b07985 (2016).

90 Wilks, T. R. *et al.* "Giant Surfactants" Created by the Fast and Efficient Functionalization of a DNA Tetrahedron with a Temperature-Responsive Polymer. *ACS Nano* **7**, 8561-8572, doi:10.1021/nn402642a (2013).

91 Li, S. & Schroeder, C. M. Synthesis and Direct Observation of Thermoresponsive DNA Copolymers. *ACS Macro Lett* **7**, 281-286, doi:10.1021/acsmacrolett.8b00016 (2018).

92 Sugawara, Y., Tamaki, T. & Yamaghchi, T. Development of an aptamer-functionalized molecular recognition gating membrane targeting a specific protein on the basis of the aggregation phenomena of DNA–PNIPAM. *Polymer* **62**, 86-93, doi:10.1016/j.polymer.2015.02.027 (2015).

93 Jeong, J., Szczepaniak, G., Das, S. R. & Matyjaszewski, K. Synthesis of RNA-Amphiphiles via Atom Transfer Radical Polymerization in the Organic Phase. *Precis Chem* **1**, 326-331, doi:10.1021/prechem.3c00042 (2023).

94 Serpell, C. J., Edwardson, T. G., Chidchob, P., Carneiro, K. M. & Sleiman, H. F. Precision polymers and 3D DNA nanostructures: emergent assemblies from new parameter space. *J Am Chem Soc* **136**, 15767-15774, doi:10.1021/ja509192n (2014).

95 Knudsen, J. B. *et al.* Routing of individual polymers in designed patterns. *Nat Nanotechnol* **10**, 892-898, doi:10.1038/nnano.2015.190 (2015).

96 Jäschke, A. *et al.* Synthesis and Analytical Characterization of RNA-Polyethylene Glycol Conjugates. *Nucleosides and Nucleotides* **15**, 1519-1529, doi:10.1080/07328319608002451 (1996).

97 Kim, S. H., Jeong, J. H., Lee, S. H., Kim, S. W. & Park, T. G. PEG conjugated VEGF siRNA for anti-angiogenic gene therapy. *J Control Release* **116**, 123-129, doi:10.1016/j.jconrel.2006.05.023 (2006).

98 Jeong, J., Szczepaniak, G., Das, S. R. & Matyjaszewski, K. Expanding the architectural horizon of nucleic-acid-polymer biohybrids by site-controlled incorporation of ATRP initiators in DNA and RNA. *Chem* **9**, 3319-3334, doi:10.1016/j.chempr.2023.07.013 (2023).

99 Averick, S. E. *et al.* Autotransfecting short interfering RNA through facile covalent polymer escorts. *J Am Chem Soc* **135**, 12508-12511, doi:10.1021/ja404520j (2013).

100 Lee, K., Povlich, L. K. & Kim, J. Label-Free and Self-Signal Amplifying Molecular DNA Sensors Based on Bioconjugated Polyelectrolytes. *Advanced Functional Materials* **17**, 2580-2587, doi:10.1002/adfm.200700218 (2007).

101 Levenson, E. A. & Kiick, K. L. DNA-polymer conjugates for immune stimulation through Toll-like receptor 9 mediated pathways. *Acta Biomater* **10**, 1134-1145, doi:10.1016/j.actbio.2013.11.022 (2014).

102 Shi, Y. *et al.* Defined positive charge patterns created on DNA nanostructures determine cellular uptake efficiency. *Nano Lett* **22**, 5330-5338, doi:10.1021/acs.nanolett.2c01316 (2022).

103 Kocak, G., Tuncer, C. & Bütün, V. pH-Responsive polymers. *Polymer Chemistry* **8**, 144-176, doi:10.1039/c6py01872f (2017).

104 Krieg, E. & Shih, W. M. Selective Nascent Polymer Catch-and-Release Enables Scalable Isolation of Multi-Kilobase Single-Stranded DNA. *Angew Chem Int Ed Engl* **57**, 714-718, doi:10.1002/anie.201710469 (2018).

105 Ramos, J., Forcada, J. & Hidalgo-Alvarez, R. Cationic polymer nanoparticles and nanogels: from synthesis to biotechnological applications. *Chem Rev* **114**, 367-428, doi:10.1021/cr3002643 (2014).

106 Tang, M. X. & Szoka, F. C. The influence of polymer structure on the interactions of cationic polymers with DNA and morphology of the resulting complexes. *Gene Therapy* **4**, 823-832, doi:10.1038/sj.gt.3300454 (1997).

107 Xia, F. *et al.* On the Binding of Cationic, Water-Soluble Conjugated Polymers to DNA: Electrostatic and Hydrophobic Interactions. *Journal of the American Chemical Society* **132**, 1252-1254, doi:10.1021/ja908890q (2010).

108 Averick, S. E. *et al.* Preparation of Cationic Nanogels for Nucleic Acid Delivery. *Biomacromolecules* **13**, 3445-3449, doi:10.1021/bm301166s (2012).

109 Kumar, R. *et al.* Polymeric Delivery of Therapeutic Nucleic Acids. *Chemical Reviews* **121**, 11527-11652, doi:10.1021/acs.chemrev.0c00997 (2021).

110 Kabanov, A. V. & Kabanov, V. A. Interpolyelectrolyte and block ionomer complexes for gene delivery: physico-chemical aspects. *Advanced Drug Delivery Reviews* **30**, 49-60, doi:10.1016/S0169-409X(97)00106-3 (1998).

111 Noir, R., Kotera, M., Pons, B., Remy, J.-S. & Behr, J.-P. Oligonucleotide−Oligospermine Conjugates (Zip Nucleic Acids): A Convenient Means of Finely Tuning Hybridization Temperatures. *Journal of the American Chemical Society* **130**, 13500-13505, doi:10.1021/ja804727a (2008).

112 Abraham, J. N., Gour, N., Bolisetty, S., Mezzenga, R. & Nardin, C. Controlled aggregation of peptide–DNA hybrids into amyloid-like fibrils. *European Polymer Journal* **65**, 268-275, doi:10.1016/j.eurpolymj.2015.02.009 (2015).

113 Gour, N. *et al.* Label-free, optical sensing of the supramolecular assembly into fibrils of a ditryptophan-DNA hybrid. *Chem Commun (Camb)* **50**, 6863-6865, doi:10.1039/c4cc02631d (2014).

114 Zhang, X. *et al.* DNA Nanoparticle Based 2D Biointerface to Study the Effect of Dynamic RGD Presentation on Stem Cell Adhesion and Migration. *Small*, e2311402, doi:10.1002/smll.202311402 (2024).

115 Zhao, F., Frandsen, M., Capodaglio, S. & Sleiman, H. F. DNA-Mediated Peptide Assembly into Protein Mimics. *J Am Chem Soc* **146**, 1946-1956, doi:10.1021/jacs.3c08984 (2024).

116 Danielsen, M. B., Mao, H. & Lou, C. Peptide-DNA conjugates as building blocks for de novo design of hybrid nanostructures. *Cell Reports Physical Science* **4**, doi:10.1016/j.xcrp.2023.101620 (2023).

117 Buchberger, A., Simmons, C. R., Fahmi, N. E., Freeman, R. & Stephanopoulos, N. Hierarchical Assembly of Nucleic Acid/Coiled-Coil Peptide Nanostructures. *J Am Chem Soc* **142**, 1406-1416, doi:10.1021/jacs.9b11158 (2020).

118 Kye, M., Zhang, Z. & Lim, Y.-b. Self-assembling cyclic peptide-oligonucleotide conjugates: Synthetic strategies and the effect of cyclic topology on self-assembly and base pairing. *Peptide Science* **113**, e24193, doi:10.1002/pep2.24193 (2021).

119 Kubo, T., Morikawa, M., Ohba, H. & Fujii, M. Synthesis of DNA−Peptide Conjugates by Solid-Phase Fragment Condensation. *Organic Letters* **5**, 2623-2626, doi:10.1021/ol034721p (2003).

120 Williams, B. A. & Chaput, J. C. Synthesis of peptide-oligonucleotide conjugates using a heterobifunctional crosslinker. *Curr Protoc Nucleic Acid Chem* **Chapter 4**, Unit4 41, doi:10.1002/0471142700.nc0441s42 (2010).

121 Stephanopoulos, N. *et al.* Bioactive DNA-peptide nanotubes enhance the differentiation of neural stem cells into neurons. *Nano Lett* **15**, 603-609, doi:10.1021/nl504079q (2015).

122 Chotera, A., Sadihov, H., Cohen-Luria, R., Monnard, P. A. & Ashkenasy, G. Functional Assemblies Emerging in Complex Mixtures of Peptides and Nucleic Acid-Peptide Chimeras. *Chemistry* **24**, 10128-10135, doi:10.1002/chem.201800500 (2018).

123 Serrano, C. M., Freeman, R., Godbe, J., Lewis, J. A. & Stupp, S. I. DNA-Peptide Amphiphile Nanofibers Enhance Aptamer Function. *ACS Appl Bio Mater* **2**, 2955-2963, doi:10.1021/acsabm.9b00310 (2019).

124 Jin, J. *et al.* Peptide Assembly Directed and Quantified Using Megadalton DNA Nanostructures. *ACS Nano* **13**, 9927-9935, doi:10.1021/acsnano.9b04251 (2019).

125 Daly, M. L., Gao, Y. & Freeman, R. Encoding Reversible Hierarchical Structures with Supramolecular Peptide-DNA Materials. *Bioconjug Chem* **30**, 1864-1869, doi:10.1021/acs.bioconjchem.9b00271 (2019).

126 Wang, B. *et al.* Short intrinsically disordered polypeptide-oligonucleotide conjugates for programmed self-assembly of nanospheres with temperature-dependent size controllability. *Soft Matter* **17**, 1184-1188, doi:10.1039/d0sm01817a (2021).

127 Hafenstine, G. R., Domaille, D. W., Cha, J. N. & Goodwin, A. P. Self-assembly and reassembly of fiber-forming dipeptides for pH-triggered DNA delivery. *Journal of Polymer Science Part A: Polymer Chemistry* **53**, 183-187, doi:10.1002/pola.27319 (2014).

128 Harrison, J. G. & Balasubramanian, S. Synthesis and hybridization analysis of a small library of peptide-oligonucleotide conjugates. *Nucleic Acids Research* **26**, 3136-3145, doi:10.1093/nar/26.13.3136 (1998).

129 Chen, C.-P. *et al.* A Concise Method for the Preparation of Peptide and Arginine-Rich Peptide-Conjugated Antisense Oligonucleotide. *Bioconjugate Chemistry* **14**, 532-538, doi:10.1021/bc034004f (2003).

130 Basu, S. & Wickstrom, E. Solid phase synthesis of a d-peptide-phosphorothioate oligodeoxynucleotide conjugate from two arms of a polyethylene glycol-polystyrene support. *Tetrahedron Letters* **36**, 4943-4946, doi:10.1016/0040-4039(95)00898-M (1995).

131 Tetzlaff, C. N., Schwope, I., Bleczinski, C. F., Steinberg, J. A. & Richert, C. A convenient synthesis of 5′-amino-5′-deoxythymidine and preparation of peptide-DNA hybrids. *Tetrahedron Letters* **39**, 4215-4218, doi:10.1016/S0040-4039(98)00788-6 (1998).

132 Kusmierz, C. D., Bujold, K. E., Callmann, C. E. & Mirkin, C. A. Defining the Design Parameters for in Vivo Enzyme Delivery Through Protein Spherical Nucleic Acids. *ACS CENTRAL SCIENCE* **6**, 815-822, doi:10.1021/acscentsci.0c00313 (2020).

133 Ebrahimi, S. B., Samanta, D., Kusmierz, C. D. & Mirkin, C. A. Protein transfection via spherical nucleic acids. *Nat Protoc* **17**, 327-357, doi:10.1038/s41596-021-00642-x (2022).

134 Hayes, O. G., McMillan, J. R., Lee, B. & Mirkin, C. A. DNA-Encoded Protein Janus Nanoparticles. *J Am Chem Soc* **140**, 9269-9274, doi:10.1021/jacs.8b05640 (2018).

135 Hayes, O. G., Partridge, B. E. & Mirkin, C. A. Encoding hierarchical assembly pathways of proteins with DNA. *Proc Natl Acad Sci U S A* **118**, doi:10.1073/pnas.2106808118 (2021).

136 Robinson, P. K. Enzymes: principles and biotechnological applications. *Essays Biochem* **59**, 1-41, doi:10.1042/bse0590001 (2015).

137 Timm, C. & Niemeyer, C. M. Assembly and purification of enzyme-functionalized DNA origami structures. *Angew Chem Int Ed Engl* **54**, 6745-6750, doi:10.1002/anie.201500175 (2015).

138 Numajiri, K., Yamazaki, T., Kimura, M., Kuzuya, A. & Komiyama, M. Discrete and Active Enzyme Nanoarrays on DNA Origami Scaffolds Purified by Affinity Tag Separation. *Journal of the American Chemical Society* **132**, 9937-9939, doi:10.1021/ja104702q (2010).

139 Qian, L. *et al.* The Dawn of a New Era: Targeting the "Undruggables" with Antibody-Based Therapeutics. *Chem Rev* **123**, 7782-7853, doi:10.1021/acs.chemrev.2c00915 (2023).

140 Wagenbauer, K. F. *et al.* Programmable multispecific DNA-origami-based T-cell engagers. *Nat Nanotechnol* **18**, 1319-1326, doi:10.1038/s41565-023-01471-7 (2023).

141 Weickert, P. & Stingele, J. DNA-Protein Crosslinks and Their Resolution. *Annu Rev Biochem* **91**, 157-181, doi:10.1146/annurev-biochem-032620-105820 (2022).

142 Hoyt, E. A., Cal, P. M. S. D., Oliveira, B. L. & Bernardes, G. J. L. Contemporary approaches to site-selective protein modification. *Nature Reviews Chemistry* **3**, 147-171, doi:10.1038/s41570-019-0079-1 (2019).

143 Ang, Y. S. & Yung, L.-Y. L. Protein–DNA Conjugates with a Discrete Number of Oligonucleotide Strands for Highly Reproducible Protein Quantification by the DNA Proximity Assay. *Analytical Chemistry* **95**, 12071-12079, doi:10.1021/acs.analchem.3c02033 (2023).

144 Zhou, Z., Xiang, Y., Tong, A. & Lu, Y. Simple and efficient method to purify DNA-protein conjugates and its sensing applications. *Anal Chem* **86**, 3869-3875, doi:10.1021/ac4040554 (2014).

145 Samanta, D., Ebrahimi, S. B., Kusmierz, C. D., Cheng, H. F. & Mirkin, C. A. Protein Spherical Nucleic Acids for Live-Cell Chemical Analysis. *J Am Chem Soc* **142**, 13350-13355, doi:10.1021/jacs.0c06866 (2020).

146 Huang, C., Han, Z., Evangelopoulos, M. & Mirkin, C. A. CRISPR Spherical Nucleic Acids. *J Am Chem Soc* **144**, 18756-18760, doi:10.1021/jacs.2c07913 (2022).

147 Marcher, A., Palmfeldt, J., Nisavic, M. & Gothelf, K. V. A Reagent for Amine-Directed Conjugation to IgG1 Antibodies. *Angew Chem Int Ed Engl* **60**, 6539-6544, doi:10.1002/anie.202013911 (2021).
148 Nielsen, T. B. *et al.* Peptide-Directed DNA-Templated Protein Labelling for The Assembly of a Pseudo-IgM. *Angew Chem Int Ed Engl* **58**, 9068-9072, doi:10.1002/anie.201903134 (2019).
149 Rosen, C. B. *et al.* Template-directed covalent conjugation of DNA to native antibodies, transferrin and other metal-binding proteins. *Nat Chem* **6**, 804-809, doi:10.1038/nchem.2003 (2014).
150 Xu, L., Kuan, S. L. & Weil, T. Contemporary Approaches for Site-Selective Dual Functionalization of Proteins. *Angew Chem Int Ed Engl* **60**, 13757-13777, doi:10.1002/anie.202012034 (2021).
151 Trads, J. B., Torring, T. & Gothelf, K. V. Site-Selective Conjugation of Native Proteins with DNA. *Acc Chem Res* **50**, 1367-1374, doi:10.1021/acs.accounts.6b00618 (2017).
152 Xin, L., Zhou, C., Yang, Z. & Liu, D. Regulation of an enzyme cascade reaction by a DNA machine. *Small* **9**, 3088-3091, doi:10.1002/smll.201300019 (2013).
153 Wang, C., Yue, L. & Willner, I. Controlling biocatalytic cascades with enzyme–DNA dynamic networks. *Nature Catalysis* **3**, 941-950, doi:10.1038/s41929-020-00524-7 (2020).
154 Spratt, J. *et al.* Multivalent insulin receptor activation using insulin-DNA origami nanostructures. *Nat Nanotechnol*, doi:10.1038/s41565-023-01507-y (2023).
155 Youssef, S., Tsang, E., Samanta, A., Kumar, V. & Gothelf, K. V. Reversible Protection and Targeted Delivery of DNA Origami with a Disulfide-Containing Cationic Polymer. *Small*, e2301058, doi:10.1002/smll.202301058 (2023).
156 Yu, L. *et al.* CytoDirect: A Nucleic Acid Nanodevice for Specific and Efficient Delivery of Functional Payloads to the Cytoplasm. *J Am Chem Soc* **145**, 27336-27347, doi:10.1021/jacs.3c07491 (2023).
157 Paloja, K. *et al.* Balancing the Nanoscale Organization in Multivalent Materials for Functional Inhibition of the Programmed Death-1 Immune Checkpoint. *ACS Nano* **18**, 1381-1395, doi:10.1021/acsnano.3c06552 (2024).
158 Stahl, S. *et al.* Affibody Molecules in Biotechnological and Medical Applications. *Trends Biotechnol* **35**, 691-712, doi:10.1016/j.tibtech.2017.04.007 (2017).
159 Frejd, F. Y. & Kim, K. T. Affibody molecules as engineered protein drugs. *Exp Mol Med* **49**, e306, doi:10.1038/emm.2017.35 (2017).
160 Winegar, P. H. *et al.* DNA-Directed Protein Packing within Single Crystals. *Chem* **6**, 1007-1017, doi:10.1016/j.chempr.2020.03.002 (2020).
161 Figg, C. A., Winegar, P. H., Hayes, O. G. & Mirkin, C. A. Controlling the DNA Hybridization Chain Reaction. *J Am Chem Soc* **142**, 8596-8601, doi:10.1021/jacs.0c02892 (2020).
162 Jbara, M. *et al.* Oligonucleotide Bioconjugation with Bifunctional Palladium Reagents. *Angew Chem Int Ed Engl* **60**, 12109-12115, doi:10.1002/anie.202103180 (2021).
163 Reinking, H. K. & Stingele, J. Protein-oligonucleotide conjugates as model substrates for DNA-protein crosslink repair proteases. *STAR Protoc* **2**, 100591, doi:10.1016/j.xpro.2021.100591 (2021).
164 Li, S. *et al.* A DNA nanorobot functions as a cancer therapeutic in response to a molecular trigger in vivo. *Nat Biotechnol* **36**, 258-264, doi:10.1038/nbt.4071 (2018).
165 Chan, Y. H., van Lengerich, B. & Boxer, S. G. Lipid-anchored DNA mediates vesicle fusion as observed by lipid and content mixing. *Biointerphases* **3**, FA17, doi:10.1116/1.2889062 (2008).
166 Takahashi, K., Matsuo, M., Banno, T. & Toyota, T. Micrometer-sized network structure of novel DNA-lipid conjugates induced by heat stimulation. *Soft Matter* **11**, 7053-7058, doi:10.1039/c5sm01456e (2015).

167 Zhang, Y., Peng, R., Xu, F. & Ke, Y. Hierarchical Self-Assembly of Cholesterol-DNA Nanorods. *Bioconjug Chem* **30**, 1845-1849, doi:10.1021/acs.bioconjchem.9b00322 (2019).

168 Miller, G. P. & Kool, E. T. A Simple Method for Electrophilic Functionalization of DNA. *Organic Letters* **4**, 3599-3601, doi:10.1021/ol0264915 (2002).

169 Chan, Y.-H. M., van Lengerich, B. & Boxer, S. G. Effects of linker sequences on vesicle fusion mediated by lipid-anchored DNA oligonucleotides. *Proceedings of the National Academy of Sciences* **106**, 979-984, doi:10.1073/pnas.0812356106 (2009).

170 Rawle, R. J., Boxer, S. G. & Kasson, P. M. Disentangling Viral Membrane Fusion from Receptor Binding Using Synthetic DNA-Lipid Conjugates. *Biophys J* **111**, 123-131, doi:10.1016/j.bpj.2016.05.048 (2016).

171 van Lengerich, B., Rawle, R. J., Bendix, P. M. & Boxer, S. G. Individual vesicle fusion events mediated by lipid-anchored DNA. *Biophys J* **105**, 409-419, doi:10.1016/j.bpj.2013.05.056 (2013).

172 van Lengerich, B., Rawle, R. J. & Boxer, S. G. Covalent attachment of lipid vesicles to a fluid-supported bilayer allows observation of DNA-mediated vesicle interactions. *Langmuir* **26**, 8666-8672, doi:10.1021/la904822f (2010).

173 Webster, E. R., Liu, K. N., Rawle, R. J. & Boxer, S. G. Modulating the Influenza A Virus-Target Membrane Fusion Interface With Synthetic DNA-Lipid Receptors. *Langmuir* **38**, 2354-2362, doi:10.1021/acs.langmuir.1c03247 (2022).

174 Wolfrum, C. *et al.* Mechanisms and optimization of in vivo delivery of lipophilic siRNAs. *Nat Biotechnol* **25**, 1149-1157, doi:10.1038/nbt1339 (2007).

175 Dong, Y. *et al.* Folding DNA into a Lipid-Conjugated Nanobarrel for Controlled Reconstitution of Membrane Proteins. *Angew Chem Int Ed Engl* **57**, 2072-2076, doi:10.1002/anie.201710147 (2018).

176 Yang, Y. *et al.* Self-assembly of size-controlled liposomes on DNA nanotemplates. *Nat Chem* **8**, 476-483, doi:10.1038/nchem.2472 (2016).

177 Gosse, C. *et al.* Micelles of Lipid−Oligonucleotide Conjugates: Implications for Membrane Anchoring and Base Pairing. *The Journal of Physical Chemistry B* **108**, 6485-6497, doi:10.1021/jp031188m (2004).

178 Raouane, M. *et al.* Synthesis, characterization, and in vivo delivery of siRNA-squalene nanoparticles targeting fusion oncogene in papillary thyroid carcinoma. *J Med Chem* **54**, 4067-4076, doi:10.1021/jm2000272 (2011).

179 Matsuura, K., Akasaka, T., Hibino, M. & Kobayashi, K. Facile Synthesis of Stable and Lectin-Recognizable DNA-Carbohydrate Conjugates via Diazo Coupling. *Bioconjugate Chemistry* **11**, 202-211, doi:10.1021/bc9901191 (2000).

180 Yokoyama, K. *et al.* Synthesis and biological properties of DNA-sugar conjugates. *Nucleic Acids Symposium Series* **1**, 73-74, doi:10.1093/nass/1.1.73 (2001).

181 Karskela, M., Helkearo, M., Virta, P. & Lönnberg, H. Synthesis of Oligonucleotide Glycoconjugates Using Sequential Click and Oximation Ligations. *Bioconjugate Chemistry* **21**, 748-755, doi:10.1021/bc900529g (2010).

182 Matsuura, K., Hibino, M., Yamada, Y. & Kobayashi, K. Construction of Glyco-Clusters by Self-Organization of Site-Specifically Glycosylated Oligonucleotides and Their Cooperative Amplification of Lectin-Recognition. *Journal of the American Chemical Society* **123**, 357-358, doi:10.1021/ja001945j (2001).

183 Sheppard, T. L., Wong, C. H. & Joyce, G. F. Nucleoglycoconjugates: design and synthesis of a new class of DNA-carbohydrate conjugates. *Angew Chem Int Ed Engl* **39**, 3660-3663, doi:10.1002/1521-3773(20001016)39:20<3660::AID-ANIE3660>3.0.CO;2-L (2000).

184 Avino, A. *et al.* Synthesis and in vitro inhibition properties of siRNA conjugates carrying glucose and galactose with different presentations. *Mol Divers* **15**, 751-757, doi:10.1007/s11030-011-9305-6 (2011).

185 Yan, H., Aguilar, A. L. & Zhao, Y. Preparation of carbohydrate-oligonucleotide conjugates using the squarate spacer. *Bioorg Med Chem Lett* **17**, 6535-6538, doi:10.1016/j.bmcl.2007.09.078 (2007).
186 Zhao, Y., Tram, K. & Yan, H. Synthesis and characterization of mannosylated oligoribonucleotides. *Carbohydr Res* **344**, 2137-2143, doi:10.1016/j.carres.2009.08.033 (2009).
187 Akasaka, T., Matsuura, K., Emi, N. & Kobayashi, K. Conjugation of Plasmid DNAs with Lactose via Diazocoupling Enhances Resistance to Restriction Enzymes and Acquires Binding Affinity to Galactose-Specific Lectin. *Biochemical and Biophysical Research Communications* **260**, 323-328, doi:10.1006/bbrc.1999.0830 (1999).
188 Forget, D., Renaudet, O., Defrancq, E. & Dumy, P. Efficient preparation of carbohydrate–oligonucleotide conjugates (COCs) using oxime bond formation. *Tetrahedron Letters* **42**, 7829-7832, doi:10.1016/S0040-4039(01)01682-3 (2001).
189 Schlegel, M. K., Hutter, J., Eriksson, M., Lepenies, B. & Seeberger, P. H. Defined presentation of carbohydrates on a duplex DNA scaffold. *Chembiochem* **12**, 2791-2800, doi:10.1002/cbic.201100511 (2011).

Acknowledgements

T.J. acknowledges financial support from the Alexander von Humboldt Foundation through a Feodor-Lynen Return Fellowship. ChatGPT versions 3.5 and 4o have been used to improve the language of the article and draft the conclusion section.

Competing interests

The authors declare no competing interests.

II. MOTIVATION AND OBJECTIVES

Motivated by Nature's precision, DNA nanotechnology sets new standards for highly defined nanomaterials. By combining with other material classes like polymers or proteins to create precise hybrid materials, the applications of DNA nanotechnology is tremendously expanded. For the material formation, different approaches like *grafting from*, *grafting to* or *grafting onto* strategies pave the way for a better accessibility. However, creating such DNA materials and architectures is usually very complex and only possible in small batches. The yields are low, and the assemblies are usually susceptible to decomposition. Within this thesis, the focus is on the DNA-polymer hybrid class to implement a robust strategy for a reliable architecture construction and functionalization. Therefore, the formation and purification of functional DNA-polymer materials should be optimized in view of a simple, applicability and resource-saving manner.

The first attempt was to optimize the DNA-polymer conjugate formation in terms of robustness towards different polymers as well as obtaining high yields. Choosing between the *grafting to* and the *grafting from* technique, the *grafting to* method seems the more adjustable with the potential to upscale the formation of conjugates. Moreover, the *grafting from* method is limited by its lack of robustness against impurities and variability in different monomers, restricting its potential as a universal technique. Via reversible addition-fragmentation chain-transfer polymerization (RAFT) a water-soluble polymer, containing an NHS group, was synthesized, acting as a model polymer. We aimed for poly *N,N*-Dimethylacrylamide (P(DMA)) with a molecular weight of 20 kDa to optimize reaction conditions and solvent mixtures. P(DMA) is highly water soluble without any phase separation, facilitate the reaction between the DNA and polymer. For reaction optimization, the solvent seems to be a promising parameter, due to the importance of solubility for the reaction. For a successful reaction of the polymer with the DNA in general, both functional ends need to be accessible to react. If the solubility would be insufficient, the molecules can collapse in solution shielding the reactive ends. These obtained results for optimization would then be applied to other polymers of three different polymer families (acrylates, methacrylates, acrylamides) with different behaviors like phase separation or higher hydrophobicity to explore the versatility of the previously applied reaction conditions. Furthermore, testing the variability of the reaction towards different sized polymers, the system would be applied to lower and higher molecular weight polymers underline the universality of the chosen method.

In the next step, we intend to optimize the processing of the purification to obtain pure DNA-polymer conjugates. In general, the *grafting to* strategy uses an excess of the cheaper components

in order to drive higher yields during the reaction. Here, the excess of polymer leads often to problems during purification due to the similar chemical properties of polymer and conjugate as well as an overlay of retention times during purification. This usually limits the resolution as well as the possible amount that can be purified. Therefore, a method and protocol was developed where the peak resolution is independent of the aforementioned properties, even with larger quantities. Furthermore, we aimed to make a separation of the conjugate and the unreacted DNA possible, interesting for scaling up the conjugate formation due to the recovery of the expensive, unreacted DNA strands. By testing different purification strategies such as spin filtration, reverse phase HPLC and size exclusion chromatography and anion exchange chromatography, the most promising purification method was established and optimized to implement a robust, versatile method and increase the accessibility of DNA-polymer conjugates to the community.

As a proof of concept, the synthesized DNA-polymer conjugates would be utilized to introduce functional patterns on DNA-origami. DNA-origami facilitate the creation of highly defined nano architectures and thus expanding the engineering of nanoobjects to a new level. Combining these architectures with the controllability and functionality of DNA-polymer conjugates give rise a new class of functional hybrid structures and grant, due to the customizable functionalization patterns and properties, new application possibilities. Accordingly, DNA-origami structures in tube and rectangle shapes, featuring protruding sticky sequences on their surfaces, were selected as targets. The strategy entails the conjugation of polymers to the complementary DNA strands, followed by annealing to the DNA architecture, thereby enabling the creation of various multifunctional surfaces and polymer contours on a single architecture.

This thesis endeavors to develop a straightforward and widely applicable approach to synthesizing DNA-polymer conjugates, while addressing the challenges associated with purification through the implementation of a reliable method to achieve high purity and the ability to recover utilized reactants. Moreover, the project envisions the decoration of DNA-origami architectures by annealing with DNA-polymer conjugates, aiming for high controllability and definition in nanometer resolution and thus introducing a toolbox of possible functional patterns for DNA-origami.

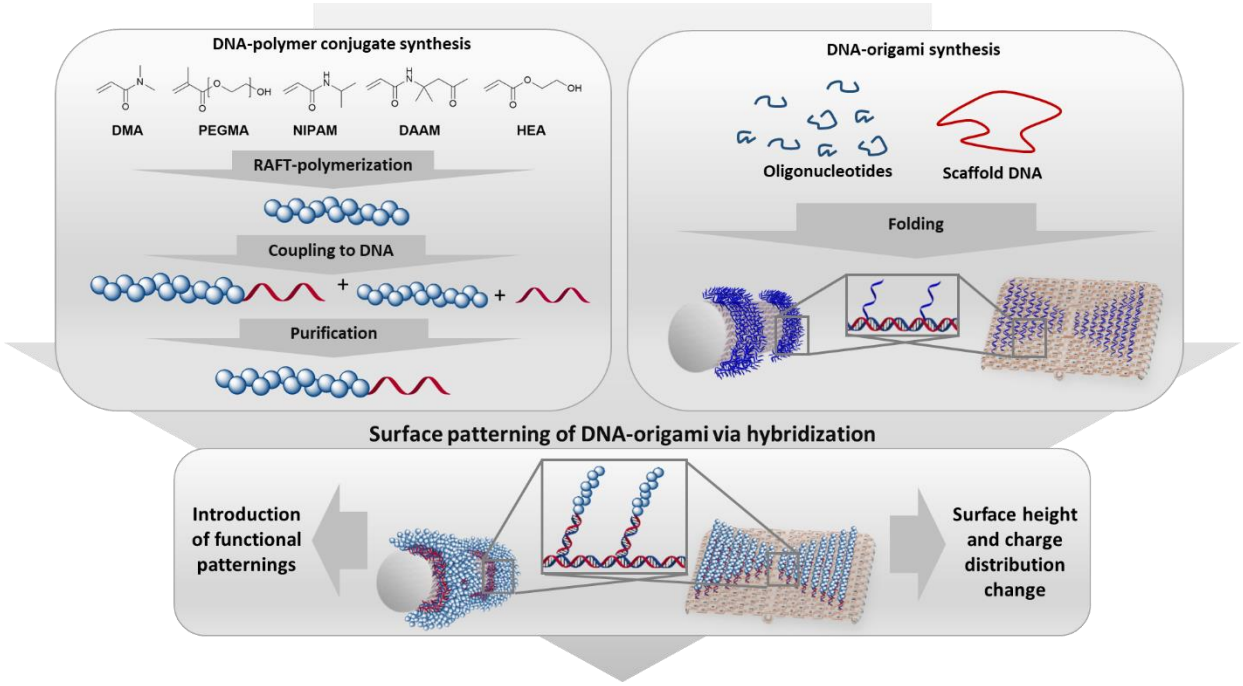

Figure 12: Schematic presentation of the thesis approach to create DNA-polymer conjugates and use them to create polymer patterns on DNA-origami surface with nanometer resolution.

III. RESULTS AND DISCUSSIONS

III.I NANOSCALE PATTERNING OF POLYMERS ON DNA ORIGAMI

Publication:	**"Nanoscale patterning of polymers on DNA origami"**
Authors:	**Nico Alleva**, Pia Winterwerber, Colette J. Whitfield, David Y. W. Ng* and Tanja Weil*
Published in:	Journal of Material Chemistry B, 2022, 10, 7512-7517
DOI:	10.1039/D2TB00812B
Date of Publication:	8th June 2022

Author Contribution:

Nico Alleva	Conceptualization, polymer synthesis via RAFT polymerization, characterization of polymers, testing solvent conditions for coupling, transferring system to other DNA-polymer conjugates, experiments for conjugate to DNA-origami annealing, preparation and analysis of PAGE/Agarose gels, AFM measurements. Writing the manuscript.
Pia Winterwerber	Initial introduction to the project and expertise
Colette J. Whitfield	Initial introduction to the project and expertise
David Y. W. Ng/ Tanja Weil	The project was processed under the supervision of both; acquiring funding; edited manuscript

Funding	Deutsche Forschungsgemeinschaft (DFG, German Research Foundation) – Project No. 364549901 – TRR 234 CataLight (B01) and the Max Planck Society for Open Access Funding

Copyrights:

Graphical Abstract:

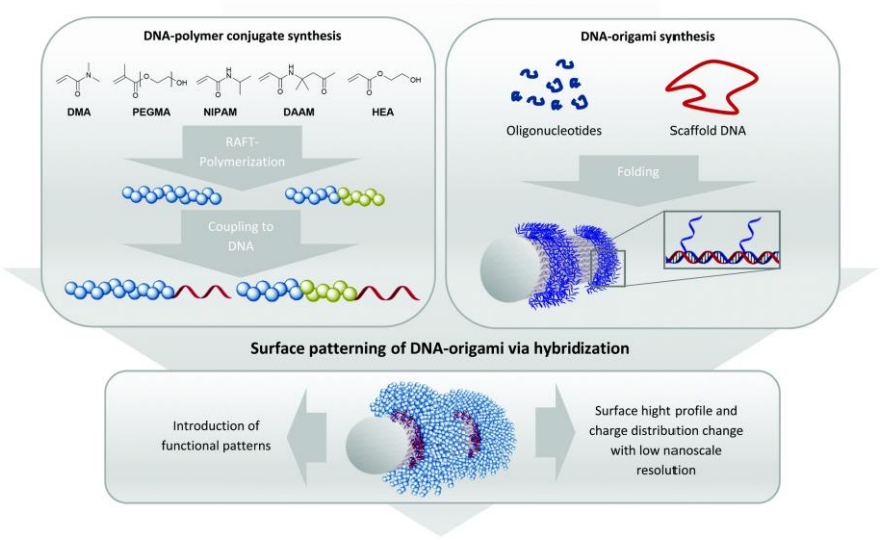

Summary:

DNA-polymer architectures have garnered increased interest in recent years owing to their programmability and unique properties for special applications such biosensors One approach to fabricating these hybrid nanostructures involves annealing single-stranded DNA-polymer conjugates onto the surface of DNA architectures. This method necessitates complementary strands protruding from the surface, as well as well-defined conjugates to achieve patterning. Various strategies, including the *grafting to* and *grafting from* method, can be employed to obtain DNA-polymer conjugates. While the *grafting from* approach requires an oxygen-free environment and is typically conducted on a small scale, the *grafting to* method is generally considered more robust in terms of reaction control and accessibility.

The publication presented herein describes a versatile and robust method for the synthesis of DNA-polymer conjugates comprising polymers from different polymer families such as acrylates, methacrylates, and acrylamides. Through optimization of reaction conditions, high yields were achieved even for polymers prone to phase separation or exhibiting brush-like structures. Notably, the method demonstrated success in synthesizing DNA-polymer conjugates with high molecular weight polymers, overcoming previous limitations in yield for larger polymers. Subsequently, the synthesized conjugates were applied to DNA-origami structures of various shapes, resulting in

excellent surface patterning with nanometer scale precision. Moreover, a step-by-step annealing process employing different conjugates on a single DNA-origami architecture showcased the method's potential for creating multifunctional DNA-polymer hybrid materials.

Journal of Materials Chemistry B

ROYAL SOCIETY OF CHEMISTRY

COMMUNICATION

View Article Online
View Journal | View Issue

Cite this: *J. Mater. Chem. B*, 2022, 10, 7512

Received 13th April 2022,
Accepted 4th June 2022

DOI: 10.1039/d2tb00812b

rsc.li/materials-b

Nanoscale patterning of polymers on DNA origami†

Nico Alleva, Pia Winterwerber, Colette J. Whitfield, David Y. W. Ng * and Tanja Weil*

The combination of DNA–origami and synthetic polymers paves the way to a new class of structurally precise biohybrid nanomaterials for diverse applications. Herein, we introduce the grafting to method with high conversions (70–90%) under ambient conditions to generate DNA–polymer conjugates, which can hybridized precisely to DNA–origami architectures. We generated homo and block copolymers from three different polymer families (acrylates, methacrylates and acrylamides), coupled them to single stranded DNA (ssDNA) and pattern different DNA–origami architectures to demonstrate the formation of precise surface nanopatterns.

In recent years, DNA–polymer hybrid materials have received increasing interest as biosensors[1] or drug delivery systems.[2] Due to the high versatility of the synthetic polymer component, a wide range of properties, particularly those that promote dynamic and responsive behaviour (*i.e.* pH, temperature), have been combined with the unique programmability offered by DNA nanotechnology.[3] DNA–polymer nanostructures have been realized and structure formations has been studied. One of the most elaborate example exploits the polyanionic character of DNA with hydrophobic polymers to create amphiphilic conjugates that assemble into micelles.[4] Amphiphilic micelles have been made thermo-responsive by conjugation of the temperature-responsive polymer poly(*N*-isopropylacrylamide) (P(NIPAM)) and thus conferring its lower critical solution temperature (LCST) behaviour onto the eventual micelles.[5] These studies have since been expanded to include multi-responsiveness, not only from polymers, but also from oligonucleotides, such as the pH induced interconversion of "i-motif" structures.[6] In combination with the bioactivity of DNA–aptamer nanostructures, advanced drug delivery systems based on DNA–polymer conjugates have been developed.[7]

Importantly, the unique facet of DNA–polymer conjugates lies in a versatile platform to create architectures of higher complexity where DNA nanotechnology can be used to guide polymers with high precision in the nanoscale.[8] This strategy entails the use of DNA–origami as a template, where a long single-stranded (ss) DNA is folded by short oligonucleotides, so called staple strands, into complex 3-D DNA origami architectures like rectangles, tubes, stars or many other architectures.[9] As each grid position on DNA–origami can be independently functionalized, radical initiators[10] and/or photocatalysts[11] have been patterned to promote polymerization at the designated locations. However, conducting polymerization reactions directly on DNA–origami requires stringent conditions such as high ionic strength buffers with divalent cations Mg^{2+}/Ca^{2+}, low reaction volumes typically below 100 µl and mild reaction conditions during polymerization. This significantly limits both the monomer scope and polymerization technique. Additionally, it is often difficult to characterize the polymers (*i.e.* molecular weights, dispersity) grafted from the DNA origami due to its very low quantities. Herein, we circumvent these

Max Planck Institute for Polymer Research, Ackermannweg 10, 55128 Mainz, Germany. E-mail: david.ng@mpip-mainz.mpg.de, weil@mpip-mainz.mpg.de

† Electronic supplementary information (ESI) available. See DOI: https://doi.org/10.1039/d2tb00812b

David Y. W. Ng

David received his BSc in Chemistry with first class honours in 2009 at the National University of Singapore. In 2010, his PhD studies on dendrimer–protein transporters was funded by the Max Planck Institute for Polymer Research (MPIP) to work under the supervision of Prof. Tanja Weil in Ulm. David graduated with summa cum laude in 2014 and led a junior group until 2016. He then moved to the MPIP and formed the synthetic life-like systems group focusing on constructing dynamic bioactive structures in living cells. In 2021, he is appointed to concurrently lead the BioCore facility of the MPIP.

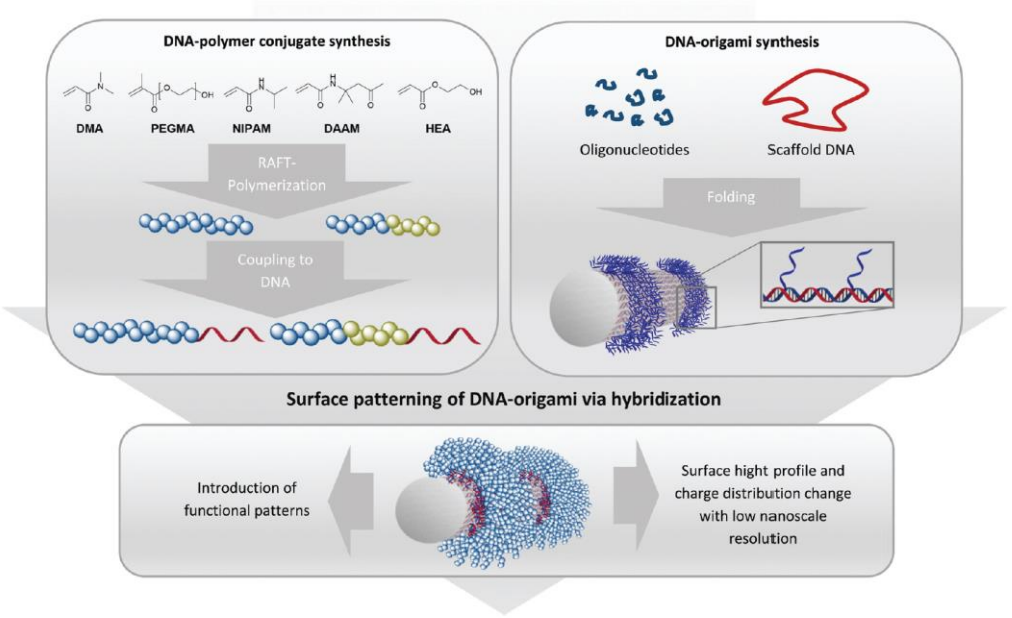

Fig. 1 Concept of the combination of the grafting to method for generating DNA–polymer conjugates and the surface coating of DNA–origami due to protruding single stranded sticky sequences on the surface. The selected monomers form polymers with different features to diversify the inherent properties of DNA–origami nano-objects. The monomers were polymerized *via* RAFT polymerization and then coupled to single stranded DNA *via* NHS–amine conjugation chemistry under mild and ambient conditions. This versatile method generates a wide range of DNA–polymer conjugates for precise surface patterning of DNA–origami nanostructures.

limitations by adapting the grafting to approach, where polymers are synthesized in organic solvents (Fig. 1) before binding to DNA–origami for creating precise 3-D polymeric nanopatterns. This approach is already used in literature for the creation of functional DNA–polymer conjugates for *e.g.* fluorescent polythiophenes to form patterned DNA–origami in a high precise way.[8,12]

In order to position polymer chains onto DNA–origami, staple strands corresponding to the designated positions have to be elongated by a sticky DNA sequence. These extensions protrude as a ssDNA from the DNA–origami surface, allowing complementary sequences appended onto the polymer chains to recognize.[13] Hence, polymer chains with different sets of sticky DNA sequences can self-assemble onto their corresponding sites to afford a customizable architecture. As such, this technique grants access towards achieving precise geometric shapes that cannot be constructed *via* conventional polymer synthesis methods.[14,15] Three different kinds of monomer backbone (acrylates, methacrylates and acrylamides) were selected to underline the versatility of the approach. Technically, the production of 1–1 DNA–polymer conjugates can be performed *via* the grafting from or the grafting to method. In the grafting from method, the DNA block contains an initiator molecule and polymerization of the monomer proceeds *in situ* to form the respective DNA–polymer conjugate.[16] However, the polymerization reaction has to be performed under conditions that accommodate the monomer, polymer and DNA components and there is a general loss of controllability and dispersity of the resultant polymers. On the contrary, the grafting to method synthesizes the polymer independently, which also facilitates characterization and easy scalability. After successful synthesis, bioconjugation to the DNA strand furnishes the target conjugate. As the polymer is synthesized prior the bioconjugation, the polymer block can be tailored with high flexibility even if the polymer chain is hydrophobic.[17] Due to these advantages, the grafting to method opens access to various DNA–polymer conjugates containing homo and block copolymers with hydrophilic and hydrophobic monomer units.[18]

Dimethyl acrylamide (DMA), oligoethylene glycol acrylate (OEGMA), *N*-isopropyl acrylamide (NIPAM), hydroxyethyl acrylate (HEA) and diacetone acrylamide (DAAM) were polymerized *via* reversible–addition–fragmentation chain-transfer polymerization (RAFT) to form the homo polymers and block copolymers (Fig. 2a). These monomers constitute widely used classes in the polymer community with DMA and OEGMA promoting aqueous solubility[19] whereas NIPAM, HEA and DAAM are common functional monomers in self-assembly systems.[16,20]

View Article Online
Journal of Materials Chemistry B Communication

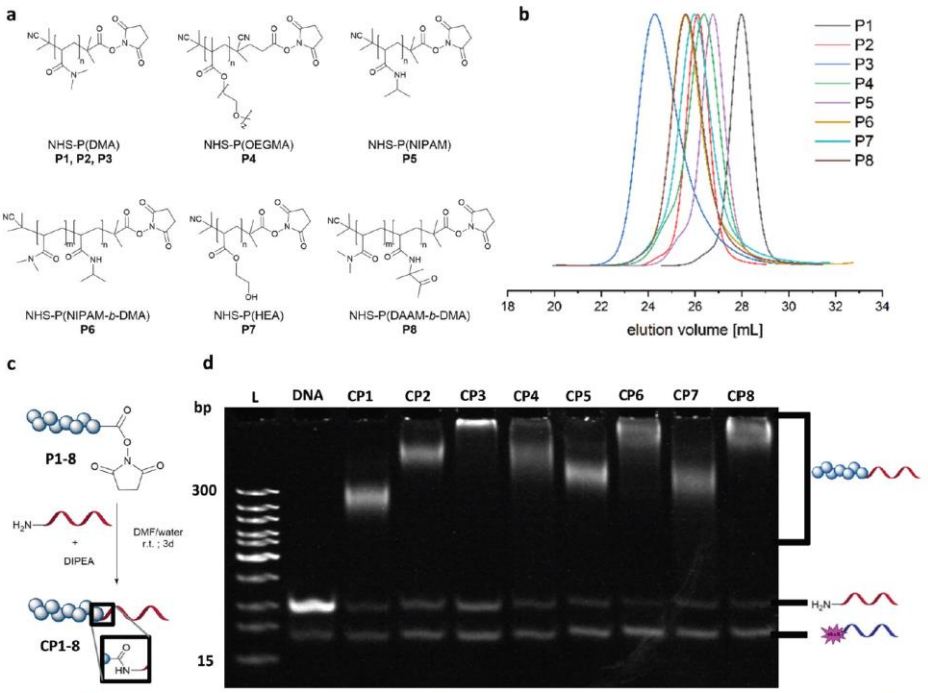

Fig. 2 (a) Obtained polymers after CTA group removal, containing the NHS group for bioconjugation to DNA. (B) GPC traces of the NHS polymers P1–P8 as measured by DMF GPC using polymethylmethacrylate (PMMA) as calibration standard. (c) Schematic representation of the coupling reaction of the generated NHS polymers with the 5′ amino oligonucleotide using DIPEA as the auxiliary base. (D) DNA and DNA–polymer conjugation reaction solutions analysed by 15% PAGE, stained with SYBR Gold. Complementary rhodamine DNA was used for hybridization to obtain better staining. L: DNA ladder; DNA: used 5′amino oligonucleotide; CP1–CP8: coupling reaction solutions of P1–P8 with 5′amino oligonucleotide (StA).

As with RAFT polymerization, the control over dispersity and chain length can be accomplished along with a wide selection of monomers and flexible end group modifications.[16,21] Polymerizations of DMA, NIPAM, HEA and DAAM were performed with 2-(dodecylthiocarbonothioylthio)-2-methylpropionic acid *N*-hydroxysuccinimide ester (NHS-DDMAT) acting as the chain transfer agent (CTA) in dioxane or DMF. Block co-polymerization consisting of hydrophobic P(DAAM) and hydrophilic P(DMA) were synthesized to demonstrate the robustness of the functionalization reaction and subsequent patterning. To prevent side reactions during the subsequent bioconjugation reaction with oligonucleotides, the CTA group of the NHS-polymers was removed post polymerization with an excess of azobisisobutyronitrile (AIBN) in dioxane at 75 °C. The obtained NHS–polymers revealed narrow molecular weight distributions ($Đ$ = 1.08–1.27, Table S3, ESI†) and a wide range of polymers with different molecular weights were synthesized (9.6–48.6 kDa, analysed by GPC (Fig. 2(b)). To perform the bioconjugation reaction of the NHS-functionalized polymers with the 5′amino oligonucleotide (complementary sticky A (StA^c; 5′-NH_2-TTTTCTCT ACCACCTACTA-3′)[13] or complementary sticky E (StE^c; 5′-NH_2-CAGTCAGTCAGTCAGTCAGT-3′)[15]) (Fig. 2c), the solvent has a high impact on the conversion. The accessibility of the reactive functionalities drives the reaction efficiency and therefore requires a good solvent that prevents aggregation of the polymer and the oligonucleotide chains. Optimization on the solvent conditions was performed in acetonitrile (ACN), dimethylformamide (DMF), water and mixtures thereof using **P2** as a model polymer, monitored by native polyacrylamide gel electrophoresis (PAGE) (Fig. S2 and S3, ESI†). In comparison, DMF : water (3 : 1) was the best reaction solvent to afford a conversion between 70–90% (Fig. 2d), quantified by integrating the band intensity of the PAGE gels (Fig. S1 and Table S2, ESI†). The PAGE revealed that the conversion depends on the chain length of the respective polymer, which is exemplarily shown for the DMA polymers (**P1–P3**) with increasing intensity of the unreacted 5′amino oligonucleotide. Comparing across polymer families, P(NIPAM-*b*-DMA) (**P6**) showed higher conversions than P(DMA) (**P2–P3**) and even the functionalization of P(OEGMA) (**P4**) proceeds well despite its brush like structure. Importantly, the reaction conditions were also robust for amphiphilic type block copolymer P(DAAM-*b*-DMA) **P8**, with an estimated conversion of ~90%.

Next, the DNA–polymer conjugates were patterned onto the surface of DNA origami nanotubes. First, the DNA–DMA conjugates of three different polymer chain length (**P1**: 9.6 kDa; **P2**:

View Article Online
Communication
Journal of Materials Chemistry B

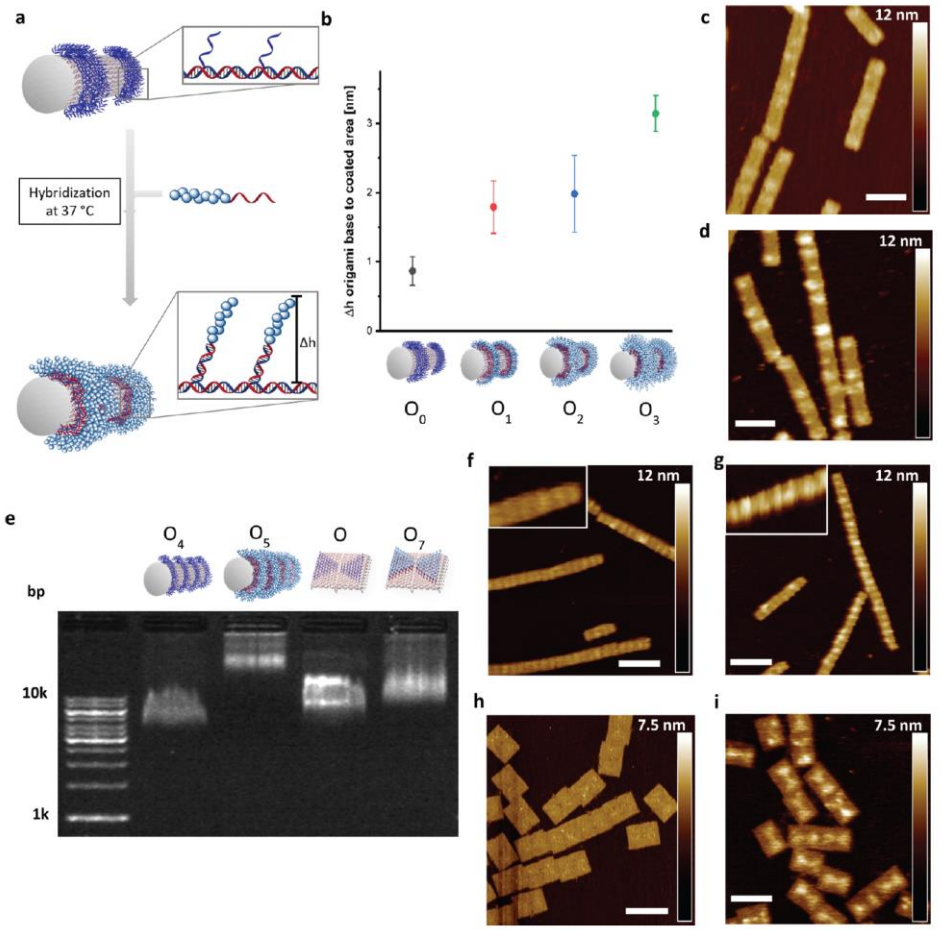

Fig. 3 (a) Schematic representation of the DNA–origami coating with DNA–polymer conjugates by hybridization at 37 °C. (b) Height changes of the DNA origami surface obtained *via* AFM, where the respective uncoated and the coated sections on the origami nanostructures were measured to obtain the height difference (n = 10 times for each coating). Heights from Fig. S5–S8 and Tables S4–S7. (c) Uncoated DNA–origami imaged by AFM. Scale bar = 80 nm. (d) DNA–origami coated with CP3 imaged by AFM. Scale bar = 80 nm. (e) Monitoring of the coated and uncoated DNA–origami tube and rectangle containing StA by 1% agarose gel, stained with SYBR Gold; L: DNA ladder; O_4: uncoated DNA–origami; O_5: coated DNA–origami with CP3; O_6: uncoated DNA–origami; O_7: coated DNA–origami with CP2. (f–i) Respective DNA–origami architectures uncoated and coated with the respective DNA–polymer conjugate; tube: CP3; rectangle: CP2. Scale bar = 120 nm.

22.1 kDa; **P3**: 48.6 kDa), were purified *via* spin filtration to remove unreacted amino oligonucleotides. Subsequently, the conjugates were hybridized to the DNA–origami tube containing patterned StA sequences (Fig. 3a). The attachment was performed in origami buffer (1 mM Na_2EDTA, 5 mM NaCl, 5 mM Tris, 12 mM $MgCl_2$ pH 8) at 37 °C for 1 h. The resulting architectures (**O_1**, **O_2**, **O_3**) were monitored *via* atomic force microscopy (AFM) to determine the height profile of the DMA coated DNA–origami against uncoated DNA–origami (**O_0**) (Fig. 3b). The increase in height as a function of polymer weight demonstrated successful hybridization of the polymer chains and showed a nonlinear dependence between polymer length and height change. The trend is expected due to the increase in chain collapse as the molecular weight of the polymer chains increases. As such, the z-axis contribution per monomer is weighted less as the polymer grows larger. The attachment of the polymers was independently characterized using agarose gel, with shifts in molecular weight to charge ratios corresponding to the size of the polymers used (Fig. S4, ESI†).

To show the flexibility to accommodate patterns of varying shapes and of different origami templates, a DNA–origami tube containing four StA rings (**O_4**) and a DNA–origami tile with two

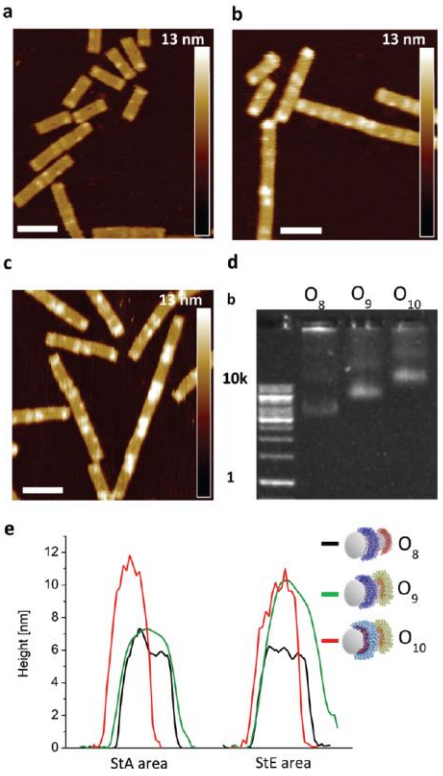

Fig. 4 (a) Uncoated DNA–origami (O_8) monitored *via* AFM. Scale bar = 100 nm (b) DNA–origami (O_9) with StE^c-P7 monitored *via* AFM. Scale bar = 100 nm (c) DNA–origami (O_{10}) coated with StE^c-P7 and CP2. Scale bar = 100 nm (d) Coated and uncoated DNA–origami monitored with 1% agarose gel, stained with SYBR Gold. O_8 is uncoated, O_9 is coated with StE^c-P7 and O_{10} is coated with CP2 and StE^c-P7. (e) AFM topographic images reveal a significant increase in height of the respective coating area.

StA triangles (**O_6**) were hybridized with **CP2** or **CP3** and imaged *via* AFM (Fig. 3f–i). The topological height change observed in the AFM image and the band shift in the agarose gel (Fig. 3e) indicate that the patterning of the polymeric architectures was successful, demonstrating the nanoscale resolution of the coating, even for larger (~50 kDa) DNA–polymer conjugates. Further customization can be achieved by using different sticky sequences to assemble different polymers onto a single nano-object. A DNA–origami tube patterned with StE and StA sequences (**O_8**) was hybridized with **StE^c-P7** conjugate and **CP2** (Fig. 4). The recognition between each set of sticky sequences and their complementary binding partners was characterized stepwise. Using **O_8**, hybridization was performed with **StE^c-P7** to form **O_9**. The attachment of **StE^c-P7** was observed *via* AFM only on one end of the DNA–origami tube resulting in a height difference of ~3–4 nm (Fig. 4e), thus underlining the specificity of the hybridization reaction. The influence of the attached polymers in terms of molecular weight and charge change of the DNA–origami were determined by agarose gel electrophoresis (Fig. 4d). With both **StE^c-P7** and **CP2** present, the designated two-ring structure was formed.

Collectively, we showed that the grafting to strategy present several advantages over the grafting from strategy. First, the polymers can be fully characterized prior to patterning. This allows us to attribute material characteristics to each polymer scaffold and composition. In addition, the methodology is more modular, where polymer combinations one origami can be easily achieved. Furthermore, the grafting to strategy showed better sustainability and cost effectiveness evaluated by Eco Scale,[22] a green metric factor (see ESI†).

In conclusion, we have introduced a robust grafting to procedure under ambient conditions with high conversions to achieve various DNA–polymer conjugates containing homo and block copolymers. These DNA–polymer conjugates from widely used polymer families (methacrylates acrylates and acrylamides) show conserved DNA-based recognition properties to their complementary sequences. The hybridization process was also not affected by the steric demand of the polymer chain, which was demonstrated by varying the molecular weight from ~10 kDa to 50 kDa. The attachment of the polymers to the DNA–origami was demonstrated on both tube and tile origamis. Different polymer chains, each equipped with a unique set of sticky sequences, can be attached onto each origami nano-object in a convenient manner also applicable for non-polymer chemists. With the rising importance of precisely engineered interfaces in nanotechnology and biomedicine, hybrid DNA–polymer conjugates remain one of the most accessible strategies to achieve coatings with nanoscale precision.

Conflicts of interest

There are no conflicts to declare.

Acknowledgements

The authors acknowledge the financial support by the Deutsche Forschungsgemeinschaft (DFG, German Research Foundation) – Project No. 364549901 – TRR 234 CataLight (B01) and the Max Planck Society for Open Access Funding.

References

1 J. M. Gibbs, S.-J. Park, D. R. Anderson, K. J. Watson, C. A. Mirkin and S. T. Nguyen, *J. Am. Chem. Soc.*, 2005, **127**, 1170–1178.
2 H. Kang, H. Liu, X. Zhang, J. Yan, Z. Zhu, L. Peng, H. Yang, Y. Kim and W. Tan, *Langmuir*, 2011, **27**, 399–408.
3 (*a*) F. E. Alemdaroglu, K. Ding, R. Berger and A. Herrmann, *Angew. Chem., Int. Ed.*, 2006, **45**, 4206–4210; (*b*) F. Cavalieri, A. Postma, L. Lee and F. Caruso, *ACS Nano*, 2009, **3**, 234–240.

4 T. R. Wilks, J. Bath, J. W. de Vries, J. E. Raymond, A. Herrmann, A. J. Turberfield and R. K. O'Reilly, *ACS Nano*, 2013, **7**, 8561–8572.
5 K. Isoda, N. Kanayama, M. Fujita, T. Takarada and M. Maeda, *Chem. – Asian J.*, 2013, **8**, 3079–3084.
6 Z. Zhao, L. Wang, Y. Liu, Z. Yang, Y.-M. He, Z. Li, Q.-H. Fan and D. Liu, *Chem. Commun.*, 2012, **48**, 9753–9755.
7 L. Yang, H. Sun, Y. Liu, W. Hou, Y. Yang, R. Cai, C. Cui, P. Zhang, X. Pan, X. Li, L. Li, B. S. Sumerlin and W. Tan, *Angew. Chem., Int. Ed.*, 2018, **130**, 17294–17298.
8 J. B. Knudsen, L. Liu, A. L. Bank Kodal, M. Madsen, Q. Li, J. Song, J. B. Woehrstein, S. F. J. Wickham, M. T. Strauss, F. Schueder, J. Vinther, A. Krissanaprasit, D. Gudnason, A. A. A. Smith, R. Ogaki, A. N. Zelikin, F. Besenbacher, V. Birkedal, P. Yin, W. M. Shih, R. Jungmann, M. Dong and K. V. Gothelf, *Nat. Nanotechnol.*, 2015, **10**, 892–898.
9 P. W. K. Rothemund, *Nature*, 2006, **440**, 297–302.
10 Y. Tokura, Y. Jiang, A. Welle, M. H. Stenzel, K. M. Krzemien, J. Michaelis, R. Berger, C. Barner-Kowollik, Y. Wu and T. Weil, *Angew. Chem., Int. Ed.*, 2016, **128**, 5786–5791.
11 P. Winterwerber, S. Harvey, D. Y. W. Ng and T. Weil, *Angew. Chem., Int. Ed.*, 2020, **59**, 6144–6149.
12 J. Zessin, F. Fischer, A. Heerwig, A. Kick, S. Boye, M. Stamm, A. Kiriy and M. Mertig, *Nano Lett.*, 2017, **17**, 5163–5170.
13 P. Winterwerber, C. J. Whitfield, D. Y. W. Ng and T. Weil, *Angew. Chem., Int. Ed.*, 2021, e202111226.
14 N. P. Agarwal, M. Matthies, F. N. Gür, K. Osada and T. L. Schmidt, *Angew. Chem., Int. Ed.*, 2017, **56**, 5460–5464.
15 J. Schill, B. J. H. M. Rosier, B. Gumí Audenis, E. Magdalena Estirado, T. F. A. de Greef and L. Brunsveld, *Angew. Chem., Int. Ed.*, 2021, **60**, 7612–7616.
16 T. Lückerath, K. Koynov, S. Loescher, C. J. Whitfield, L. Nuhn, A. Walther, C. Barner-Kowollik, D. Y. W. Ng and T. Weil, *Angew. Chem., Int. Ed.*, 2020, **59**, 15474–15479.
17 S. Hansson, V. Trouillet, T. Tischer, A. S. Goldmann, A. Carlmark, C. Barner-Kowollik and E. Malmström, *Biomacromolecules*, 2013, **14**, 64–74.
18 M. Safak, F. E. Alemdaroglu, Y. Li, E. Ergen and A. Herrmann, *Adv. Mater.*, 2007, **19**, 1499–1505.
19 (*a*) S. Maiez-Tribut, J. P. Pascault, E. R. Soulé, J. Borrajo and R. J. J. Williams, *Macromolecules*, 2007, **40**, 1268–1273; (*b*) K. G. Neoh and E. T. Kang, *Polym. Chem.*, 2011, **2**, 747–759.
20 A. Khan, T. H. Khan, A. M. El-Toni, A. Aldalbahi, J. Alam and T. Ahamad, *Mater. Lett.*, 2019, **235**, 197–201.
21 S. Goldmann, D. Quémener, P.-E. Millard, T. P. Davis, M. H. Stenzel, C. Barner-Kowollik and A. H. Müller, *Polymer*, 2008, **49**, 2274–2281.
22 K. Aken, L. Strekowski and L. Patiny, *Beilstein J. Org. Chem.*, 2006, **2**, 3.

III.II A VERSATILE AND EFFICIENT METHOD TO ISOLATE DNA–POLYMER CONJUGATES

Publication: **"A Versatile and Efficient Method to Isolate DNA–Polymer Conjugates"**

Authors: **Nico Alleva**, Katharina Eigen, David Y. W. Ng* and Tanja Weil*

Published in: ACS Macro Letters, **2023**, 12, 9, 1257-1263

DOI: 10.1021/acsmacrolett.3c00371

Date of Publication: 1st September 2023

Author Contribution:

Nico Alleva	Conceptualization, synthesis of all DNA-polymer conjugates used, testing all methods for successful purification of the conjugates, introducing and optimizing the AEC purification method for all DNA-polymer conjugates, performing all analytics. Writing the manuscript.
Katharina Eigen	Under the supervision of Nico Alleva she worked on her master thesis on this project and researched the basics of the method introducing the gradient into the method and tested several conditions and method lengths.
David Y. W. Ng/ Tanja Weil	The project was processed under the supervision of both; acquiring funding; edited manuscript

Funding Deutsche Forschungsgemeinschaft (DFG, German Research Foundation), Project No. 364549901-TRR 234 CataLight (B08), and the Max Planck Society for Open access Funding

Graphical Abstract:

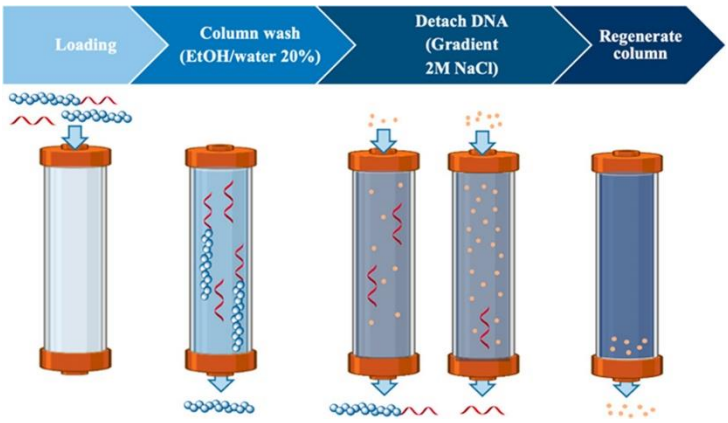

Summary:

DNA-polymer conjugates form a hybrid class of interesting properties by combining the definition of DNA with the attributes of polymers like responsiveness or phase separation. These conjugates develop increasing potential as materials for niche applications like biosensors or self-healing, responsive hydrogels. To create these conjugates, the *grafting to* strategy is commonly used as an upscale method to couple functionalized DNA to functionalized polymer chains. Here the advantage towards the *grafting from* method, is the pre-synthesis and analysis of the polymer leading to higher defined conjugates as well as bring more robust towards impurities during conjugate formations. The downside of this method is the difficult purification post conjugation due to the unreacted educts, which have normally similar chemical properties and molecular size hindering the separation.

This publication addresses the purification challenges by testing different purification methods and optimizing the protocol for broad applicability across different types of conjugates. After testing several purification methods like size exclusion chromatography (SEC), spin filtration, reverse phase HPLC (RP-HPLC), anion exchange chromatography emerged as the most promising method. Anion exchange chromatography allows the interaction of the negative charged molecules with the positive charged resin, whereby uncharged molecules can be removed. Initial experiments with a model conjugate demonstrated successful removal of polymers and efficient separation of conjugates from unreacted DNA during the elution step. By fine-tuning the sodium chloride solution gradient in the elution step, reliable separation was achieved, allowing for the potential reuse of unreacted DNA. Furthermore, the purification protocol was applied successful to several conjugates containing different sized polymer- as well as DNA-blocks.

ACS Macro Letters

pubs.acs.org/macroletters
Letter

A Versatile and Efficient Method to Isolate DNA–Polymer Conjugates

Nico Alleva, Katharina Eigen, David Y. W. Ng,* and Tanja Weil*

Cite This: ACS Macro Lett. 2023, 12, 1257–1263
Read Online

ABSTRACT: We present a facile and adaptable method to purify and isolate DNA–polymer conjugates from different uncharged homo, random, or block copolymer families. Anion exchange chromatography is used to separate the reaction solution and retrieve the excess unreacted polymer and oligonucleotide. The stationary phase has a high efficiency (25 nmol of DNA per run), facilitating the purification of large batches without compromising the peak shape and resolution. To demonstrate the versatility of this method, different types of polymers, including acrylates, methacrylates, and acrylamides containing hydrophilic and hydrophobic blocks, were purified with high yields. Additionally, DNA–polymer conjugates with various DNA block lengths were also successfully purified, further highlighting the broad applicability of this method.

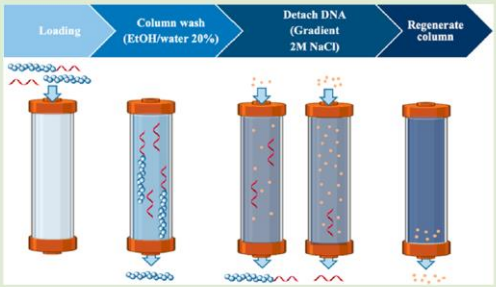

DNA–polymer conjugates have seen a significant expansion in recent years due to the increasing accessibility of DNA, resulting in seminal developments ranging from gene therapy[1,2] to drug delivery[3−6] and biosensing.[7−9] Exploiting the fidelity of DNA technology, they can be used to construct sophisticated shapes and patterns that are only a few nanometers in size, leading to new possibilities for the design and construction of precision nanoscale devices.[10,11] Furthermore, functional polymer or polymer-coated DNA architectures lead to an enhanced cellular uptake, thereby increasing pharmaceutical applications, for instance as drug carriers.[12−14] Additionally, by varying the length and composition, they can provide diverse architectures including micelles, vesicles, and tubes.[15] The individual control over the polymer and DNA length, composition, and chemical handles enables broad engineering of conjugate properties for targeted applications.[14,16]

To prepare DNA–polymer conjugates, the *grafting-to* method is commonly used, which involves using excess amounts of the less expensive polymer to achieve high conversion rates.[10,17−19] However, this often leads to the challenge of removing the unreacted polymer after the reaction. Because of the high amount of free polymer and the amphiphilic nature of the conjugates, spin filtration with molecular weight cutoffs often results in long purification times and major product loss.[10] Other methods such as reversed-phase high performance liquid chromatography (HPLC) easily reach their capacity limits, requiring extensive optimization of the stationary and mobile phases according to different polymer scaffolds and molecular weights. Alternatively, size exclusion chromatography (SEC) is particularly inefficient for smaller DNA blocks and the often amphiphilic nature of the conjugates.[20] As such, the full integration of polymer science into DNA nanotechnology has not been fully realized due to these pervasive challenges.

To address this limitation, we expand existing approaches of purifying DNA–polymer conjugates with strong anion exchange chromatography,[21,22] explore its broad applicability toward DNA lengths, different polymer scaffolds, and molecular weights, and compare it with other techniques like HPLC, SEC, and spin filtration. The strategy of this method relies on the negative charge of the DNA block to interact with the positively charged stationary phase. Excess uncharged polymer moves freely through the column and is eluted. Subsequent change in the mobile phase with a gradient of NaCl solution is used to elute DNA containing molecules and allows separation of the DNA–polymer conjugate from minor amounts of unreacted oligonucleotide. Within this method, polymers of three different polymer families (acrylates, acrylamides, and methacrylates) with molecular weight between 9 and 48 kDa were purified as well as conjugates with different DNA block lengths (10, 19, and 40 bases).

Adopting the *grafting-to* strategy, the polymer block is synthesized using polymerization techniques via reversible

Received: June 20, 2023
Accepted: August 29, 2023
Published: September 1, 2023

https://doi.org/10.1021/acsmacrolett.3c00371
ACS Macro Lett. 2023, 12, 1257−1263

ACS Macro Letters pubs.acs.org/macroletters Letter

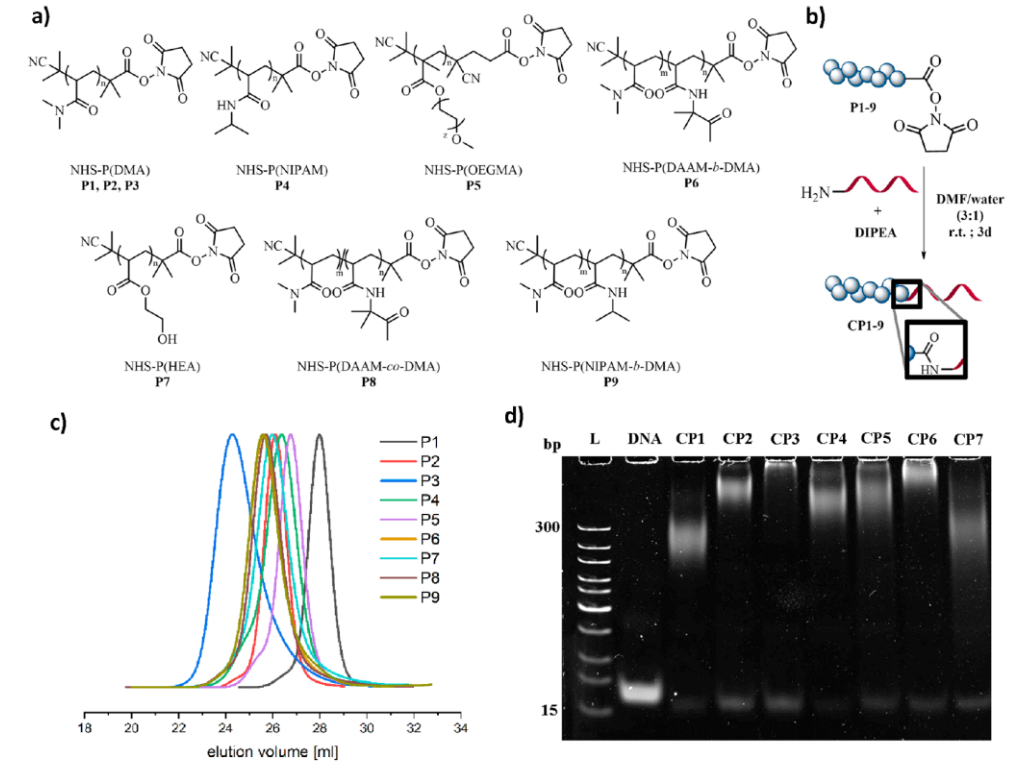

Figure 1. (a) Chemical structure of the NHS polymers used for coupling with the respective DNA. Synthesized via RAFT. (b) General reaction scheme of the NHS coupling to an amine-functionalized oligonucleotide. (c) Elution diagrams of the NHS polymers **P1**−**P9** as measured by DMF SEC using poly(methyl methacrylate) (PMMA) as standard. (d) PAGE gel of the obtained reaction solutions after coupling **P1**−**P7** to 19-base-long oligonucleotide. L: DNA ladder; DNA: used 19-base-long oligonucleotide; **CP1**−**CP7** respective coupling reaction solution of **P1**−**P7**. Using SYBR Gold for staining (2×).

addition−fragmentation chain transfer (RAFT), which incorporates a functional end-group. Subsequently, the polymer is covalently attached to a complementary functional group on the DNA block. In this case, the strategy was performed using NH_2-functionalized oligonucleotide and NHS-activated polymers prepared by RAFT polymerization.[10] The coupling was performed in a DMF/water (3:1) mixture using 50 equiv of the polymer, with DIPEA as an auxiliary base (Figure 1b). The reaction solution was analyzed using polyacrylamide gel electrophoresis (PAGE) to confirm the formation of the DNA−polymer conjugate and to monitor remaining oligonucleotides (Figures 1d and S22). Using the general conditions above, polymers (P(DMA), **P1**, 9.6 kDa; P(DMA), **P2**, 22 kDa; P(DMA), **P3**, 48 kDa; P(NIPAM), **P4**, 21 kDa; P(OEGMA), **P5**, 21 kDa; P(DAAM-*b*-DMA), **P6**, 26 kDa; P(HEA), **P7**, 22 kDa; P(DAAM-*co*-DMA) **P8**, 26 kDa; P(NIPAM-*b*-DMA) **P9**, 30 kDa) and DNA of various lengths (**SDNA**, 10 base long; **DNA**, 19 base long; **LDNA**, 40 base long) were prepared and coupled. P(DMA) (**P1**−**P3**) with varying molecular weights was selected to establish a reliable method and to investigate the impact of polymer block length on the conjugation efficiency. P(NIPAM) (**P4**) and P(HEA) (**P7**) were employed to demonstrate how changes in the properties of the polymer block, specifically hydrophilicity and hydrophobicity, affect the method. The brush-like P(OEGMA) (**P5**) represents a sterically demanding polymer which potentially influences the binding to the stationary phase. Block copolymers P(DAAM-*b*-DMA) (**P6**) and P(NIPAM-*b*-DMA) (**P9**) as well as random copolymer P(DAAM-*co*-DMA) (**P8**) were also included to demonstrate the robustness of the technique toward complex polymer designs. Additionally, DNA block lengths were varied to show the ease of method adaptation caused by charge and differences in hydrophilicity.

Following polymer to DNA coupling, DMF and DIPEA were removed via spin filtration, and the obtained solution was diluted with water to a final volume of 2 mL, from which 1 mL (25 nmol of DNA) is loaded onto the column (Cytiva HiRes Q 5/50; 5 × 50 mm^2 bed dimensions). The purification method contains several steps to prepare/equilibrate the column, separate the components of the reaction solution, and elute them fractionwise (Figure S1). Detection at 260 nm during purification takes into consideration the characteristic absorption of DNA.[23] Additionally, as the polymer absorbs mostly at 240 nm, it is also tracked simultaneously (Figure S2). To prepare the column, the stationary phase is initially washed and equilibrated with water (flow rate: 0.7 mL/min; 5 CV;

https://doi.org/10.1021/acsmacrolett.3c00371
ACS Macro Lett. 2023, 12, 1257−1263

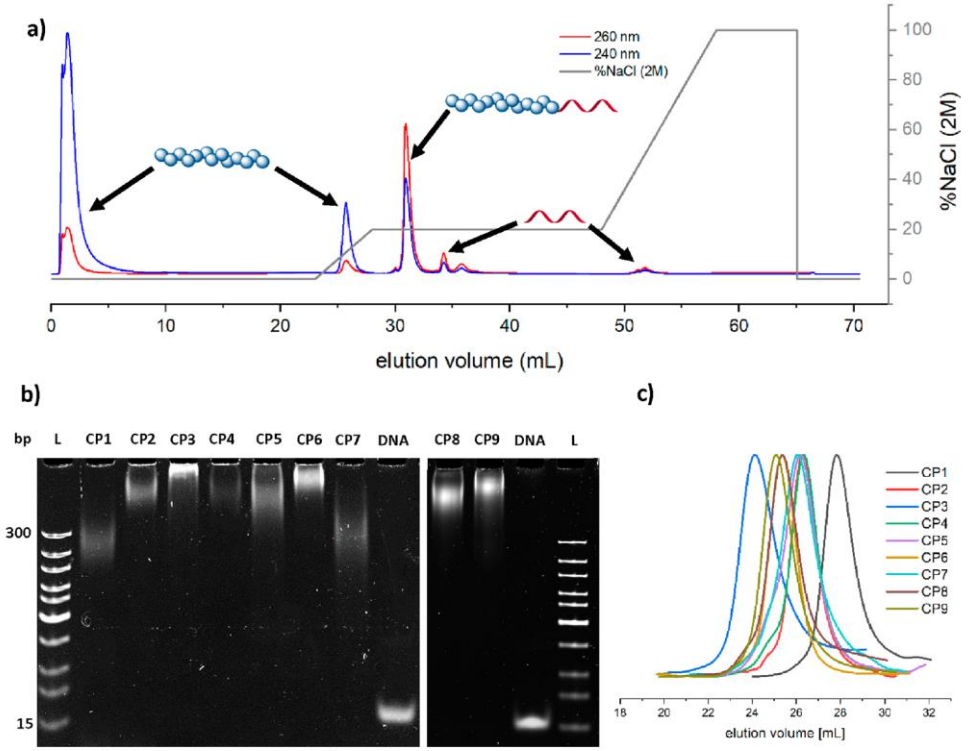

Figure 2. (a) Elution diagram of the **CP2** reaction solution run with contemporaneous detection of absorbance at 240 nm (polymer block) and 260 nm (oligonucleotide block). (b) PAGE gel electrophoresis of the respective purified conjugates **CP1−CP9**. L: DNA ladder; **CP1−CP9**: respective pure conjugates; DNA: 19-base oligonucleotide as comparison. Stained with SYBR Gold (2×). (c) Elution diagrams of the conjugates **CP1−CP9** measured by DMF SEC using poly(methyl methacrylate) (PMMA) as standard.

Figure S3) before loading with the diluted reaction solution (Figure S4). Both DNA and the DNA−polymer conjugate are negatively charged, allowing the molecules to bind to the positively charged resin.[24] The sample loading is achieved via a 1 mL sample loop and applying 3 mL of water as the loading volume. Subsequently, the column is washed with EtOH/water (20% EtOH, v/v, 20 CV) to remove the unbound, excess free polymer from the solution (Figure S5). Next, stepwise elution is performed by applying a NaCl gradient to control the separation of the bound components (Figure S6). Post elution, the column is washed with 2 M NaCl solution to remove any remaining bound components (Figure S7). Finally, the stationary phase is equilibrated with pure water, and a new run can begin (Figure S8). Because of the charged resin's high binding affinity towards DNA, 25 nmol of DNA per run can be purified without a loss of resolution or purity of the conjugate, despite the small size of the column.

The versatility of the method was demonstrated using NHS-functionalized polymers from three different monomer families (acrylates, methacrylates, and acrylamides) coupled to the 19-base oligonucleotide (Figure 1a). First, using DMA as the scaffold, the polymer length of P(DMA) was varied, comprising a short (P(DMA) ∼9.6 kDa; **P1**), middle (P(DMA) ∼22 kDa; **P2**), and a longer (P(DMA) ∼48 kDa; **P3**) chain to test if the purification remained robust. The elution diagram for the DNA−polymer conjugate **CP2** (Figure 2a) indicates that during loading and washing most of the polymer was successfully removed from the column. Subsequently, the eluent was changed to a gradient of NaCl (0−2 M) solution. As the NaCl solution concentration increases from 0 to 0.4 M, further unbound polymer was eluted from the column. At 0.4 M NaCl, the mobile phase was held isocratic to elute the DNA−polymer conjugate followed by the unreacted DNA oligonucleotide. Thereafter, gradient elution from 0.4 to 2 M NaCl was implemented to regenerate the stationary phase, removing any remaining bound components. Surprisingly, the elution diagrams (Figures 2a and S9−S10) showed no significant changes during purification of the corresponding DNA−polymer conjugates **CP1−CP3** (elution volumes: CP1, 31.3 mL; CP2, 31.0 mL; CP3, 30.3 mL). However, the trend shows that the larger the polymer block, the faster the conjugate elutes. We postulate that as the polymer segment increase in size, its collapsed volume increases correspondingly, which affects the accessibility to the DNA block and lowers the binding affinity to the stationary phase. Characterization of the purified DNA−P(DMA) conjugates via PAGE (Figure 2b) and SEC (Figure 2c) demonstrates the successful isolation. The respective yields range from ∼67% to quantitative (Table S2).

https://doi.org/10.1021/acsmacrolett.3c00371
ACS Macro Lett. 2023, 12, 1257−1263

ACS Macro Letters pubs.acs.org/macroletters Letter

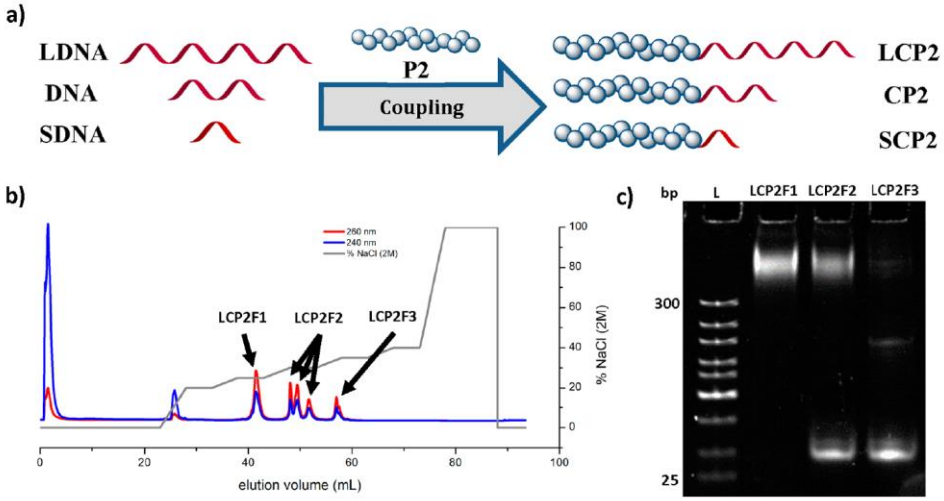

Figure 3. (a) Schematic representation of the coupling reaction of the generated NHS-P(DMA) (**P2**) to the oligonucleotides of different lengths (10, 19, and 40 bases). (b) Elution diagram of the method development profile of the **LCP2** reaction solution to find the optimal gradient for the conjugate elution. Here the gradient, starting at 20% was every 5 CV increased by 5% to 40%. (c) PAGE of the **LCP2** test run fractions as shown in b). L: DNA ladder; **LCP2F1−3**: respective fractions. Stained with SYBR Gold (2×).

Subsequently, the methodology was applied to a broader range of polymer species, including the more hydrophilic poly(hydroxyl acrylate) (P(HEA), ∼22 kDa; **P7**) and the more hydrophobic and thermoresponsive[25−27] poly(*N*-isopropylacrylamide) (P(NIPAM), ∼21 kDa; **P4**). Despite the varying hydrophilic character of the polymer block, the elution profiles of **CP4** and **CP7** had no significant impact on the separation efficiency (elution volume: **CP4**: 31.5 mL, Figure S11; **CP7**: 31.8 mL, Figure S14). Good to excellent yields were obtained for **CP4** (∼98%) and **CP7** (∼70%). The next attempt was to purify more sterically demanding DNA−polymer conjugates by using poly(oligo(ethylene glycol) methacrylate) (P(OEGMA), ∼21 kDa; **P5**). The elution profile remained unaffected during the purification process (Figure S12). The elution volume of **CP5** is 30.7 mL, with a yield of ∼63% (Table S2). The excess of unreacted brush-like polymer could also be eliminated, as confirmed by SEC (Figure 2c).

The established method was further tested with an amphiphilic block copolymer, which is known to undergo partial phase separation.[28] A diacetone acrylamide−DMA block copolymer (P(DAAM-*b*-DMA), ∼26 kDa; **P6**) and a *N*-isopropylacrylamide−DMA block copolymer (P(NIPAM-*b*-DMA), ∼30 kDa; **P9**) were synthesized, coupled to DNA to afford **CP6** and **CP9**, and purified using the proposed method. Consistent with the other polymer species tested, no major changes were noted during the purification step, as the elution volume is 31.1 mL for **CP6** (Figure S13) and 31.0 mL for **CP9** (Figure S17). An isolated yield of ∼60% for **CP6** and ∼72% for **CP9** was obtained, which was similar to that of the brush-like **CP5** conjugate. For comparative purposes, a random diacetone acrylamide−DMA copolymer (P(DAAM-*co*-DMA ∼26 kDa, **P8**) was subjected to coupling and purified, giving an elution time for **CP8** of 31.6 mL (Figure S16) and 93% yield. This enhanced yield could be attributed to the reduced phase separation of the polymer during the purification process. These results indicate the method's universal applicability for a broad range of water-soluble DNA/polymer conjugates with uncharged polymer segments.

Although the variation in polymer lengths and composition had a minimal impact on the chromatographic separation, the length of the DNA segment contributes to the total charge and should therefore influence the elution profile. To this end, we selected 10-base (NH_2-CCACCTACTA; **SDNA**) and 40-base (NH_2-GAAGATAAAAACATTTGATTTTTTCTCTACCACCTACTA; **LDNA**) oligonucleotides in addition to the 19-base counterpart (Figure 3a). With the different oligonucleotides, polymer **P2** was used as the model polymer and coupled to the DNA strand via the same NHS chemistry. As an initial assessment, PAGE confirmed the successful reactions (Figure 4a). For the purification of the long DNA−polymer conjugate, we used the same gradient optimized for the 19-base oligonucleotide (Figure S15). However, unlike the 19-base DNA−polymer conjugates, the 40-base counterpart (**LCP2**) eluted at a high retention volume (51−53 mL) together with the unreacted oligonucleotide at higher NaCl concentrations (0.85−1.2 M). Hence, the gradient was modified in order to resolve the separation. We developed a stepwise gradient method to identify the optimal NaCl concentration for elution (Figure 3b). The individual peak fractions were collected, and PAGE was performed to identify the components (Figure 3c). We found that 0.5 M NaCl was the optimal concentration to selectively elute the conjugate, **LCP2**. Using this knowledge, the original elution diagram was modified with a gradient run until 0.5 M, which was then held isocratic to successfully separate the conjugate **LCP2** from the free oligonucleotide (Figure 4b). Because of the gradient adjustment, which was necessary for **LCP2**, we applied a similar approach for **SCP2** by reducing the gradient to 0.3 M NaCl (Figure 4d), resulting in pure conjugate as verified via PAGE gel analysis (Figure 4e). This experiment series demonstrates the method's ease and flexibility in purifying DNA−polymer conjugates with varying DNA block lengths commonly used within DNA nano-

https://doi.org/10.1021/acsmacrolett.3c00371
ACS Macro Lett. 2023, 12, 1257−1263

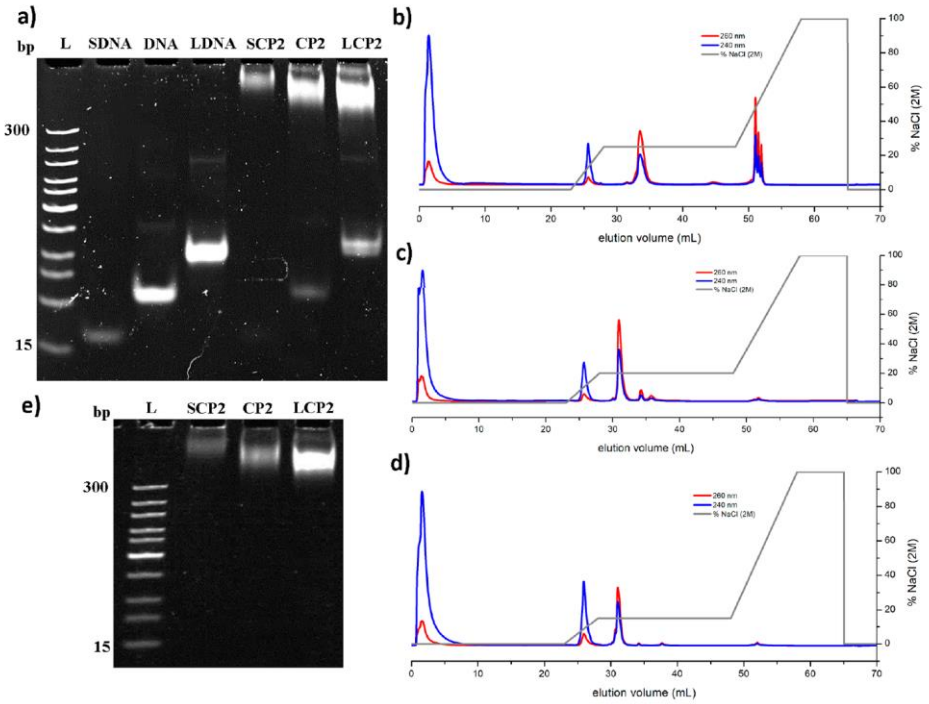

Figure 4. (a) PAGE gel electrophoresis of the pure oligonucleotides and of the reaction solutions after coupling with **P2**. L: DNA ladder; **SDNA**: short oligonucleotide (10 base long); **DNA**: middle oligonucleotide (19 base long); **LDNA**: long oligonucleotide (40 base long); **SCP2**: reaction solution of **P2** coupled with **SDNA**; **CP2**: reaction solution of **P2** coupled with DNA; **LCP2**: reaction solution of **P2** coupled with **LDNA**. Stained with SYBR Gold (2×). (b–d) Elution diagram of the whole purification run of the coupling reactions of **LCP2**, **CP2**, and **SCP2** with **P2** with contemporaneous detection of absorbance at 240 nm (polymer block) and 260 nm (oligonucleotide block). (b) **LDNA** reaction solution. (c) **DNA** reaction solution. (d) **SDNA** reaction solution. (e) PAGE gel electrophoresis of the obtained pure conjugates of **SCP2**, **CP2**, and **LCP2**. L: DNA ladder; **SCP2**/**CP2**/**LCP2**: pure conjugate of the respective conjugate was obtained after purification. Stained with SYBR Gold (2×).

technology. Based on straightforward method development protocols, further variation of the DNA block lengths can be easily resolved by the NaCl gradient during elution.

Using **CP2** as a model DNA–polymer conjugate, we compare our method against analytical scale HPLC and SEC as well as with spin filtration alone. The HPLC studies (Jupiter C18, 5 μm, 300 Å) were performed first using the reaction mixture of **CP2** (8 μL, 1 nmol), containing 75% (v/v) DMF. Stepwise gradient of acetonitrile/water elution shows several peaks divided into five fractions (F1: 1.25–3.75 mL; F2: 16–16.8 mL; F3: 16.8–17.8 mL; F4: 19–21 mL; F5: 22–22.6 mL) (Figure S18d,e). PAGE gel (Figure S18f) revealed an incomplete separation of the unreacted oligonucleotide and **CP2**. While F1 shows no conjugate or DNA, F2–F4 include **CP2** as well as unreacted oligonucleotide, whereas F5 contains only **CP2**. Intensity measurements of the bands revealed a yield of 13% for F5 (Table S5). Removal of DMF by spin filtration prior to HPLC separation did not improve the peak resolution (Figure S19). However, the yields of pure fractions F3 and F4 were increased to 45% (Table S5). These results show that even in an analytical scale, purification of **CP2** and separation from unreacted oligonucleotide are not optimal. Separate attempts using analytical SEC performed with 8 μL (1 nmol) reaction solution of CP2 fail to show visible separation due to the large excess of polymer (50 equiv) present (Figure S20). Purification solely by the spin filtration method (8 cycles) with 10 and 30 kDa molecular weight cutoff were similarly unsuccessful. In each case, the PAGE gel (Figure S21) indicated the continued presence of free oligonucleotide after purification. Overall, these methods present very limited success in isolating pure DNA–polymer conjugates.

The purification efficiency of the method relies on the accessibility of the DNA block to the anionic stationary phase, which is in turn dictated by the length of the polymer block and the steric component of the side-chains. Given a fixed oligonucleotide length of 19 bases, purification efficiency decreases with increasing polymer length (yields: **CP1** (~9.6 kDa, quantitative), **CP2** (~22 kDa, 96%), **CP3** (~48 kDa, 67%)). Second, polymers with side-chain bulk such as that of P(OEGMA), **CP5**, or amphiphilic block copolymers like **CP6** reduced the ionic interactions between the oligonucleotide to the column, which in turn lowered the yields. In general, polymers with a molecular weight between 10 and 50 kDa with small, homogeneous side-chains are ideal for this purification method.

In conclusion, we have introduced a versatile and adaptable purification method with high efficiency to purify DNA–polymer conjugates containing various classes of polymers

https://doi.org/10.1021/acsmacrolett.3c00371
ACS Macro Lett. 2023, 12, 1257–1263

(acrylates, methacrylates, and acrylamides) and oligonucleotide lengths. Compared to other performed methods like HPLC, spin filtration, or SEC, anion exchange chromatography consistently provides high yields in preparative scale. The purification method is largely independent of the polymer, and even sterically demanding, brush-like DNA–polymer conjugates were isolated successfully. Moreover, complex DNA–polymer conjugates like DNA–P(DAAM-*b*-DMA) and P-(NIPAM-*b*-DMA), with a high tendency to phase separate, could also be purified without loss in resolution. The purification of DNA blocks of different lengths is easily adaptable, which will widen the range of applications of this method in the community. As the unreacted oligonucleotide can also be separated, reuse would also be possible. This reported approach is reliable for water-soluble, noncharged polymer block within DNA–polymer conjugates and can be scaled according to the column dimensions holding the stationary phase. The increased ease of purification and isolation of DNA–polymer conjugates will create greater access and application in nanoscale engineering, biomedicine, and polymer science.

■ ASSOCIATED CONTENT

Supporting Information

The Supporting Information is available free of charge at https://pubs.acs.org/doi/10.1021/acsmacrolett.3c00371.

Detailed information about the polymer synthesis, the coupling reactions, and the purification method (PDF)

■ AUTHOR INFORMATION

Corresponding Authors

David Y. W. Ng – *Max Planck Institute for Polymer Research, 55128 Mainz, Germany;* orcid.org/0000-0002-0302-0678; Email: david.ng@mpip-mainz.mpg.de

Tanja Weil – *Max Planck Institute for Polymer Research, 55128 Mainz, Germany;* orcid.org/0000-0002-5906-7205; Email: weil@mpip-mainz.mpg.de

Authors

Nico Alleva – *Max Planck Institute for Polymer Research, 55128 Mainz, Germany*

Katharina Eigen – *Max Planck Institute for Polymer Research, 55128 Mainz, Germany*

Complete contact information is available at: https://pubs.acs.org/10.1021/acsmacrolett.3c00371

Author Contributions

CRediT: **Nico Alleva** conceptualization, data curation, formal analysis, investigation, methodology, supervision, visualization, writing-original draft, writing-review & editing; **Katharina Eigen** data curation, investigation, writing-review & editing; **David Y.W. Ng** conceptualization, funding acquisition, investigation, project administration, resources, supervision, writing-original draft, writing-review & editing; **Tanja Weil** conceptualization, funding acquisition, investigation, project administration, resources, supervision, writing-original draft, writing-review & editing.

Funding

Open access funded by Max Planck Society.

Notes

The authors declare no competing financial interest.

■ ACKNOWLEDGMENTS

The authors acknowledge the financial support by the Deutsche Forschungsgemeinschaft (DFG, German Research Foundation), Project No. 364549901-TRR 234 CataLight (B08), and the Max Planck Society for Open access Funding.

■ REFERENCES

(1) Ogris, M.; Walker, G.; Blessing, T.; Kircheis, R.; Wolschek, M.; Wagner, E. Tumor-targeted gene therapy: strategies for the preparation of ligand-polyethylene glycol-polyethylenimine/DNA complexes. *J. Controlled Release* **2003**, *91* (1–2), 173–181.

(2) Alemdaroglu, F. E.; Alemdaroglu, N. C.; Langguth, P.; Herrmann, A. DNA Block Copolymer Micelles – A Combinatorial Tool for Cancer Nanotechnology. *Adv. Mater.* **2008**, *20* (5), 899–902.

(3) Kang, H.; Liu, H.; Zhang, X.; Yan, J.; Zhu, Z.; Peng, L.; Yang, H.; Kim, Y.; Tan, W. Photoresponsive DNA-cross-linked hydrogels for controllable release and cancer therapy. *Langmuir* **2011**, *27* (1), 399–408.

(4) Kedracki, D.; Maroni, P.; Schlaad, H.; Vebert-Nardin, C. Polymer-Aptamer Hybrid Emulsion Templating Yields Bioresponsive Nanocapsules. *Adv. Funct. Mater.* **2014**, *24* (8), 1133–1139.

(5) Rodríguez-Pulido, A.; Kondrachuk, A. I.; Prusty, D. K.; Gao, J.; Loi, M. A.; Herrmann, A. Light-triggered sequence-specific cargo release from DNA block copolymer-lipid vesicles. *Angew. Chem., Int. Ed.* **2013**, *52* (3), 1008–1012.

(6) Pokholenko, O.; Gissot, A.; Vialet, B.; Bathany, K.; Thiéry, A.; Barthélémy, P. Lipid oligonucleotide conjugates as responsive nanomaterials for drug delivery. *J. Mater. Chem.. B* **2013**, *1* (39), 5329–5334.

(7) Gibbs, J. M.; Park, S.-J.; Anderson, D. R.; Watson, K. J.; Mirkin, C. A.; Nguyen, S. T. Polymer-DNA hybrids as electrochemical probes for the detection of DNA. *J. Am. Chem. Soc.* **2005**, *127* (4), 1170–1178.

(8) Chen, T.; Wu, C. S.; Jimenez, E.; Zhu, Z.; Dajac, J. G.; You, M.; Han, D.; Zhang, X.; Tan, W. DNA micelle flares for intracellular mRNA imaging and gene therapy. *Angew. Chem., Int. Ed.* **2013**, *52* (7), 2012–2016.

(9) Yu, S.; Dong, R.; Chen, J.; Chen, F.; Jiang, W.; Zhou, Y.; Zhu, X.; Yan, D. Synthesis and self-assembly of amphiphilic aptamer-functionalized hyperbranched multiarm copolymers for targeted cancer imaging. *Biomacromolecules* **2014**, *15* (5), 1828–1836.

(10) Alleva, N.; Winterwerber, P.; Whitfield, C. J.; Ng, D. Y. W.; Weil, T. Nanoscale patterning of polymers on DNA origami. *J. Mater. Chem. B* **2022**, *10* (37), 7512–7517.

(11) Tokura, Y.; Jiang, Y.; Welle, A.; Stenzel, M. H.; Krzemien, K. M.; Michaelis, J.; Berger, R.; Barner-Kowollik, C.; Wu, Y.; Weil, T. Bottom-Up Fabrication of Nanopatterned Polymers on DNA Origami by In Situ Atom-Transfer Radical Polymerization. *Angew. Chem., Int. Ed.* **2016**, *55*, 5692–5697.

(12) Winterwerber, P.; Whitfield, C. J.; Ng, D. Y. W.; Weil, T. Multi-Wellenlängen-Photopolymerisation von stabilen Poly(katecholamin)-DNA-Origami-Nanostrukturen. *Angew. Chem., Int. Ed.* **2022**, *61*, No. e202111226.

(13) Sun, H.; Yang, L.; Thompson, M. P.; Schara, S.; Cao, W.; Choi, W.; Hu, Z.; Zang, N.; Tan, W.; Gianneschi, N. C. Recent Advances in Amphiphilic Polymer-Oligonucleotide Nanomaterials via Living/Controlled Polymerization Technologies. *Bioconjugate chem.* **2019**, *30* (7), 1889–1904.

(14) Whitfield, C. J.; Zhang, M.; Winterwerber, P.; Wu, Y.; Ng, D. Y. W.; Weil, T. Functional DNA-Polymer Conjugates. *Chem. Rev.* **2021**, *121*, 11030–11084.

(15) Peterson, A. M.; Heemstra, J. M. Controlling self-assembly of DNA-polymer conjugates for applications in imaging and drug delivery. *Wiley Interdiscip. Rev.: Nanomed. Nanobiotechnol* **2015**, *7*, 282–297.

(16) Lueckerath, T.; Strauch, T.; Koynov, K.; Barner-Kowollik, C.; Ng, D. Y. W.; Weil, T. DNA-Polymer Conjugates by Photoinduced RAFT Polymerization. *Biomacromolecules* **2019**, *20*, 212−221.
(17) Peng, L.; Wu, C. S.; You, M.; Han, D.; Chen, Y.; Fu, T.; Ye, M.; Tan, W. Engineering and Applications of DNA-Grafting Polymer Materials. *Chem. Sci.* **2013**, *4*, 1928−1938.
(18) Oh, J. S.; Wang, Y.; Pine, D. J.; Yi, G.-R. High-Density PEO- b -DNA Brushes on Polymer Particles for Colloidal Superstructures. *Chem. Mater.* **2015**, *27*, 8337−8344.
(19) Hansson, S.; Trouillet, V.; Tischer, T.; Goldmann, A. S.; Carlmark, A.; Barner-Kowollik, C.; Malmström, E. Grafting efficiency of synthetic polymers onto biomaterials: a comparative study of grafting-from versus grafting-to. *Biomacromolecules* **2013**, *14*, 64−74.
(20) Rubner, M. M.; Achatz, D. E.; Mader, H. S.; Stolwijk, J. A.; Wegener, J.; Harms, G. S.; Wolfbeis, O. S.; Wagenknecht, H.-A. DNA "Nanolamps": "Clicked" DNA Conjugates with Photon Upconverting Nanoparticles as Highly Emissive Biomaterial. *ChemPlusChem.* **2012**, *77*, 129−134.
(21) Zimmermann, J.; Kwak, M.; Musser, A. J.; Herrmann, A. Amphiphilic DNA Block Copolymers: Nucleic Acid-Polymer Hybrid Materials for Diagnostics and Biomedicine. In *Bioconjugation Protocols*; Humana Press: 2011; pp 239−266.
(22) Kwak, M.; Gao, J.; Prusty, D. K.; Musser, A. J.; Markov, V. A.; Tombros, N.; Stuart, M. C. A.; Browne, W. R.; Boekema, E. J.; ten Brinke, G.; Jonkman, H. T.; van Wees, B. J.; Loi, M. A.; Herrmann, A. DNA Block Copolymer Doing It All: From Selection to Self-Assembly of Semiconducting Carbon Nanotubes. *Angew. Chem., Int. Ed.* **2011**, *50* (14), 3206−3210.
(23) Gallagher, S. R.; Desjardins, P. R. Quantitation of DNA and RNA with absorption and fluorescence spectroscopy. *Curr. Protoc. Mol. Biol.* **2006**, *76*, Appendix 3, Appendix 3D,.
(24) Budelier, K.; Schorr, J. Purification of DNA by anion-exchange chromatography. *Curr. Protoc. Mol. Biol.* **1998**, Chapter 2, Unit2.1B,.
(25) Murata, M.; Kaku, W.; Anada, T.; Soh, N.; Katayama, Y.; Maeda, M. Thermo responsive DNA/Polymer Conjugate for Intelligent Antisense Strategy. *Chem. Lett.* **2003**, *32*, 266−267.
(26) Feng, C.; Zhu, T.; Jiang, Z.; Ren, C.; Ma, Y. Temperature−regulated non-monotonic behavior of DNA immobilization on poly(N−isopropylacrylamide) (PNIPAm)−grafted surface. *Colloids Surf., A* **2022**, *640*, No. 128507.
(27) Yang, T.; Fu, J.; Zheng, S.; Yao, H.; Jin, Y.; Lu, Y.; Liu, H. Biomolecular logic devices based on stimuli-responsive PNIPAM-DNA film electrodes and bioelectrocatalysis of natural DNA with Ru(bpy)32+ as mediator. *Biosens. Bioelectron.* **2018**, *108*, 62−68.
(28) Lückerath, T.; Koynov, K.; Loescher, S.; Whitfield, C. J.; Nuhn, L.; Walther, A.; Barner-Kowollik, C.; Ng, D. Y. W.; Weil, T. DNA-Polymer Nanostructures by RAFT Polymerization and Polymerization-Induced Self-Assembly. *Angew. Chem., Int. Ed.* **2020**, *59*, 15474−15479.

https://doi.org/10.1021/acsmacrolett.3c00371
ACS Macro Lett. 2023, 12, 1257−1263

III.III EXCURSUS: PEPTIDE BISPECIFICS INHIBITING HIV-1 INFECTION BY AN ORTHOGONAL CHEMICAL AND SUPRAMOLECULAR STRATEGY

Publication:	**"Peptide Bispecifics Inhibiting HIV-1 Infection by an Orthogonal Chemical and Supramolecular Strategy"**
Authors:	Dominik Schauenburg[#], Fabian Zech[#], Astrid Johanna Heck, Pascal von Maltitz, Mirja Harms, Siska Führer, **Nico Alleva**, Jan Münch, Seah Ling Kuan*, Frank Kirchhoff*, and Tanja Weil*
Published in:	Bioconjugate Chemistry, **2023**, 34, 9, 1645–1652
DOI:	10.1021/acs.bioconjchem.3c00314
Date of Publication:	4th September 2023

Author Contribution:

Dominik Schauenburg	Upscaling the synthesis of the bis-sulfone-PEG-maleimide linker and the conjugation of the VIRIP to the bis-sulfone-PEG-maleimide linker. He performed material characterization (LC-MS, ESI, NMR). He was involved in scientific discussions and wrote large parts of the manuscript.
Fabian Zech	Preparation of the overview schematics and performed the infection and toxicity assays presented in Figures 2A/B, 5, S15, and S16.
Astrid Heck	Initiation of the project. She designed, planned and performed the synthesis of the bis-sulfone-PEG-maleimide linker. She was synthesizing the biotin-PEG-SH and performed the bioconjugation of the different peptides: Biotin-JM#173, biotin-VIRIP and the bispecific Biotin-VIRIP-JM#173. Furthermore, she was characterizing biotinylated peptides using HABA assay and assembled them onto a Nav protein platform. She performed material characterization (LC-MS, ESI, MALDI, NMR, HPLC). She contributed to scientific discussions and wrote parts of the manuscript.

Pascal von Maltitz	Performing pre-experiments to confirm that the activity of JM#173 C was retained after modification. The validation of modified B-EPI-X4 JM#173 C and SAv-EPI-X4 JM#173 C contributed to Figure 5.
Mirja Harms	Performing pre-experiments to confirm that the activity of JM#173 C was retained after modification. The validation of modified B-EPI-X4 JM#173 C and SAv-EPI-X4 JM#173 C contributed to Figure 5.
Siska Führer	Upscaling the bioconjugation of the biotin-VIRIP and was involved in scientific discussions and the manuscript preparation.
Nico Alleva	Performed AFM analytic to visualizing the self-assembling and calculated the dispersity of the unconjugated and conjugated platform
Jan Münch	Co-conceived the study and assisted in writing the manuscript.
Seah Ling Kuan	Design and discussion of the concept, experimental design and results. Editing of the manuscript. S. L. Kuan was supervising A. J. Heck, D. Schauenburg and S. Führer
Frank Kirchhoff	Supervision, acquiring funding for the project, design and discussion of the concept and results. Editing of the manuscript.
Tanja Weil	Supervision, acquiring funding for the project, design and discussion of the concept and results. Editing of the manuscript.

Funding Deutsche Forschungsgemeinschaft (DFG, German Research Foundation)–Project number 316249678–SFB 1279 (TW: SFB 1279 A05, C01; FK: A05, JM: A06). The authors thank the mass spectrometry facility at MPIP for MS measurements. F.Z. was funded by the “Bausteinprogramm”, project number: L.SBN.0225, of Ulm University. M.H. was funded by programs for female scientists of the Equal Opportunities Unit and by the “Bausteinprogramm”, project number: L.SBN.0209, of Ulm University. M.H. also receives funding from the Baden-Württemberg Foundation.

Graphical Abstract:

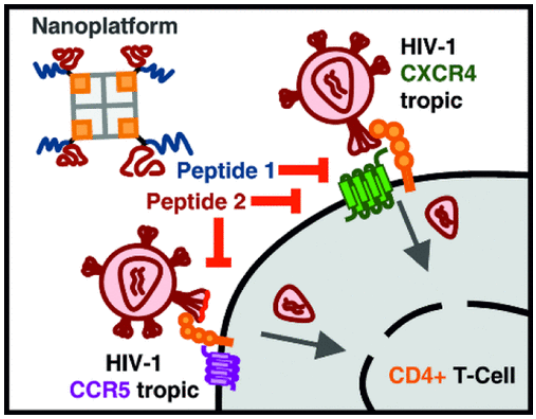

Summary and contribution:

Apart from DNA nanotechnology, alternative approaches are being explored to engineer controllable, self-assembling systems for biochemical reactions. Peptides, in particular, are frequently utilized for the assembly and construction of supramolecular systems capable of specific interactions with targets such as viruses. Therefore, various peptide chains can be combined forming a multivalent system with multifunctionality. Herein, streptavidin as a nanoplatform to assemble different peptide sidechains containing biotin as an affinity group. After assembling, the functional peptide sidechains protrude from the surface and interacts with the respective target. In this study, the targeted interaction demonstrates inhibitory activity against HIV-1 variants. This approach underscores the potential of assembling peptides with diverse modes of action onto a nanoplatform, resulting in multifunctionality and broadening the scope of target interactions.

To visualize and confirm the assembly and connection of peptides, atomic force microscopy (AFM) can be employed. In this study, I conducted AFM measurements to monitor the assembly process and estimate size distribution by analyzing average height.

Given the more distant relationship between peptide assembly and DNA nanotechnology, the article and supporting information have been included in the appendix.

IV. CONCLUSION AND FUTURE PERSPECTIVES

The objective of this thesis was to develop a straightforward method for creating DNA-polymer conjugates, thereby increasing their accessibility and enabling new applications for these promising hybrid materials. The principal achievements of this research are (1) the accessibility of DNA-polymer conjugates through the implementation of a straightforward and reliable grafting technique and (2) a novel purification method utilizing anion exchange chromatography, which is capable of purifying a diverse range of conjugates possessing varying properties and block sizes. In this way, polymers were patterned onto DNA-origami architectures using an annealing strategy, enabling the creation of precisely defined nanostructures that even allowed the generation of multiple polymer patterns assembled on a single DNA nanostructure. Despite the challenges associated with the formation of DNA-polymer conjugates via the grafting strategy, including low yields due to steric hindrance from the polymer chain and DNA sequence, the advantages of this approach, including high controllability and definition of the resulting conjugates, outweigh these limitations. Consequently, a universal optimization strategy of this process was devised, resulting in the ability to generate amphiphilic and sterically demanding conjugates with high yields, which can be purified based on the newly established purification protocol using anion exchange chromatography. These functional DNA-polymer conjugates offer the opportunity to functionalize DNA origami in a precise manner, thereby introducing novel properties to these hybrid nanoobjects.

The first project sought to identify the optimal reaction parameters for the grafting strategy, which involves the coupling of DNA sequences to polymers. The selected model reaction involved the coupling of an amino- to an NHS-group, whereby the polymer was modified with an NHS group and the DNA sequence was amino functionalized. The NHS functionalization is a well-established, commercially available method that is readily accessible and highly reliable. Following the synthesis of a model polymer (P(DMA); MW: 20 kDa) via RAFT polymerization, with the NHS group appended, the reaction was tested in a number of conditions. The grafting technique typically yields low levels of success, largely due to the steric hindrance of the chains towards the functional groups. Furthermore, the disparity in polarity between DNA and the polymer necessitated careful consideration to address solubility issues. Evaluation of different reaction solvents revealed that DMF:water (3:1) yielded the most promising results, with high yields observed. These conditions were then applied to polymers from three distinct monomer families (methacrylates, acrylates, and acrylamides) with highly successful results. Following

these findings, the purification process was optimized with the objective of enhancing existing isolation methods through the implementation of high-throughput techniques. A DNA-P(DMA) conjugate was employed as a representative model to evaluate the efficacy of various purification techniques, including SEC, RP-HPLC, and spin filtration. The results demonstrated that these techniques were not optimal. Anion exchange chromatography was identified as a potentially viable alternative, offering a straightforward method for the removal of uncharged polymers following their loading into the column. Further refinement, incorporating a sodium chloride solution gradient, facilitated the successful separation of unreacted DNA and conjugates, thereby enabling the reuse of unreacted DNA. The developed purification protocol was successfully employed to effectively purify a diverse array of DNA-polymer conjugates, encompassing both phase-separating and thermo-responsive variants, with high yields. Furthermore, the methodology was readily applicable to conjugates comprising diverse DNA and polymer block sizes, with gradient modifications tailored to enhance outcomes corresponding to varying DNA lengths.

In the next part, the functionalized DNA-polymer conjugates were used to functionalize the surface of diverse DNA-origami nanostructures through annealing, resulting in highly defined patterns with nanometer resolution. This demonstrated the programmability of these hybrid materials. A variety of origami architectures, including rectangles and tubes, were successfully modified with multiple polymer patterns. In order to expand the library of patterns, DNA-origami were modified with patterns in ring and rectangle shape, thereby confirming the generality of this new strategy. AFM studies revealed a distinct, dense polymer pattern with nanometer resolution, even for high molecular weight DNA-polymer conjugates. Furthermore, the conjugates were used to create multiple patterning of different polymers on one DNA architecture, which was utilized by different complementary DNA sequences to introduce programmable multifunctionality.

The expertise gained in the characterization of self-assembling biohybrid nanostructures is also relevant to the characterization of other self-assembling nanostructures. For example, in a collaborative effort, the protein streptavidin formed a precise supramolecular complex with HIV-1 inhibitory peptides. This nanostructure was characterized by atomic force microscopy (AFM) both before and after assembly, providing essential insights into structural features, size parameters and dispersity after assembly.

In light of prospective applications, DNA-polymer nanostructures present a number of promising avenues, particularly in the context of biomedical applications. The emergence of the SARS-CoV-2 virus and the subsequent development of novel RNA vaccines have elevated the profile of

DNA/RNA-based materials within the field of modern pharmaceuticals. Nonetheless, challenges emerged in vaccine applications, such as instability, which had to be addressed through extensive RNA modifications or encapsulation within liposomes. Consequently, DNA-polymer materials may present an attractive alternative due to their enhanced stability and their capacity to form morphologies that stabilize DNA through steric shielding effects. Nevertheless, the successful realization of these applications is contingent upon the reliability and precision of the material formation process. Our research indicates that an effective approach to the assembly of DNA-polymer hybrid materials is the optimization of reaction conditions in order to facilitate scalability and the production of highly pure materials. This is of particular importance in the context of medical applications, given the necessity for rigorous purity standards. By combining the aforementioned synthesis method with the recently developed purification protocol, it is possible to obtain these bioconjugates in a very high degree of purity. A significant advantage of this purification protocol is its scalability, which permits the purification of larger batches without compromising resolution or peak separation.

The findings presented in this thesis pave the way for the synthesis of a diverse range of DNA-polymer conjugates through a single formation strategy. The use of DNA-polymer conjugates as functional materials or for the surface functionalization of diverse DNA architectures is a promising avenue of research. By leveraging the precision of DNA annealing, these conjugates enable the creation of 3D DNA-polymer architectures with nanometer resolution, which may be of interest for diverse applications in nanotechnology and medicine. This work introduces the integration of DNA-polymer conjugates into applications requiring access to large-scale, very pure materials, thereby expanding the potential for DNA nanotechnology.

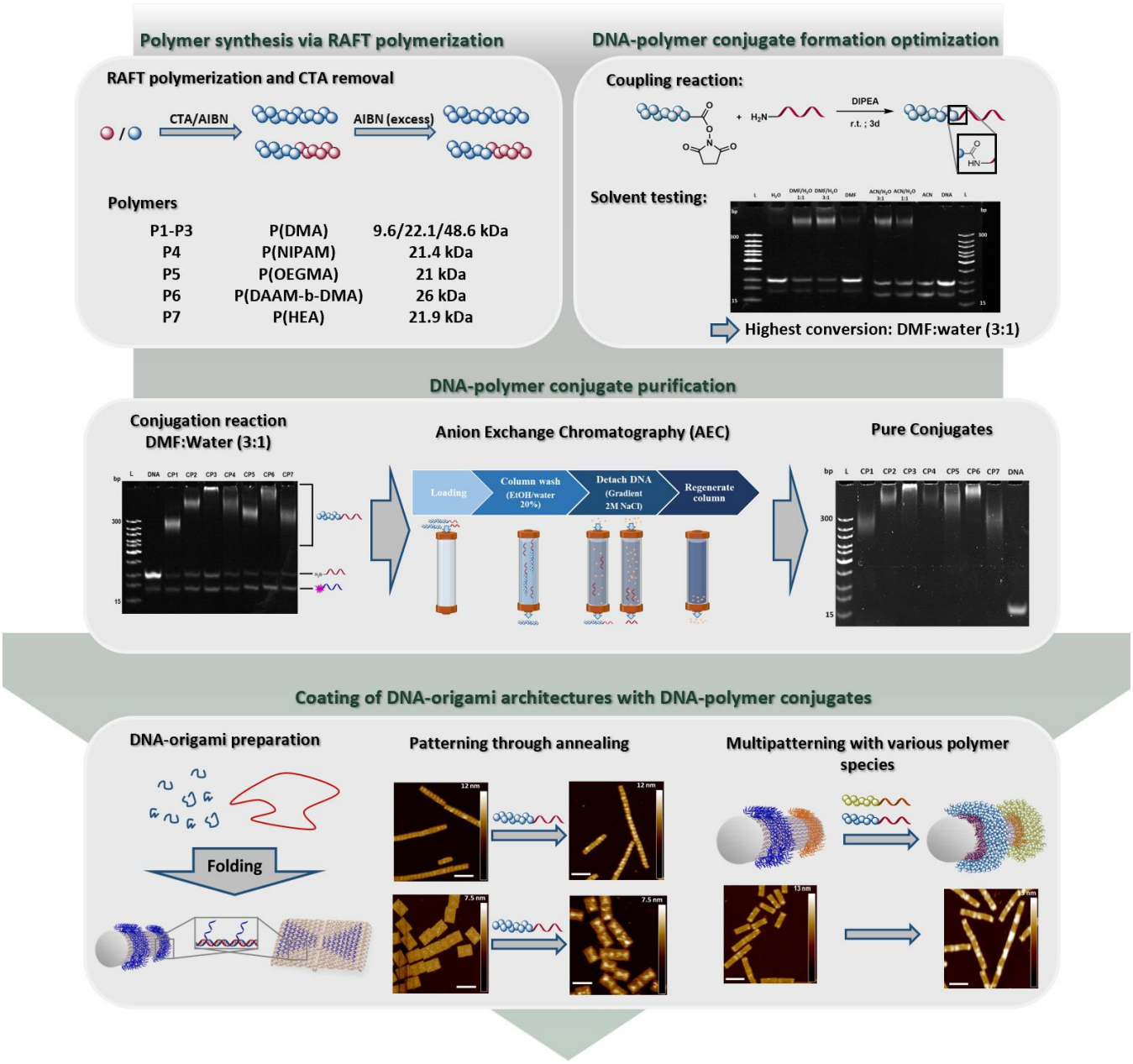

Figure 13: Schematic presentation about the applied strategies and obtained results to create DNA-polymer conjugates and the usage to create polymer patterns on DNA-origami surface with nanometer resolution.

V. REFERENCES

(1) *Raus aus der Plastikfalle: Wie du deinen Plastic Footprint reduzieren kannst - Rachel Salt - Google Books*. https://books.google.de/books?hl=de&lr=&id=SE-5EAAAQBAJ&oi=fnd&pg=PP1&dq=plastikproduktion+weltweit+2023&ots=_kGxBpu5NE&sig=pUJf-rMq_E8Gd_WsSod76JtSqjQ#v=onepage&q=plastikproduktion%20weltweit%202023&f=false (accessed 2024-04-02).

(2) Handbook of Radical Polymerization. *Handbook of Radical Polymerization* **2002**. https://doi.org/10.1002/0471220450.

(3) *The Chemistry of Radical Polymerization - Graeme Moad, D.H. Solomon - Google Books*. https://books.google.de/books?hl=de&lr=&id=EPA0NcrQIOIC&oi=fnd&pg=PP1&dq=radical+polymerization+mechanism&ots=OJphXHpKuh&sig=7GWhVSeEjldNkCHqwB3elvJgrcA#v=onepage&q=radical%20polymerization%20mechanism&f=false (accessed 2024-04-02).

(4) *Anionic Polymerization: Principles and Practice - Maurice Morton - Google Books*. https://books.google.de/books?hl=de&lr=&id=IhBjOTVx6MIC&oi=fnd&pg=PP1&dq=anionic+polymerization&ots=8xIrQ-OkK1&sig=oK4nQxJXNyINjXyC1mjmLRjk01A#v=onepage&q=anionic%20polymerization&f=false (accessed 2024-04-02).

(5) Hadjichristidis, N.; Pitsikalis, M.; Pispas, S.; Iatrou, H. Polymers with Complex Architecture by Living Anionic Polymerization. *Chem Rev* **2001**, *101* (12), 3747–3792. https://doi.org/10.1021/CR9901337.

(6) Hong, K.; Uhrig, D.; Mays, J. W. Living Anionic Polymerization. *Curr Opin Solid State Mater Sci* **1999**, *4* (6), 531–538. https://doi.org/10.1016/S1359-0286(00)00011-5.

(7) Corrigan, N.; Jung, K.; Moad, G.; Hawker, C. J.; Matyjaszewski, K.; Boyer, C. Reversible-Deactivation Radical Polymerization (Controlled/Living Radical Polymerization): From Discovery to Materials Design and Applications. *Prog Polym Sci* **2020**, *111*, 101311. https://doi.org/10.1016/J.PROGPOLYMSCI.2020.101311.

(8) Shipp, D. A. Reversible-Deactivation Radical Polymerizations. *Polymer Reviews* **2011**, *51* (2), 99–103. https://doi.org/10.1080/15583724.2011.566406.

(9) Ouchi, M.; Sawamoto, M. Sequence-Controlled Polymers via Reversible-Deactivation Radical Polymerization. *Polymer Journal 2018 50:1* **2017**, *50* (1), 83–94. https://doi.org/10.1038/pj.2017.66.

(10) Tokura, Y.; Jiang, Y.; Welle, A.; Stenzel, M. H.; Krzemien, K. M.; Michaelis, J.; Berger, R.; Barner-Kowollik, C.; Wu, Y.; Weil, T. Bottom-Up Fabrication of Nanopatterned Polymers on DNA Origami by In Situ Atom-Transfer Radical Polymerization. *Angewandte Chemie* **2016**, *128* (19), 5786–5791. https://doi.org/10.1002/ANGE.201511761.

(11) Kato, M.; Kamigaito, M.; Sawamoto, M.; Higashimura, T. Polymerization of Methyl Methacrylate with the Carbon Tetrachloride/Dichlorotris-(Triphenylphosphine)Ruthenium(II)/ Methylaluminum Bis(2,6-Di-Tert-Butylphenoxide)

Initiating System: Possibility of Living Radical Polymerization. *Macromolecules* **1995**, *28* (5), 1721–1723. https://doi.org/10.1021/MA00109A056.

(12) Wang, J. S.; Matyjaszewski, K. Controlled/"Living" Radical Polymerization. Atom Transfer Radical Polymerization in the Presence of Transition-Metal Complexes. *J Am Chem Soc* **1995**, *117* (20), 5614–5615. https://doi.org/10.1021/JA00125A035.

(13) Peng, C. H.; Kong, J.; Seeliger, F.; Matyjaszewski, K. Mechanism of Halogen Exchange in ATRP. *Macromolecules* **2011**, *44* (19), 7546–7557. https://doi.org/10.1021/MA201035U.

(14) Tang, W.; Matyjaszewski, K. Kinetic Modeling of Normal ATRP, Normal ATRP with [CuII]0, Reverse ATRP and SR&NI ATRP. *Macromol Theory Simul* **2008**, *17* (7–8), 359–375. https://doi.org/10.1002/MATS.200800050.

(15) Tang, W.; Matyjaszewski, K. Effect of Ligand Structure on Activation Rate Constants in ATRP. *Macromolecules* **2006**, *39* (15), 4953–4959. https://doi.org/10.1021/MA0609634.

(16) Afonso, M. B. A.; Cruz, T. R.; Silva, Y. F.; Pereira, J. C. A.; Machado, A. E. H.; Goi, B. E.; Lima-Neto, B. S.; Carvalho-Jr, V. P. Ruthenium(II) Complexes of Schiff Base Derived from Cycloalkylamines as Pre-Catalysts for ROMP of Norbornene and ATRP of Methyl Methacrylate. *J Organomet Chem* **2017**, *851*, 225–234. https://doi.org/10.1016/J.JORGANCHEM.2017.09.043.

(17) Lee, J.; Grandner, J. M.; Engle, K. M.; Houk, K. N.; Grubbs, R. H. In Situ Catalyst Modification in Atom Transfer Radical Reactions with Ruthenium Benzylidene Complexes. *J Am Chem Soc* **2016**, *138* (22), 7171–7177. https://doi.org/10.1021/JACS.6B03767.

(18) Maria, S.; Biedroń, T.; Poli, R.; Kubisa, P. Atom Transfer Radical Polymerization of Methyl Acrylate with Molybdenum Halides as Catalysts in an Ionic Liquid. *J Appl Polym Sci* **2007**, *105* (1), 278–281. https://doi.org/10.1002/APP.26046.

(19) Stoffelbach, F.; Haddleton, D. M.; Poli, R. Controlled Radical Polymerization of Alkyl Acrylates and Styrene Using a Half-Sandwich Molybdenum(III) Complex Containing Diazadiene Ligands. *Eur Polym J* **2003**, *39* (11), 2099–2105. https://doi.org/10.1016/S0014-3057(03)00152-6.

(20) Mukumoto, K.; Li, Y.; Nese, A.; Sheiko, S. S.; Matyjaszewski, K. Synthesis and Characterization of Molecular Bottlebrushes Prepared by Iron-Based ATRP. *Macromolecules* **2012**, *45* (23), 9243–9249. https://doi.org/10.1021/MA3020867.

(21) Wang, Y.; Zhang, Y.; Parker, B.; Matyjaszewski, K. ATRP of MMA with Ppm Levels of Iron Catalyst. *Macromolecules* **2011**, *44* (11), 4022–4025. https://doi.org/10.1021/MA200771R.

(22) Simakova, A.; Averick, S. E.; Konkolewicz, D.; Matyjaszewski, K. Aqueous ARGET ATRP. *Macromolecules* **2012**, *45* (16), 6371–6379. https://doi.org/10.1021/MA301303B.

(23) Pan, J. L.; Li, Z.; Zhang, L. F.; Cheng, Z. P.; Zhu, X. L. Iron-Mediated AGET ATRP of Styrene and Methyl Methacrylate Using Ascorbic Acid Sodium Salt as Reducing Agent. *Chinese Journal of Polymer Science (English Edition)* **2014**, *32* (8), 1010–1018. https://doi.org/10.1007/S10118-014-1481-2/METRICS.

(24) Paterson, S. M.; Brown, D. H.; Chirila, T. V.; Keen, I.; Whittaker, A. K.; Baker, M. V. The Synthesis of Water-Soluble PHEMA via ARGET ATRP in Protic Media. *J Polym Sci A Polym Chem* **2010**, *48* (18), 4084–4092. https://doi.org/10.1002/POLA.24194.

(25) Lou, Q.; Shipp, D. A. Recent Developments in Atom Transfer Radical Polymerization (ATRP): Methods to Reduce Metal Catalyst Concentrations. *ChemPhysChem* **2012**, *13* (14), 3257–3261. https://doi.org/10.1002/CPHC.201200166.

(26) Wang, Y.; Han, G.; Duan, W.; Zhang, W. ICAR ATRP in PEG with Low Concentration of Cu(II) Catalyst: A Versatile Method for Synthesis of Block Copolymer Nanoassemblies under Dispersion Polymerization. *Macromol Rapid Commun* **2019**, *40* (2), 1800140. https://doi.org/10.1002/MARC.201800140.

(27) Konkolewicz, D.; Magenau, A. J. D.; Averick, S. E.; Simakova, A.; He, H.; Matyjaszewski, K. ICAR ATRP with Ppm Cu Catalyst in Water. *Macromolecules* **2012**, *45* (11), 4461–4468. https://doi.org/10.1021/MA300887R.

(28) Pan, X.; Malhotra, N.; Dadashi-Silab, S.; Matyjaszewski, K.; Pan, X.; Malhotra, N.; Dadashi-Silab, S.; Matyjaszewski, K. A Simplified Fe-Based PhotoATRP Using Only Monomers and Solvent. *Macromol Rapid Commun* **2017**, *38* (13), 1600651. https://doi.org/10.1002/MARC.201600651.

(29) Chmielarz, P.; Fantin, M.; Park, S.; Isse, A. A.; Gennaro, A.; Magenau, A. J. D.; Sobkowiak, A.; Matyjaszewski, K. Electrochemically Mediated Atom Transfer Radical Polymerization (EATRP). *Prog Polym Sci* **2017**, *69*, 47–78. https://doi.org/10.1016/J.PROGPOLYMSCI.2017.02.005.

(30) Kutahya, C.; Aykac, F. S.; Yilmaz, G.; Yagci, Y. LED and Visible Light-Induced Metal Free ATRP Using Reducible Dyes in the Presence of Amines. *Polym Chem* **2016**, *7* (39), 6094–6098. https://doi.org/10.1039/C6PY01417H.

(31) Liu, X.; Zhang, L.; Cheng, Z.; Zhu, X. Metal-Free Photoinduced Electron Transfer–Atom Transfer Radical Polymerization (PET–ATRP) via a Visible Light Organic Photocatalyst. *Polym Chem* **2016**, *7* (3), 689–700. https://doi.org/10.1039/C5PY01765C.

(32) Nicolas, J.; Guillaneuf, Y.; Lefay, C.; Bertin, D.; Gigmes, D.; Charleux, B. Nitroxide-Mediated Polymerization. *Prog Polym Sci* **2013**, *38* (1), 63–235. https://doi.org/10.1016/J.PROGPOLYMSCI.2012.06.002.

(33) Grubbs, R. B. Nitroxide-Mediated Radical Polymerization: Limitations and Versatility. *Polymer Reviews* **2011**, *51* (2), 104–137. https://doi.org/10.1080/15583724.2011.566405.

(34) Sciannamea, V.; Jérôme, R.; Detrembleur, C. In-Situ Nitroxide-Mediated Radical Polymerization (NMP) Processes: Their Understanding and Optimization. *Chem Rev* **2008**, *108* (3), 1104–1126. https://doi.org/10.1021/CR0680540.

(35) Siegenthaler, K. O.; Studer, A. Nitroxide-Mediated Radical Polymerization/Increase of Steric Demand in Nitroxides. How Much Is Too Much? *Macromolecules* **2006**, *39* (4), 1347–1352. https://doi.org/10.1021/MA0513463.

(36) Hawker, C. J.; Bosman, A. W.; Harth, E. New Polymer Synthesis by Nitroxide Mediated Living Radical Polymerizations. *Chem Rev* **2001**, *101* (12), 3661–3688. https://doi.org/10.1021/CR990119U.

(37) Fleischmann, S.; Komber, H.; Appelhans, D.; Voit, B. I. Synthesis of Functionalized NMP Initiators for Click Chemistry: A Versatile Method for the Preparation of Functionalized Polymers and Block Copolymers. *Macromol Chem Phys* **2007**, *208* (10), 1050–1060. https://doi.org/10.1002/MACP.200700046.

(38) Wu, L.; Glebe, U.; Böker, A. Surface-Initiated Controlled Radical Polymerizations from Silica Nanoparticles, Gold Nanocrystals, and Bionanoparticles. *Polym Chem* **2015**, *6* (29), 5143–5184. https://doi.org/10.1039/C5PY00525F.

(39) Chevigny, C.; Gigmes, D.; Bertin, D.; Jestin, J.; Boué, F. Polystyrene Grafting from Silica Nanoparticles via Nitroxide-Mediated Polymerization (NMP): Synthesis and SANS Analysis with the Contrast Variation Method. *Soft Matter* **2009**, *5* (19), 3741–3753. https://doi.org/10.1039/B906754J.

(40) Lee, Y.; Boyer, C.; Kwon, M. S. Photocontrolled RAFT Polymerization: Past, Present, and Future. *Chem Soc Rev* **2023**, *52* (9), 3035–3097. https://doi.org/10.1039/D1CS00069A.

(41) Keddie, D. J. A Guide to the Synthesis of Block Copolymers Using Reversible-Addition Fragmentation Chain Transfer (RAFT) Polymerization. *Chem Soc Rev* **2013**, *43* (2), 496–505. https://doi.org/10.1039/C3CS60290G.

(42) Barner-Kowollik, C.; Buback, M.; Charleux, B.; Coote, M. L.; Drache, M.; Fukuda, T.; Goto, A.; Klumperman, B.; Lowe, A. B.; Mcleary, J. B.; Moad, G.; Monteiro, M. J.; Sanderson, R. D.; Tonge, M. P.; Vana, P. Mechanism and Kinetics of Dithiobenzoate-Mediated RAFT Polymerization. I. The Current Situation. *J Polym Sci A Polym Chem* **2006**, *44* (20), 5809–5831. https://doi.org/10.1002/POLA.21589.

(43) Perrier, S.; Takolpuckdee, P.; Westwood, J.; Lewis, D. M. Versatile Chain Transfer Agents for Reversible Addition Fragmentation Chain Transfer (RAFT) Polymerization to Synthesize Functional Polymeric Architectures. *Macromolecules* **2004**, *37* (8), 2709–2717. https://doi.org/10.1021/MA035468B.

(44) Destarac, M. On the Critical Role of RAFT Agent Design in Reversible Addition-Fragmentation Chain Transfer (RAFT) Polymerization. *Polymer Reviews* **2011**, *51* (2), 163–187. https://doi.org/10.1080/15583724.2011.568130.

(45) Boyer, C.; Bulmus, V.; Davis, T. P.; Ladmiral, V.; Liu, J.; Perrier, S. Bioapplications of RAFT Polymerization. *Chem Rev* **2009**, *109* (11), 5402–5436. https://doi.org/10.1021/CR9001403.

(46) Reyhani, A.; Nothling, M. D.; Ranji-Burachaloo, H.; McKenzie, T. G.; Fu, Q.; Tan, S.; Bryant, G.; Qiao, G. G. Blood-Catalyzed RAFT Polymerization. *Angewandte Chemie International Edition* **2018**, *57* (32), 10288–10292. https://doi.org/10.1002/ANIE.201802544.

(47) Chen, M.; Moad, G.; Rizzardo, E. Thiocarbonylthio End Group Removal from RAFT-Synthesized Polymers by a Radical-Induced Process. *J Polym Sci A Polym Chem* **2009**, *47* (23), 6704–6714. https://doi.org/10.1002/POLA.23711.

(48) Moad, G.; Rizzardo, E.; Thang, S. H. End-Functional Polymers, Thiocarbonylthio Group Removal/Transformation and Reversible Addition–Fragmentation–Chain Transfer (RAFT) Polymerization. *Polym Int* **2011**, *60* (1), 9–25. https://doi.org/10.1002/PI.2988.

(49) Postma, A.; Davis, T.; Moad, G.; Macromolecules, M. O. 39; S.-; 2005, undefined. Thermolysis of RAFT-Synthesized Polymers. A Convenient Method for Trithiocarbonate Group Elimination. *academia.eduA Postma, TP Davis, G Moad, MS O@# 39; SheaMacromolecules, 2005•academia.edu*.

(50) Barner-Kowollik, Christopher. Handbook of RAFT Polymerization. 543.

(51) Willcock, H.; O'Reilly, R. K. End Group Removal and Modification of RAFT Polymers. *Polym Chem* **2010**, *1* (2), 149–157. https://doi.org/10.1039/B9PY00340A.

(52) Watson, J. D.; Crick, F. H. C. Molecular Structure of Nucleic Acids: A Structure for Deoxyribose Nucleic Acid. *Nature 1953 171:4356* **1953**, *171* (4356), 737–738. https://doi.org/10.1038/171737a0.

(53) *DNA Structure and Function - Richard R. Sinden - Google Books*. https://books.google.de/books?hl=de&lr=&id=Q6Yd-qYvx9UC&oi=fnd&pg=PR17&dq=dna+structure&ots=XlYCTjWoam&sig=xHmxkEIKyGT6ucTd8W00fGUskgI#v=onepage&q=dna%20structure&f=false (accessed 2024-04-02).

(54) Ghosh, A.; Bansal, M. A Glossary of DNA Structures from A to Z. *urn:issn:0907-4449* **2003**, *59* (4), 620–626. https://doi.org/10.1107/S0907444903003251.

(55) Seeman, N. C. Nucleic Acid Junctions and Lattices. *J Theor Biol* **1982**, *99* (2), 237–247. https://doi.org/10.1016/0022-5193(82)90002-9.

(56) Song, Q.; Hu, Y.; Yin, A.; Wang, H.; Yin, Q. DNA Holliday Junction: History, Regulation and Bioactivity. *International Journal of Molecular Sciences 2022, Vol. 23, Page 9730* **2022**, *23* (17), 9730. https://doi.org/10.3390/IJMS23179730.

(57) Shlyakhtenko, L. S.; Potaman, V. N.; Sinden, R. R.; Gall, A. A.; Lyubchenko, Y. L. Structure and Dynamics of Three-Way DNA Junctions: Atomic Force Microscopy Studies. *Nucleic Acids Res* **2000**, *28* (18), 3472–3477. https://doi.org/10.1093/NAR/28.18.3472.

(58) Wilkinson, S.; Diechtierow, M.; Estabrook, R. A.; Schmidt, F.; Hüben, M.; Weinhold, E.; Reich, N. O. Molecular Scale Architecture: Engineered Three- and Four-Way Junctions. *Bioconjug Chem* **2008**, *19* (2), 470–475. https://doi.org/10.1021/BC700270K.

(59) Seeman, N. C. DNA Components for Molecular Architecture. *Acc Chem Res* **1997**, *30* (9), 357–363. https://doi.org/10.1021/AR9601407/ASSET/AR9601407.FP.PNG_V03.

(60) Feldkamp, U.; Niemeyer, C. M. Rational Design of DNA Nanoarchitectures. *Angewandte Chemie International Edition* **2006**, *45* (12), 1856–1876. https://doi.org/10.1002/ANIE.200502358.

(61) Rothemund, P. W. K. Folding DNA to Create Nanoscale Shapes and Patterns. *Nature 2006 440:7082* **2006**, *440* (7082), 297–302. https://doi.org/10.1038/nature04586.

(62) Kuzuya, A.; Komiyama, M. DNA Origami: Fold, Stick, and Beyond. *Nanoscale* **2010**, *2* (3), 309–321. https://doi.org/10.1039/B9NR00246D.

(63) Saccà, B.; Niemeyer, C. M. DNA Origami: The Art of Folding DNA. *Angewandte Chemie International Edition* **2012**, *51* (1), 58–66. https://doi.org/10.1002/ANIE.201105846.

(64) Hong, F.; Zhang, F.; Liu, Y.; Yan, H. DNA Origami: Scaffolds for Creating Higher Order Structures. *Chem Rev* **2017**, *117* (20), 12584–12640. https://doi.org/10.1021/ACS.CHEMREV.6B00825.

(65) Castro, C. E.; Kilchherr, F.; Kim, D. N.; Shiao, E. L.; Wauer, T.; Wortmann, P.; Bathe, M.; Dietz, H. A Primer to Scaffolded DNA Origami. *Nature Methods 2011 8:3* **2011**, *8* (3), 221–229. https://doi.org/10.1038/nmeth.1570.

(66) Wang, X.; Li, S.; Jun, H.; John, T.; Zhang, K.; Fowler, H.; Doye, J. P. K.; Chiu, W.; Bathe, M. Planar 2D Wireframe DNA Origami. *Sci Adv* **2022**, *8* (20), 39. https://doi.org/10.1126/SCIADV.ABN0039.

(67) Douglas, S. M.; Dietz, H.; Liedl, T.; Högberg, B.; Graf, F.; Shih, W. M. Self-Assembly of DNA into Nanoscale Three-Dimensional Shapes. *Nature 2009 459:7245* **2009**, *459* (7245), 414–418. https://doi.org/10.1038/nature08016.

(68) Ke, Y.; Douglas, S. M.; Liu, M.; Sharma, J.; Cheng, A.; Leung, A.; Liu, Y.; Shih, W. M.; Yan, H. Multilayer DNA Origami Packed on a Square Lattice. *J Am Chem Soc* **2009**, *131* (43), 15903–15908. https://doi.org/10.1021/JA906381Y.

(69) Ke, Y.; Voigt, N. V.; Gothelf, K. V.; Shih, W. M. Multilayer DNA Origami Packed on Hexagonal and Hybrid Lattices. *J Am Chem Soc* **2012**, *134* (3), 1770–1774. https://doi.org/10.1021/JA209719K.

(70) Ke, Y.; Bellot, G.; Voigt, N. V.; Fradkov, E.; Shih, W. M. Two Design Strategies for Enhancement of Multilayer–DNA-Origami Folding: Underwinding for Specific Intercalator Rescue and Staple-Break Positioning. *Chem Sci* **2012**, *3* (8), 2587–2597. https://doi.org/10.1039/C2SC20446K.

(71) Chandrasekhar, S.; Prakash, P. S.; Schmidt, T. L. Stability and Stabilization of DNA Nanostructures in Biomedical Applications. *DNA Origami: Structures, Technology, and Applications* **2022**, 333–377. https://doi.org/10.1002/9781119682561.CH16.

(72) Zhang, F.; Jiang, S.; Wu, S.; Li, Y.; Mao, C.; Liu, Y.; Yan, H. Complex Wireframe DNA Origami Nanostructures with Multi-Arm Junction Vertices. *Nature Nanotechnology 2015 10:9* **2015**, *10* (9), 779–784. https://doi.org/10.1038/nnano.2015.162.

(73) Wang, X.; Jun, H.; Bathe, M. Programming 2D Supramolecular Assemblies with Wireframe DNA Origami. *J Am Chem Soc* **2022**, *144* (10), 4403–4409. https://doi.org/10.1021.

(74) Huang, K.; Yang, D.; Tan, Z.; Chen, S.; Xiang, Y.; Mi, Y.; Mao, C.; Wei, B. Self-Assembly of Wireframe DNA Nanostructures from Junction Motifs. *Angewandte Chemie International Edition* **2019**, *58* (35), 12123–12127. https://doi.org/10.1002/ANIE.201906408.

(75) Kahn, J. S.; Xiong, Y.; Huang, J.; Gang, O. Cascaded Enzyme Reactions over a Three-Dimensional, Wireframe DNA Origami Scaffold. *JACS Au* **2022**, *2* (2), 357–366. https://doi.org/10.1021/JACSAU.1C00387.

(76) Piskunen, P.; Nummelin, S.; Shen, B.; Kostiainen, M. A.; Linko, V. Increasing Complexity in Wireframe DNA Nanostructures. *Molecules 2020, Vol. 25, Page 1823* **2020**, *25* (8), 1823. https://doi.org/10.3390/MOLECULES25081823.

(77) Hannewald, N.; Winterwerber, P.; Zechel, S.; Ng, D. Y. W.; Hager, M. D.; Weil, T.; Schubert, U. S. DNA Origami Meets Polymers: A Powerful Tool for the Design of Defined Nanostructures. *Angewandte Chemie International Edition* **2021**, *60* (12), 6218–6229. https://doi.org/10.1002/ANIE.202005907.

(78) Bartnik, K.; Barth, A.; Pilo-Pais, M.; Crevenna, A. H.; Liedl, T.; Lamb, D. C. A DNA Origami Platform for Single-Pair Förster Resonance Energy Transfer Investigation of DNA-DNA Interactions and Ligation. *J Am Chem Soc* **2020**, *142* (2), 815–825. https://doi.org/10.1021/JACS.9B09093.

(79) Winterwerber, P.; Harvey, S.; Ng, D. Y. W.; Weil, T. Photocontrolled Dopamine Polymerization on DNA Origami with Nanometer Resolution. *Angewandte Chemie International Edition* **2020**, *59* (15), 6144–6149. https://doi.org/10.1002/ANIE.201911249.

(80) Kong, G.; Xiong, M.; Liu, L.; Hu, L.; Meng, H. M.; Ke, G.; Zhang, X. B.; Tan, W. DNA Origami-Based Protein Networks: From Basic Construction to Emerging Applications. *Chem Soc Rev* **2021**, *50* (3), 1846–1873. https://doi.org/10.1039/D0CS00255K.

(81) Knappe, G. A.; Wamhoff, E. C.; Bathe, M. Functionalizing DNA Origami to Investigate and Interact with Biological Systems. *Nature Reviews Materials 2022 8:2* **2022**, *8* (2), 123–138. https://doi.org/10.1038/s41578-022-00517-x.

(82) Rajendran, A.; Endo, M.; Sugiyama, H. Single-Molecule Analysis Using DNA Origami. *Angewandte Chemie International Edition* **2012**, *51* (4), 874–890. https://doi.org/10.1002/ANIE.201102113.

(83) Balakrishnan, D.; Wilkens, G. D.; Heddle, J. G. Delivering DNA Origami to Cells. *Nanomedicine* **2019**, *14* (7), 911–925. https://doi.org/10.2217/NNM-2018-0440.

(84) Acuna, G. P.; Bucher, M.; Stein, I. H.; Steinhauer, C.; Kuzyk, A.; Holzmeister, P.; Schreiber, R.; Moroz, A.; Stefani, F. D.; Liedl, T.; Simmel, F. C.; Tinnefeld, P. Distance Dependence of Single-Fluorophore Quenching by Gold Nanoparticles Studied on DNA Origami. *ACS Nano* **2012**, *6* (4), 3189–3195. https://doi.org/10.1021/NN2050483.

(85) Glembockyte, V.; Grabenhorst, L.; Trofymchuk, K.; Tinnefeld, P. DNA Origami Nanoantennas for Fluorescence Enhancement. *Acc Chem Res* **2021**, *54* (17), 3338–3348. https://doi.org/10.1021/ACS.ACCOUNTS.1C00307.

(86) Winterwerber, P.; Whitfield, C. J.; Ng, D. Y. W.; Weil, T. Multiple Wavelength Photopolymerization of Stable Poly(Catecholamines)-DNA Origami Nanostructures**. *Angewandte Chemie International Edition* **2022**, *61* (8), e202111226. https://doi.org/10.1002/ANIE.202111226.

(87) Monferrer, A.; Kohler, F.; Sigl, C.; Schachtner, M.; Peterhoff, D.; Asbach, B.; Wagner, R.; Dietz, H. DNA Origami Traps for Large Viruses. *Cell Rep Phys Sci* **2023**, *4* (1), 101237. https://doi.org/10.1016/J.XCRP.2022.101237.

(88) Rodríguez-Franco, H. J.; Weiden, J.; Bastings, M. M. C. Stabilizing Polymer Coatings Alter the Protein Corona of DNA Origami and Can Be Engineered to Bias the Cellular Uptake. *ACS Polymers Au* **2023**, *3* (4), 344–353. https://doi.org/10.1021/ACSPOLYMERSAU.3C00009.

(89) Agarwal, N. P.; Matthies, M.; Gür, F. N.; Osada, K.; Schmidt, T. L. Block Copolymer Micellization as a Protection Strategy for DNA Origami. *Angewandte Chemie* **2017**, *129* (20), 5552–5556. https://doi.org/10.1002/ANGE.201608873.

(90) Ward, M. A.; Georgiou, T. K. Thermoresponsive Polymers for Biomedical Applications. *Polymers 2011, Vol. 3, Pages 1215-1242* **2011**, *3* (3), 1215–1242. https://doi.org/10.3390/POLYM3031215.

(91) Kocak, G.; Tuncer, C.; Bütün, V. PH-Responsive Polymers. *Polym Chem* **2016**, *8* (1), 144–176. https://doi.org/10.1039/C6PY01872F.

(92) Deirram, N.; Zhang, C.; Kermaniyan, S. S.; Johnston, A. P. R.; Such, G. K.; Deirram, N.; Zhang, C.; Kermaniyan, S. S.; Such, G. K.; Johnston, A. P. R. PH-Responsive Polymer Nanoparticles for Drug Delivery. *Macromol Rapid Commun* **2019**, *40* (10), 1800917. https://doi.org/10.1002/MARC.201800917.

(93) Daoud, M.; Joanny, J. F. Conformation of Branched Polymers. *Journal de Physique* **1981**, *42* (10), 1359–1371. https://doi.org/10.1051/JPHYS:0198100420100135900.

(94) Wang, W.; Liu, H.; Mu, M.; Yin, H.; Feng, Y. CO2-Induced Reversible Morphology Transition from Giant Worms to Polymersomes Assembled from a Block-Random Segmented Copolymer. *Polym Chem* **2015**, *6* (15), 2900–2908. https://doi.org/10.1039/C5PY00053J.

(95) Blanazs, A.; Madsen, J.; Battaglia, G.; Ryan, A. J.; Armes, S. P. Mechanistic Insights for Block Copolymer Morphologies: How Do Worms Form Vesicles? *J Am Chem Soc* **2011**, *133* (41), 16581–16587. https://doi.org/10.1021/JA206301A.

(96) Peng, L.; Wu, C. S.; You, M.; Han, D.; Chen, Y.; Fu, T.; Ye, M.; Tan, W. Engineering and Applications of DNA-Grafted Polymer Materials. *Chem Sci* **2013**, *4* (5), 1928–1938. https://doi.org/10.1039/C2SC21198J.

(97) Jonášová, E. P.; Stokke, B. T. Bioresponsive DNA-Co-Polymer Hydrogels for Fabrication of Sensors. *Curr Opin Colloid Interface Sci* **2016**, *26*, 1–8. https://doi.org/10.1016/J.COCIS.2016.07.001.

(98) Gačanin, J.; Synatschke, C. V; Weil, T.; Gačanin, J.; Synatschke, C. V; Weil, T. Biomedical Applications of DNA-Based Hydrogels. *Adv Funct Mater* **2020**, *30* (4), 1906253. https://doi.org/10.1002/ADFM.201906253.

(99) Li, F.; Tang, J.; Geng, J.; Luo, D.; Yang, D. Polymeric DNA Hydrogel: Design, Synthesis and Applications. *Prog Polym Sci* **2019**, *98*, 101163. https://doi.org/10.1016/J.PROGPOLYMSCI.2019.101163.

(100) Jin, Y.; Wang, H.; Li, X.; Zhu, H.; Sun, D.; Sun, X.; Liu, H.; Zhang, Z.; Cao, L.; Gao, C.; Wang, H.; Liang, X. J.; Zhang, J.; Yang, X. Multifunctional DNA Polymer-Assisted Upconversion Therapeutic Nanoplatform for Enhanced Photodynamic Therapy. *ACS Appl Mater Interfaces* **2020**, *12* (24), 26832–26841. https://doi.org/10.1021/ACSAMI.0C03274.

(101) Hamner, K. L.; Alexander, C. M.; Coopersmith, K.; Reishofer, D.; Provenza, C.; Maye, M. M. Using Temperature-Sensitive Smart Polymers to Regulate DNA-Mediated Nanoassembly and Encoded Nanocarrier Drug Release. *ACS Nano* **2013**, *7* (8), 7011–7020. https://doi.org/10.1021/NN402214E.

(102) Westover, T. R.; Aryal, B. R.; Ranasinghe, D. R.; Uprety, B.; Harb, J. N.; Woolley, A. T.; Davis, R. C. Impact of Polymer-Constrained Annealing on the Properties of DNA Origami-Templated Gold Nanowires. *Langmuir* **2020**, *36* (24), 6661–6667. https://doi.org/10.1021/ACS.LANGMUIR.0C00594.

(103) Messina, M. S.; Messina, K. M. M.; Bhattacharya, A.; Montgomery, H. R.; Maynard, H. D. Preparation of Biomolecule-Polymer Conjugates by Grafting-from Using ATRP, RAFT, or ROMP. *Prog Polym Sci* **2020**, *100*, 101186. https://doi.org/10.1016/J.PROGPOLYMSCI.2019.101186.

(104) Lueckerath, T.; Strauch, T.; Koynov, K.; Barner-Kowollik, C.; Ng, D. Y. W.; Weil, T. DNA-Polymer Conjugates by Photoinduced RAFT Polymerization. *Biomacromolecules* **2019**, *20* (1), 212–221. https://doi.org/10.1021/ACS.BIOMAC.8B01328.

(105) Lückerath, T.; Koynov, K.; Loescher, S.; Whitfield, C. J.; Nuhn, L.; Walther, A.; Barner-Kowollik, C.; Ng, D. Y. W.; Weil, T. DNA–Polymer Nanostructures by RAFT Polymerization and Polymerization-Induced Self-Assembly. *Angewandte Chemie International Edition* **2020**, *59* (36), 15474–15479. https://doi.org/10.1002/ANIE.201916177.

(106) Kovaliov, M.; Cohen-Karni, D.; Burridge, K. A.; Mambelli, D.; Sloane, S.; Daman, N.; Xu, C.; Guth, J.; Kenneth Wickiser, J.; Tomycz, N.; Page, R. C.; Konkolewicz, D.; Averick, S. Grafting Strategies for the Synthesis of Active DNase I Polymer Biohybrids. *Eur Polym J* **2018**, *107*, 15–24. https://doi.org/10.1016/J.EURPOLYMJ.2018.07.041.

(107) Jia, F.; Lu, X.; Tan, X.; Zhang, K. Facile Synthesis of Nucleic Acid–Polymer Amphiphiles and Their Self-Assembly. *Chemical Communications* **2015**, *51* (37), 7843–7846. https://doi.org/10.1039/C5CC01934F.

(108) Wilks, T. R.; Bath, J.; De Vries, J. W.; Raymond, J. E.; Herrmann, A.; Turberfield, A. J.; O'Reilly, R. K. "giant Surfactants" Created by the Fast and Efficient Functionalization of a DNA Tetrahedron with a Temperature-Responsive Polymer. *ACS Nano* **2013**, *7* (10), 8561–8572. https://doi.org/10.1021/NN402642A.

(109) Zhang, C.; Hao, L.; Calabrese, C. M.; Zhou, Y.; Choi, C. H. J.; Xing, H.; Mirkin, C. A. Biodegradable DNA-Brush Block Copolymer Spherical Nucleic Acids Enable Transfection Agent-Free Intracellular Gene Regulation. *Small* **2015**, *11* (40), 5360–5368. https://doi.org/10.1002/SMLL.201501573.

(110) Arbona, J. M.; Aimé, J. P.; Elezgaray, J. Folding of Small Origamis. *Journal of Chemical Physics* **2012**, *136* (6). https://doi.org/10.1063/1.3682472/191924.

(111) Vuong, S.; Stefan, L.; Lejault, P.; Rousselin, Y.; Denat, F.; Monchaud, D. Identifying Three-Way DNA Junction-Specific Small-Molecules. *Biochimie* **2012**, *94* (2), 442–450. https://doi.org/10.1016/J.BIOCHI.2011.08.012.

(112) Reshetnikov, R. V.; Stolyarova, A. V.; Zalevsky, A. O.; Panteleev, D. Y.; Pavlova, G. V.; Klinov, D. V.; Golovin, A. V.; Protopopova, A. D. A Coarse-Grained Model for DNA Origami. *Nucleic Acids Res* **2018**, *46* (3), 1102–1112. https://doi.org/10.1093/NAR/GKX1262.

(113) Rothemund, P. W. K. Folding DNA to Create Nanoscale Shapes and Patterns. *Nature 2006 440:7082* **2006**, *440* (7082), 297–302. https://doi.org/10.1038/nature04586.

(114) Dey, S.; Fan, C.; Gothelf, K. V.; Li, J.; Lin, C.; Liu, L.; Liu, N.; Nijenhuis, M. A. D.; Saccà, B.; Simmel, F. C.; Yan, H.; Zhan, P. DNA Origami. *Nature Reviews Methods Primers 2021 1:1* **2021**, *1* (1), 1–24. https://doi.org/10.1038/s43586-020-00009-8.

(115) Ijäs, H.; Hakaste, I.; Shen, B.; Kostiainen, M. A.; Linko, V. Reconfigurable DNA Origami Nanocapsule for PH-Controlled Encapsulation and Display of Cargo. *ACS Nano* **2019**, *13* (5), 5959–5967. https://doi.org/10.1021/ACSNANO.9B01857.

ChatGPT was used throughout the entire work to make texts more readable and improve comprehensibility. Neither data nor content was adopted/generated by ChatGPT.

Mendeley was used as the citation program. ChemDraw Professional 16.0, bioRender and Power Point were used for graphics and drawings.

VI. APPENDIX

SUPPORTING INFORMATION: NANOSCALE PATTERNING OF POLYMERS ON DNA ORIGAMI

Electronic Supplementary Material (ESI) for Journal of Materials Chemistry B.

Electronic Supplementary Information

Nanoscale patterning of polymers on DNA-origami

Nico Alleva, Pia Winterwerber, Colette J. Whitfield, David Y. W. Ng,* Tanja Weil*

Corresponding Author:

E-Mail: David Ng david.ng@mpip-mainz.mpg.de

Tanja Weil weil@mpip-mainz.mpg.de

Max Planck Institute for Polymer Research, Mainz 55128, Germany

CHEMICALS

Diethyl ether (Honeywell), petrolium ether (30-40 °C, Fisher Scientific), dichloromethane (Fisher Scientific), TEMED (Roth, >98.5%, p a), GeneRuler 1kb DNA ladder (Thermofisher), GeneRuler Ultra Low Range DNA Ladder (Thermofisher), tris-borate-EDTA buffer (Sigma Aldrich, 10x concentrate), nuclease-free water (QIAGEN), *N,N*-diisopropylethylamine (Roth, >99,5%), chloroform-d (Sigma Aldrich, 99.8 atom %), deuterium oxide (Sigma Aldrich, 99.9 atom %), 1,4-dioxane (Sigma Aldrich, anhydrous, 99.8%), dimethyl form amide (ACROS, extra dry, 99.8%), 4-cyano-4-(phenylcarbonothioylthio)pentanoic acid *N*-succinimidyl ester (Sigma Aldrich) and 2-(dodecylthiocarbonothioylthio)-2-methylpropionsöure-*N*-hydroxysuccinimidester (Sigma Aldrich) were used as received.

2,2′-Azobis(2-methylpropionitrile) (Fluka analytics, >98%) was recrystallized in methanol prior usage.

Poly(ethylene glycol) methyl ether methacrylate (PEGMA, Sigma Aldrich, average M_n = 300 g/mol, stabilized with 100 ppm MeHQ and 300 ppm BHT), 2-hydroxyethyl acrylate (HEA, Acros, 97%, stabilized), *N,N*-dimethylacrylamide (DMA, Sigma Aldrich, 99%, stabilized with 500 ppm MeHQ) were purified prior polymerization by removing the stabiliser with a small column filled with alumina.

N-Isopropyl acrylamide (NIPAM, TCI, >98%, stabilized with MeHQ) and diacetone acrylamide (DAAM, Alfa Aesar, 99%,) were purified prior polymerization by dissolving in dioxan and removing the stabiliser with a small column filled with alumina.

PROCEDURES AND METHODS

POLYMERIZATION

For the polymerization of homo polymers or the first block of the block copolymers, the monomer, CTA and AIBN were dissolved in the polymerization solvent, purged with argon for 45-90 min and heated up to the respective temperature. The ratio of initiator to CTA was 1:10. After the reaction time, the reaction mixture was cooled down with an ice bath and a precipitate was formed in the respective precipitation solvent (Table S3). The collected solid was again dissolved and precipitated twice. The obtained solid was dried under vacuum.

The second block was obtained by dissolving the first block (macro CTA) in the polymerization solvent, adding AIBN and monomer, purged with argon for 45-90 min and heated up to respective temperature. After the reaction time, the reaction solution was cooled with an ice bath and precipitated in the precipitation solvent. The obtained solid was collected and dried under vacuum.

Table S3 shows the respective solvents, reagents and reaction parameters for the respective polymerization.

To calculate the amounts of monomer, initiator and CTA formula 1 was used:

$$X_n = \frac{p[M]_0}{(p'[RAFT]_0 + 2fp''[I]_0)} \quad (1)$$

Where $[RAFT]_0$, $[I]_0$ and $[M]_0$ are the starting concentrations of CTA, initiator and monomer. The fractional conversions of the monomer, CTA and initiator are p, p' and p'', here set to 1. f is the functionality of the initiator and X_n is the degree of polymerization. The scale for the polymerization was 0.5 g to 1 g of monomer.

CTA REMOVAL

The obtained polymer was dissolved in dioxane and an excess of AIBN was added. The reaction solution was heated up to 80 °C. After the reaction time, the reaction solution was cooled in an ice bath, and the polymer was participated in the respective precipitation solvent (Table S3). The obtained polymer was dried under vacuum and analysed with SEC (DMF, PMMA standard) and ^{1}H-NMR (300 MHz).

CONJUGATION REACTION

For a typical conjugation reaction, 5'amino-oligonucleotide (StA^C: NH_2-TTTTCTCTACCACCTACTA or StE^C: NH_2-CAGTCAGTCAGTCAGTCAGT) (10 nmol), polymer (50 equiv.) and DIPEA (200 equiv.) were mixed in the respective reaction solvent, to a total volume of 80 µL and shacken for 44-69 h at room temperature. After the reaction time, 1 µL of the reaction solution was diluted and analysed with PAGE.

The obtained reaction solution was purified via spin filtration (Amicon Ultra-6 mL Centrifugal Filters MWCO 10k or 30k) by adding 5 mL to the reaction solution and centrifuge for 1 h. This was repeated 10 times.

ORIGAMI SYNTHESIS

DNA origami nanostructures were prepared by mixing the respective staple strands (8 equiv.), folding strands (16 equiv.) and scaffold DNA (M13mp18) in origami buffer (1 mM Na_2EDTA, 5 mM NaCl, 5 mM TRIS, 12 mM $MgCl_2$ pH 8) and a temperature program run, starting at 70 °C and cooling down to 20 °C over 2 h (0.5 °C/min to 35 °C, 1 °C/min to 20 °C). The obtained DNA origami structures were purified by precipitation from PEG solution (15% PEG_{8000}, 5 mM TRIS buffer, 1 mM Na_2EDTA buffer, 0.505 M NaCl) with a 1:1 reaction solution to PEG solution ratio. The mixtures were centrifuged for 25 min at 12 xg at room temperature. The supernatant was removed, the DNA origami was redissolved in origami buffer and precipitated again from PEG solution. This procedure was repeated twice. The concentration was determined by measuring the absorption at 260 nm with Spark® 20M with Nanoquant plate™. The DNA origami were stored at 4 °C.

Table S 1: DNA-origami used in the experiments. For StA, the respective staple strand was elongated with the StA sequence. For StE, the respective staple strand was elongated with the StE sequence. To create DNA-origami tubes, the normal staple strand (number) was changed to the respective folding strand listed in Table S9.

Origami	Sequences different then staple strand or folding strand:
O_0	StA: 53-60; 63-74; 77-98; 158-179; 182-203 Folding strand (for tube): 1, 25, 27, 28, 51, 52, 75, 76, 99, 100, 111, 132, 133, 156, 157, 180, 181, 204, 205, 216
O_4	StA: 31-50, 81-98, 113, 115, 117, 118, 120, 122, 124, 125, 127, 129, 131, 134, 136, 138, 140, 142, 144, 146, 148, 150, 152, 154, 182-200 Folding strand (for tube): 1, 25, 27, 28, 51, 52, 75, 76, 99, 100, 111, 132, 133, 156, 157, 180, 181, 204, 205, 216
O_6	StA: 13-15, 17, 19, 37-44, 46, 59-70, 72, 81, 83, 85, 87, 89, 91, 93, 95, 119-122, 124, 140-147, 148, 162-173, 175, 184, 186-188, 190, 192, 194, 196, 198
O_8	StA: 161, 163, 165, 167, 169, 171, 173, 175, 177, 179, 182-200 StE: 56, 58, 60, 62, 64, 66, 68, 70, 72, 74, 77, 79, 81-98 Folding strand (for tube): 1, 25, 27, 28, 51, 52, 75, 76, 99, 100, 111, 132, 133, 156, 157, 180, 181, 204, 205, 216

ORIGAMI ANNEALING

To anneal the DNA-polymer conjugates to DNA origami, DNA origami (10 nM, final concentration) and DNA-polymer conjugate (50 equiv.) were mixed in origami buffer (1 mM Na_2EDTA, 5 mM NaCl, 5 mM TRIS, 12 mM $MgCl_2$ pH 8) to a total volume of 40 µL. The sample was heated up to 37 °C for 1 h and cooled to 30 °C and kept at 30 °C overnight. The obtained reaction solution was purified via spin filtration (Amicon Ultra-0.5 mL Centrifugal Filters MWCO 100K) by adding 400 µL origami buffer to the reaction solution and centrifuge 5 min at 5xg. The filtrate was removed and the purification was repeated two more times. The supernatant was collected, and the concentration was determined by measuring the absorption at 260 nm with Spark® 20M with Nanoquant plate™.

PAGE

The PAGE gel (15%) was manufactured by mixing 40% acrylamide/bis-acrylamide solution 37.5:1 (5.63 mL), 10x tris/borate/EDTA buffer (TBE buffer) (1.5 mL), water (7.9 mL), tetramethylethylenediamine (TEMED) (7.5 µL and 10% ammonium persulfate (APS) solution (75 µL) and casting the gel.

For monitoring the conjugation reaction via PAGE, 1 µL of diluted reaction solution (1:12.5, 10 fmol DNA) was hybridized with the complementary Rh6G-DNA sequence (100 µM, 20 fmol, 2 equiv.) in 10x origami buffer (0.5 µL) and nuclease-free water (1.5 µL) to a total volume of 5 µL. The obtained solution was heated to 35°C for 30 min (hybridization). The reaction solution was the cooled down to room temperature, mixed with loading dye (1.7 µL, 6x Thermo Fisher) and nuclease-free water

(3.3 µL) to a total volume of 10 µL and loaded onto the gel. The gel was run fist at 100 V for 10 min and then at 150 V for 50 min on a Cell SureLockTM mini-cell electrophoresis system from Thermo Fisher using 0.5 × TBE buffer as the running buffer (44.5 mM Tris-Borate, 1 mM EDTA). Generuler ultra low range DNA ladder (Thermo Fisher) was used as the DNA ladder. Controls contain 5'amino-oligonucleotide and polymer (50 equiv.) to show that the polymer does not entangle with DNA. The gels are stained with SYBR Gold (1x, 50 mL) for 45 min at room temperature. The images were taken with G:BOX Chemi Gel Doc System from Syngene.

AGAROSE

Agarose gels (1% TBE ethidium bromide (EtBr), BioRad, ReadyAgarose Precast Gel) were used as received.

For analysing DNA origami via agarose gel electrophoresis, origami solution (10 fmol), loading dye (6x Thermo Fisher) and 1x origami buffer (1 mM Na_2EDTA, 5 mM NaCl, 5 mM TRIS, 12 mM $MgCl_2$ pH 8) with a total volume of 10 µL were loaded on the gel. The electrophoresis was conducted at 90 V for 60 min at 4 °C. The gels were stained with SYBR Gold for 1 h. The images were taken with G:BOX Chemi Gel Doc System from Syngene.

AFM

For imaging the DNA origami architectures, Bruker Dimension FastScan Bio™ atomic force microscope was used in the liquid state, which was operated in PeakForce mode. FastScan-D tips from Burker with a nominal spring constant of 0.25 Nm^{-1} were used.

For sample preparation, origami solution (40 µL, 0.5-2 nM in origami buffer) was added to a circular mica substrate (20 mm) and incubated for 10-15 min. The excess liquid was removed and 300 µL origami buffer was added to the mica to measure in liquid. Images were analysed with NanoScope Analysis 1.9.

GPC

GPC experiments were performed on a PSS SECurity instrument comprising an auto sampler, a column oven with three GRAM columns (10^3, 10^3 and 10^2 Å, 300 × 8 mm, 10 µm particle size) and a RI as well as an UV detector (Agilent Technologies 1260 Infinity). DMF containing 1 g/L lithium bromide was used as the eluent at a flowrate of 1 mL/min. Poly(methyl methacrylate) (1600 kDa–800 Da) served as the calibration standard for molecular weight measurements. The samples were filtered (0.4 µm) prior to injection. The data were fitted with OriginPro 2021.

NMR

NMR spectra were recorded on a Burker Avance (300 MHz) NMR spectrometer, using solvent signals of deuterated chloroform (δ=7.26) or deuterated water (δ=4.80) as reference. The data were processed with MestReNova 14.2.1.

RESULTS AND DISCUSSION

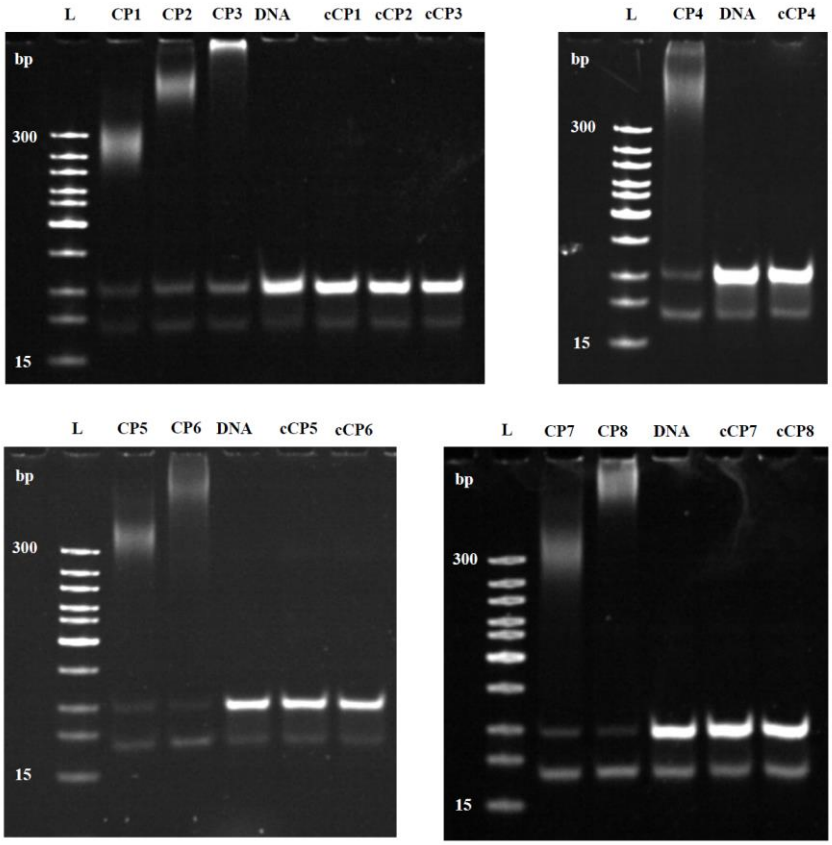

Figure S 1: PAGE gel (15%) of conjugation reaction of P1-P8 with 5'amino oligonucleotide and controls, stained with SYBR Gold. The controls contain the same amount of the respective polymer and 5'amino oligonucleotide without DIPEA and without reaction time to show that the oligonucleotide is not entangling with the respective polymer. L: DNA ladder; CP: respective conjugation reaction solution; cCP: control of respective conjugation reaction.

Table S 2: Conversion determination using the software ImageJ to analyse intensity and calculate conversion of the respective conjugation reaction. Used PAGE gels are shown in Figure 2 and S1.

	Intensity I	Intensity II	Conversion I	Conversion II
DNA	71.85	74.80		
CP1	13.55	15.43	81%	93%
CP2	18.05	20.04	75%	88%
CP3	22.51	24.55	69%	80%

	Intensity I	Intensity II	Conversion I	Conversion II
DNA	99.80	87.78		
CP4	28.57	22.91	71%	94%

	Intensity I	Intensity II	Conversion I	Conversion II
DNA	56.53	52.26		
CP5	16.71	13.62	71%	93%
CP6	15.46	12.58	73%	97%

	Intensity I	Intensity II	Conversion I	Conversion II
DNA	54.07	57.79		
CP7	5.83	6.95	89%	94%
CP8	4.77	5.79	91%	96%

Table S 3: Overview of the synthesized polymers, polymerization parameters and purification solvents.

Polymer	M_w (SEC)	Đ (SEC)	Amount I. Block (SEC)	Used CTA	Polym. solvent	Precipitation solvent	Reaction Temp.	Reaction time
P(DMA) (P1, P2, P3)	9649	1.08	/	NHS-DDMAT	dioxane	diethyl ether	70 °C	18 h
	22125	1.08					70 °C	18 h
	48637	1.27					65 °C	4 h
P(PEGMA) (P4)	21090	1.19	/	NHS-CPADB	dioxane	diethyl ether (-20 °C, phase separation)	70 °C	20.5 h
P(NIPAM) (P5)	17078	1.11	/	NHS-DDMAT	dioxane	diethyl ether	75 °C	19 h
P(NIPAM-*b*-DMA) (P6)	30445	1.19	43%	NHS-DDMAT	dioxane	diethyl ether	I. Block: 70 °C II. Block: 65 °C	15 h 17 h
P(HEA) (P7)	23264	1.27	/	NHS-DDMAT	DMF	diethyl ether	70 °C	16 h
P(DAAM-*b*-DMA) (P8)	26013	1.20	29%	NHS-DDMAT	dioxane	petrol ether	I. Block: 70 °C II. Block: 55 °C	17 h 21 h

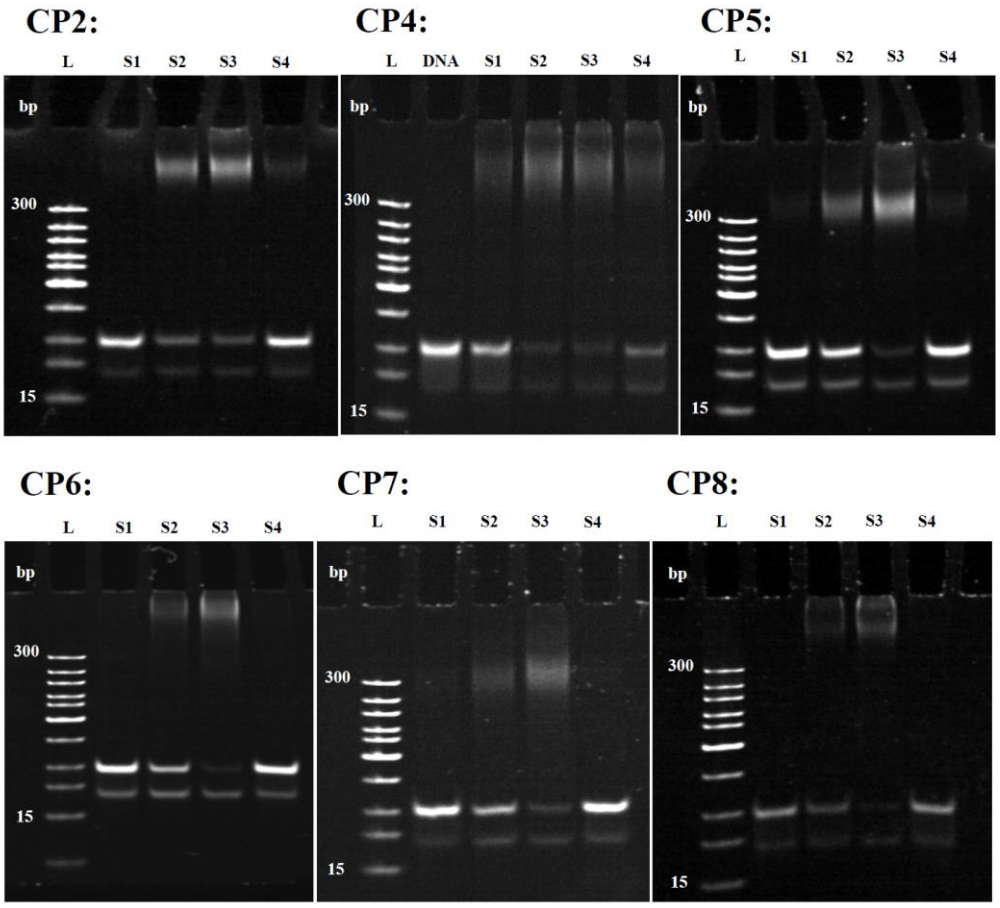

Figure S 2: PAGE gels (15%) of the respective polymer conjugation reactions accomplished in different solvent mixtures; S1 water, S2 DMF/water (1:1), S3 DMF/water (3:1) and S4 DMF. Stained with SYBR Gold.

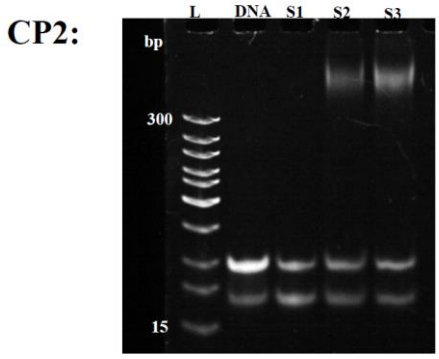

Figure S 3: PAGE gels (15%) of the respective polymer conjugation reaction of P2 accomplished in different solvent mixtures of ACN; S1 ACN, S2 ACN/water (1:1), S3 ACN/water (3:1). Stained with SYBR Gold.

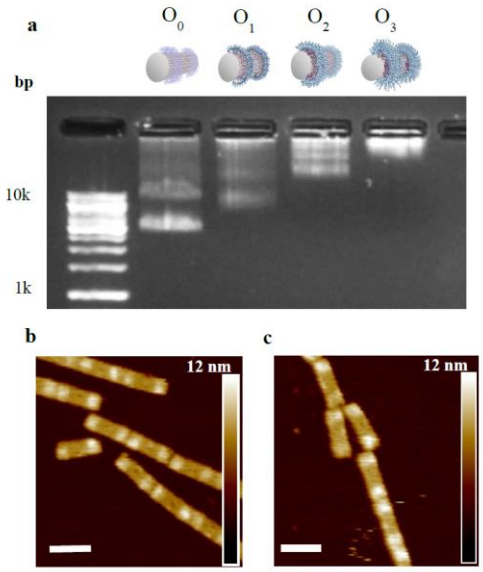

Figure S 4: c) Monitoring of the coated and uncoated DNA-origami (O_0-O_3) containing StA with CP1-CP3 by 1% agarose gel, stained with SYBR Gold. L: DNA ladder; O_0: uncoated DNA-origami; O_{1-3}: Coated DNA-origami (from left to right). b) Monitored DNA-origami (O_1) coated with CP1 via AFM. Scale bar = 80 nm c) Monitored DNA-origami (O_2) coated with CP2 via AFM. Scale bar = 80 nm.

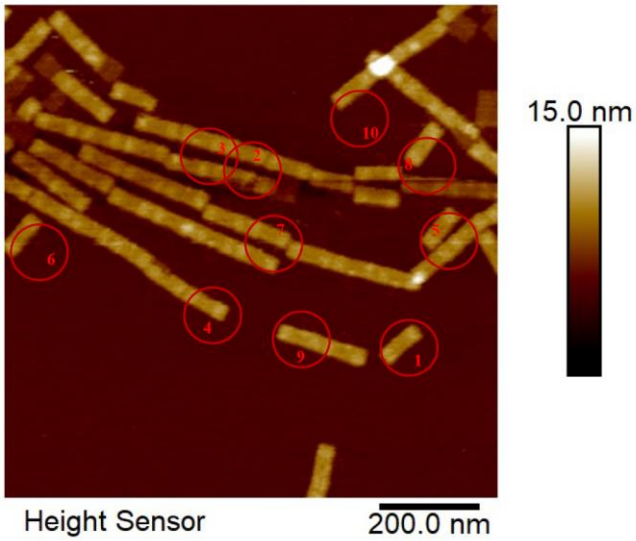

Figure S 5: AFM images of DNA origami (O_0) and marked DNA tubes which were used for height measurement. Results of height measurement are shown in Table S 4.

Table S 4: Heights of the uncoated DNA-origami (O_0)

Origami	Max height base	Max height coated area
1	4.82	5.69
2	4.88	5.54
3	4.65	5.61
4	5.11	6.00
5	4.63	5.57
6	4.45	5.68
7	4.84	5.28
8	4.95	5.82
9	5.04	6.02
10	5.09	5.90

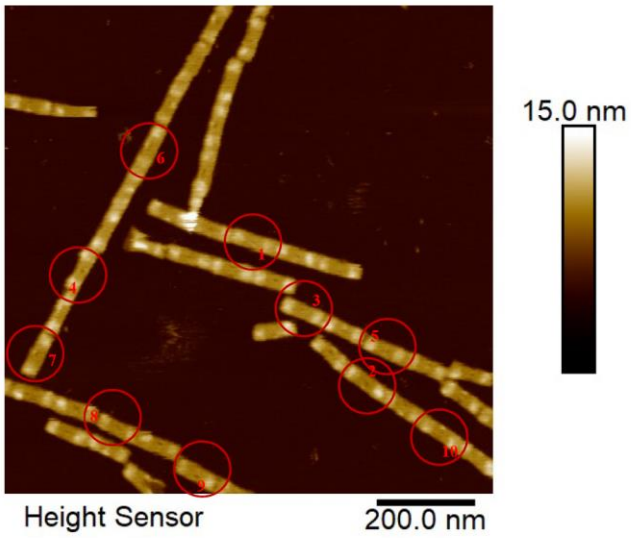

Figure S 6: AFM images of the coated DNA origami (O_1) and marked DNA tubes which were used for height measurement. Results of height measurement is shown in Table S 5.

Table S 5: Heights of the coated DNA-origami (O_1)

Origami	Max height base	Max height coated area
1	5.66	7.05
2	5.00	6.49
3	5.38	7.38
4	5.41	7.67
5	5.31	7.22
6	5.21	7.16
7	5.49	7.37
8	4.69	6.86
9	5.01	6.04
10	4.96	6.78

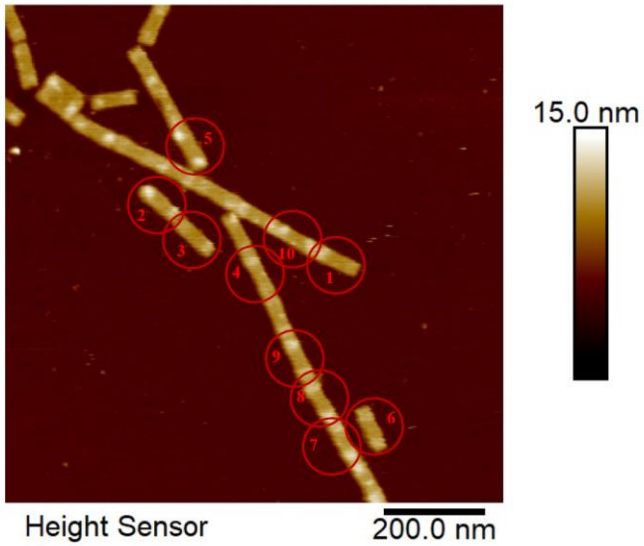

Figure S 7: AFM image of coated DNA origami (O_2) and marked DNA tubes which were used for height measurement. Results of height measurement is shown in Table S 6.

Table S 6: Heights of the coated DNA-origami (O_2)

Origami	Max height base	Max height coated area
1	4.99	6.10
2	5.76	8.40
3	5.28	6.88
4	5.47	7.43
5	5.86	8.72
6	5.65	6.96
7	5.80	7.62
8	5.80	7.87
9	5.45	7.79
10	5.74	7.84

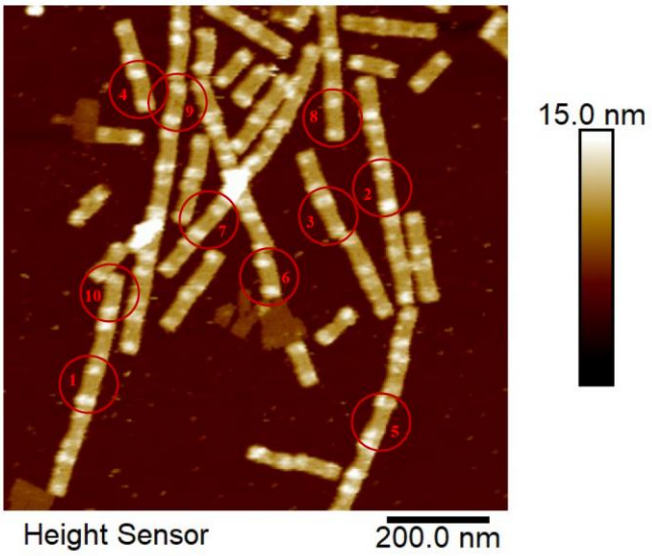

Figure S 8: AFM images of coated DNA origami (O_3) and marked DNA tubes which were used for height measurement. Results of height measurement are shown in Table S 7.

Table S 7: Heights of the coated DNA-origami (O_3)

Origami	Max height base	Max height coated area
1	5.72	8.98
2	6.22	9.34
3	5.94	8.59
4	5.88	9.41
5	5.94	9.11
6	5.72	9.01
7	5.54	8.51
8	5.47	8.37
9	5.41	8.83
10	5.92	9.03

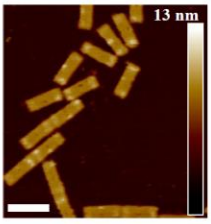

Figure S 9: AFM images of uncoated DNA origami (O_8) containing StA and StE sequences.

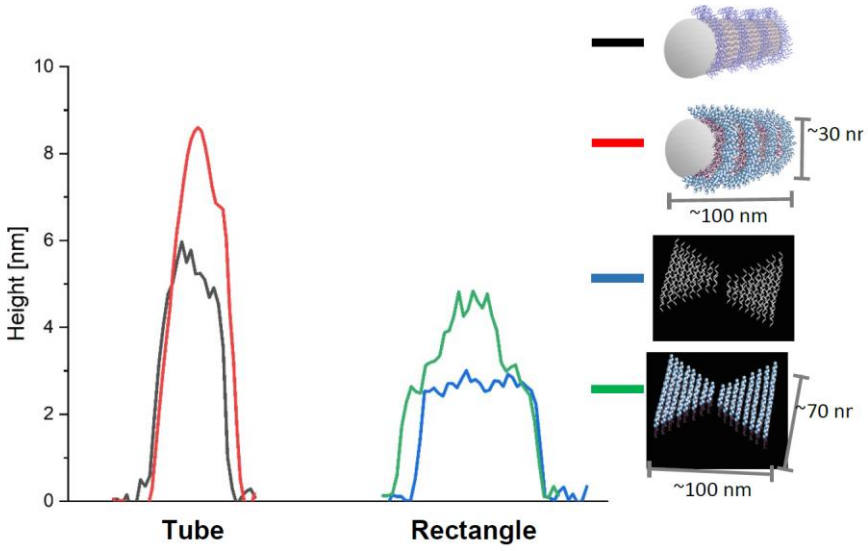

Figure S 10: AFM topographic images of O_4, O_5, O_6 and O_7 (Figure 3 f,g,h,i) reveal a significant increase in height of the respective coating area.

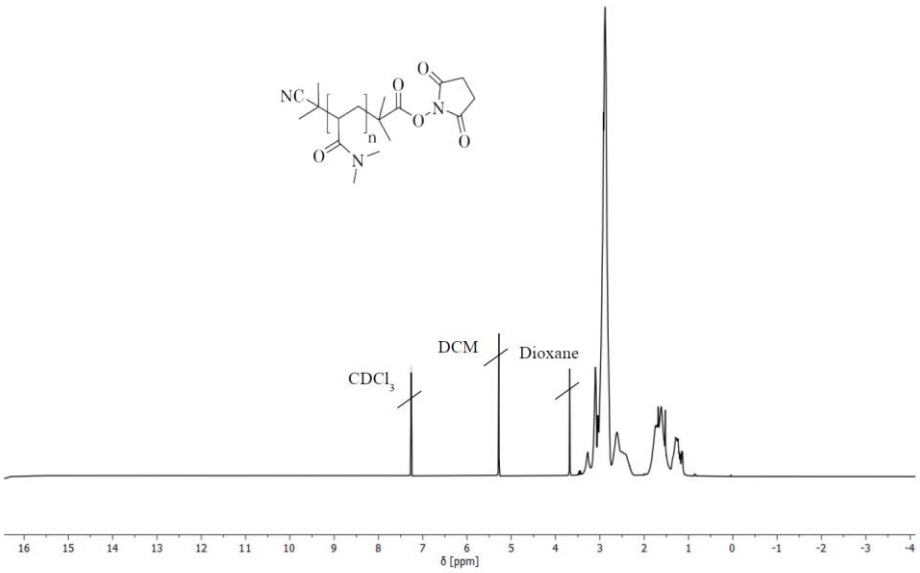

Figure S 11:^{1}H-NMR of P1 synthesized by RAFT polymerization. CTA group was removed with an excess of AIBN.

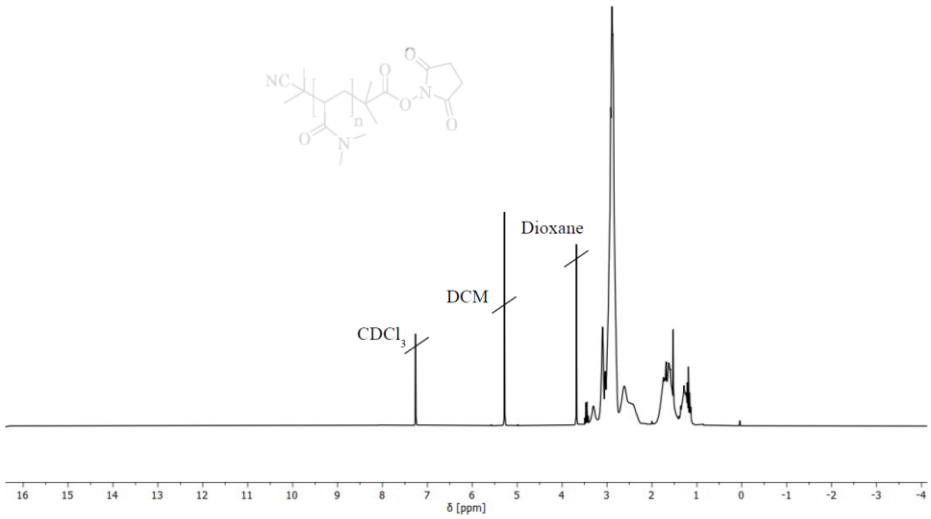

Figure S 12: ^{1}H-NMR of P2 synthesized by RAFT polymerization. CTA group was removed with an excess of AIBN.

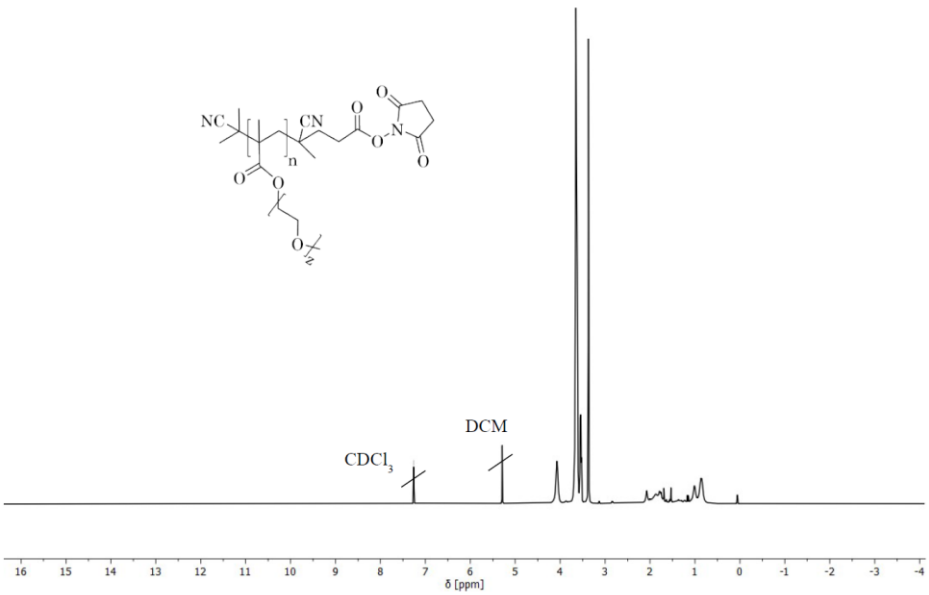

Figure S13: ^{1}H-NMR of P4 synthesized by RAFT polymerization. CTA group was removed with an excess of AIBN.

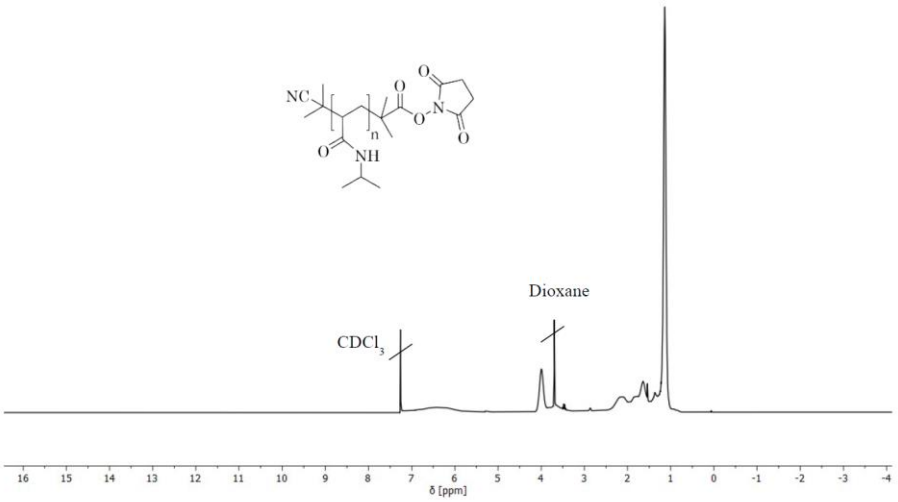

Figure S 14: ^{1}H-NMR of P5 synthesized by RAFT polymerization. CTA group was removed with an excess of AIBN.

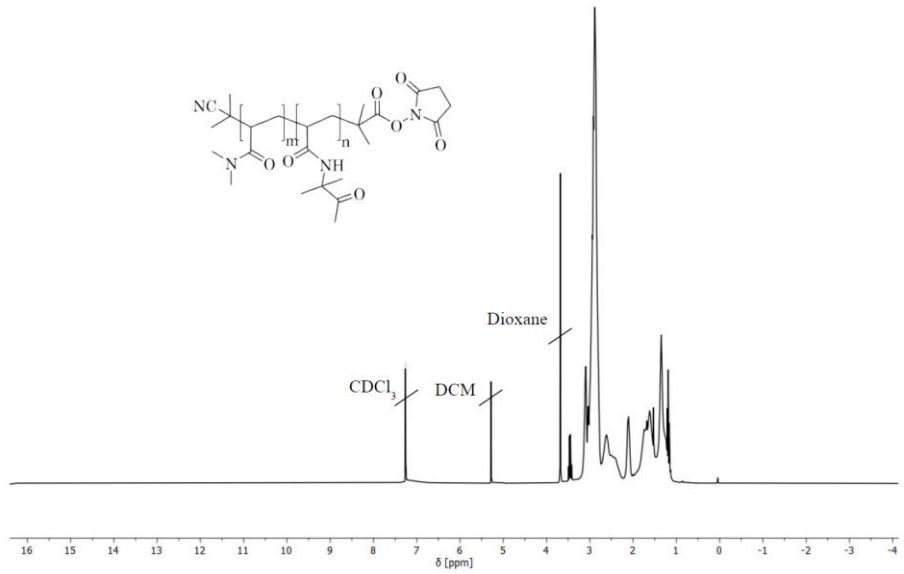

Figure S 15: ^{1}H-NMR of P8 synthesized by RAFT polymerization. CTA group was removed with an excess of AIBN.

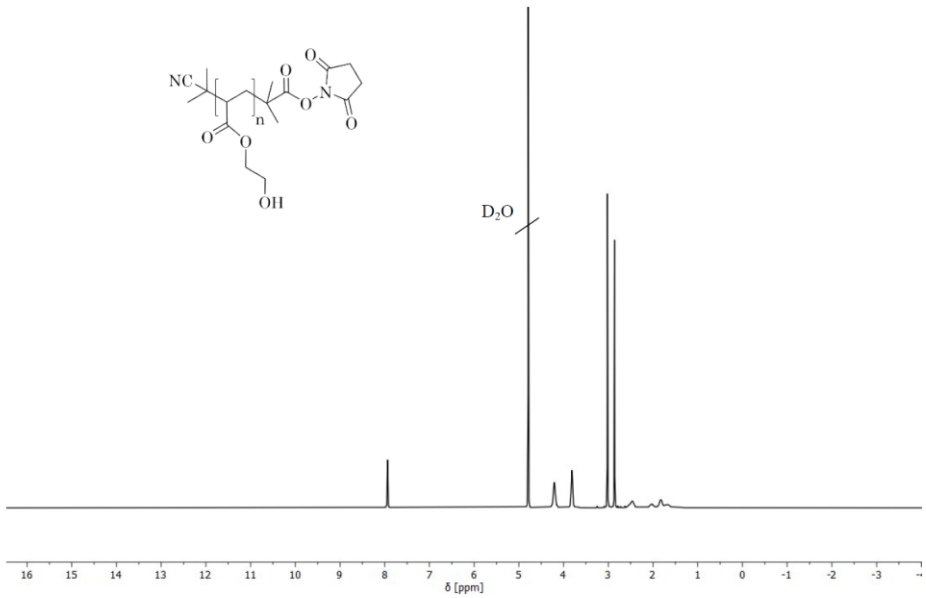

Figure S 16: ^{1}H-NMR of P7 synthesized by RAFT polymerization. CTA group was removed with an excess of AIBN.

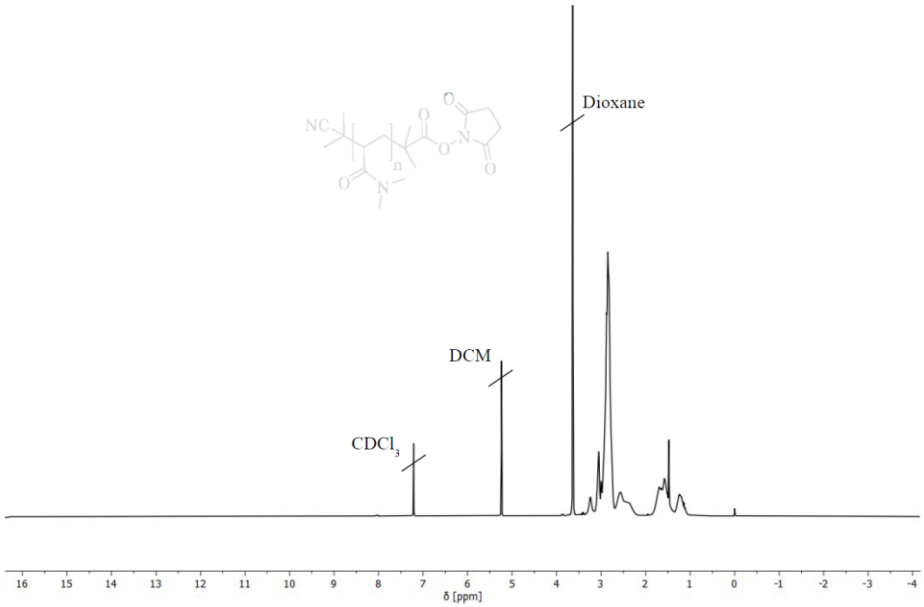

Figure S 17: ^{1}H-NMR of P3 synthesized by RAFT polymerization. CTA group was removed with an excess of AIBN.

Table S 8: Staple sequences for DNA-origami synthesis.

Name	Sequence
1	CAAGCCCAATAGGAACCCATGTACAAACAGTT
2	AATGCCCCGTAACAGTGCCCGTATCTCCCTCA
3	TGCCTTGACTGCCTATTTCGGAACAGGGATAG
4	GAGCCGCCCCACCACCGGAACCGCGACGGAAA
5	AACCAGAGACCCTCAGAACCGCCAGGGGTCAG
6	TTATTCATAGGGAAGGTAAATATTCATTCAGT
7	CATAACCCGAGGCATAGTAAGAGCTTTTTAAG
8	ATTGAGGGTAAAGGTGAATTATCAATCACCGG
9	AAAAGTAATATCTTACCGAAGCCCTTCCAGAG
10	GCAATAGCGCAGATAGCCGAACAATTCAACCG
11	CCTAATTTACGCTAACGAGCGTCTAATCAATA
12	TCTTACCAGCCAGTTACAAAATAAATGAAATA
13	ATCGGCTGCGAGCATGTAGAAACCTATCATAT
14	CTAATTTATCTTTCCTTATCATTCATCCTGAA
15	GCGTTATAGAAAAAGCCTGTTTAGAAGGCCGG
16	GCTCATTTTCGCATTAAATTTTTGAGCTTAGA
17	AATTACTACAAATTCTTACCAGTAATCCCATC
18	TTAAGACGTTGAAAACATAGCGATAACAGTAC
19	TAGAATCCCTGAGAAGAGTCAATAGGAATCAT
20	CTTTTACACAGATGAATATACAGTAAACAATT
21	TTTAACGTTCGGGAGAAACAATAATTTTCCCT
22	CGACAACTAAGTATTAGACTTTACAATACCGA
23	GGATTTAGCGTATTAAATCCTTTGTTTTCAGG
24	ACGAACCAAAACATCGCCATTAAATGGTGGTT
25	GAACGTGGCGAGAAAGGAAGGGAACAAACTAT
26	TAGCCCTACCAGCAGAAGATAAAAACATTTGA
27	CGGCCTTGCTGGTAATATCCAGAACGAACTGA
28	CTCAGAGCCACCACCCTCATTTTCCTATTATT
29	CTGAAACAGGTAATAAGTTTTAACCCCTCAGA
30	AGTGTACTTGAAAGTATTAAGAGGCCGCCACC
31	GCCACCACTCTTTTCATAATCAAACCGTCACC
32	GTTTGCCACCTCAGAGCCGCCACCGATACAGG
33	GACTTGAGAGACAAAAGGGCGACAAGTTACCA
34	AGCGCCAACCATTTGGGAATTAGATTATTAGC
35	GAAGGAAAATAAGAGCAAGAAACAACAGCCAT

36	GCCCAATACCGAGGAAACGCAATAGGTTTACC
37	ATTATTTAACCCAGCTACAATTTTCAAGAACG
38	TATTTTGCTCCCAATCCAAATAAGTGAGTTAA
39	GGTATTAAGAACAAGAAAAATAATTAAAGCCA
40	TAAGTCCTACCAAGTACCGCACTCTTAGTTGC
41	ACGCTCAAAATAAGAATAAACACCGTGAATTT
42	AGGCGTTACAGTAGGGCTTAATTGACAATAGA
43	ATCAAAATCGTCGCTATTAATTAACGGATTCG
44	CTGTAAATCATAGGTCTGAGAGACGATAAATA
45	CCTGATTGAAAGAAATTGCGTAGACCCGAACG
46	ACAGAAATCTTTGAATACCAAGTTCCTTGCTT
47	TTATTAATGCCGTCAATAGATAATCAGAGGTG
48	AGATTAGATTTAAAAGTTTGAGTACACGTAAA
49	AGGCGGTCATTAGTCTTTAATGCGCAATATTA
50	GAATGGCTAGTATTAACACCGCCTCAACTAAT
51	CCGCCAGCCATTGCAACAGGAAAAATATTTTT
52	CCCTCAGAACCGCCACCCTCAGAACTGAGACT
53	CCTCAAGAATACATGGCTTTTGATAGAACCAC
54	TAAGCGTCGAAGGATTAGGATTAGTACCGCCA
55	CACCAGAGTTCGGTCATAGCCCCCGCCAGCAA
56	TCGGCATTCCGCCGCCAGCATTGACGTTCCAG
57	AATCACCAAATAGAAAATTCATATATAACGGA
58	TCACAATCGTAGCACCATTACCATCGTTTTCA
59	ATACCCAAGATAACCCACAAGAATAAACGATT
60	ATCAGAGAAAGAACTGGCATGATTTTATTTTG
61	TTTTGTTTAAGCCTTAAATCAAGAATCGAGAA
62	AGGTTTTGAACGTCAAAAATGAAAGCGCTAAT
63	CAAGCAAGACGCGCCTGTTTATCAAGAATCGC
64	AATGCAGACCGTTTTTATTTTCATCTTGCGGG
65	CATATTTAGAAATACCGACCGTGTTACCTTTT
66	AATGGTTTACAACGCCAACATGTAGTTCAGCT
67	TAACCTCCATATGTGAGTGAATAAACAAAATC
68	AAATCAATGGCTTAGGTTGGGTTACTAAATTT
69	GCGCAGAGATATCAAAATTATTTGACATTATC
70	AACCTACCGCGAATTATTCATTTCCAGTACAT
71	ATTTTGCGTCTTTAGGAGCACTAAGCAACAGT
72	CTAAAATAGAACAAAGAAACCACCAGGGTTAG
73	GCCACGCTATACGTGGCACAGACAACGCTCAT

74	GCGTAAGAGAGAGCCAGCAGCAAAAAGGTTAT
75	GGAAATACCTACATTTTGACGCTCACCTGAAA
76	TATCACCGTACTCAGGAGGTTTAGCGGGGTTT
77	TGCTCAGTCAGTCTCTGAATTTACCAGGAGGT
78	GGAAAGCGACCAGGCGGATAAGTGAATAGGTG
79	TGAGGCAGGCGTCAGACTGTAGCGTAGCAAGG
80	TGCCTTTAGTCAGACGATTGGCCTGCCAGAAT
81	CCGGAAACACACCACGGAATAAGTAAGACTCC
82	ACGCAAAGGTCACCAATGAAACCAATCAAGTT
83	TTATTACGGTCAGAGGGTAATTGAATAGCAGC
84	TGAACAAACAGTATGTTAGCAAACTAAAAGAA
85	CTTTACAGTTAGCGAACCTCCCGACGTAGGAA
86	GAGGCGTTAGAGAATAACATAAAAGAACACCC
87	TCATTACCCGACAATAAACAACATATTTAGGC
88	CCAGACGAGCGCCCAATAGCAAGCAAGAACGC
89	AGAGGCATAATTTCATCTTCTGACTATAACTA
90	TTTTAGTTTTTCGAGCCAGTAATAAATTCTGT
91	TATGTAAACCTTTTTTAATGGAAAAATTACCT
92	TTGAATTATGCTGATGCAAATCCACAAATATA
93	GAGCAAAAACTTCTGAATAATGGAAGAAGGAG
94	TGGATTATGAAGATGATGAAACAAAATTTCAT
95	CGGAATTATTGAAAGGAATTGAGGTGAAAAAT
96	ATCAACAGTCATCATATTCCTGATTGATTGTT
97	CTAAAGCAAGATAGAACCCTTCTGAATCGTCT
98	GCCAACAGTCACCTTGCTGAACCTGTTGGCAA
99	GAAATGGATTATTTACATTGGCAGACATTCTG
100	TTTTTATAAGTATAGCCCGGCCGTCGAG
101	AGGGTTGATTTTATAAATCCTCATTAAATGATATTC
102	ACAAACAATTTTAATCAGTAGCGACAGATCGATAGC
103	AGCACCGTTTTTTAAAGGTGGCAACATAGTAGAAAA
104	TACATACATTTTGACGGGAGAATTAACTACAGGGAA
105	GCGCATTATTTTGCTTATCCGGTATTCTAAATCAGA
106	TATAGAAGTTTTCGACAAAAGGTAAAGTAGAGAATA
107	TAAAGTACTTTTCGCGAGAAAACTTTTTATCGCAAG
108	ACAAAGAATTTTATTAATTACATTTAACACATCAAG
109	AAAACAAATTTTTTCATCAATATAATCCTATCAGAT
110	GATGGCAATTTTAATCAATATCTGGTCACAAATATC
111	AAACCCTCTTTTACCAGTAATAAAAGGGATTCACCAGTCACACGTTTT

112	CCGAAATCCGAAAATCCTGTTTGAAGCCGGAA
113	CCAGCAGGGGCAAAATCCCTTATAAAGCCGGC
114	GCATAAAGTTCCACACAACATACGAAGCGCCA
115	GCTCACAATGTAAAGCCTGGGGTGGGTTTGCC
116	TTCGCCATTGCCGGAAACCAGGCATTAAATCA
117	GCTTCTGGTCAGGCTGCGCAACTGTGTTATCC
118	GTTAAAATTTTAACCAATAGGAACCCGGCACC
119	AGACAGTCATTCAAAAGGGTGAGAAGCTATAT
120	AGGTAAAGAAATCACCATCAATATAATATTTT
121	TTTCATTTGGTCAATAACCTGTTTATATCGCG
122	TCGCAAATGGGGCGCGAGCTGAAATAATGTGT
123	TTTTAATTGCCCGAAAGACTTCAAAACACTAT
124	AAGAGGAACGAGCTTCAAAGCGAAGATACATT
125	GGAATTACTCGTTTACCAGACGACAAAAGATT
126	GAATAAGGACGTAACAAAGCTGCTCTAAAACA
127	CCAAATCACTTGCCCTGACGAGAACGCCAAAA
128	CTCATCTTGAGGCAAAAGAATACAGTGAATTT
129	AAACGAAATGACCCCCAGCGATTATTCATTAC
130	CTTAAACATCAGCTTGCTTTCGAGCGTAACAC
131	TCGGTTTAGCTTGATACCGATAGTCCAACCTA
132	TGAGTTTCGTCACCAGTACAAACTTAATTGTA
133	CCCCGATTTAGAGCTTGACGGGGAAATCAAAA
134	GAATAGCCGCAAGCGGTCCACGCTCCTAATGA
135	GAGTTGCACGAGATAGGGTTGAGTAAGGGAGC
136	GTGAGCTAGTTTCCTGTGTGAAATTTGGGAAG
137	TCATAGCTACTCACATTAATTGCGCCCTGAGA
138	GGCGATCGCACTCCAGCCAGCTTTGCCATCAA
139	GAAGATCGGTGCGGGCCTCTTCGCAATCATGG
140	AAATAATTTTAAATTGTAAACGTTGATATTCA
141	GCAAATATCGCGTCTGGCCTTCCTGGCCTCAG
142	ACCGTTCTAAATGCAATGCCTGAGAGGTGGCA
143	TATATTTTAGCTGATAAATTAATGTTGTATAA
144	TCAATTCTTTTAGTTTGACCATTACCAGACCG
145	CGAGTAGAACTAATAGTAGTAGCAAACCCTCA
146	GAAGCAAAAAAGCGGATTGCATCAGATAAAAA
147	TCAGAAGCCTCCAACAGGTCAGGATCTGCGAA
148	CCAAAATATAATGCAGATACATAAACACCAGA
149	CATTCAACGCGAGAGGCTTTTGCATATTATAG

150	ACGAGTAGTGACAAGAACCGGATATACCAAGC
151	AGTAATCTTAAATTGGGCTTGAGAGAATACCA
152	GCGAAACATGCCACTACGAAGGCATGCGCCGA
153	ATACGTAAAAGTACAACGGAGATTTCATCAAG
154	CAATGACACTCCAAAAGGAGCCTTACAACGCC
155	AAAAAAGGACAACCATCGCCCACGCGGGTAAA
156	TGTAGCATTCCACAGACAGCCCTCATCTCCAA
157	GTAAAGCACTAAATCGGAACCCTAGTTGTTCC
158	AGTTTGGAGCCCTTCACCGCCTGGTTGCGCTC
159	AGCTGATTACAAGAGTCCACTATTGAGGTGCC
160	ACTGCCCGCCGAGCTCGAATTCGTTATTACGC
161	CCCGGGTACTTTCCAGTCGGGAAACGGGCAAC
162	CAGCTGGCGGACGACGACAGTATCGTAGCCAG
163	GTTTGAGGGAAAGGGGGATGTGCTAGAGGATC
164	CTTTCATCCCCAAAAACAGGAAGACCGGAGAG
165	AGAAAAGCAACATTAAATGTGAGCATCTGCCA
166	GGTAGCTAGGATAAAAATTTTTAGTTAACATC
167	CAACGCAATTTTTGAGAGATCTACTGATAATC
168	CAATAAATACAGTTGATTCCCAATTTAGAGAG
169	TCCATATACATACAGGCAAGGCAACTTTATTT
170	TACCTTTAAGGTCTTTACCCTGACAAAGAAGT
171	CAAAAATCATTGCTCCTTTTGATAAGTTTCAT
172	TTTGCCAGATCAGTTGAGATTTAGTGGTTTAA
173	AAAGATTCAGGGGGTAATAGTAAACCATAAAT
174	TTTCAACTATAGGCTGGCTGACCTTGTATCAT
175	CCAGGCGCTTAATCATTGTGAATTACAGGTAG
176	CGCCTGATGGAAGTTTCCATTAAACATAACCG
177	TTTCATGAAAATTGTGTCGAAATCTGTACAGA
178	ATATATTCTTTTTTCACGTTGAAAATAGTTAG
179	AATAATAAGGTCGCTGAGGCTTGCAAAGACTT
180	CGTAACGATCTAAAGTTTTGTCGTGAATTGCG
181	ACCCAAATCAAGTTTTTTGGGGTCAAAGAACG
182	TGGACTCCCTTTTCACCAGTGAGACCTGTCGT
183	TGGTTTTTAACGTCAAAGGGCGAAGAACCATC
184	GCCAGCTGCCTGCAGGTCGACTCTGCAAGGCG
185	CTTGCATGCATTAATGAATCGGCCCGCCAGGG
186	ATTAAGTTCGCATCGTAACCGTGCGAGTAACA
187	TAGATGGGGGGTAACGCCAGGGTTGTGCCAAG

188	ACCCGTCGTCATATGTACCCCGGTAAAGGCTA
189	CATGTCAAGATTCTCCGTGGGAACCGTTGGTG
190	TCAGGTCACTTTTGCGGGAGAAGCAGAATTAG
191	CTGTAATATTGCCTGAGAGTCTGGAAAACTAG
192	CAAAATTAAAGTACGGTGTCTGGAAGAGGTCA
193	TGCAACTAAGCAATAAAGCCTCAGTTATGACC
194	TTTTTGCGCAGAAAACGAGAATGAATGTTTAG
195	AAACAGTTGATGGCTTAGAGCTTATTTAAATA
196	ACTGGATAACGGAACAACATTATTACCTTATG
197	ACGAACTAGCGTCCAATACTGCGGAATGCTTT
198	CGATTTTAGAGGACAGATGAACGGCGCGACCT
199	CTTTGAAAAGAACTGGCTCATTATTTAATAAA
200	GCTCCATGAGAGGCTTTGAGGACTAGGGAGTT
201	ACGGCTACTTACTTAGCCGGAACGCTGACCAA
202	AAAGGCCGAAAGGAACAACTAAAGCTTTCCAG
203	GAGAATAGCTTTTGCGGGATCGTCGGGTAGCA
204	ACGTTAGTAAATGAATTTTCTGTAAGCGGAGT
205	TTTTCGATGGCCCACTACGTAAACCGTC
206	TATCAGGGTTTTCGGTTTGCGTATTGGGAACGCGCG
207	GGGAGAGGTTTTTGTAAAACGACGGCCATTCCCAGT
208	CACGACGTTTTTGTAATGGGATAGGTCAAAACGGCG
209	GATTGACCTTTTGATGAACGGTAATCGTAGCAAACA
210	AGAGAATCTTTTGGTTGTACCAAAAACAAGCATAAA
211	GCTAAATCTTTTCTGTAGCTCAACATGTATTGCTGA
212	ATATAATGTTTTCATTGAATCCCCCTCAAATCGTCA
213	TAAATATTTTTTGGAAGAAAAATCTACGACCAGTCA
214	GGACGTTGTTTTTCATAAGGGAACCGAAAGGCGCAG
215	ACGGTCAATTTTGACAGCATCGGAACGAACCCTCAG
216	CAGCGAAAATTTTACTTTCAACAGTTTCTGGGATTTTGCTAAACTTTT
Loop1	AACATCACTTGCCTGAGTAGAAGAACT
Loop2	TGTAGCAATACTTCTTTGATTAGTAAT
Loop3	AGTCTGTCCATCACGCAAATTAACCGT
Loop4	ATAATCAGTGAGGCCACCGAGTAAAAG
Loop5	ACGCCAGAATCCTGAGAAGTGTTTTT
Loop6	TTAAAGGGATTTTAGACAGGAACGGT
Loop7	AGAGCGGGAGCTAAACAGGAGGCCGA
Loop8	TATAACGTGCTTTCCTCGTTAGAATC
Loop9	GTACTATGGTTGCTTTGACGAGCACG

Loop10	GCGCTTAATGCGCCGCTACAGGGCGC

Table S 9: Folding strands (tube) for DNA-origami synthesis.

Name	Sequence
F1	CGGCCTTGATAGGAACCCATGTACAAACAGTT
F25	TGAGTTTCCGAGAAAGGAAGGGAACAAACTAT
F27	CAAGCCCACTGGTAATATCCAGAACGAACTGA
F28	CCGCCAGCCACCACCCTCATTTTCCTATTATT
F51	CTCAGAGCCATTGCAACAGGAAAAATATTTTT
F52	GGAAATACACCGCCACCCTCAGAACTGAGACT
F75	CCCTCAGACTACATTTTGACGCTCACCTGAAA
F76	GAAATGGATACTCAGGAGGTTTAGCGGGGTTT
F99	TATCACCGTTATTTACATTGGCAGACATTCTG
F132	GAACGTGGGTCACCAGTACAAACTTAATTGTA
F133	TGTAGCATTAGAGCTTGACGGGGAAATCAAAA
F156	CCCCGATTTCCACAGACAGCCCTCATCTCCAA
F157	CGTAACGACTAAATCGGAACCCTAGTTGTTCC
F180	GTAAAGCATCTAAAGTTTTGTCGTGAATTGCG
F181	ACGTTAGTCAAGTTTTTTGGGGTCAAAGAACG
F204	ACCCAAATAAATGAATTTTCTGTAAGCGGAGT
F100	GTCACACGTTTTTATAAGTATAGCCCGGCCGTCGAG
F205	TGCTAAACTTTTCGATGGCCCACTACGTAAACCGTC
N-111	AAACCCTCTTTTACCAGTAATAAAAGGGATTCACCA
N-216	CAGCGAAATTTTAACTTTCAACAGTTTCTGGGATTT

Table S 10: Used StA and StE elongations for DNA-origami synthesis and their respective complementary sequences used for the coupling reaction.

Name	Sequence
StA	TTTTTTTAGTAGGTGGTAGAG
StA^c	NH_2-TTTTCTCTACCACCTACTA
StE	TTTTTTTACTGACTGACTGACTGACTG
StE^c	NH_2-CAGTCAGTCAGTCAGTCAGT

Eco Scale Calculations (Aken et al., *Beilstein J. Org. Chem.* **2006**, *2*, 3)

Eco Scale of the current *grafting to* strategy:

Yield:		(100-70)/2 to (100-90)/2
Price:	over 50$ for 10 mmol	5
Safety:	DMF (flammable)	5
	DIPEA (toxic)	5
Setup:	common procedure (eppi tube)	0
Temperature:	Room temp (>24 h)	1
	Heating (>1 h) (37 °C)	2

Workup: simple spin filtration		0

Total: 23 - 33 (depending on yield)
Eco Scale: 100-(23 to 33) = 67 to 77 (70% to 90% yield)

Grafting from method of "Bottom-Up Fabrication of Nanopatterned Polymers on DNA Origami by In Situ Atom-Transfer Radical Polymerization" (Tokura et. al, *Angew. Chem. Int. Ed.* **2016**, *128*, 5786–5791.)

Here we calculated the Eco Scale for the introduction of the DNA-initiator to the origami surface and the *in situ* polymerization. Therefore, it was needed to make some assumptions for example the yield of this technique.

Yield:		(100-80)/2= 10
Price:	over 50$ for 10 mmol	5
Safety:	DMF (flammable)	5
	$CuBr_2$ (ecological damage)	5
Setup:	Instruments for controlled addition of chemicals	1
	Pressure equipment (freeze pump)	3
	Special glassware (Schlenk)	1
	Inert gas (Argon for polym.)	1
Temperature/time:	Heating, > 1 h	3
	Cooling, < 0 °C	5
Workup:	simple spin filtration, precipitation	0

Total: 39
Eco Scale: 100-(39) = 61

SUPPORTING INFORMATION: A VERSATILE AND EFFICIENT METHOD TO ISOLATE DNA–POLYMER CONJUGATES

Electronic Supplementary Information

A Versatile and Efficient Method to Isolate DNA-Polymer Conjugates

Nico Alleva, Katharina Eigen, David Y. W. Ng, Tanja Weil

Corresponding Author:

E-Mail: David Ng david.ng@mpip-mainz.mpg.de

Tanja Weil weil@mpip-mainz.mpg.de

Max Planck Institute for Polymer Research, Mainz 55128, Germany

CHEMICALS

Diethyl ether (Honeywell), petrolium ether (30-40 °C, Fisher Scientific), dichloromethane (Fisher Scientific),Tetramethylethylenediamine (TEMED) (Roth, >98.5%, p a), GeneRuler Ultra Low Range DNA Ladder (Thermofisher), tris-borate-EDTA buffer (Sigma Aldrich, 10x concentrate), nuclease-free water (QIAGEN), *N,N*-diisopropylethylamine (Roth, >99,5%), 1,4-dioxane (Sigma Aldrich, anhydrous, 99.8%), dimethylformamide (ACROS, extra dry, 99.8%), 4-cyano-4-(phenylcarbonothioylthio)pentanoic acid *N*-succinimidyl ester (Sigma Aldrich) and 2-(dodecylthiocarbonothioylthio)-2-methylpropionic acid *N*-hydroxysuccinimide ester (Sigma Aldrich) were used as received.

2,2'-Azobis(2-methylpropionitrile) (Fluka analytics, >98%) was recrystallized in methanol prior use.

Poly(ethylene glycol) methyl ether methacrylate (PEGMA, Sigma Aldrich, average M_n = 300 g/mol, stabilized with 100 ppm MeHQ and 300 ppm BHT), *N,N*-dimethylacrylamide (DMA, Sigma Aldrich, 99%, stabilized with 500 ppm MeHQ) and 2-hydroxyethyl acrylate (HEA, Acros, 97%, stabilized) were purified prior polymerization by removing the stabiliser with a small column filled with alumina.

N-Isopropyl acrylamide (NIPAM, TCI, >98%, stabilized with MeHQ) and diacetone acrylamide (DAAM, Alfa Aesar, 99%,) were purified by dissolving in dioxan and removing the stabiliser with a small column filled with alumina.

PROCEDURES AND METHODS

POLYMERIZATION

The polymerization procedure was carried out as described by Alleva et al. 2022[1]

For the polymerization of homo polymers or the first block of the block copolymers, the monomer, CTA and AIBN were dissolved in the polymerization solvent, purged with argon for 45-90 min and heated up to the respective temperature. The ratio of initiator to CTA was 1:10. After the reaction time, the reaction mixture was cooled down with an ice bath and a precipitate was formed in the respective precipitation solvent (Table S1). The collected solid was again dissolved and precipitated twice. The obtained solid was dried under vacuum.

The second block was obtained by dissolving the first block (macro CTA) in the polymerization solvent, adding AIBN and monomer, purged with argon for 45-90 min and heated up to respective temperature. After the reaction time, the reaction solution was cooled with an ice bath and precipitated in the precipitation solvent. The obtained solid was collected and dried under vacuum.

CTA REMOVAL

The polymerization procedure was carried out as described by Alleva et al. 2022[1]

The obtained polymer was dissolved in dioxane and an excess of AIBN was added. The reaction solution was heated up to 80 °C. After the reaction time, the reaction solution was cooled in an ice bath, and the polymer was participated in the respective precipitation solvent (Table S1). The obtained polymer was dried under vacuum and analysed with SEC (DMF, PMMA standard).

CONJUGATION REACTION

For a typical conjugation reaction, oligonucleotide (SDNA: NH_2-CCACCTACTA ; DNA: NH_2-TTTTCTCTACCACCTACTA or LDNA; NH_2-AGAAGATAAAAACATTTGATTTTTTCTCTACCACCTACTA) (50 nmol), polymer (50 equiv.) and DIPEA (200 equiv.) were mixed in a DMF/water (3:1) mixture to a total volume of 400 µL (125 µM DNA) and shaken for at least 48 h at room temperature. After the reaction time, 2.5 µL of the reaction solution was diluted and analysed with PAGE.

PAGE

The PAGE gel (15%) was prepared by mixing tetramethylethylenediamine (TEMED) (7.5 µL), 40% acrylamide/bis-acrylamide solution 37.5:1 (5.63 mL), 10x TRIS-borate-EDTA buffer (TBE buffer) (1.5 mL), water (7.9 mL) and 10% ammonium persulfate (APS) solution (75 µL) and casting the gel.

For monitoring the conjugation reaction via PAGE, 1 µL of diluted reaction solution (25 pmol DNA, for SDNA 62.5 pmol due to its smaller size and less intercalation of the dye) was mixed with water and loading dye (1.7 µL, 6x Thermo Fisher) to a total

volume of 10 µL and loaded onto the gel. The gel was run first at 100 V for 10 min and then at 150 V for 45–50 min on a Cell SureLockTM mini-cell electrophoresis system from Thermo Fisher using 0.5 × TBE buffer as the running buffer (44.5 mM Tris-Borate, 1 mM EDTA). Gene ruler ultra-low range DNA ladder (Thermo Fisher) was used as the DNA ladder. The gels are stained with SYBR Gold (2×, 50 mL) for 45 min at room temperature. The images were taken with ChemiDoc Touch Imaging System from Bio-Rad or G:BOX Chemi Gel Doc System from Syngene. For intensity measurement ImageJ was used to determine the intensity of the respective band.

SEC

Polymer measured with SEC: 10–20 mg of dry polymer was measured via the SEC method stated below.

Preparing the obtained DNA-polymer conjugate for SEC: 100–200 µL of the obtained conjugate solution was freeze dried. The obtained solid was measured via the SEC method stated below.

For the purification approach, 8 µL (1 nmol) were diluted with DMF to 100 µL and injected.

SEC experiments were performed on a PSS SECurity instrument comprising an auto sampler, a column oven with three GRAM columns (10^3, 10^3 and 10^2 Å, 300 × 8 mm, 10 µm particle size) and a RI as well as an UV detector (Agilent Technologies 1260 Infinity). DMF containing 1 g/L lithium bromide was used as the eluent at a flowrate of 1 mL/min. Poly(methyl methacrylate) (1600 kDa–800 Da) served as the calibration standard for molecular weight measurements. The samples were filtered (0.4 µm) prior to injection. The data were fitted with OriginPro 2021.

SPIN FILTRATION (SF) FOR PURIFICATION

For the spin filtration, 200 µL of reaction solution, containing 25 nmol DNA were given to the respective spinfilter ((Amicon Ultra-6 mL Centrifugal Filters MWCO 10k or 30k cutoff) and were centrifuged 8 times for 1 hour. After each centrifugation the filtrate was discarded, the filter was refilled with 6 mL water and the solution was mixed. Centrifuged at 3900 rpm.

HIGH PRESSURE LIQUID CHROMATOGRAPHY (HPLC) FOR PURIFICATION

HPLC instrument from Shimadzu was used including an auto sampler, a column oven and a fraction collector. The samples were purified by analytical HPLC using the column Jupiter 5 µm C18 300A (4.6 × 150 mm, 5 µm at a flowrate of 1 mL/min. The elution protocol started with the mobile phase from 5% solvent B (HPLC grade acetonitrile) and 95% solvent C (0.1 M triethylammonium acetate buffer), raising to 15% B, then to 25% B and then increasing to 100% B, hold it for 20 min then decreasing to 5% B in 4 min. The absorbance was monitored at 240 nm and 260 nm. 8 µL (1 nmol) were injected.

TECAN ABSORBANCE MEASUREMENT

To determine the concentration of the obtained DNA–polymer conjugate solutions after the purification, Tecan Spark was used to measure the absorbance at 260 nm. Extinction coefficient of the SDNA block: 83720 $L \cdot mol^{-1} \cdot cm^{-1}$ DNA block: 187700 $L \cdot mol^{-1} \cdot cm^{-1}$ LDNA block: 344186 $L \cdot mol^{-1} \cdot cm^{-1}$; d = 0.5 mm.

ANION EXCHANGE COLUMN

Cytiva Capto™ HiRes Q 5/50 was used for the purification of DNA–polymer conjugates. The column was stored at 20% EtOH/water.

ÄKTA SYSTEM

The ÄKTA pure™ system was used as the device for using the anion exchange column.

PREPARING REACTION SOLUTION FOR AKTA PURIFICATION

The included DMF of the obtained reaction solutions were removed via spin filtration (Amicon Ultra-6 mL Centrifugal Filters MWCO 2k or 10k) by adding 5 mL nuclease-free water to the reaction solution and centrifuge for 1 h. This was repeated three times.

ÄKTA PURIFICATION METHOD

The following pictures/screenshots show the purification method, used with the ÄKTA pure™ with the anion exchange column Cytiva Capto™ HiRes Q 5/50 build in. The screenshots show the method applied for all conjugate purifications containing the 19 base oligonucleotide. The gradient is driven to 20% and held then isocratic. Please notice that for the short 10 base oligonucleotide the gradient is driven to 15% instead of 20% and for the long 40 base oligonucleotide the gradient is driven to 25%. All other parameters, pressures, flow rates etc. are the same.

Figure S1: Overview of the single steps of the purification method

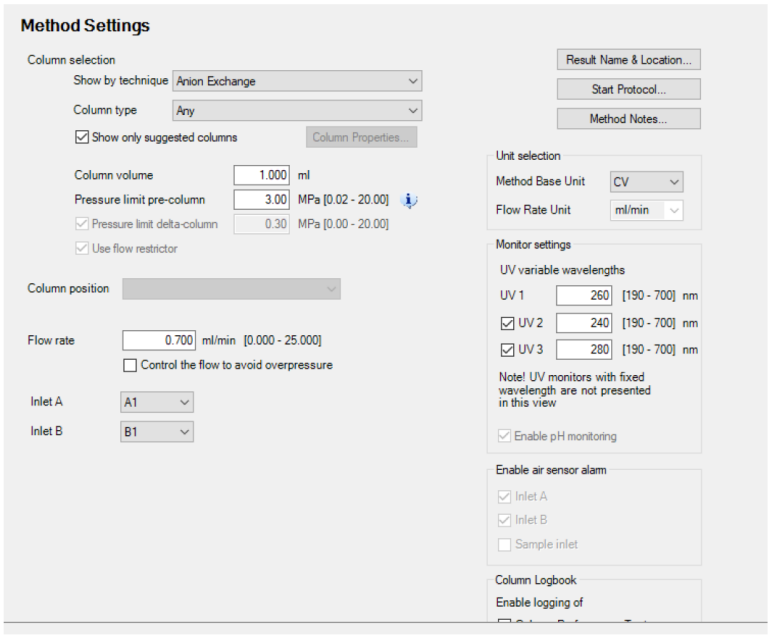

Figure S2: General method settings. A1 is water and B1 is NaCl solution (2M).

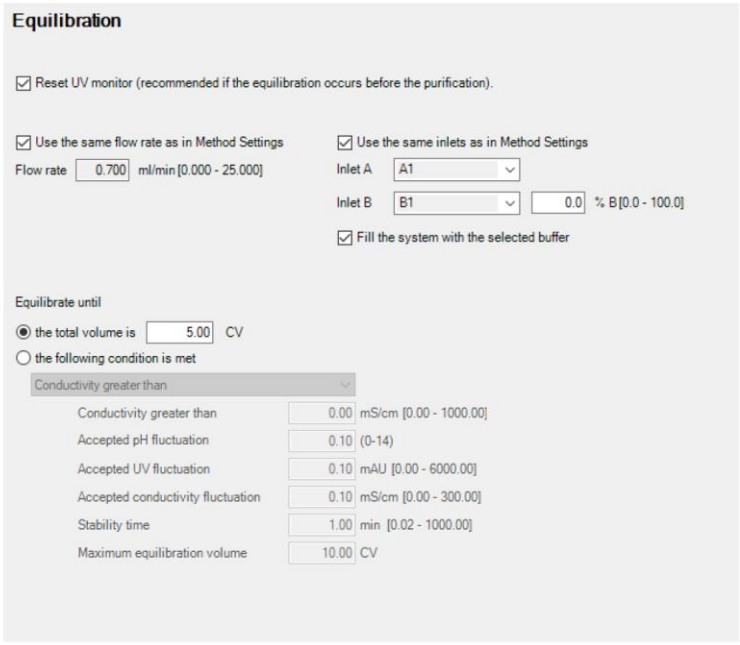

Figure S3: Equilibration step.

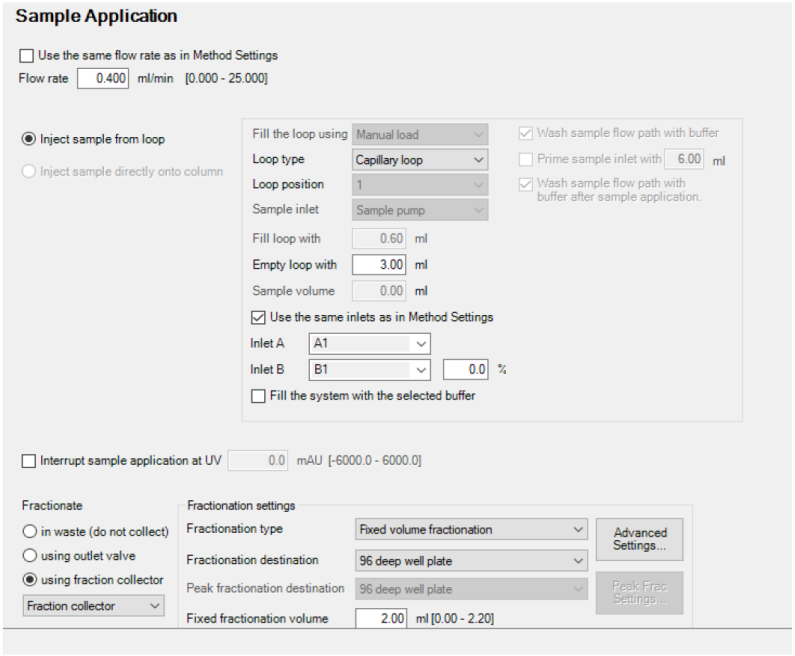

Figure S4: Sample application step.

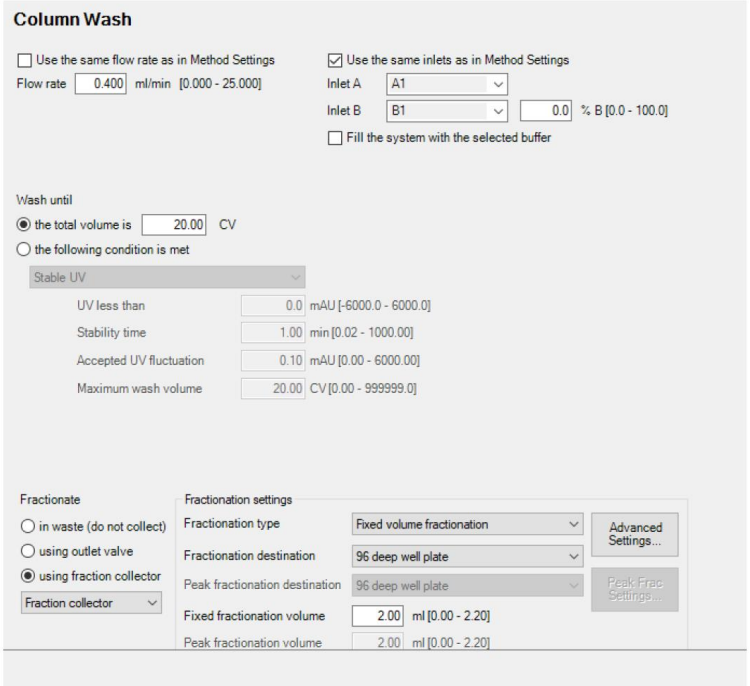

Figure S5: First column wash step to remove the uncharged, unreacted polymer excess.

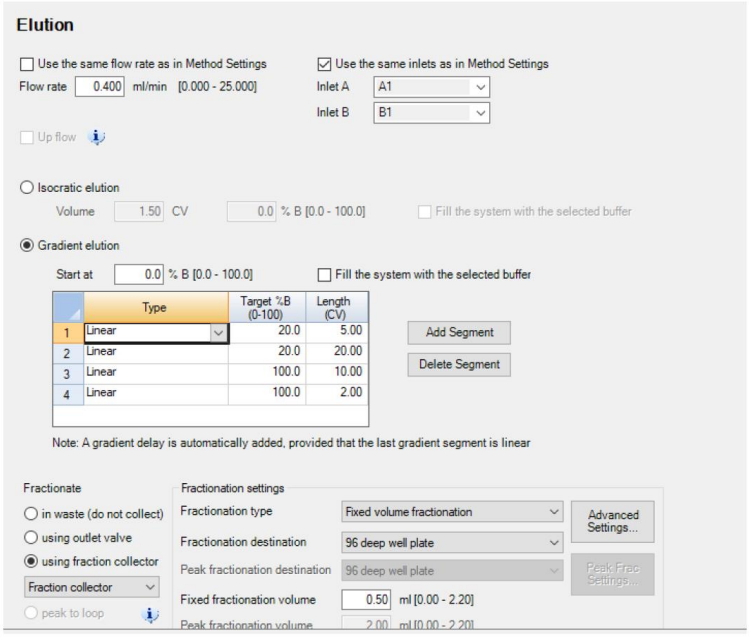

Figure S6: Elution step. In this step the gradient is driven to the respective limit to elute the DNA-polymer conjugate and at higher concentrations the unreacted oligonucleotide.

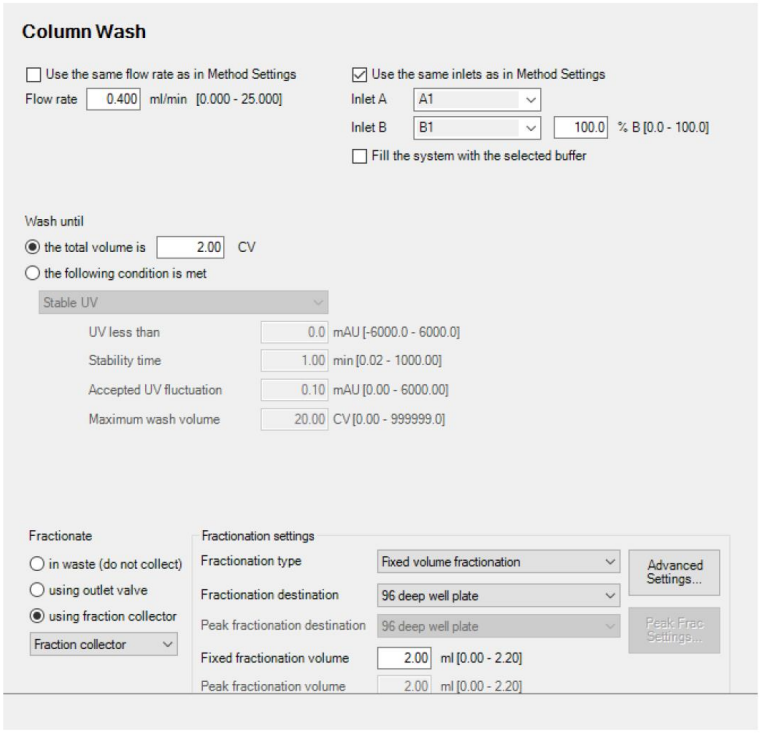

Figure S7: Column wash step with 100% NaCl (2M) solution to remove all leftovers from the column.

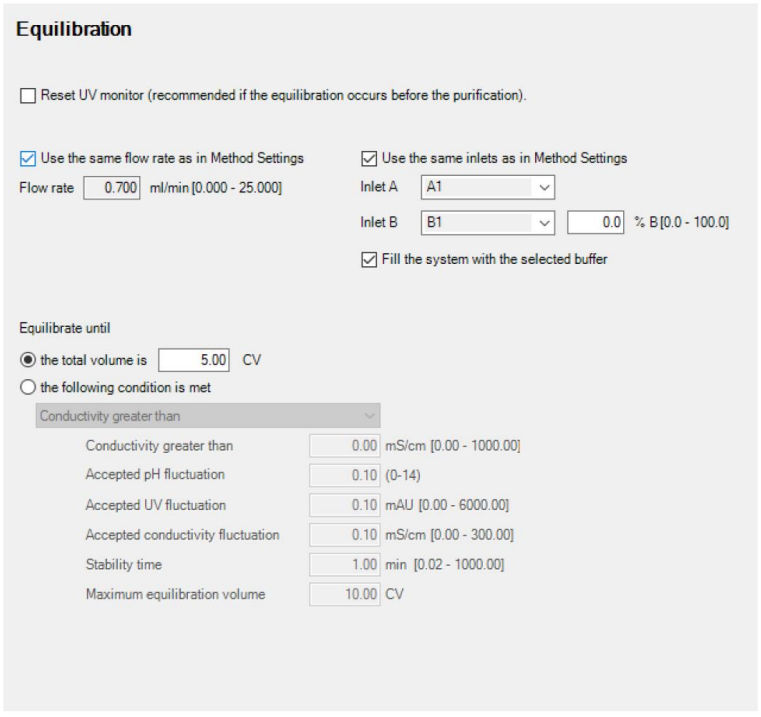

Figure S8: Equilibration step to remove NaCl leftovers and set the milieu to water again.

POST-PREPARATION OF THE OBTAINED PURE CONJUGATE SOLUTION FROM ÄKTA

The obtained solutions contain NaCl due to the purification process. To remove the salt, the solutions were diluted with nuclease-free water and spin filtered with Amicon Ultra-6 mL Centrifugal Filters MWCO 10k for 20 min. This process is repeated three times.

Results and Discussion:

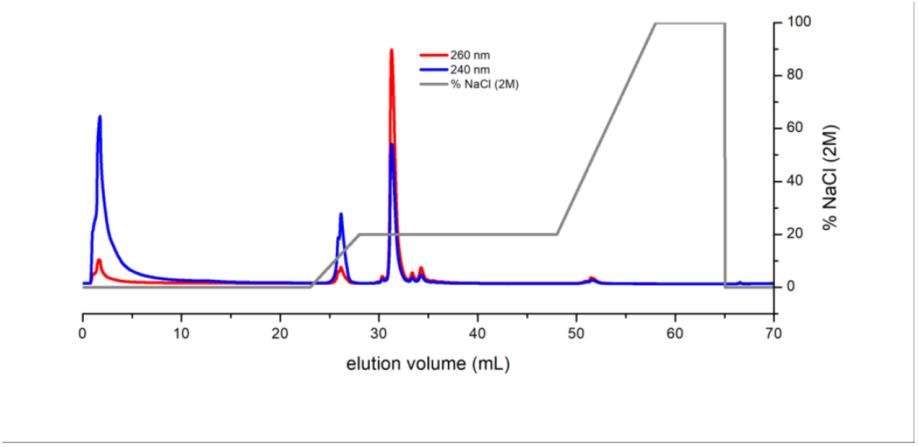

Figure S9: Elution diagram of CP1 reaction solution.

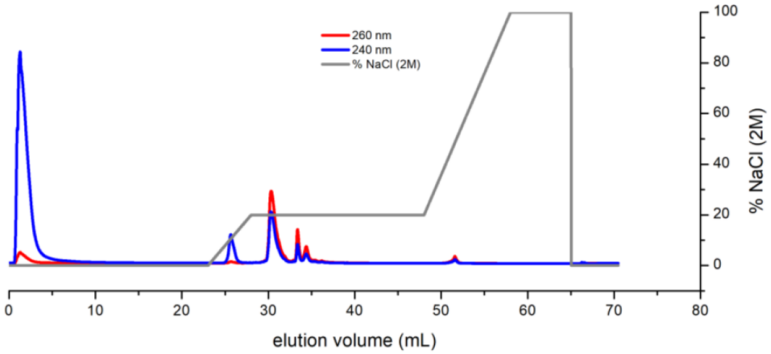

Figure S10: Elution diagram of CP3 reaction solution.

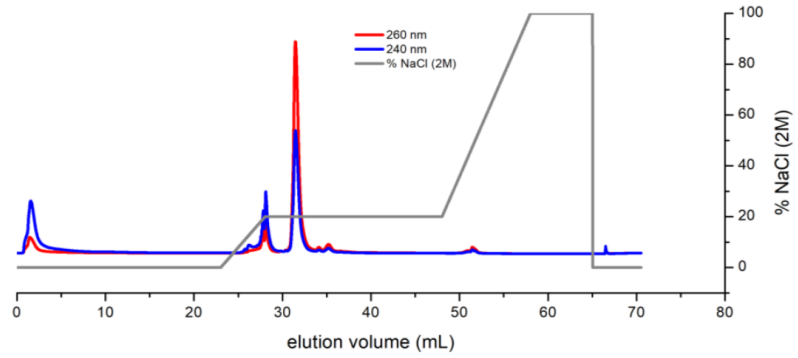

Figure S11: Elution diagram of the CP4 reaction solution.

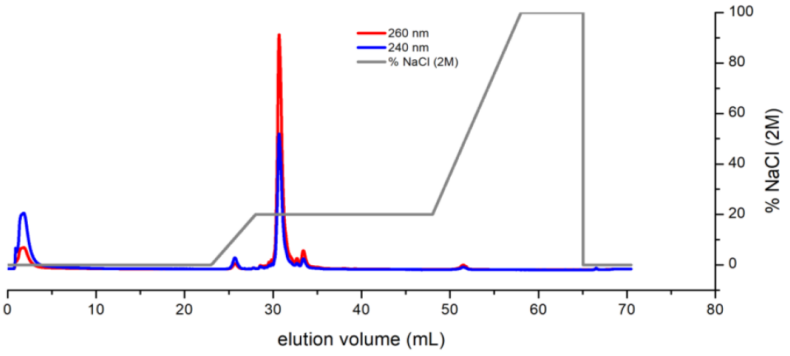

Figure S12: Elution diagram of the CP5 reaction solution.

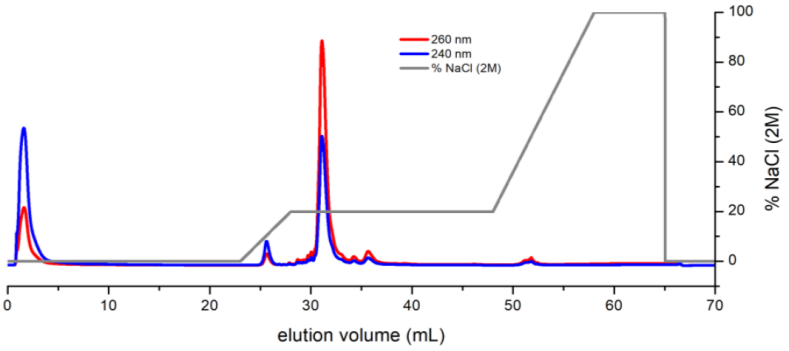

Figure S13: Elution diagram of the CP6 reaction solution.

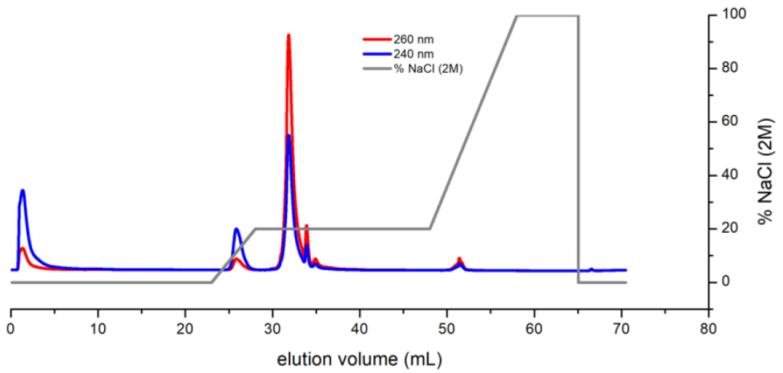

Figure S14: Elution diagram of the CP7 reaction solution.

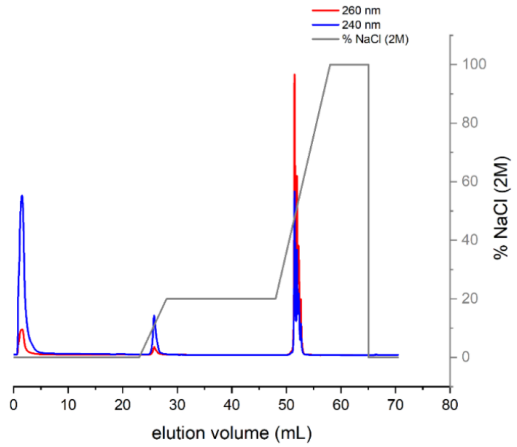

Figure S15: Elution diagram of LCP2 from the first applied gradient. The diagram shows clearly, that the conjugate and also the unreacted oligonucleotide eluate at higher NaCl concentration.

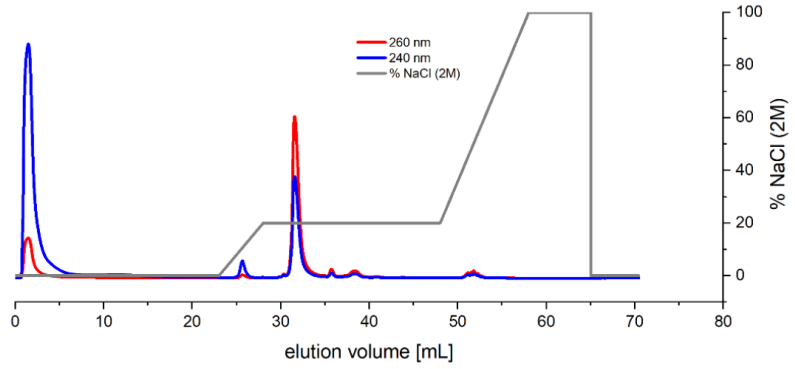

Figure S16: Elution diagram of the CP8 reaction solution.

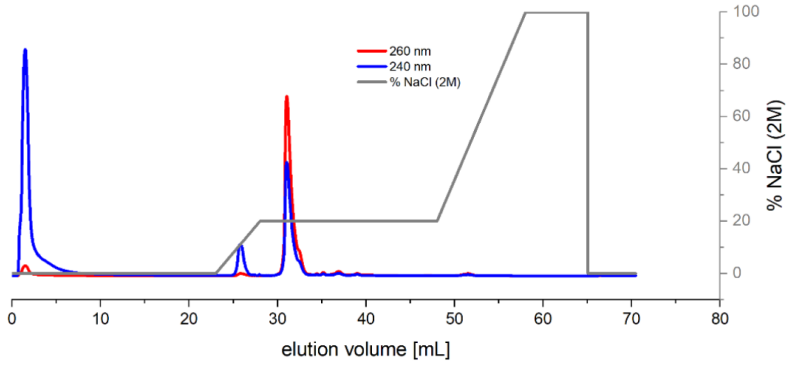

Figure S17: Elution diagram of the CP9 reaction solution.

Table S1: Overview of the synthesized polymers, polymerization parameters and purification solvents.[1]

Polymer	M_w (SEC)	Đ (SEC)	Amount I. Block (SEC)	Used CTA	Polym. solvent	Precipitation solvent	Reaction Temp.	Reaction time
P(DMA) (P1, P2, P3)	9649	1.08	/	NHS-DDMAT	dioxane	diethyl ether	70 °C	18 h
	22125	1.08					70 °C	18 h
	48637	1.27					65 °C	4 h
P(NIPAM) (P4)	21448	1.12	/	NHS-DDMAT	dioxane	diethyl ether	70 °C	16 h
P(PEGMA) (P5)	21090	1.19	/	NHS-CPADB	dioxane	diethyl ether (- 20 °C, phase separation)	70 °C	20.5 h
P(DAAM-*b*-DMA) (P6)	26013	1.20	29%	NHS-DDMAT	dioxane	petrol ether	I. Block: 70 °C II. Block: 55 °C	17 h 21 h
P(HEA) (P7)	21978	1.28	/	NHS-DDMAT	DMF	diethyl ether	60 °C	17 h
P(DAAM-*co*-DMA) (P8)	26614	1.22	2:7 (NMR)	NHS-DDMAT	dioxane	petrolether	70 °C	17 h
P(NIPAM-*b*-DMA) (P9)	30445	1.19	43%	NHS-DDMAT	dioxane	diethylether	I. Block: 70 °C II. Block: 65 °C	15 h 17 h

Table S2: Overview of the synthesized polymers, the conversion of the coupling reaction with the 19 base oligonucleotide[1], the yield after purification and the molecular weight/dispersity of the conjugates given by SEC, measured in DMF. Yield after purification is calculated with conversion of the coupling reaction= 100%.

Polymer	M_w (SEC)	Đ (SEC)	Conversion (%)[1]	Yield after purification (%)	M_w conjugate (SEC)	Đ conjugate (SEC)
P(DMA) (P1, P2, P3)	9649	1.08	~93	Quantitative	11081	1.21
	22125	1.08	~88	~96	22761	1.21
	48637	1.27	~80	~67	46077	1.34
P(NIPAM) (P4)	21448	1.12	~93	~98	23936	1.19
P(OEGMA) (P5)	21090	1.19	~94	~63	23600	1.26
P(DAAM-*b*-DMA) (P6)	26013	1.20	~96	~60	33841	1.11
P(HEA) (P7)	21978	1.28	~94	~70	23278	1.33
P(DAAM-*co*-DMA) (P8)	26614	1.22	~69	~93	27791	1.25
P(NIPAM-*b*-DMA) (P9)	30445	1.19	~97	~72	31817	1.34

Table S3: Conversion determination using ImageJ intensity calculator to calculate conversion of the CP8 conjugation reaction. Used PAGE gels are shown in Figure S22

	Intensity	Conversion
DNA	307.37	
CP8	96.07	69%

Table S4: Conversion determination using ImageJ intensity calculator to calculate conversion and the yield after ÄKTA of the LDNA, LCP2, SDNA and SCP2. Used PAGE gel is shown in Figure 4a

	Intensity	Conversion	Yield after ÄKTA if conv. Is 100%
LDNA	2457		
LCP2	1137	54%	81.4%
SDNA	/		
SCP2	/	Quant.	73.5%

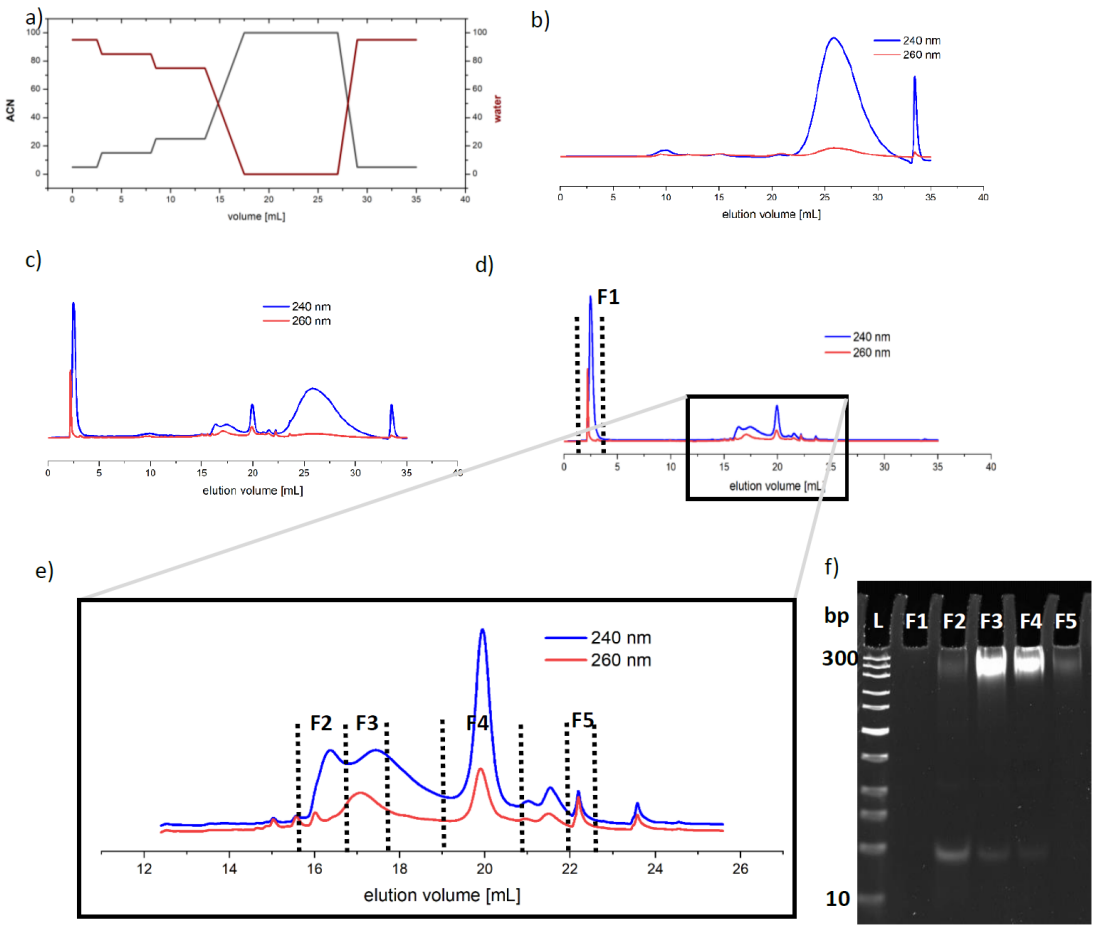

Figure S18: HPLC purification method for the reaction solution **CP2** after coupling. a) Applied stepwise gradient of the purification method with Acetonitrile (ACN) and water as solvents. b) elution diagram with absorption detection of the solvents as baseline. c) elution diagram of the reaction solution purification d) elution diagram with deducted solvent absorption. e) Magnification of the elution diagram in d) for better peak observation. f) PAGE gel (15%) of the respective fractions. Stained with SYBR Gold (2x).

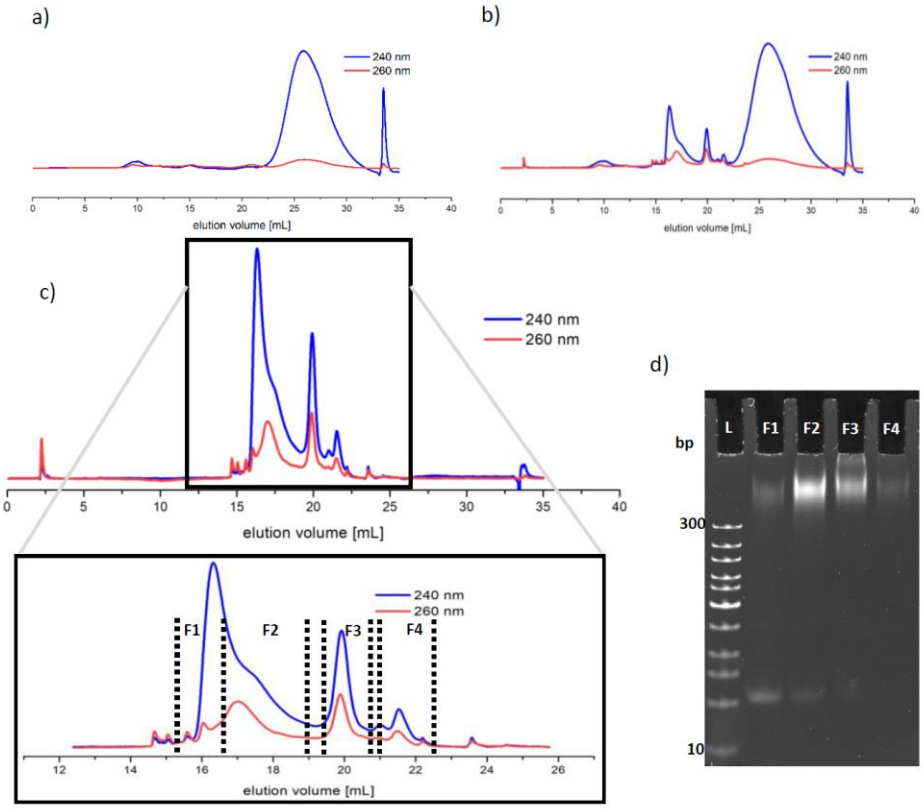

Figure S19: HPLC purification method for the spin filtered reaction solution **CP2** (DMF removed) after coupling with the same stepwise gradient. a) elution diagram with absorption detection of the solvents as baseline. b) elution diagram of the reaction solution purification c) HPLC elution diagram with deducted solvent absorption of the **CP2** reaction solution purification without DMF. Magnification of the elution diagram for the respective fractions. d) PAGE gel (15%) of the respective fractions of the conducted **CP2** reaction solution purification containing DMF. Stained with SYBR Gold (2x).

Table S5: Intensity of the obtained conjugate CP2 from the respective fraction from the PAGE gels shown in Figure S18 and S19 and the calculated proportion from the whole conjugate intensity.

With DMF:		
Fraction	Intensity (ImageJ)	Proportion
1	0	0
2	5.955	13.2%
3	17.352	38.4%
4	15.850	35.1%
5	5.980	13.2%
Without DMF:		
1	5.362	14.6%
2	14.850	40.4%
3	11.683	31.8%
4	4.846	13.2%

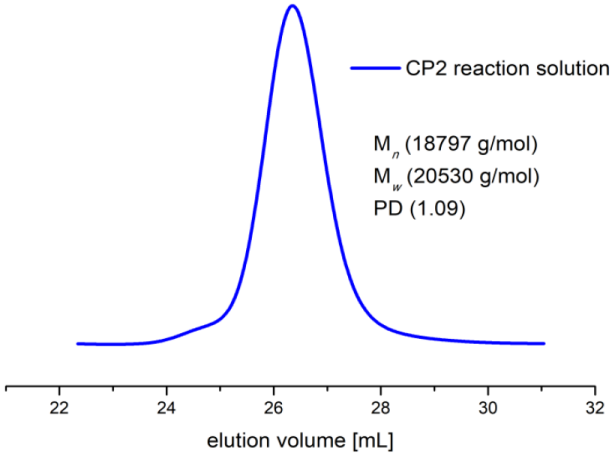

Figure S20: Elution diagrams of the conjugates **CP2** reaction solution measured by DMF SEC using polymethylmethacrylate (PMMA) as standard.

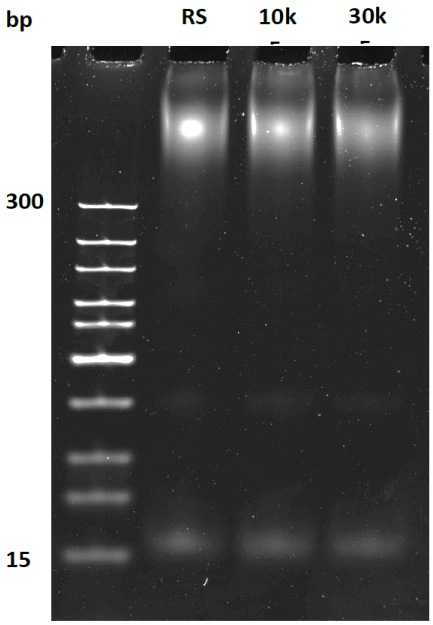

Figure S21: PAGE gel (15%) of the spin filtration of CP2 reaction solution using 10k and 30k cutoff spinfilter. Staine with SYBR Gold (2x).

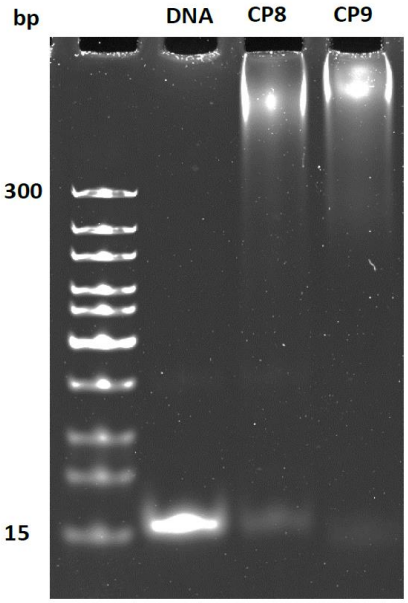

Figure S22: PAGE gel (15%) of the CP8 and CP9 reaction solution. Staine with SYBR Gold (2x).

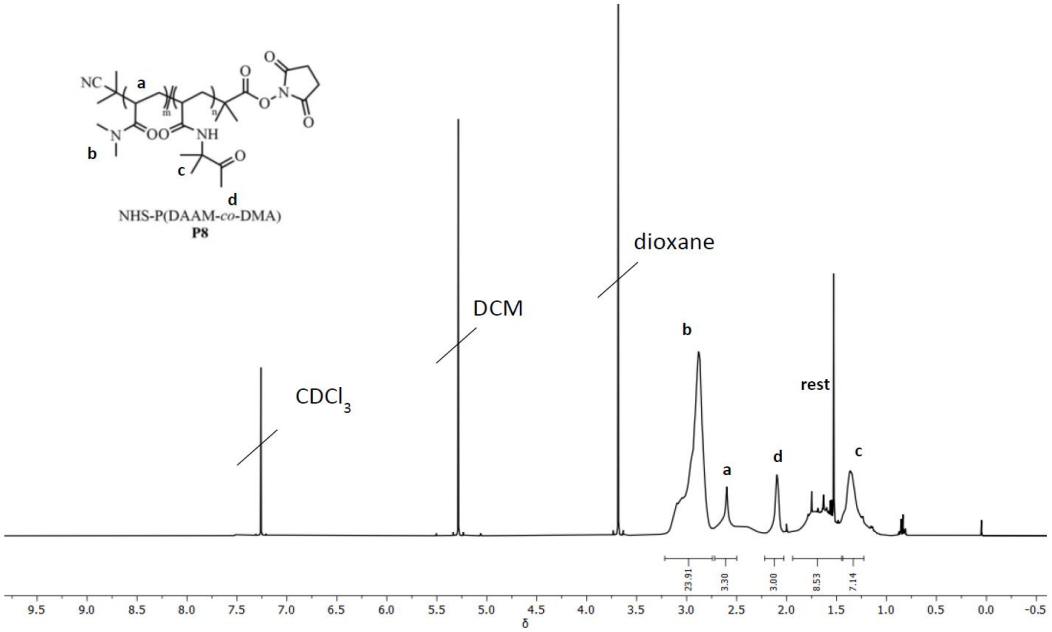

Figure S23: ^{1}H-NMR of P8 synthesized by RAFT polymerization. CTA group was removed with an excess of AIBN.

REFERENCES

(1) Alleva, N.; Winterwerber, P.; Whitfield, C. J.; Ng, D. Y. W.; Weil, T. Nanoscale patterning of polymers on DNA origami. *J. Mater. Chem. B* **2022**, *10*, 7512–7517.

PEPTIDE BISPECIFICS INHIBITING HIV-1 INFECTION BY AN ORTHOGONAL CHEMICAL AND SUPRAMOLECULAR STRATEGY

Bioconjugate Chemistry

Editors' Choice
Open Access

pubs.acs.org/bc

Article

Peptide Bispecifics Inhibiting HIV-1 Infection by an Orthogonal Chemical and Supramolecular Strategy

Dominik Schauenburg,[§] Fabian Zech,[§] Astrid Johanna Heck, Pascal von Maltitz, Mirja Harms, Siska Führer, Nico Alleva, Jan Münch, Seah Ling Kuan,* Frank Kirchhoff,* and Tanja Weil*

Cite This: *Bioconjugate Chem.* 2023, 34, 1645−1652

Read Online

ACCESS | Metrics & More | Article Recommendations | Supporting Information

ABSTRACT: Viral infections pose a significant threat to human health, and effective antiviral strategies are urgently needed. Antiviral peptides have emerged as a promising class of therapeutic agents due to their unique properties and mechanisms of action. While effective on their own, combining antiviral peptides may allow us to enhance their potency and to prevent viral resistance. Here, we developed an orthogonal chemical strategy to prepare a heterodimeric peptide conjugate assembled on a protein-based nanoplatform. Specifically, we combined the optimized version of two peptides inhibiting HIV-1 by distinct mechanisms. Virus-inhibitory peptide (VIRIP) is a 20 amino acid fragment of α1-antitrypsin that inhibits HIV-1 by targeting the gp41 fusion peptide. Endogenous peptide inhibitor of CXCR4 (EPI-X4) is a 16-residue fragment of human serum albumin that prevents HIV-1 entry by binding to the viral CXCR4 co-receptor. Optimized forms of both peptides are assembled on supramolecular nanoplatforms through the streptavidin−biotin interaction. We show that the construct consisting of the two different peptides (SAv-VIR-102C9-EPI-X4 JM#173-C) shows increased activity against CCR5- and CXCR4-tropic HIV-1 variants. Our results are a proof of concept that peptides with different modes of action can be assembled on nanoplatforms to enhance their antiviral activity.

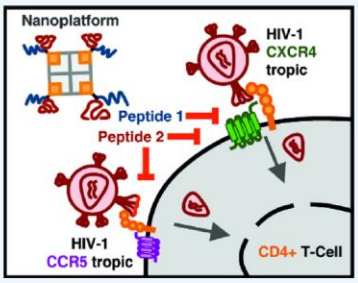

INTRODUCTION

Viral diseases pose substantial threats to public health, socioeconomic stability, and global economic structures, as vividly underscored by the recent SARS-CoV-2 pandemic. Additionally, other pandemic pathogens, like HIV-1, remain inadequately controlled, with approximately 1.7 million new HIV-1 infections and ~700,000 AIDS-related deaths reported for 2020.[1] Increasing drug resistance further exacerbates the challenges faced by current antiretroviral treatment strategies. In addition, effective and specific drugs are only available for a very limited number of viral pathogens[2,3] underscoring the urgent need for novel therapeutic interventions. Most antiviral drugs target viral enzymes to inhibit viral replication.[2] This requires cellular uptake, which increases the potential for adverse effects. Consequently, therapeutic agents designed to block viral entry into cells provide a promising approach. The process of viral infection is multistage, involving attachment, anchoring, fusion, and eventual entry into host cells, each step offering targets for inhibitory agents. Furthermore, many viruses rely on multiple cellular receptors for infection, which also present potential intervention points. For instance, the initial step in HIV-1 replication involves the attachment of the viral envelope glycoprotein gp120 to the cellular CD4 receptor. This attachment triggers conformational changes that allow gp120 to bind to the CCR5 or CXCR4 co-receptors, subsequently allowing the insertion of the fusion peptide of the viral transmembrane protein gp41 into the target cell membrane. This sequence concludes with the formation of a six-helix bundle, pulling the viral and cellular membranes together to achieve fusion. Essentially all HIV-1 variants are critically dependent on CCR5 or CXCR4 for infection. CCR5 is critical for HIV-1 transmission and used during chronic infection, while CXCR4- and/or dual-tropic viral variants emerge in up to 50% AIDS patients and are associated with poor prognosis.[4,5] All of these forms of HIV-1 may coexist in infected individuals and need to be targeted for effective therapy and to prevent resistance.[5]

Two entry inhibitors have so far been approved for clinical treatment of HIV-1 infection: Maraviroc (brand name Selzentry) blocks the CCR5 co-receptor on the surface of the host cell but is inactive against HIV-1 strains using CXCR4 for viral entry.[6] The peptidic fusion inhibitor enfuvirtide (brand name Fuzeon) binds to helical regions in the viral gp41 and prevents six-helix bundle formation required for fusion of the viral and host cell membranes.[7] Additional co-receptor

Received: July 14, 2023
Revised: August 18, 2023
Published: September 4, 2023

https://doi.org/10.1021/acs.bioconjchem.3c00314
Bioconjugate Chem. 2023, 34, 1645−1652

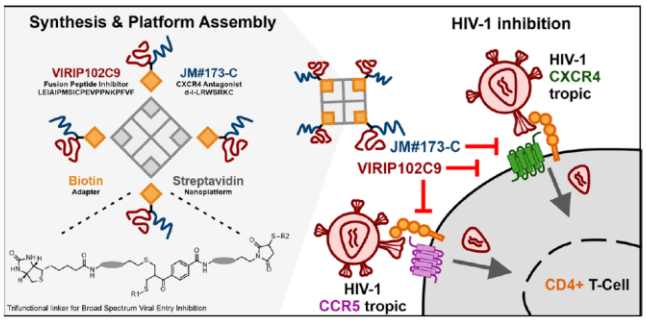

Figure 1. Overview showing the design of the linker for the synthesis of the bispecific VIR-102C9/EPI-X4 JM#173-C and a representation of the antiviral activity of the tetravalent VIR-102C9/EPI-X4 JM#173-C assembled on streptavidin.

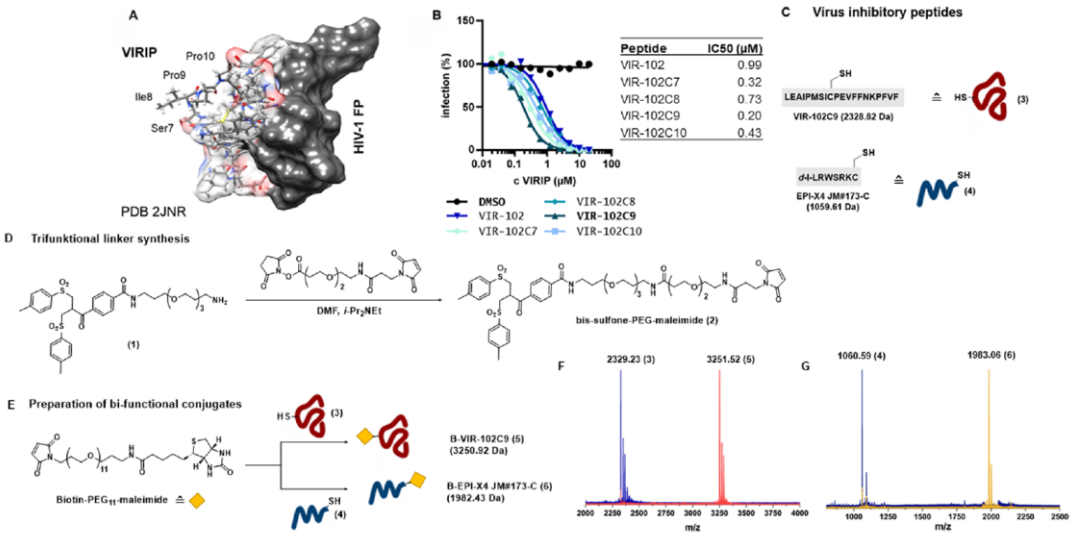

Figure 2. (A) NMR structure of VIR-165 binding the HIV-1 fusion peptide (PDB 2JNR).[17] VIR-165 positions 7−10 are highlighted. Image is created using UCSF Chimera 1.13.1.[23] (B) Inhibition of wild-type HIV-1 NL4-3 by single-cysteine VIRIP derivatives. (C) Single letter code and molecular weight of VIR-102C9 (**3**) and EPI-X4 JM#173-C (**4**). (D) Synthesis of the linker bis-sulfone-PEG-maleimide (**2**). (E) Bioconjugation of B-VIR-102C9 (**5**) and B-EPI-X4 JM#173-C (**6**) conjugate. (F) MALDI-TOF spectrum of unconjugated (blue) and biotinylated VIR-102C9 peptide (red). (G) MALDI-TOF spectrum of unconjugated (blue) and biotinylated EPI-X4 JM#173-C peptide (orange). Full spectra of **5** and **6** are available in the SI.

antagonists and fusion inhibitors have been suggested as possible therapeutic candidates. For example, derivatives of the endogenous peptide inhibitor of CXCR4 (EPI-X4), a 16 amino acid fragment of human serum albumin, act as highly specific CXCR4 antagonists and efficiently inhibit CXCR4 (X4)-tropic HIV-1 strains (Figure 1).[8,9] Recently, optimized variants of EPI-X4 have been developed, e.g., the seven amino acid EPI-X4 JM#173, which is stable in blood plasma for more than 8 h.[10] Optimized EPI-X4 derivatives show promise as therapeutic agents for CXCR4-linked diseases, exhibiting anti-inflammatory and anticancer functions in preclinical mouse models.[11,12] Thus, they are currently further developed for therapeutic applications.[13−16] VIRIP is the only known inhibitor for the gp41 fusion peptide and prevents anchoring of the virus into the cellular membrane. It consists of 20 amino acids corresponding to the C-proximal region of α1-antitrypsin (Figure 2A).[17] VIRIP-based inhibitors are active against all HIV-1 variants including multiresistant strains due to their distinct mode of action.[17−19]

Intravenous infusion of the optimized VIRIP derivative (VIR-576) reduced the mean plasma viral load by up to 98% without causing severe adverse effects.[18] In addition, it has been demonstrated that VIRIP-based inhibitors pose a very high barrier to HIV-1 resistance.[19] However, monotherapy with VIR-576 showed fast clearances and required infusion of high doses of the peptide.[17,18] Altogether, HIV-1 entry can be targeted by agents that block CD4 receptor or CXCR4 and CCR5 co-receptor engagement, as well as steps involved in membrane fusion. Combining antiretroviral peptides with different modes of action may enhance their potency,[20] prevent the development of drug resistance, and increase the bioavailability and in vivo half-life due to their enlarged size

https://doi.org/10.1021/acs.bioconjchem.3c00314
Bioconjugate Chem. 2023, 34, 1645−1652

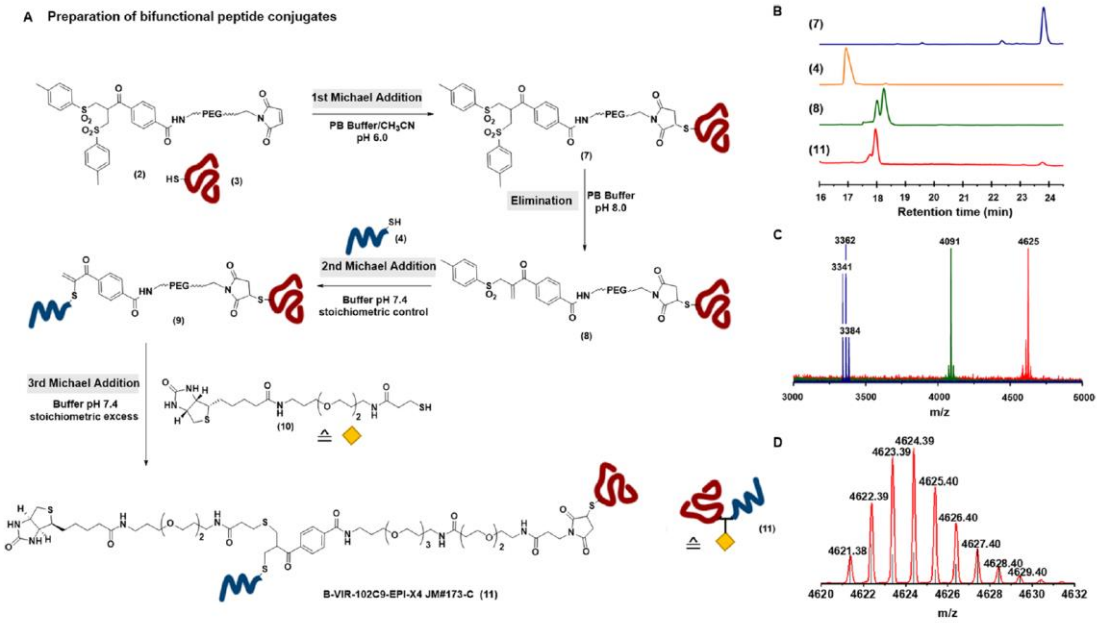

Figure 3. (A) Bioconjugation of B-VIR-102C9-EPI-X4 JM#173-C peptide conjugate (**11**). (B) HPLC spectrum of VIR-102C9 bis-sulfone (**7**), EPI-X4 JM#173-C peptide (**4**), VIR-102C9-EPI-X4 JM#173-C vinyl thioether as a racemic mixture (**9**) and B-VIR-102C9-EPI-X4 JM#173-C conjugate (**11**). (C) MALDI-TOF spectrum of VIR-102C9 bis-sulfone (**7**) (blue), VIR-102C9-EPI-X4 JM#173-C vinyl thioether (**9**) (green), and B-VIR-102C9-EPI-X4 JM#173-C conjugate (**11**) (red). Full spectra of **7**, **9**, and **11** are available in the SI. (D) Isotopic pattern of deconvoluted TOF MS ESI spectrum in positive mode of B-VIR-102C9-EPI-X4 JM#173-C (**11**). Deconvoluted spectrum for **11** showing molecular weight. Exact mass determined for m/z = $[M+5H]^+$ calc: 925.823, found 925.2822.

and combined action. While solid-phase peptide synthesis or native chemical ligation can be used to combine two different peptide sequences, there are limitations. For example, spacers such as poly(ethylene glycol) could be required to ensure that the active amino acids are sufficiently extended and both peptide sequences remain exposed to address the receptors or binding to particles. In other instances, extension of the second peptide sequence from an internal amino acid could be required where the N- or C-termini are critical for activity.[21,22]

To overcome these limitations and generate new antiviral peptide bispecifics, we devised a pH-controlled, stepwise chemical conjugation strategy to prepare and assemble optimized versions of the EPI-X4 derivative JM#173 and the anchoring inhibitor VIRIP (Figure 1). As a proof of concept, we prepared a streptavidin hybrid that contains four copies of the bispecific EPI-X4 JM#173-C and the VIRIP variant 102C9. We demonstrate that this construct inhibits HIV-1 in nanomolar concentrations and shows enhanced activity against CCR5 (R5)- and CXCR4-tropic HIV-1.

■ RESULTS AND DISCUSSION

Design of Mono-Peptide and Dipeptide Antiviral Conjugates. To enable the assembly of two antiviral peptides to a supramolecular protein platform, i.e., streptavidin (SAv), we had to further include a biotin group (B) that allows binding to four pockets in tetrameric SAv. Thus, a linker with three sites for chemical functionalization was required. To ensure ease of synthesis of the peptide sequences and minimal influence on the bioactivity of the antiviral peptides, a single cysteine was introduced into each of the peptide sequences. As the N- and C-termini are important for the antiviral activity of VIRIP,[17] we screened a series of variants with internal cysteines (Figure 2B,C) and selected VIR-102C9 (**3**) with the lowest IC50 (0.20 μM) for further study. In comparison, EPI-X4 derivatives interact with CXCR4 via the seven N-terminal amino acid residues.[11] Thus, to maintain CXCR4 binding and antiviral activity after conjugation, a C-terminal cysteine was incorporated into EPI-X4 JM#173 and termed JM#173-C, (**4**, Figure 2C). One of the major challenges is to ensure selectivity in a sequential manner with the different thiol-containing peptides.[24] Specifically, the linker requires three reactive sites for successive Michael additions of natural amino acids (cysteine sidechains) and biotin thiol in a chemoselective fashion. Thus, we designed a linker, which allows pH-controlled reaction of different thiol-containing molecules of interest (Figure 2D). As a first thiol-reactive group, we chose the well-known maleimide reagent, which can undergo Michael addition even under slightly acidic reaction conditions, due to its high reactivity.[25,26] As a second chemical handle, we applied a bis-sulfone that is activated only in slightly alkaline condition, for disulfide re-bridging[27] or for two successive thiol conjugations (Figure 2D).[28]

We began our studies with the preparation of bifunctional conjugates (**5** and **6**) consisting of the individual antiviral peptide (VIR-102C9, **3** or EPI-X4 JM#173-C, **4**) and a biotin group for assembly. Biotinylation of the peptides was performed using a commercially available biotin-PEG_{11}-maleimide (see Figure 2E) under neutral, buffered conditions. We obtained bifunctional conjugates B-VIR-102C9 (**5**) and B-EPI-X4 JM#173-C (**6**) in 62 and 67% yields, respectively. The

https://doi.org/10.1021/acs.bioconjchem.3c00314
Bioconjugate Chem. 2023, 34, 1645−1652

peptides were identified by MALDI-ToF mass spectrometry through their m/z at 3252 and 1983 $[M + H]^+$, respectively. Monopeptides **5** and **6** were further assembled to the tetrameric biotin-binding protein (SAv) and used as controls for comparison with the bifunctional construct derived from the newly designed B-VIR-102C9-EPI-X4 JM#173-C (**11**, see Figure 3A).

To allow multimerization of different antiviral peptides on SAv, we aimed to conjugate the HIV-1 fusion peptide inhibitor VIR-102C9 (**3**) and the CXCR4 antagonist EPI-X4 JM#173-C (**4**) to our newly designed linker molecule (**2**). In the first step, we conjugated VIR-102C9 selectively to the maleimide under slightly acidic conditions (pH 6.0) to afford VIR-102C9 bis-sulfone (**7**) and VIR-102C9 allyl sulfone (**8**) after HPLC purification. β-Ketosulfones are prone to undergo elimination reactions under strongly basic conditions to yield α,β-unsaturated carbonyl compounds.[29] A small peak was observed in the chromatogram which could be due to a trace amount of elimination of the sulfinic acid in acidic pH. However, due to the fast reaction rate of the maleimide-thiol addition, this will not have a substantial effect on the chemoselectivity.[27] Furthermore, the products were purified by HPLC. Thereafter, **7** was incubated at pH 8.0 enabling the elimination of the first *p*-toluoyl sulfinic acid to gain the thiol-reactive allyl sulfone (**8**). The second cysteine-containing peptide (EPI-X4 JM#173-C, **4**) was added to the mixture resulting in conjugate addition and, sequential elimination of the second *p*-toluoyl sulfinic acid, to afford VIR-102C9-EPI-X4 JM#173-C vinyl thioether (**9**). This generates another Michael acceptor, to which was added a biotin-PEG_3-thiol (**10**). The whole course of the successive reactions was followed with HPLC (Figure 3B). After this three-step one-pot reaction, we isolated the bifunctional peptide conjugate (**11**, B-VIR-EPI-X4 JM#173-C) for supramolecular protein hybrids with precise stoichiometry with an overall yield of 14%. The identity was confirmed by HR-ESI-MS (Figure 3D).

Supramolecular Assembly of Biotinylated Peptides onto Protein Platforms. We aimed to investigate the bioactivity of the bispecific antiviral peptides in one supramolecular platform. Due to their strong binding affinity to biotin ($k_D = 10^{-15}$ M),[30] the well-documented bio-applicability,[31,32] and their ability to bind up to four equivalents of the native ligand, we chose the avidin-like protein streptavidin as a supramolecular platform. First, we investigated the number of biotinylated conjugates required to saturate the four binding pockets per SAv, in comparison to its native ligand biotin. We applied the 2(4-hydoxyphenylazo)benzoic acid (HABA)-assay for this purpose (see Figure 4A,B). The diazo-compound HABA binds to the biotin pockets of avidin-like proteins with lower affinity than biotin itself ($k_D = 5 \times 10^{-6}$ M).[33] Thus, it is replaced by the natural ligand, if present.[33,34] Since the complex of HABA with SAv shows characteristic absorbance at 500 nm, upon saturation of all four binding pockets with biotin, the absorbance intensity at 500 nm does not decrease further.[33−35] For the HABA assay, we examined the displacement using increasing equivalents of the biotinylated peptides **5**, **6**, and **11** (Figure 4B). Four equivalents of biotinylated peptides (**5**, **6**, or **11**) per SAv were required for the assembly. Supramolecular assemblies for subsequent biological investigations were performed by mixing **5**, **6**, or **11** with SAv in phosphate buffer at physiological pH, followed by ultraspin filtration purification. In this way, SAv-VIR-102C9 (**12**), SAv-EPI-X4 JM#173-C (**13**), and SAv-VIR-102C9-EPI-X4 JM#173-C (**14**) were generated, respectively. The height tomographic image of SAv-VIR-102C9-EPI-X4 JM#173-C (**14**) was obtained using atomic force microscopy (AFM). AFM shows particles with a maximum height of 8 nm (SI Figure S14). The average height was determined to be 5.5 ± 0.8 nm and showed particle homogeneity (SI Figure S14, Table S1), similar to SAv protein constructs reported in the literature.[36] Notably, we did not observe larger aggregates.

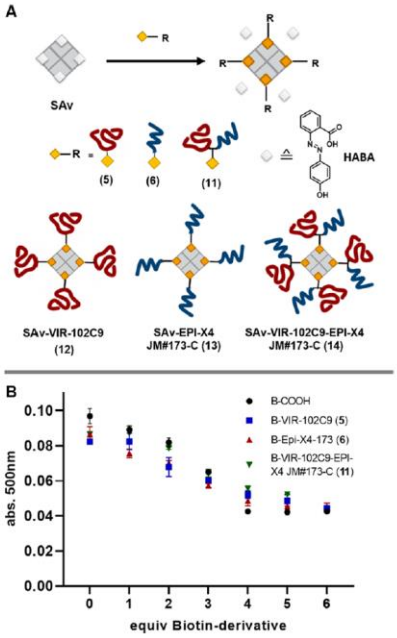

Figure 4. (A) Schematic representation of the supramolecular assembly of biotinylated peptides onto the streptavidin (SAv) platform. (B) Absorbance at 500 nm plotted against biotin and biotinylated peptides to determine stoichiometry required to saturate biotin-binding pockets on SAv. (For **11**, a maximum of five equivalents were used in the HABA assay).

Effect of SAv-Coupled VIR-102C9 and EPI-X4 JM#173-C Derivatives on CXCR4- and CCR5-Tropic HIV Infection. Next, we investigated the antiviral activity of the multifunctional protein constructs SAv-VIR-102C9 (**12**), SAv-EPI-X4 JM#173-C (**13**), and SAv-VIR-102C9-EPI-X4 JM#173-C (**14**), in vitro. To confirm the sustained antiviral activity of the mono- and multivalent biotin- (B) and SAv-coupled peptides, we conducted HIV-1 infection assays with TZM-bl reporter cells, derived from a HeLa cell clone engineered to stably express CD4, CCR5, and CXCR4.[37] As a result, TZM-bl cells are highly susceptible to HIV-1 infection and commonly used for studies on viral entry, tropism, neutralization, and drug sensitivity.[38] TZM-bl reporter cells were pretreated with increasing concentrations of the mono- and multivalent compounds and subsequently infected with the well-characterized X4-tropic HIV-1 NL4-3 molecular clone or an R5-tropic derivative thereof that differs in the V3 region of the viral envelope glycoprotein from the parental virus (Figure 5A).[39] B-VIR-102C9 (**5**) inhibited both X4- and R5-tropic HIV-1 NL4-3 constructs with mean 50% inhibitory concentrations (IC50) of ∼1.1 and ∼1.2 μM, respectively. The

https://doi.org/10.1021/acs.bioconjchem.3c00314
Bioconjugate Chem. 2023, 34, 1645−1652

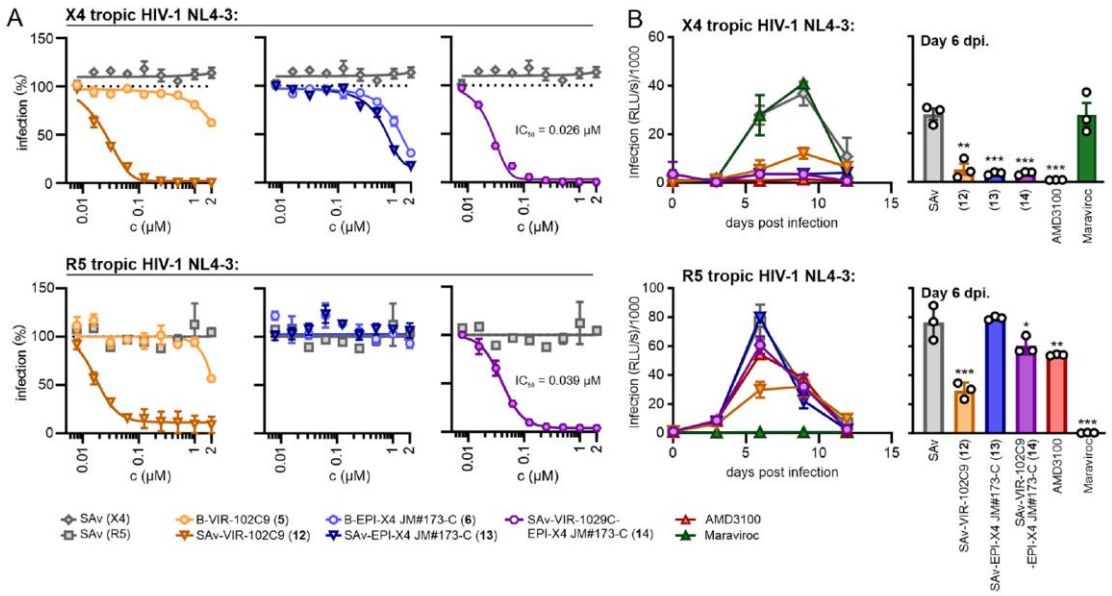

Figure 5. Antiviral activity of single- and multivalent VIR-102C9/EPI-X4 JM#173-C conjugates. Concentrations indicate the molarity of the tested biotin-conjugated peptides or of the SAv conjugates with four copies of mono- or bispecific peptides respectively. (A) TZM-bl cells were pretreated with the indicated amounts of the single or multivalent compound and infected with X4- or R5-tropic HIV-1. Three days post-infection, a β-galactosidase assay was performed. IC50 values are given in the SI (Table S2). (B) Human PBMCs were isolated, stimulated, and pretreated with 1 μM of the indicated single- or multivalent compound, Maraviroc (MVC/50 nM) or AMD3100 (1 μM). The cells were infected with X4- or R5-tropic HIV-1. Infectious virus yield was determined by infection of TZM-bl reporter cells with PBMC culture supernatants obtained at the indicated day post-infection (dpi). Each curve indicates three biological replicates ± SEM. $^{**}p$ <0.01, $^{***}p$ <0.001 (one-way ANOVA with reference to SAv).

multivalent SAv-VIR-102C9 construct (**12**) showed 11- and 18-fold enhanced antiviral activity (IC50 values of ~25 and 100 nM or ~17 and 68 nM per construct or VIR-102C9 content, respectively) compared to the single peptide **5** against X4- and R5-tropic HIV-1 NL4-3. As expected, B-EPI-X4 JM#173-C (**6**) inhibited X4-tropic HIV-1 NL4-3 (IC50: ~1 μM) but was inactive against the R5-tropic derivative. SAv-EPI-X4 JM#173-C (**13**) inhibited X4-tropic HIV-1 NL4-3 with an IC50 of 0.73 μM per construct and 2.92 μM per peptide. In this case, the multivalent construct did not show enhanced antiviral potency compared to the monomeric peptide **6**. Finally, **14** containing both inhibitory peptides (SAv-VIR-102C9-EPI-X4 JM#173-C) efficiently inhibited both X4- (IC50: 26 nM per construct; 104 nM per bivalent peptide) and R5-tropic (IC50: 39 nM per construct; 156 nM per peptide) HIV-1 NL4-3 infection. Construct **14** showed ~11- and 8-fold increased inhibitory activity against X4- and R5-tropic HIV-1, compared to monomeric VIR-102C9 (**5**). Taken together, our results support a clear multivalency effect in constructs containing VIR-102C9 (**12**, **14**), possibly because the HIV-1 envelope glycoprotein is a trimer and targeting of several gp41 fusion peptides might be required for effective inhibition. Notably, none of the compounds were cytotoxic at the used concentrations (SI Figure S15).

To examine the efficiency of the mono- and multivalent SAv-coupled compounds in inhibiting spreading HIV-1 infection in primary viral target cells, we infected activated peripheral blood mononuclear cells (PBMCs) from three human donors in the presence and absence of the compounds. Infectious virus production was determined by infection of TZM-bl indicator cells with PBMC culture supernatants obtained at different days post-infection (dpi). Predictably, AMD3100, a CXCR4 antagonist clinically approved for mobilizing hematopoietic stem cells,[40] blocked X4-tropic HIV-1, while the CCR5-antagonist Maraviroc (MVC) prevented R5-tropic HIV-1 replication. All three multivalent constructs (**12**, **13**, and **14**) significantly reduced the replication of X4-tropic HIV-1. VIR-109C2 containing assemblies (**12**, **14**) also reduced the replication of R5-tropic HIV-1 although less efficiently than MVC (Figure 5B). Altogether, the coupled peptides maintained their activity against HIV-1 in primary human cells.

■ CONCLUSIONS

In this work, we present the synthesis and supramolecular assembly to prepare peptide bispecifics targeting the HIV-1 gp41 fusion peptide or the CXCR4 co-receptor as a proof-of-concept approach for the combination of antiviral peptides acting by different mechanisms on tetrameric SAv. We were able to link three different thiol-reactive moieties in one system using a bis-sulfone moiety in combination with a maleimide functionality. Our procedure offers chemoselectivity by a simple pH control. Notably, we were able to combine two peptide sequences through an internal amino acid modification, which cannot be easily accomplished by standard solid-phase peptide synthesis. With this, therapeutic peptides can be conjugated by adding a natural amino acid side chain and functionalized with an affinity group (biotin), for assembly to

https://doi.org/10.1021/acs.bioconjchem.3c00314
Bioconjugate Chem. 2023, 34, 1645−1652

form tetravalent bispecifics on a protein nanoplatform. We confirmed the inhibitory effects of the tetravalent SAv-peptide constructs against R5- and X4-tropic HIV-1 variants. Remarkably, the tetravalent SAv-VIR-102C9 and SAv-VIR-102C9-EPI-X4 JM#173-C showed increased inhibitory activity against both X4- (11-fold) and R5-tropic (8-fold) HIV-1, compared to B-VIR-102C9. Our results further revealed that the bispecific tetravalent construct **14** shows increased activity against both X4- and R5-tropic HIV-1 variants. The approach presented herein is not limited to VIR-102C9, EPI-X4 JM#173-C, and Bt-SH but can be used as a versatile platform for the conjugation of any thiol-containing peptides or targeting units. The chemical strategy and supramolecular platform described here can emerge as a convenient tool for the preparation of multifunctional bispecific peptides for potential antiviral treatments including expansion to peptides that target two different viruses. Besides combining two peptides, VIRIP-derived drugs act by a unique mechanism and can be combined with other antiviral drugs with careful chemical design. Finally, our approach offers perspectives for other diseases, such as targeted cancer therapy by addressing two different target receptors on the cell surface.

■ ASSOCIATED CONTENT

Supporting Information

The Supporting Information is available free of charge at https://pubs.acs.org/doi/10.1021/acs.bioconjchem.3c00314.

Full experimental procedures and characterization data for new compounds (PDF)

■ AUTHOR INFORMATION

Corresponding Authors

Seah Ling Kuan − *Max-Planck Institute for Polymer Research, 55128 Mainz, Germany;* orcid.org/0000-0003-3945-4491; Email: kuan@mpip-mainz.mpg.de

Frank Kirchhoff − *Institute of Molecular Virology, Ulm University Medical Center, 89081 Ulm, Germany;* Email: frank.kirchhoff@uni-ulm.de

Tanja Weil − *Max-Planck Institute for Polymer Research, 55128 Mainz, Germany;* orcid.org/0000-0002-5906-7205; Email: weil@mpip-mainz.mpg.de

Authors

Dominik Schauenburg − *Max-Planck Institute for Polymer Research, 55128 Mainz, Germany*

Fabian Zech − *Institute of Molecular Virology, Ulm University Medical Center, 89081 Ulm, Germany*

Astrid Johanna Heck − *Max-Planck Institute for Polymer Research, 55128 Mainz, Germany*

Pascal von Maltitz − *Institute of Molecular Virology, Ulm University Medical Center, 89081 Ulm, Germany*

Mirja Harms − *Institute of Molecular Virology, Ulm University Medical Center, 89081 Ulm, Germany*

Siska Führer − *Max-Planck Institute for Polymer Research, 55128 Mainz, Germany*

Nico Alleva − *Max-Planck Institute for Polymer Research, 55128 Mainz, Germany*

Jan Münch − *Institute of Molecular Virology, Ulm University Medical Center, 89081 Ulm, Germany;* orcid.org/0000-0001-7316-7141

Complete contact information is available at: https://pubs.acs.org/10.1021/acs.bioconjchem.3c00314

Author Contributions

[§]D.S. and F.Z. contributed equally to this work.

Funding

German Research Foundation DFG for funding SFB 1279, Project number 316249678; Ulm University "Bausteinprogramm", Project numbers: L.SBN.0225 and L.SBN.0209. Open access funded by Max Planck Society.

Notes

The authors declare the following competing financial interest(s): J.M., F.K., and M.H. are co-inventors of pending and issued patents that claim to use EPI-X4 (ALB408-423) and derivatives for the therapy of CXCR4-associated diseases.

■ ACKNOWLEDGMENTS

This project was funded by the Deutsche Forschungsgemeinschaft (DFG, German Research Foundation)−Project number 316249678−SFB 1279 (TW: SFB 1279 A05, C01; FK: A05, JM: A06). The authors thank the mass spectrometry facility at MPIP for MS measurements. F.Z. was funded by the "Bausteinprogramm", project number: L.SBN.0225, of Ulm University. M.H. was funded by programs for female scientists of the Equal Opportunities Unit and by the "Bausteinprogramm", project number: L.SBN.0209, of Ulm University. M.H. also receives funding from the Baden-Württemberg Foundation.

■ REFERENCES

(1) *Global HIV & AIDS statistics — Fact sheet | UNAIDS.* https://www.unaids.org/en/resources/fact-sheet (accessed Dec, 2022).

(2) Cihlar, T.; Fordyce, M. Current Status and Prospects of HIV Treatment. *Curr. Opin. Virol.* **2016**, *18*, 50−56.

(3) Jordan, S. C.; Zakowski, P.; Tran, H. P.; Smith, E. A.; Gaultier, C.; Marks, G.; Zabner, R.; Lowenstein, H.; Oft, J.; Bluen, B.; Le, C.; Shane, R.; Ammerman, N.; Vo, A.; Chen, P.; Kumar, S.; Toyoda, M.; Ge, S.; Huang, E. Compassionate Use of Tocilizumab for Treatment of SARS-CoV-2 Pneumonia. *Clin. Infect. Dis.* **2020**, *71*, 3168−3173.

(4) Grande, F.; Occhiuzzi, M. A.; Rizzuti, B.; Ioele, G.; De Luca, M.; Tucci, P.; Svicher, V.; Aquaro, S.; Garofalo, A. CCR5/CXCR4 Dual Antagonism for the Improvement of HIV Infection Therapy. *Molecules* **2019**, *24*, No. 550.

(5) Berger, E. A.; Murphy, P. M.; Farber, J. M. Chemokine Receptors As HIV-1 Coreceptors: Roles in Viral Entry, Tropism, and Disease. *Annu. Rev. Immunol.* **1999**, *17*, 657−700.

(6) Hayn, M.; Blötz, A.; Rodríguez, A.; Vidal, S.; Preising, N.; Ständker, L.; Wiese, S.; Stürzel, C. M.; Harms, M.; Gross, R.; Jung, C.; Kiene, M.; Jacob, T.; Pöhlmann, S.; Forssmann, W. G.; Münch, J.; Sparrer, K. M. J.; Seuwen, K.; Hahn, B. H.; Kirchhoff, F. Natural Cystatin C Fragments Inhibit GPR15-Mediated HIV and SIV Infection without Interfering with GPR15L Signaling. *Proc. Natl. Acad. Sci. U.S.A.* **2021**, *118*, No. e2023776118.

(7) Zhu, X.; Zhu, Y.; Ye, S.; Wang, Q.; Xu, W.; Su, S.; Sun, Z.; Yu, F.; Liu, Q.; Wang, C.; Zhang, T.; Zhang, Z.; Zhang, X.; Xu, J.; Du, L.; Liu, K.; Lu, L.; Zhang, R.; Jiang, S. Improved Pharmacological and Structural Properties of HIV Fusion Inhibitor AP3 over Enfuvirtide: Highlighting Advantages of Artificial Peptide Strategy. *Sci. Rep.* **2015**, *5*, No. 13028.

(8) Zirafi, O.; Kim, K.-A.; Ständker, L.; Mohr, K. B.; Sauter, D.; Heigele, A.; Kluge, S. F.; Wiercinska, E.; Chudziak, D.; Richter, R.; Moepps, B.; Gierschik, P.; Vas, V.; Geiger, H.; Lamla, M.; Weil, T.; Burster, T.; Zgraja, A.; Daubeuf, F.; Frossard, N.; Hachet-Haas, M.; Heunisch, F.; Reichetzeder, C.; Galzi, J.-L.; Pérez-Castells, J.; Canales-Mayordomo, A.; Jiménez-Barbero, J.; Giménez-Gallego, G.; Schneider, M.; Shorter, J.; Telenti, A.; Hocher, B.; Forssmann, W.-G.; Bonig, H.; Kirchhoff, F.; Münch, J. Discovery and Characterization of an Endogenous CXCR4 Antagonist. *Cell Rep.* **2015**, *11*, 737−747.

(9) Buske, C.; Kirchhoff, F.; Münch, J. EPI-X4, a Novel Endogenous Antagonist of CXCR4. *Oncotarget* **2015**, *6*, 35137.
(10) Harms, M.; Almeida-Hernández, Y.; Alfonso, A. R.; Habib, M.; Gilg, A.; Albers, D.; Ahmed, N.; Abadi, A.; Weidinger, G.; Ständker, L.; Wiese, S.; Sanchez-Garcia, E.; Münch, J. Development of N-Terminally Modified Variants of the CXCR4-Antagonizing Peptide EPI-X4 with Increased Plasma Stability. *Authorea Prepr.* **2022**, DOI: 10.22541/AU.166733107.78559129/V1.
(11) Harms, M.; Habib, M. M. W.; Nemska, S.; Nicolò, A.; Gilg, A.; Preising, N.; Sokkar, P.; Carmignani, S.; Raasholm, M.; Weidinger, G.; Kizilsavas, G.; Wagner, M.; Ständker, L.; Abadi, A. H.; Jumaa, H.; Kirchhoff, F.; Frossard, N.; Sanchez-Garcia, E.; Münch, J. An Optimized Derivative of an Endogenous CXCR4 Antagonist Prevents Atopic Dermatitis and Airway Inflammation. *Acta Pharm. Sin. B* **2021**, *11*, 2694−2708.
(12) Kaiser, L. M.; Harms, M.; Sauter, D.; Rawat, V. P. S.; Glitscher, M.; Hildt, E.; Tews, D.; Hunter, Z.; Münch, J.; Buske, C. Targeting of CXCR4 by the Naturally Occurring CXCR4 Antagonist EPI-X4 in Waldenström's Macroglobulinemia. *Cancers* **2021**, *13*, No. 826.
(13) Sokkar, P.; Harms, M.; Stürzel, C.; Gilg, A.; Kizilsavas, G.; Raasholm, M.; Preising, N.; Wagner, M.; Kirchhoff, F.; Ständker, L.; Weidinger, G.; Mayer, B.; Münch, J.; Sanchez-Garcia, E. Computational Modeling and Experimental Validation of the EPI-X4/CXCR4 Complex Allows Rational Design of Small Peptide Antagonists. *Commun. Biol.* **2021**, *4*, No. 1113.
(14) Harms, M.; Hansson, R. F.; Carmali, S.; Almeida-Hernández, Y.; Sanchez-Garcia, E.; Münch, J.; Zelikin, A. N. Dimerization of the Peptide CXCR4-Antagonist on Macromolecular and Supramolecular Protraction Arms Affords Increased Potency and Enhanced Plasma Stability. *Bioconjugate Chem.* **2022**, *33*, 594−607.
(15) Rodríguez-Alfonso, A.; Heck, A.; Ruiz-Blanco, Y. B.; Gilg, A.; Ständker, L.; Kuan, S. L.; Weil, T.; Sanchez-Garcia, E.; Wiese, S.; Münch, J.; Harms, M. Advanced EPI-X4 Derivatives Covalently Bind Human Serum Albumin Resulting in Prolonged Plasma Stability. *Int. J. Mol. Sci.* **2022**, *23*, 15029.
(16) Gaonkar, R. H.; Schmidt, Y. T.; Mansi, R.; Almeida-Hernandez, Y.; Sanchez-Garcia, E.; Harms, M.; Münch, J.; Fani, M. Development of a New Class of CXCR4-Targeting Radioligands Based on the Endogenous Antagonist EPI-X4 for Oncological Applications. *J. Med. Chem.* **2023**, *66*, 8484−8497.
(17) Münch, J.; Ständker, L.; Adermann, K.; Schulz, A.; Schindler, M.; Chinnadurai, R.; Pöhlmann, S.; Chaipan, C.; Biet, T.; Peters, T.; Meyer, B.; Wilhelm, D.; Lu, H.; Jing, W.; Jiang, S.; Forssmann, W.-G.; Kirchhoff, F. Discovery and Optimization of a Natural HIV-1 Entry Inhibitor Targeting the Gp41 Fusion Peptide. *Cell* **2007**, *129*, 263−275.
(18) Forssmann, W.-G.; The, Y.-H.; Stoll, M.; Adermann, K.; Albrecht, U.; Tillmann, H.-C.; Barlos, K.; Busmann, A.; Canales-Mayordomo, A.; Giménez-Gallego, G.; Hirsch, J.; Jiménez-Barbero, J.; Meyer-Olson, D.; Münch, J.; Pérez-Castells, J.; Ständker, L.; Kirchhoff, F.; Schmidt, R. E. Short-Term Monotherapy in HIV-Infected Patients with a Virus Entry Inhibitor Against the Gp41 Fusion Peptide. *Sci. Transl. Med.* **2010**, *2*, 63re3.
(19) Müller, J. A.; Glöckle, A.; Gawanbacht, A.; Geyer, M.; Münch, J.; Kirchhoff, F. Reduced Susceptibility to VIRIP-Based HIV-1 Entry Inhibitors Has a High Genetic Barrier and Severe Fitness Costs. *J. Virol.* **2018**, *92*, No. e00733-18.
(20) Gaynor, K. U.; Vaysburd, M.; Harman, M. A. J.; Albecka, A.; Jeffrey, P.; Beswick, P.; Papa, G.; Chen, L.; Mallery, D.; McGuinness, B.; Van Rietschoten, K.; Stanway, S.; Brear, P.; Lulla, A.; Ciazynska, K.; Chang, V. T.; Sharp, J.; Neary, M.; Box, H.; Herriott, J.; Kijak, E.; Tatham, L.; Bentley, E. G.; Sharma, P.; Kirby, A.; Han, X.; Stewart, J. P.; Owen, A.; Briggs, J. A. G.; Hyvönen, M.; Skynner, M. J.; James, L. C. Multivalent Bicyclic Peptides Are an Effective Antiviral Modality That Can Potently Inhibit SARS-CoV-2. *Nat. Commun.* **2023**, *14*, No. 3583.
(21) Sandín, D.; Valle, J.; Chaves-Arquero, B.; Prats-Ejarque, G.; Larrosa, M. N.; González-López, J. J.; Jiménez, M. Á.; Boix, E.; Andreu, D.; Torrent, M. Rationally Modified Antimicrobial Peptides from the N-Terminal Domain of Human RNase 3 Show Exceptional Serum Stability. *J. Med. Chem.* **2021**, *64*, 11472−11482.
(22) Santos-Filho, N. A.; Righetto, G. M.; Pereira, M. R.; Piccoli, J. P.; Almeida, L. M. T.; Leal, T. C.; Camargo, I. L. B. C.; Cilli, E. M. Effect of C-Terminal and N-Terminal Dimerization and Alanine Scanning on Antibacterial Activity of the Analogs of the Peptide p-BthTX-I. *Pept. Sci.* **2022**, *114*, No. e24243.
(23) Pettersen, E. F.; Goddard, T. D.; Huang, C. C.; Couch, G. S.; Greenblatt, D. M.; Meng, E. C.; Ferrin, T. E. UCSF Chimera—a Visualization System for Exploratory Research and Analysis. *J. Comput. Chem.* **2004**, *25*, 1605−1612.
(24) Reguera, L.; Méndez, Y.; Humpierre, A. R.; Valdés, O.; Rivera, D. G. Multicomponent Reactions in Ligation and Bioconjugation Chemistry. *Acc. Chem. Res.* **2018**, *51*, 1475−1486.
(25) Ochtrop, P.; Hackenberger, C. P. R. Recent Advances of Thiol-Selective Bioconjugation Reactions. *Curr. Opin. Chem. Biol.* **2020**, *58*, 28−36.
(26) Stenzel, M. H. Bioconjugation Using Thiols: Old Chemistry Rediscovered to Connect Polymers with Nature's Building Blocks. *ACS Macro Lett.* **2013**, *2*, 14−18.
(27) Wang, T.; Wu, Y.; Kuan, S. L.; Dumele, O.; Lamla, M.; Ng, D. Y. W.; Arzt, M.; Thomas, J.; Mueller, J. O.; Barner-Kowollik, C.; Weil, T. A Disulfide Intercalator Toolbox for the Site-Directed Modification of Polypeptides. *Chem. − Eur. J.* **2015**, *21*, 228−238.
(28) Zhou, K.; Eiben, S.; Wang, Q. Coassembly of Tobacco Mosaic Virus Coat Proteins into Nanotubes with Uniform Length and Improved Physical Stability. *ACS Appl. Mater. Interfaces* **2016**, *8*, 13192−13196.
(29) Fan, B.; Men, Y.; van Rossum, S. A. P.; Li, G.; Eelkema, R. A Fuel-Driven Chemical Reaction Network Based on Conjugate Addition and Elimination Chemistry. *ChemSystemsChem* **2020**, *2*, No. e1900028.
(30) Noda, S.; Matsumoto, T.; Tanaka, T.; Kondo, A. Secretory Production of Tetrameric Native Full-Length Streptavidin with Thermostability Using Streptomyces Lividans as a Host. *Microb. Cell Fact.* **2015**, *14*, No. 5.
(31) Raabe, M.; Heck, A. J.; Führer, S.; Schauenburg, D.; Pieszka, M.; Wang, T.; Zegota, M. M.; Nuhn, L.; Ng, D. Y. W.; Kuan, S. L.; Weil, T. Assembly of PH-Responsive Antibody-Drug-Inspired Conjugates. *Macromol. Biosci.* **2021**, No. 2100299.
(32) Bosch, T.; Lennertz, A.; Duhr, C.; Fink, E.; Samtleben, W. Ex Vivo Biocompatibility of Avidin-Agarose: A New Device for Direct Adsorption of Biotinylated Antibodies from Human Whole Blood. *Artif. Organs* **2000**, *24*, 696−704.
(33) GREEN, N. M. A SPECTROPHOTOMETRIC ASSAY FOR AVIDIN AND BIOTIN BASED ON BINDING OF DYES BY AVIDIN. *Biochem. J.* **1965**, *94*, 23C−24C.
(34) Janolino, V. G.; Fontecha, J.; Swaisgood, H. E. A Spectrophotometric Assay for Biotin-Binding Sites of Immobilized Avidin. *Appl. Biochem. Biotechnol.* **1996**, *56*, 1−7.
(35) Heck, A. J.; Ostertag, T.; Schnell, L.; Fischer, S.; Agrawalla, B. K.; Winterwerber, P.; Wirsching, E.; Fauler, M.; Frick, M.; Kuan, S. L.; Weil, T.; Barth, H. Supramolecular Toxin Complexes for Targeted Pharmacological Modulation of Polymorphonuclear Leukocyte Functions. *Adv. Healthc. Mater.* **2019**, *8*, No. 1900665.
(36) Ng, D. Y. W.; Fahrer, J. J.; Wu, Y.; Eisele, K.; Kuan, S. L.; Barth, H.; Weil, T. Efficient Delivery of P53 and Cytochrome C by Supramolecular Assembly of a Dendritic Multi-Domain Delivery System. *Adv. Healthc. Mater.* **2013**, *2*, 1620−1629.
(37) Platt, E. J.; Bilska, M.; Kozak, S. L.; Kabat, D.; Montefiori, D. C. Evidence That Ecotropic Murine Leukemia Virus Contamination in TZM-Bl Cells Does Not Affect the Outcome of Neutralizing Antibody Assays with Human Immunodeficiency Virus Type 1. *J. Virol.* **2009**, *83*, 8289−8292.
(38) Platt, E. J.; Wehrly, K.; Kuhmann, S. E.; Chesebro, B.; Kabat, D. Effects of CCR5 and CD4 Cell Surface Concentrations on Infections by Macrophagetropic Isolates of Human Immunodeficiency Virus Type 1. *J. Virol.* **1998**, *72*, 2855−2864.

https://doi.org/10.1021/acs.bioconjchem.3c00314
Bioconjugate Chem. 2023, 34, 1645−1652

(39) Papkalla, A.; Jan, M.; Claas, O.; Frank, K. Nef Enhances Human Immunodeficiency Virus Type 1 Infectivity and Replication Independently of Viral Coreceptor Tropism. *J. Virol.* **2002**, *76*, 8455−8459.
(40) Donzella, G. A.; Schols, D.; Lin, S. W.; Esté, J. A.; Nagashima, K. A.; Maddon, P. J.; Allaway, G. P.; Sakmar, T. P.; Henson, G.; De Clercq, E.; Moore, J. P. AMD3100, a Small Molecule Inhibitor of HIV-1 Entry via the CXCR4 Co-Receptor. *Nat. Med.* **1998**, *4*, 72−77.

https://doi.org/10.1021/acs.bioconjchem.3c00314
Bioconjugate Chem. 2023, 34, 1645−1652

SUPPORTING INFORMATION: PEPTIDE BISPECIFICS INHIBITING HIV-1 INFECTION BY AN ORTHOGONAL CHEMICAL AND SUPRAMOLECULAR STRATEGY

Supporting information

Peptide Bispecifics Inhibiting HIV-1 Infection by an Orthogonal Chemical and Supramolecular Strategy

Dominik Schauenburg[1, ‡], Fabian Zech[2, ‡], Astrid Johanna Heck[1], Pascal von Maltitz[2], Mirja Harms[2], Siska Führer[1], Nico Alleva[1], Jan Münch[2], Seah Ling Kuan[1, *], Frank Kirchhoff[2, *], Tanja Weil[1, *]

[1]Max-Planck Institute for Polymer Research, Ackermannweg 10, 55128 Mainz, Germany
[2]Institute of Molecular Virology, Ulm University Medical Center, Meyerhofstr. 1, 89081 Ulm, Germany

1. General information and materials

Unless otherwise stated, all chemicals were obtained from commercial sources (Merck, Sigma Aldrich, Fluka and Thermo Scientific, Fisher Scientific) and used without further purification. All organic solvents (acetonitrile (CH_3CN), chloroform ($CHCl_3$), dichlormethane (CH_2Cl_2), dimethylformamide (DMF), dimethyl sulfoxide (DMSO), ethyl acetate (EtOAc), methanol (CH_3OH), tetrahydrofuran (THF)) were obtained from Fisher Scientific and used without further purification (HPLC or analytical grades). H_2O used for the reactions was obtained from the Millipore purification system. Reaction progress was monitored by thin layer chromatography (TLC) using silica pre-coated aluminum sheets (0.2 mm Silica with fluorescence indicator UV 254 nm from Marcherey-Nagel). For visualization ultraviolet lamp (254 nm) or potassium permanganate staining solution (3 g $KMnO_4$, 20 g K_2CO_3, 5 mL 5% NaOH and 300 mL H_2O), ninhydrin (1.5 g ninhydrin in 500 mL methanol and 15 mL acetic acid) were used. Flash column chromatography was carried out using Merck silica gel 60 mesh (pore size 60 Å, 230–400 mesh particle size). NMR spectra were recorded on Bruker Avance 300, 500 or 700 MHz NMR spectrometer in the stated solvents (d_6-DMSO, $CDCl_3$, CD_3CN, D_2O, CD_3OD). Chemical shifts (δ) were reported as parts per million (ppm) referenced with respect to the residual solvent peaks. Multiplicity was descripted as followed: s = singlet, d = doublet, t = triplet, dd = doublet of doublets, dt = doublet of triplets, m = multiplet, br = broad. Liquid chromatography-mass spectroscopy (LC-MS) analysis was performed on a Shimadzu LC-MS 2020 equipped with an electrospray ionization source, a SPD-20A UV-Vis detector and a Kinetex EVO C18 column (2.1 × 50 mm, 2.6 µm). UV-traces are presented with subtracted blank. Maldi-ToF spectra were acquired on a Bruker Time-of-flight MS rapifleX MALDI-ToF-MS equipped with a 10 kHz scanning smartbeam 3D laser (Nd:YAG at 355 nm) and a 10 bit 5 GHz digitizer. HR-ESI-MS was recorded using WATERS SYNAPT G2-Si mass spectrometer. The absorbance was measured on a microplate reader (Tecan Spark 20M) using a Greiner 384 well UV-Star microplate or a nanodrop 1000 Spectrophotometer.

2. Organic Synthesis

2.1. Synthesis of tri-functional bis-sulfone-PEG-maleimide (2)

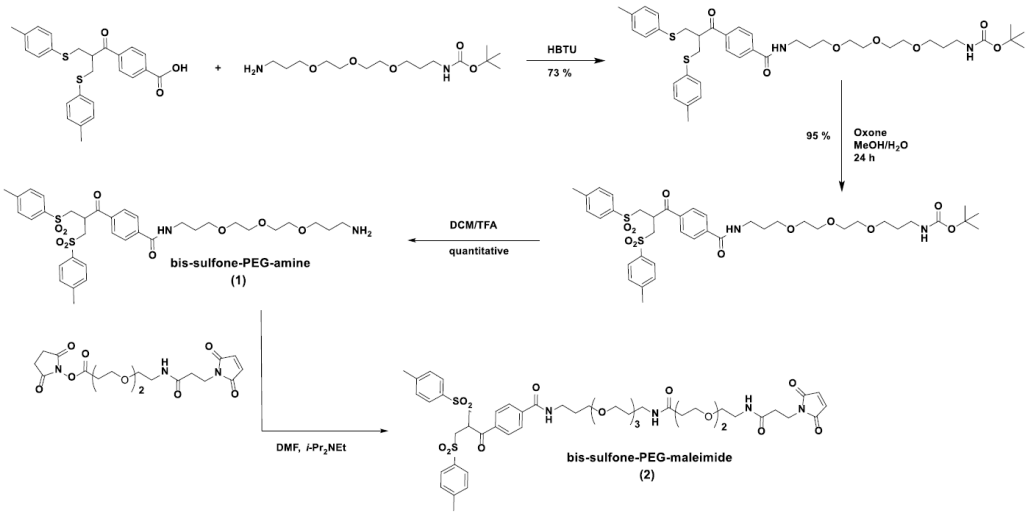

Scheme 1: Synthesis of bis-sulfone-PEG-amine as previously reported with modifications (top).[1]Synthesis route of bis-sulfone-PEG-maleimide (**2**, bottom).

N-(27-(2,5-dioxo-2,5-dihydro-1*H*-pyrrol-1-yl)-15,25-dioxo-4,7,10,17,20-pentaoxa-14,24-diazaheptacosyl)-4-(3-tosyl-2-(tosylmethyl)propanoyl)benzamide (bis-sulfone-PEG-maleimide, 2)

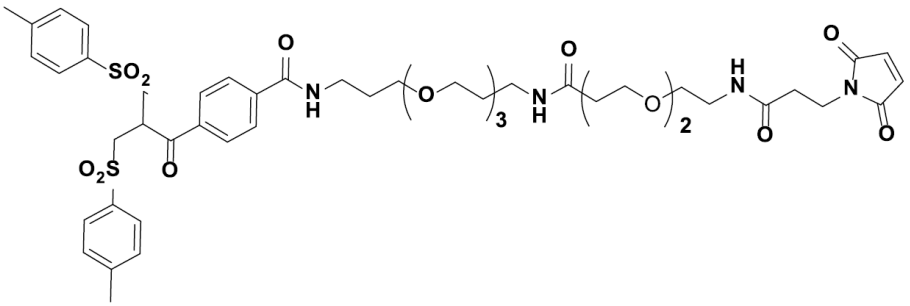

N-(3-(2-(2-(3-aminopropoxy)ethoxy)ethoxy)propyl)-4-(3-tosyl-2 (tosylmethyl)propano-yl)benzamide TFA salt (bis-sulfone-PEG-amine, **1**)[1] (100 mg, 142 µM, 1.0 equiv) was dissolved in anhydrous DMF (15 mL). To this solution *i*-Pr$_2$NEt (24.7 µl, 142 µM, 1.0 equiv) was added. In a separate vial commercially available 3-[2-[2-[[3-(2,5-Dihydro-2,5-dioxo-1H-pyrrol-1-yl)-1-oxopropyl]amino]ethoxy]ethoxy]propanoic acid

[1] Wang, Tao, et al. "A Disulfide Intercalator Toolbox for the Site- Directed Modification of Polypeptides." *Chemistry–A European Journal* 21.1 (2015): 228-238.

2,5-dioxo-1-pyrrolidinyl ester (maleimide-PEG_2-NHS, 94 mg, 212 µM, 1.5 equiv) was dissolved in 1 mL anhydrous DMF. The solution of the NHS-ester was added dropwise to the bis-sulfone PEG-amine and the mixture was stirred at rt overnight. The next day LC-MS analysis showed full conversion of the bis-sulfone PEG-amine. The solvent was removed under vacuum at rt, the residue was dissolved in CH_3CN/H_2O (1:1, v/v) containing 0.1 % formic acid and purified by preparative HPLC. ((HPLC gradient: 10% B for 4 min, 95% B in 20 min, 95% B for 3 min.)

Product containing fractions were collected as a mixture of maleimide bis-sulfone (**2**) and maleimide allyl-sulfone (**2-eli**) and lyophilized.

Note: During the amide bond coupling partial elimination of the bis-sulfone to the allyl-sulfone was observed. These two compounds can be separated by preparative HPLC however, separation at this step is not necessary since the first Michael addition to the maleimide is selective under weekly acidic conditions (pH 6.0).

Yield:(28 mg, 27.6 µmol, 39 %)

Chemical formula: $C_{49}H_{64}N_4O_{15}S_2$

LC-MS (ESI): Tr = 6.4 min, m/z = 1013.5 $[M+H]^+$ (calc. 1013.4). 1035.5 $[M+Na]^+$ (calc. 1036.4).

HR-ToF-MS (ESI): m/z = 1013.3881 $[M+H]^+$ (calc. 1013.3882).

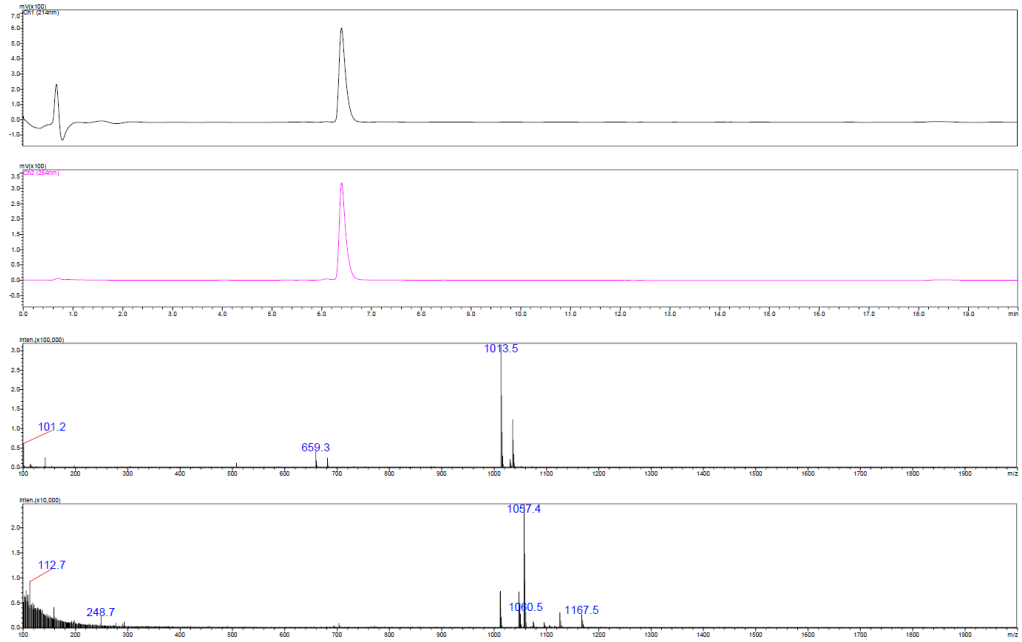

Figure S1: LC-MS spectrum of bis-sulfone PEG-maleimide, **2** (Tr = 6.4 min) at 214 nm (top) and 254 nm (bellow), B: LC-MS spectrum of bis-sulfone PEG-maleimide, **8** (Tr = 6.4 min) at 254 nm, C: LC-MS

spectrum of spectrum of bis-sulfone PEG-maleimide, **2** positive ionization mode (2nd from bottom) and negative ionization mode (bottom).

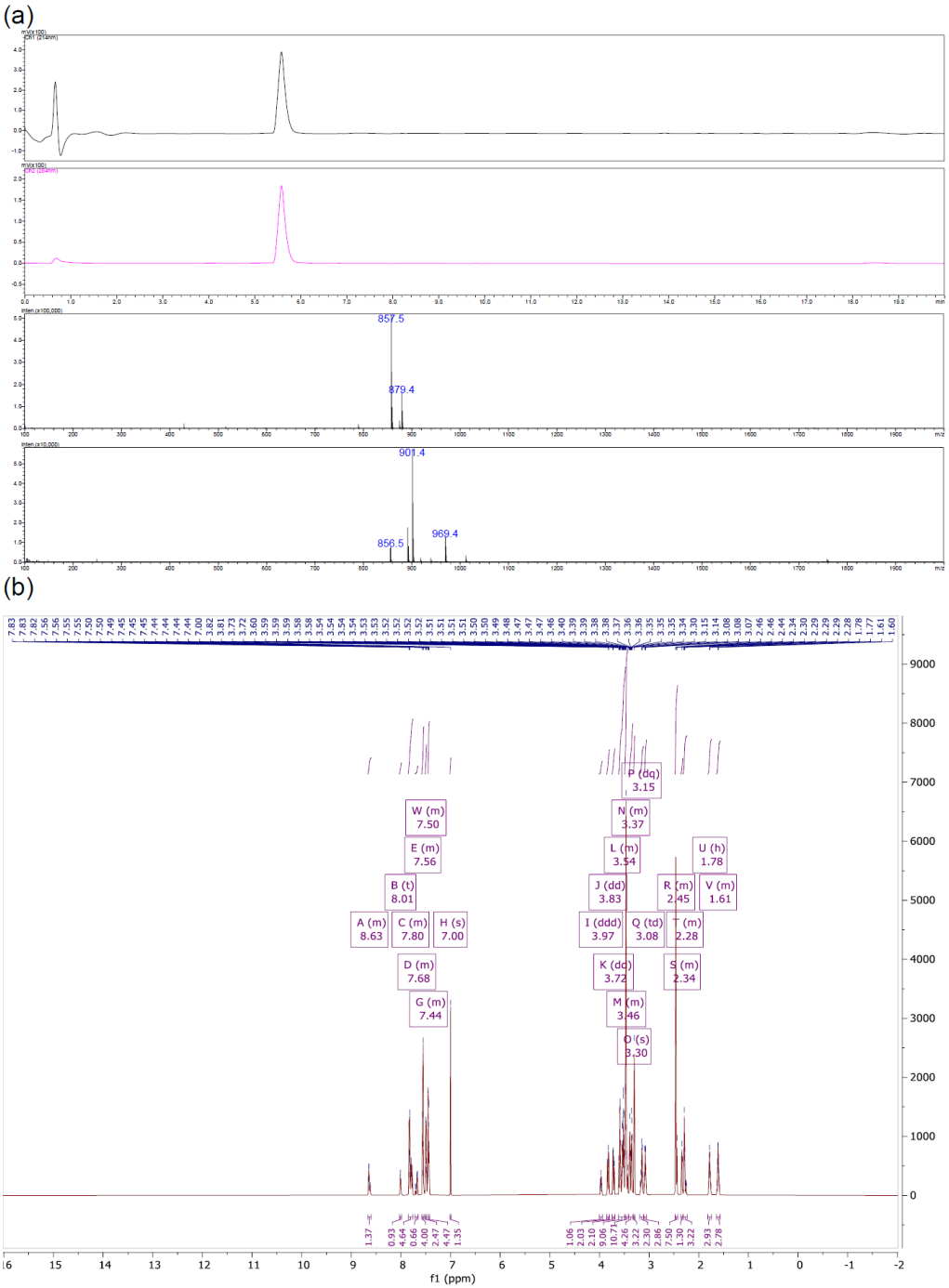

Figure S1: (a) LC-MS spectrum of allyl-sulfone PEG-maleimide **eli-2**, (Tr= 5.6 min) at 214 nm (top); LC-MS spectrum of allyl-sulfone PEG-maleimide **eli-2**, (Tr= 5.6 min) at 254 nm (below); LC-MS spectrum of spectrum of allyl-sulfone PEG-maleimide **eli-2**, positive ionization mode (m/**z** = 857.5

$[M+H]^+$) (2nd from bottom). LC-MS spectrum of allyl-sulfone PEG-maleimide **eli-2**, negative ionization mode (m/**z** = 856.5 $[M-H]^-$) (bottom) (b) ^1H NMR spectrum

2.2. Synthesis of Biotin-PEG-SH (10)

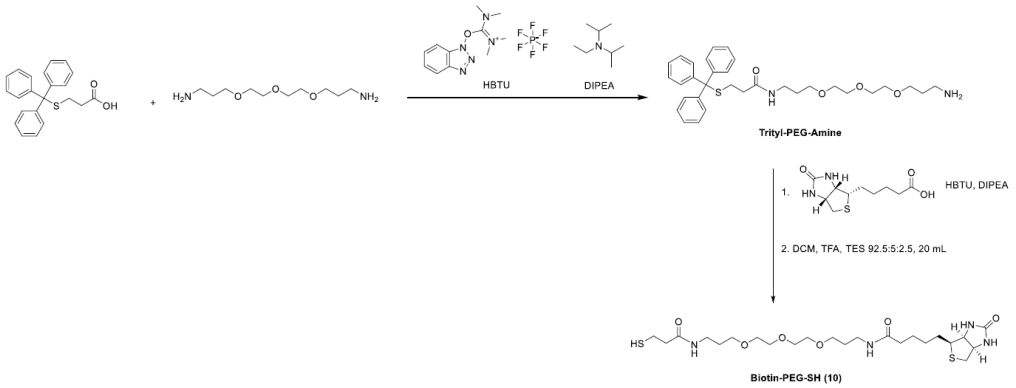

Scheme 2: Synthesis of Biotin-PEG-SH (11) in a three steps synthesis with modifications as previously reported.[2]

N-(17-mercapto-15-oxo-4,7,10-trioxa-14-azaheptadecyl)-5-((3aS,4S,6aR)-2-oxohexahydro-1H-thieno[3,4-d]imidazol-4-yl)pentanamide (10)

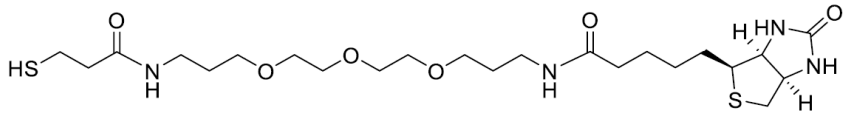

Biotin (266.15 mg, 1.09 mmol, 1.2 equiv.) was dissolved in 2 mL DMSO. HBTU (413.15 mg, 1.09 mmol, 1.2 equiv.) and DIPEA (308,78 µL, 234,67 mg, 1,82 mmol, 2 equiv.) were dissolved in 5 mL anhydrous, peptide grade DMF and added to the Biotin. The mixture was kept stirring for 15 min. Then, N-(3-(2-(2-(3-aminopropoxy)ethoxy)–ethoxy)propyl)-3-(tritylthio)propenamide (trityl-PEG3-amine, 500.0 mg, 907.84 µmol, 1 equiv) in 3 mL mL anhydrous, peptide grade DMF were added to the mixture and kept stirring over night at rt. The solvent was evaporation in vacuo and redissolved in 20 mL DCM. The solution was extracted twice with 20 mL 1M $NHCO_3$. Water phase was extracted twice with 20 mL DCM. The combined organic layers were dried over $MgSO_4$ and solvent was removed in vacuo. For trityl deprotection the crude was dissolved in 40 mL DCM, TFA, TIPS, EDT (90:5:2.5:2.5) and kept stirring for 4h. After solvent removal the crude was redissolved in MilliQ/CH_3CN with 0.1 % TFA and purified preparative HPLC, which yielded 297 mg of product **10.**

[2] Weinrich, D., Köhn, M., Jonkheijm, P., Westerlind, U., Dehmelt, L., Engelkamp, H., Christianen, P.C., Kuhlmann, J., Maan, J.C., Nüsse, D. and Schröder, H., 2010. Preparation of biomolecule microstructures and microarrays by thiol–ene photoimmobilization. *ChemBioChem*, *11*(2), pp.235-247.

Yield: 297 mg, 555 µmol, 61%.

Chemical formula: $C_{23}H_{42}N_4O_6S_2$.

LC-MS (ESI): Tr= 3.8 min, m/z = 535.4 $[M+H]^+$ (calc. 535.2619).

^{1}H-NMR ($CDCl_3$, 500 MHz):: δ = 4.59-4.46 (m, 1H, CH-CH2-S), 4.39-4.26 (m, 1H, CH-CH-S), 3.71-3.49 (m, 12H, 6 CH2-O), 3.44-3.26 (m, 4H, 2 CH2-NH), 3.22-3.06 (m, 1H, S-CH-CH), 2.91 (dd, 2 J = 12.9 Hz, 3 J = 4.7 Hz, 1H, S-CHaCH), 2.84-2.70 (m, 3H, S-CHb-CH, CH2-SH), 2.48 (t, 3 J = 6.8 Hz, 2H, CH2-CH2-SH), 2.21 (t, 3 J = 7.4 Hz, 2H, CH2-CH2-CH2-CO-NH), 1.84-1.73 (m, 4H, CO-NH-CH2-CH2), 1.72-1.57 (m, 4H, CH2-CH2-CH2-CO-NH, CH2-CH2-CH2-CO-NH), 1.50-1.35 (m, 2H, S-CH-CH2).

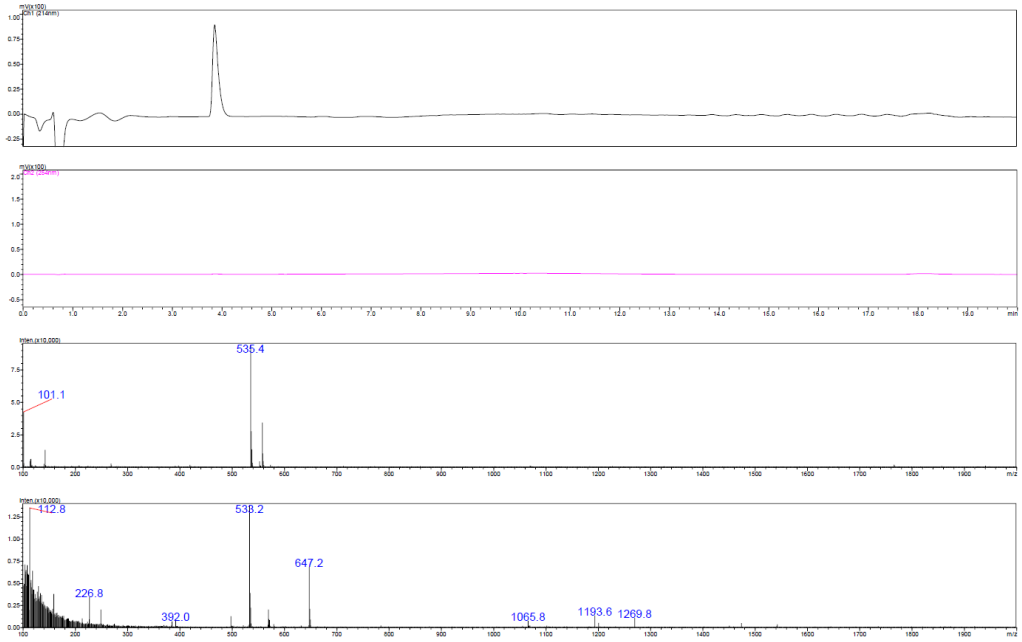

Figure S2: LC-MS spectrum of Biotin-PEG-SH (**10**) at 214 nm (top) and 254 nm (below) Tr = 3.8 min. ESI spectrum, positive ionization mode (2nd from bottom) negative ionization mode (bottom).

3. Peptide Conjugation

3.1. Biotin-PEG11-VIR-102C9 (B-VIR-102C9, 5)

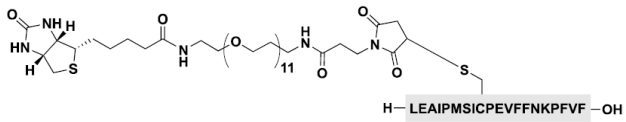

The peptide VIR-102C9 (**3**, 5.0 mg, 2.1 µmol, 1 equiv.) was dissolved in 5 mL of sodium phosphate (PB) buffer (50 mM, pH 6.8) containing 20 % CH_3CN (v/v). The reaction solution was heated to 40°C, to fully dissolve the peptide. Tris(2-carboxyethyl)phosphine) (TCEP, 1 mg/mL in PB, 537 µg, 1 equiv.) was added and the mixture stirred at 40°C for 1 h. Commercially available maleimide-PEG_{11}-biotin (Thermo Fisher Scientific, Waltham, Massachusetts, USA, 2.88 mg, 3.1 µmol, 1.5 equiv.) was dissolved in 288 µL DMF and added to the peptide solution. The mixture stirred at 40°C overnight. Solvents were removed through lyophilization and the crude product was redissolved in 2 mL MilliQ with 20 % CH_3CN (v/v) and 0.1 % TFA. Purification was achieved by semi preparative HPLC using an Eclipse XDB-C18 column (1.4 x 250 mm, 5 µm, Agilent) under acidic conditions. Mobile Phase 0.1% TFA in MilliQ was used as solvent A, and 0.1%TFA in CH_3CN was used as solvent B. (HPLC gradient: 5% B for 3 min, 95% B in 20 min, 95% B for 2 min.)

The product containing fractions were freeze dried yielding in 4.3 mg of compound **5**.

Yield: 4.3 mg, 1.32 µmol, 62 %.

Chemical Formula: $C_{154}H_{237}N_{27}O_{43}S_3$.

LC-MS (ESI): Tr = 5.4 min, m/z = 813.7 $[M+4H]^{4+}$, 1084.5 $[M+3H]^{3+}$ (calc. 1083.9), 1626.6 $[M+2H]^{2+}$ (calc. 1625.3).

ToF-MS (ESI): m/z = 813.1458 $[M+4H]^{4+}$ (calc. 813.1660), 1083.8579 $[M+3H]^{3+}$ (calc. 1083.8856), 1625.2816 $[M+2H]^{2+}$ (calc. 1625.3248).

ToF-MS (MALDI), CHCA: m/z = 3249.5168 $[M+H]^+$ (calc. 3248.6351), 3271.4811 $[M+Na]^+$ (calc. 3271.6243), 3287.4507 $[M+K]^+$ (calc. 3287.5982).

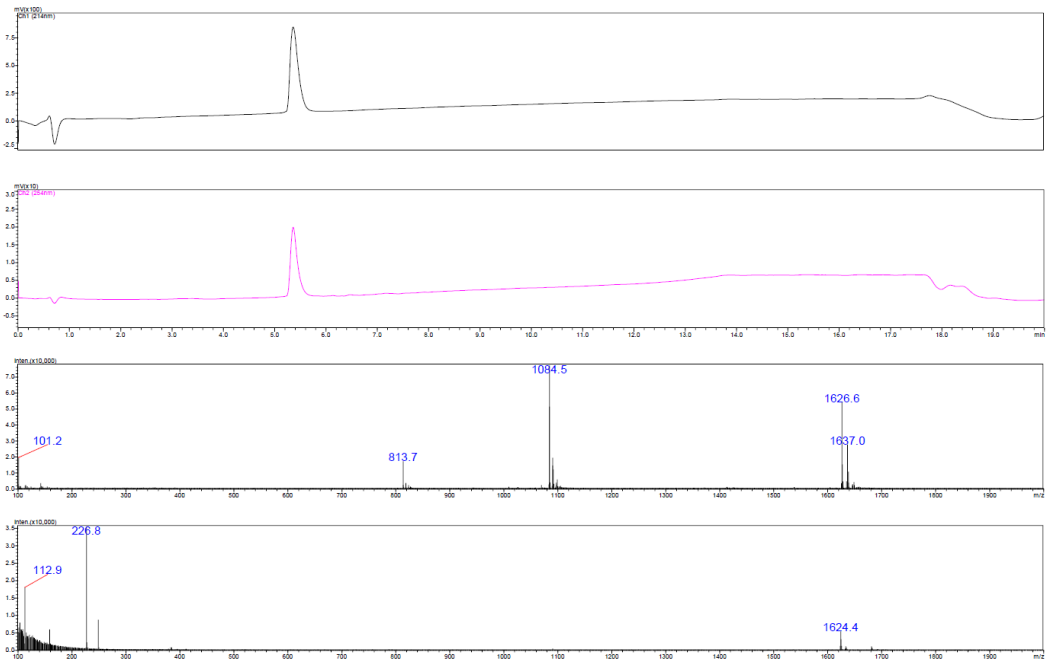

Figure S3: LC-MS spectrum of B-VIR-102C9, **5:** UV-trace at 214 nm (top) and 254 nm (Tr = 5.4 min) (bellow); ESI spectrum positive ionization mode m/z (calc.) = 3248.6 [M], m/z (found) = 1626.6 $[M+2H]^{2+}$, 1084.5 $[M+3H]^{3+}$) (2nd from bottom); ESI spectrum negative ionization mode(bottom) m/z (found) = 1624.4 $[M-2H]^{2-}$ (bottom)

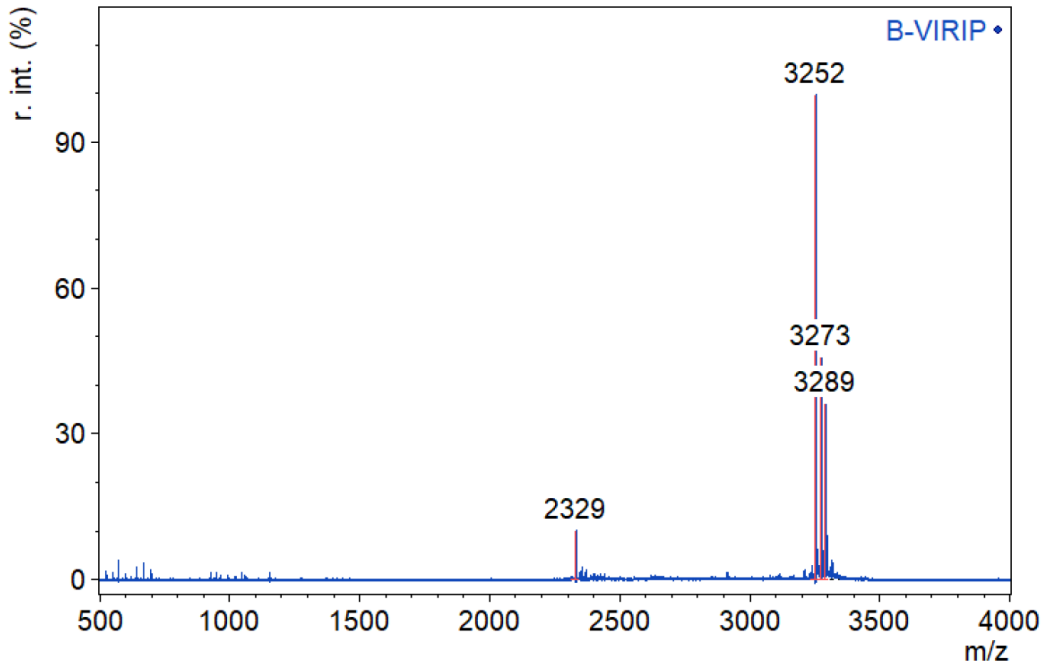

Figure S4: MALDI-ToF mass spectrum of the isolated compound ***5***. Measurement was performed using a alpha-Cyano-4-hydroxycinnamic acid (CHCA), presented as average mass. m/z = 2329 $[2+H]^+$, 3252 $[M+H]^+$, m/z = 3273 $[M+Na]^+$, 3289 $[M+K]^+$

3.2. Biotin-PEG$_{11}$- EPI-X4 JM#173-C (B-EPI-X4 JM#173-C, 6)

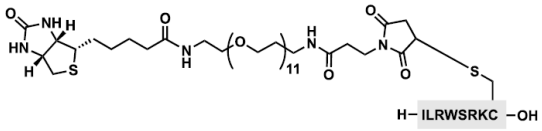

The peptide EPI-X4 JM#173-C (**4**, 5.0 mg, 4.72 µmol, 1 equiv.) was dissolved in 5 mL of sodium phosphate (PB) buffer (50 mM, pH 6.8) and Tris(2-carboxyethyl)phosphine) (TCEP, 1 mg/mL in PB, 537 µg, 1 equiv.) was added and stirred for 1 h. Commercially available maleimide-PEG$_{11}$-biotin (Thermo Fisher Scientific, Waltham, Massachusetts, USA, 2.88 mg, 3.1 µmol, 1.5 equiv.) was dissolved in 288 µL DMF and added to the peptide solution. The mixture stirred at rt overnight. Solvents were removed through lyophilization, and the crude product was redissolved in 2 mL MilliQ with 0.1 % TFA. Purification was achieved by semi preparative HPLC using an Eclipse XDB-C18 column (1.4 x 250 mm, 5 µm, Agilent) under acidic conditions. Mobile Phase 0.1% TFA in MilliQ was used as solvent A, and 0.1%TFA in CH_3CN was used as solvent B. (HPLC gradient: 5% B for 3 min, 95% B in 20 min, 95% B for 2 min.)

The product containing fractions were lyophilized and yielded 6.3 mg (67%) of compound **6**.

Yield: 6.3 mg, 3.18 µmol, 67 %.

Chemical formula: $C_{88}H_{152}N_{22}O_{25}S_2$.

ToF-MS (MALDI), CHCA : m/z = 1983 $[M+H]^+$ (calc.1982).

(a)

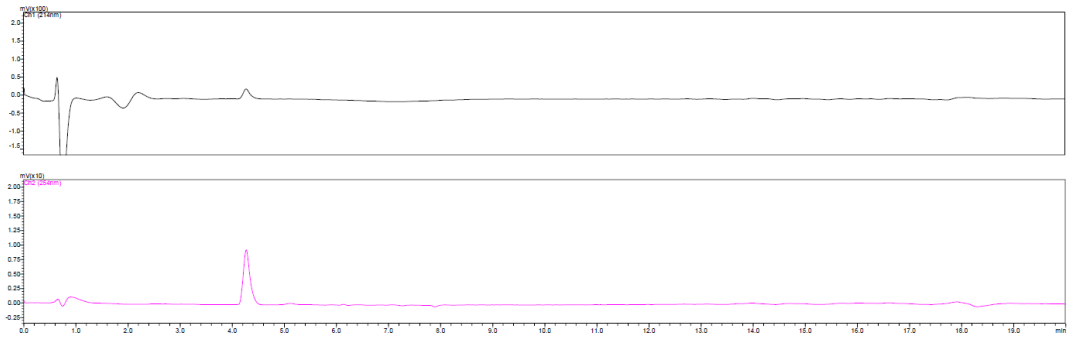

(b)

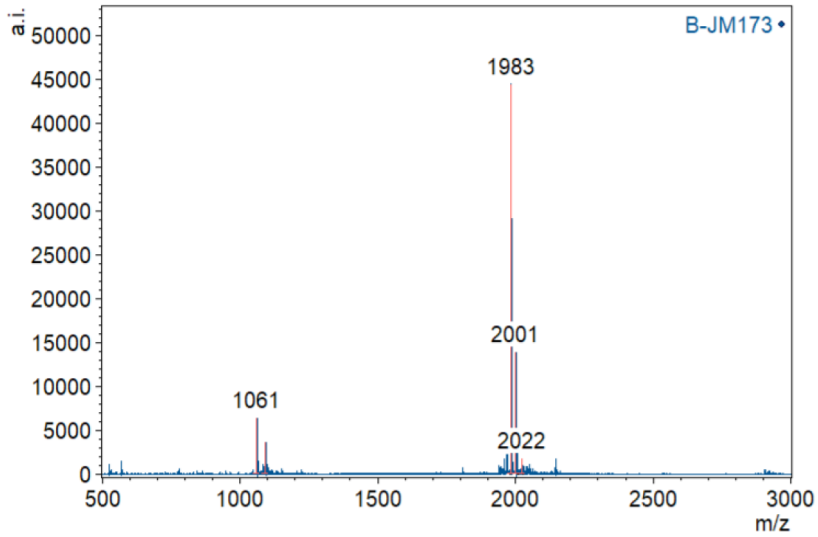

Figure S5: (a) Liquid chromatogram showing purity 214 nm (top) and 254 nm (bottom); (b) MALDI-ToF mass spectrum of the isolated compound **6**. Measurement was performed using a CHCA matrix, presented as average mass. m/z = 1983 [M+H$^+$], sodium adduct m/z = 2001 [M+Na$^+$].

3.3. VIR-102C9-bis-sulfone (7)

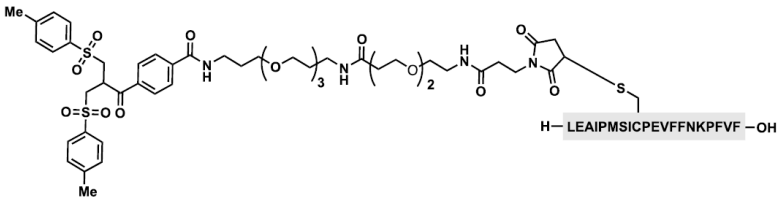

The peptide VIR-102C9 (**3**, 9.58 mg, 4.11 µmol, 1.0 equiv) and TCEP (1.03 mg, 4.11 µmol, 1.0 equiv) were dissolved in 5 ml of sodium phosphate (PB) buffer (50 mmol PB, pH 6.0, containing 40% acetonitrile, v/v) and stirred for 30 min at rt. Bis-sulfone-PEG-maleimide, (**2**, 5 mg, 4.11 µmol, 1.0 equiv) was dissolved in 3 ml PB buffer (50 mmol, pH 6.0, containing 40% acetonitrile, v/v). The reaction mixture was stirred for 2 h at rt, and purified by preparative HPLC (HPLC gradient: 5% B for 3 min, 95% B in 20 min, 95% B for 2 min.) Product containing fractions were collected as a mixture of VIR-102C9 bis-sulfone (**7**) and VIR-102C9 allyl-sulfone (**8**) and lyophilized

Note: At this step VIR-102C9 bis-sulfone and VIR-102C9 allyl-sulfone can be separated by preparative HPLC. Since the next step of reaction course is the elimination of the bis-sulfone to the allyl-sulfone under slight basic conditions (pH 8.0), no separation is required. For analytical purpose of the bis-sulfone the two species were separated.

Yield: 6.59 mg, 1.64 µmol, 40 %.

Chemical formula: $C_{162}H_{230}N_{26}O_{42}S_4$.

LC-MS (ESI) VIR-102C9 bis-sulfone: Tr = 6.6 min, m/z = 1115.0 $[M+3H]^{3+}$ (calc. 1114.0), 1672 $[M+2H]^{2+}$ (calc.1670.7850).

ToF-MS (ESI): m/z = 1670.7899 $[M+2H]^{2+}$ (calc. 1670.7850).

ToF-MS (MALDI), CHCA : m/z = 3339.8866 $[M+H]^{+}$ (calc. 3340.5617), 3361.2211 $[M+Na]^{+}$ (calc. 3362.5436), 3382.5199 $[M+ACN+H]^{+}$ (calc. 3381.8552).

LC-MS (ESI) VIR-102C9 allyl-sulfone: Tr = 6.1 min, m/z = 1593 $[M+2H]^{2+}$ (calc. 1592.7722), 1062.00 $[M+3H]^{3+}$ (calc. 1062.1839), 1592 $[M-2H]^{2-}$ (calc. 1590.7577).

ToF-MS (ESI):m/z = 1592.7870 (calc.1592.7722)

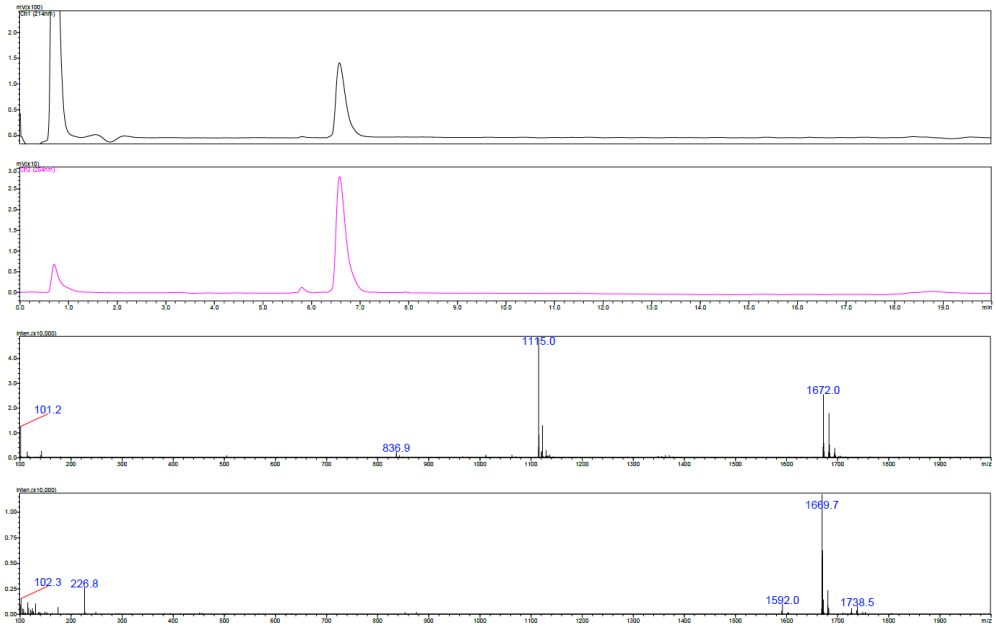

Figure S6: A: LC-MS spectrum of VIR-102C9 bis-sulfone, **7** (Tr = 6.6 min) at 214 nm (top); LC-MS spectrum of VIR-102C9 bis-sulfone **7**, (Tr = 6.6 min) at 254 nm (bellow); ESI spectrum of spectrum of VIR-102C9 bis-sulfone **7**, positive ionization mode (m/z (calc.) = 3339.6 [M], m/z (found) = $[M+2H]^{2+}$ = 1671.0 Da, $[M+3H]^{3+}$ = 1114.0 Da) (2nd from bottom); LC-MS spectrum of VIR-102C9 bis-sulfone **7**, negative ionization mode (m/z (calc.) = 3339.6 [M], m/z (found) = 1669.7 $[M-2H]^{2-}$ (bottom).

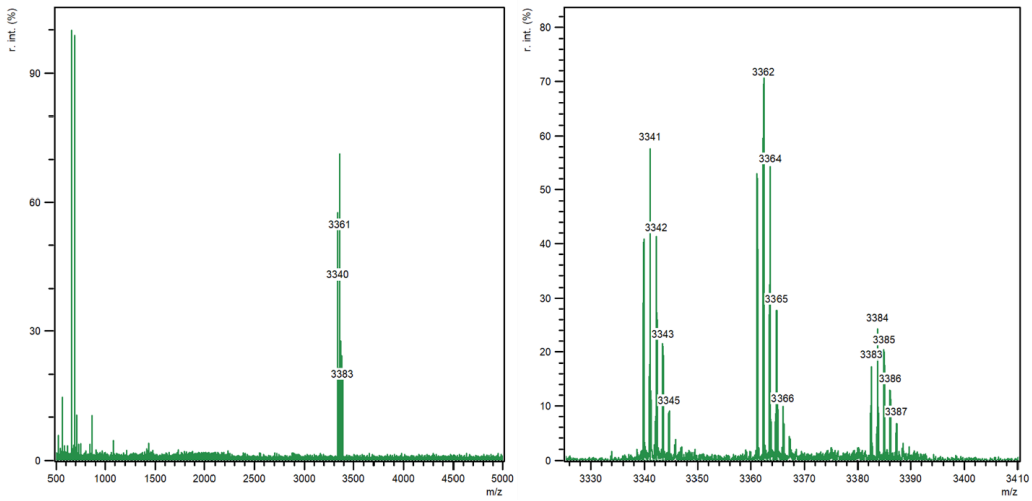

Figure S7: MALDI-ToF mass spectrum of the isolated compound **7** using CHCA matrix,presented as average mass. Full spectrum left, zoom in right. m/z = 3340 $[M+H]^{+}$.

3.4. B-VIR-102C9-EPI-X4 JM#173-C (11)

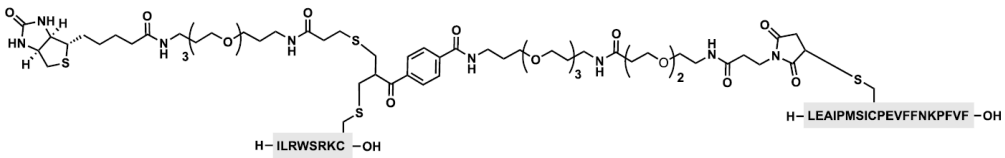

VIR-102C9 bis-sulfone **7** (5 mg, 1.5 µmol, 1.0 equiv) was dissolved in 5 ml of 50 mM PB, 10 mM EDTA, pH 8 and incubated at rt for 24 h. Elimination of the bis-sulfone to the allyl-sulfone can be monitored by LC-MS. EPI-X4 JM#173-C **3** (1.6 mg, 1.5 µmol, 1.0 equiv) was dissolved in 1 ml, 10 mM PB, 2 mM EDTA, pH 8 and TCEP (374 µg, 1.5 µM, 1.0 equiv) was added and gently agitated at rt for 30 min. The EPI-X4 JM#173-C solution was added to VIR-102C9 and shaken for 1 h at rt. Reaction was monitored using LC-MS until EPI-X4 JM#173-C peak disappeared. Biotin-PEG_3-SH **10** (8 mg, 15 µmol, 10.0 equiv) was pre-dissolved in 800 µL DMSO and added to 3.2 ml 10 mM PB, 2 mM EDTA, pH 8. TCEP (3.74 mg, 15 µmol, 10.0 equiv) was added and the mixture was kept stirring at rt for 30 min. Then Bt-PEG_3-SH solution was added to the B-VIR-102C9-EPI-X4 JM#173-C mixture and kept stirring over night at rt. The resulting mixture was purified by semi-prep HPLC (HPLC gradient: 5% B for 3 min, 95% B in 20 min, 95% B for 2 min). The product containing fractions were lyophilized to obtain 950 µg with an overall yield of 14 %.

As we observed side reactions caused by thiol exchange at higher pH that gave inconsistent yield, subsequent batches were performed using the following protocol:

VIR-102C9 bis-sulfone **7** (500 µg, 0.15 µmol, 1.0 equiv) was dissolved in 500 µL of 50 mM PB pH 8.0 and incubated at rt for 20 h under shaking. The mixture was diluted with 2 mL 50mM PB buffer pH 7.4 to decrease the pH. Then EPI-X4 JM#173-C **3** (0.16 mg, 0.15 µmol, 1.0 equiv) was dissolved in 160 µL MilliQ and added to the VIR-102C9 solution. The mixture was incubated under shaking for 1 h at 25°C. Biotin-PEG3-SH **10** (0.8 mg, 1.5 µmol, 10.0 equiv) was dissolved in 800 µL MilliQ and added to the B-VIR-102C9-EPI-X4 JM#173-C mixture and kept stirring for 14h at 25°C. The resulting mixture was purified by semi-prep HPLC. The product containing fractions were lyophilized 80 µg (12 % yield).

Chemical formula: $C_{218}H_{337}N_{47}O_{53}S_5$.

HR-ToF-MS (ESI): m/z = 925.2822 $[M+4H]^+$ (calc. 925.2823).

ToF-MS (MALDI), CHCA : m/z = 2311.6811 $[M+2H]^+$ (calc. 2311.6934), 4622.4349 $[M+H]^+$(calc. 4622.3796).

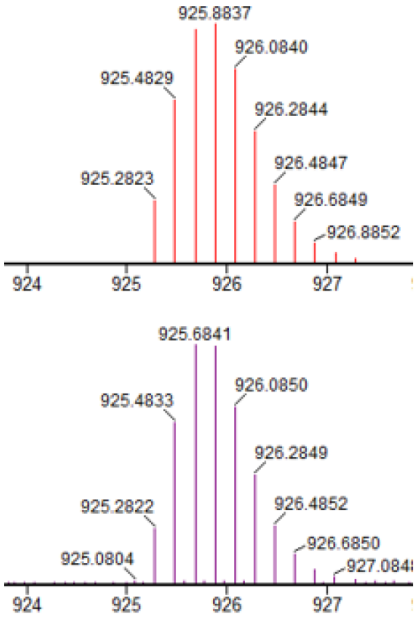

Figure S8: HR-ESI mass spectrum of the isolated compound **11.** Top: calculated isotopic pattern. Bottom: observed isotopic pattern.

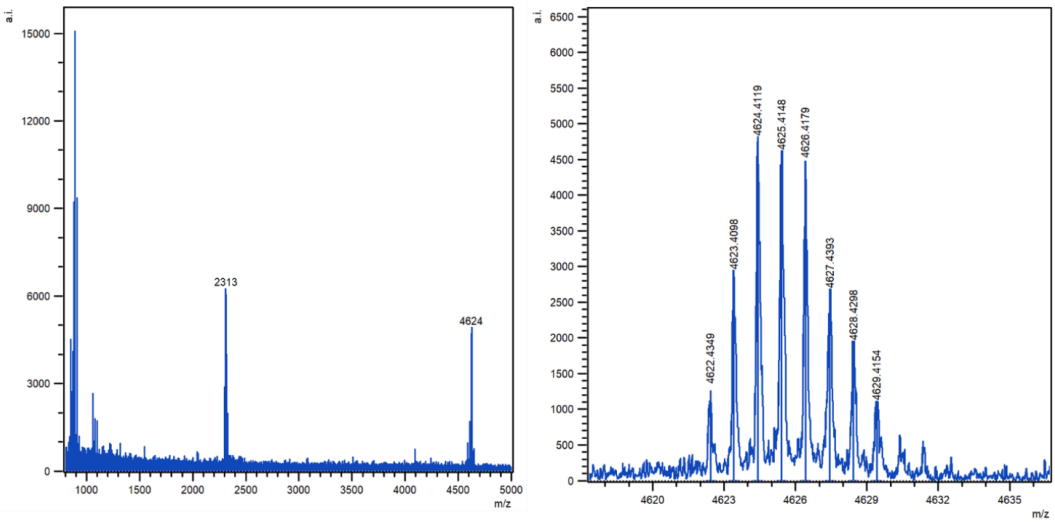

Figure S9: MALDI-ToF mass spectrum of the isolated compound **11.** left: full spectrum showing average mass. right: zoom on isotopic pattern of $[M+H]^+$.

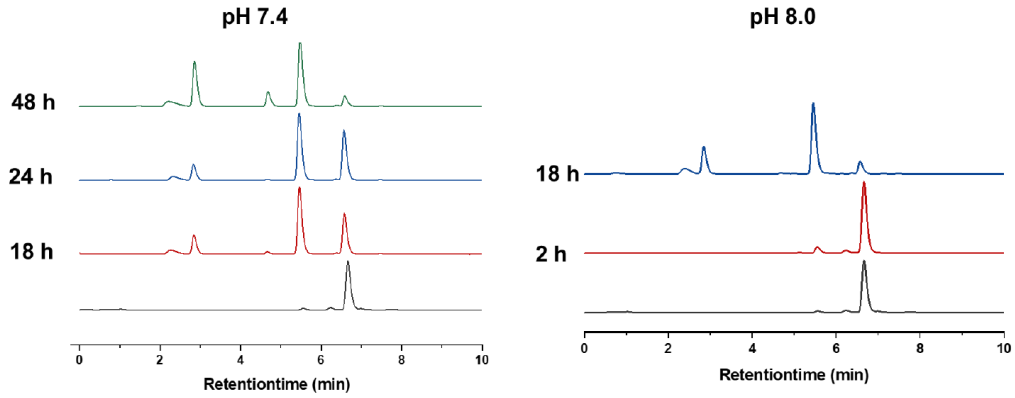

Figure S10: Monitoring of elimination process of bis-sulfone to the allyl-sulfone at pH 7.4 (left) and pH8 (right).

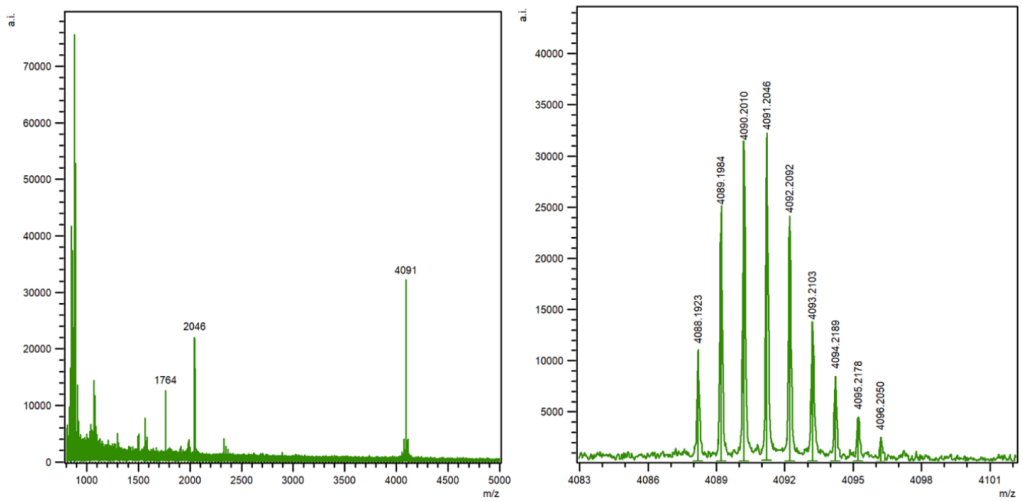

Figure S11: MALDI-ToF mass spectrum of the isolated intermediate **9.** left: full spectrum showing average mass. right: zoom on isotopic pattern of $[M+H]^+$.

4. Assembly of conjugates onto Streptavidin protein platform

4.1. 2-((4'-hydroxyphenyl)-azo) benzoic acid (HABA) – Assay

To determine the required equivalents of biotinylated peptides for saturation of the biotin binding pockets of Streptavidin (SAv, Agilent Technologies), 2-((4'-hydroxyphenyl)-azo) benzoic acid (HABA) was used. Therefore, biotin binding to SAv was analyzed by using seven vials with each 28 µL of a SAv solution (2.5 mg/mL, 1.3 nmol, 1 equiv), in phosphate buffer (50 mM, pH 7.4). Different equivalents of biotin and B-peptides (0 to six equiv. 3.18 µL, .3 nmol, 1equiv; 8.36 µL, 2.6 nmol, 2 equiv and so on) were added to each vial than buffer was added to obtain a total volume of 70 µL. For B-VIRIP-EPI-X4 JM#173-C, up to five equiv was applied. The vials were vortex, incubated for 15 min and spun down to allow complex formation. Triplets of each sample (25 µL) were introduced to a flat-bottomed transparent 384-well plate (UV-star®, Greiner Bio-one GmbH, Frickenhausen, Germany). UV-VIS absorbance spectrum was measured from 250 nm to 850 nm by using a Tecan Spark 20M microplate reader (Tecan Trading AG, Männedorf, Switzerland). The absorption at 500 nm was plotted against the biotin equivalences per protein to give the stoichiometric ratio required for saturation of all binding pockets.

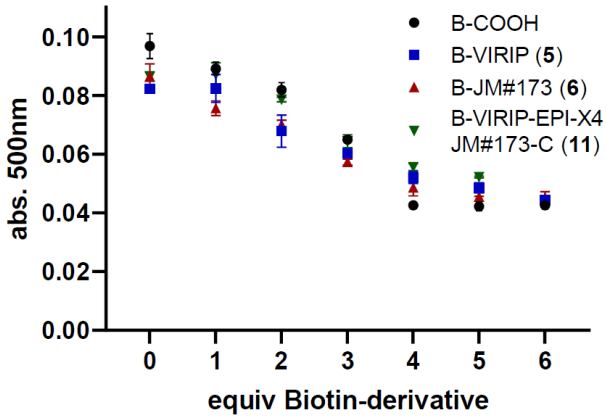

Figure S12: HABA-Assay of Biotin and Streptavidin. All peptides show saturation after 4 mol equiv. per protein (for B-VIRIP-EPI-X4 JM#173-C (**11**) assembly was performed with up to 5 equiv).

4.1.2 Atomic Force Microscopy (AFM)

30 µL of a 10 µg mL^{-1} protein solution (MilliQ H_2O) was dropped on a freshly cleaved mica plate and absorbed for 10 min at room temperature. After addition of 70 µL MilliQ H_2O samples were imaged using liquid tapping mode on a Bruker Dimension FastScan Bio AFM instrument equipped with the ScanAsyst mode with scan rates of 1.4 Hz. Images were analyzed by using NanoScope Analysis 1.8 software.

4.1.3 SDS-PAGE analysis

Preparation of samples for SDS-PAGE follows standard protocol by Bio-Rad on a Mini-Protean TGX 4-20% pre casted gel (Bio-Rad Laboratories, USA), using Laemmli protein sample buffer, with and without 10 vol% ethantiol (sample heating to 95 °C for 5 min) as denaturation and reduction steps. The gel is run in Tris/Glycine/SDS buffer (Bio-Rad Laboratories, USA) with a constant 140 V for 60 min using EXtended PS 13 (5 - 245 kDa) ladder as the reference. Samples were loaded in the gel from left to right: ladder, SAv, SAv (reducing, boiled), SAv-VIRIP, SAv-VIRIP (reducing, boiled), SAv-JM, SAv-JM (reducing, boiled), SAv-bi-specific, SAv-bi-specific (reducing, boiled).

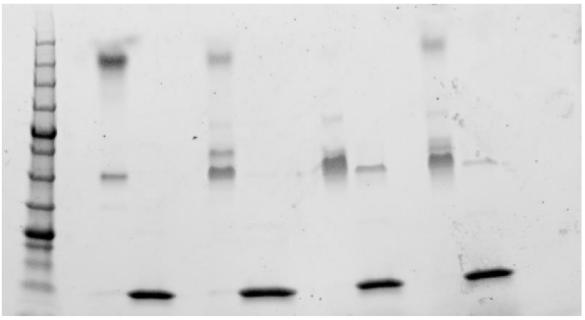

Figure S13: SDS-PAGE analysis of SAv conjugates: Leane from left to right: Leeder, SAv, SAv (reducing conditions), SAv- B-VIR-102C9, SAv-B-VIR-102C9 (reducing conditions), SAv-B-EPI-X4 JM#173-C, SAv-B- EPI-X4 JM#173-C (reducing conditions), SAv-B-VIR-102C9-EPI-X4 JM#173-C, SAv-B-VIR-102C9- EPI-X4 JM#173-C (reducing conditions).

4.2. Assembly of B-VIR-102C9 (5) on Streptavidin

1 mg Streptavidin (10 mg/mL in MilliQ water, 16,7 nmol, 1 equiv.) was added to 900 µL of PB (50 mM, pH 7.4). B-VIR-102C9 (**5**, 0.16 mg, 66,7 nmol, 4 equiv.) was dissolved in 156 µL and added to the protein. The mixture was vortex and shaken at

rt for 15 min. Purification was obtained by using 500 µL Vivaspin ultrafiltration tubes with 10 kDa MWCO and 3x 500 µL PB (50 mM, pH 7.4) spin filtration.
The concentration of the solution was determined as 1.86 mg/mL by Nanodrop absorption measurement at 280 nm and diluted to 25 µM protein concentration for further experiments. Yield was calculated based on protein absorption to be 0.93 mg (93%) of SAv in solution.

4.3. Assembly of B-EPI-X4 JM#173-C (6) on Streptavidin

1 mg Streptavidin (10 mg/mL in MilliQ water, 16,7 nmol, 1 equiv.) was added to 900 µL of PB (50 mM, pH 7.4). B-EPI-X4 JM#173-C (**6**, 0.13 mg, 66.7 nmol, 4 equiv.) was dissolved in 132 µL and added to the protein. The mixture was vortex and shaken at rt for 15 min. Purification was obtained by using 500 µL Vivaspin ultrafiltration tubes with 10 kDa MWCO and 3x 500 µL PB (50 mM, pH 7.4) spin filtration.
The concentration of the solution was determined as 1.95 mg/mL by Nanodrop absorption measurement at 280 nm and diluted to 25 µM protein concentration for further experiments. Yield was calculated based on protein absorption to be 0.90 mg (90%) of SAv in solution.

4.4. Assembly of B-VIR-102C9-EPI-X4 JM#173-C (11) on Streptavidin

1 mg Streptavidin (10 mg/mL in MilliQ water, 16,7 nmol, 1 equiv.) was added to 900 µL of PB (50 mM, pH 7.4). B-VIR-102C9-EPI-X4 JM#173-C (**11**, 0.31 mg, 66.7 nmol, 4 equiv.) was dissolved in 308 µL and added to the protein. The mixture was vortex and shaken at rt for 15 min. Purification was obtained by using 500 µL Vivaspin ultrafiltration tubes with 10 kDa MWCO and 3x 500 µL PB (50 mM, pH 7.4) spin filtration.
The concentration of the solution was determined as 1.57 mg/mL by Nanodrop absorption measurement at 280 nm and diluted to 25 µM protein concentration for further experiments. Yield was calculated based on protein absorption to be 0.82 mg (82%) of SAv in solution.

5. Atomic Force Microscopy (AFM)

Atomic Force Microscopy (AFM) of B-VIR-102C9-EPI-X4 JM#173-C (**11**) 20 µL of a 10 µg/mL protein solution was dropped on a freshly cleaved mica and absorbed for 10 min at room temperature. After subsequent washing with MilliQ H2O and addition of 70 µL MilliQ H2O samples were imaged using liquid tapping mode on a Bruker Dimension FastScan Bio AFM instrument equipped with the ScanAsyst mode with scan rates between 1 and 3 Hz. Images were analyzed by using NanoScope Analysis 1.8 software. The height of the particles were analyzed and the height distribution was determined as shown in the figure and table below by counting 24 particles.

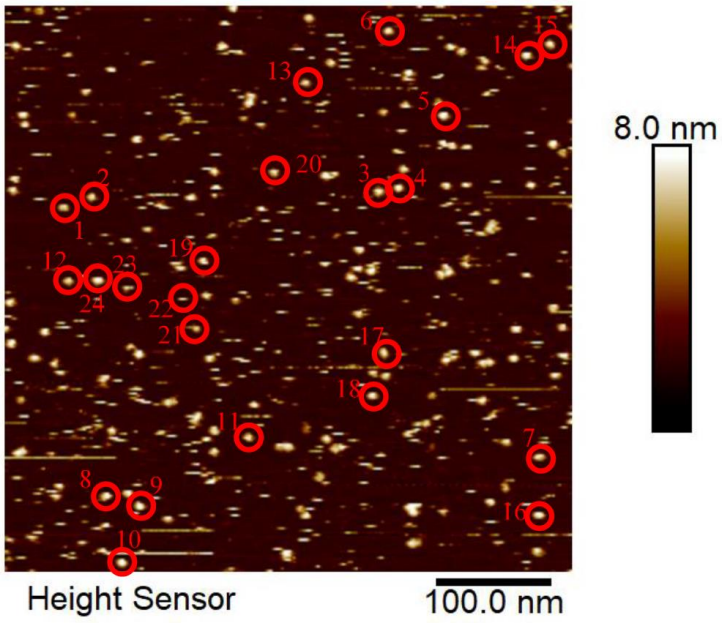

Figure S14: AFM image showing height profile and selection of particles for obtaining height profile

Table S1. Particle height distribution obtained from height profile of AFM image (Figure S14)

Number	Max. Height [nm]
1	4.496
2	4.533
3	6.145
4	5.623
5	6.366
6	6.195
7	4.647
8	6.115
9	6.074
10	5.980
11	5.591
12	4.789
13	5.483
14	5.934
15	6.016
16	6.405
17	5.886
18	5.867
19	5.231
20	5.012
21	4.515
22	3.057
23	4.927
24	5.982
Average with standard deviation	5.49 ± 0.80

6. Materials and Methods for in vitro Studies

6.1. Cell culture and Primary cells

HEK293T cells were provided and authenticated by the ATCC. TZM-bl cells were provided and authenticated by the NIH AIDS Reagent Program, Division of AIDS, NIAID. HEK293T and TZM-bl cells were maintained in Dulbecco's modified Eagle medium (DMEM) supplemented with FCS (10%), L-glutamine (2 mM), streptomycin (100 mg/mL) and penicillin (100 U/mL). Cells were cultured at 37°C, 90% humidity and 5% CO2. To obtain PBMCs, Buffy coats were collected from the blood bank (Ulm) and diluted 1:3 with PBS. Ficoll separating solution was overlaid with the diluted blood and centrifuged at 1,600 x g for 20 min without breaks. The white interface layer formed by peripheral blood mononuclear cells (PBMCs) was transferred into a fresh tube and washed twice with PBS. After separation and washing 1 x 10^6 cells/ml were cultured

in supplemented RPMI-1640 and incubated with Human T-Activator CD3/CD28 Dynabeads for 3 days.

6.2 Virus stocks

Virus stocks were generated by transient transfection of HEK293T cells using the calcium-phosphate precipitation method. One day before transfection, 0.8 x 10^6 HEK293T cells were seeded in 6-well plates (Greiner Bio-one, Frickenhausen, Germany). At a confluence of 60-80% cells were used for transfection. For the calcium-phosphate precipitation method, 5 µg DNA was mixed with 13 µl 2 M CaCl2 and the total volume was made up to 100 µl with water. This solution was added drop-wise to 100 µl of 2x HBS. The transfection cocktail was vortexed for 5 sec and added drop-wise to the cells. The transfected cells were incubated for 8-16 h before the medium was replaced by fresh supplemented DMEM. 48 h post transfection, virus stocks were prepared by collecting the supernatant and centrifuging it at 1300 rpm for 3 min.

6.3 TZM-bl infection assay

To determine infectious virus yield, 10,000 TZM-bl reporter cells/well were seeded in 96-well plates and infected with cell culture supernatants (normalized to 100.000 RLU) in triplicates on the following day. Three days p.i., cells were lysed and *β-galactosidase* reporter gene expression was determined using the GalScreen Kit (Applied Bioscience) according to the manufacturer's instructions with an Orion microplate luminometer (Berthold). Statistical analyses were performed using GraphPad PRISM 9.2 (GraphPad Software). IC50 values were calculated using the Nonlinear regression curve fit tool.

Table S2.

	B-VIR-102C9 (**5**)	SAv-VIR-102C9 (**12**)	B-EPI-X4 JM#173-C (**6**)	SAv-EPI-X4 JM#173-C (**13**)	SAv-VIR-1029C-EPI-X4 JM#173-C (**14**)
IC50 X4 (µM)	1.129	0.025	1.231	0.731	0.026

IC50 R5 (µM)	1.200	0.017	n.d.	n.d.	0.039

6.4 Cell viability

Cell viability was determined by the Cell Titer-Glo 2.0 Cell Viability Assay according to the manufacturer's instructions.

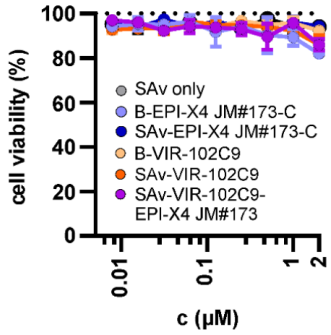

Figure S15: Cell viability of TZM-bl cells treated with increasing amounts of the antiviral peptids. TZM-bl cells were treated with increasing amounts of the indicated compounds and a SAv only control. After 48 h, cell viability was assessed by measuring ATP levels in cells lysates with the commercially available Cell Titer-Glo kit. Concentrations indicate the molarity of the tested biotin conjugated peptides or of the assembled Streptavidin conjugates with four mono- or bispecific peptides respectively. Each dot represents three biological replicates ± SEM.

6.5 Replication kinetics in PBMCs

0.75 million cells were transferred into 96 U well plates, washed twice in PBS and incubated with indicated compounds in RPMI-1640 for 1 hour at 37°C. Then, cells were infected with virus stocks previously generated by transient transfection of HEK293T cells with the respective pro-viral constructs. 16 hours post-infection, cells were washed to remove input virus. At the indicated time points, cells were spun down and ~80% (v/v) of supernatants of the PBMC cultures were aspirated and frozen at -80°C. Medium was replaced with fresh RPMI supplemented with the indicated amounts of the compounds.

6.6 Infectious virus

To determine the infectivity of virions produced in infected human |PBMCs, TZM-bl cells were seeded in 96-well plates at a density of 10,000 cells/well and infected after overnight incubation with the supernatants collected from the PBMC cultures. Three days p.i., viral infectivity was determined using a galactosidase screen kit from Tropix as recommended by the manufacturer. β-Galactosidase activities were quantified as relative light units (RLU) per second with an Orion Microplate luminometer (Berthold).

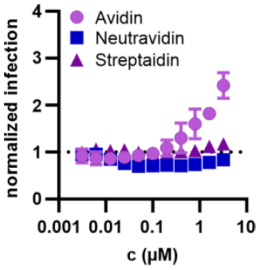

Figure S16: Neutravidin and Streptavidin do not alter HIV-1 infection efficiency. TZM-bl cells were infected with HIV-1 NL4-3 that was preincubated with increasing amounts of the carrier compounds Avidin, Neutravidin or Streptavidin. Three days post infection, a β-galactosidase assay was performed. Each dot represents three biological replicates ± SEM.

.

LIST OF THESIS PUBLICATIONS

To be submitted:

2024 **N. Alleva**[#], J. Zhang[#], D. Y. W. Ng, T. John*, T. Weil*, Functionalizing nucleic acids: synthesis and purification strategies for bioconjugates

Accepted:

2023 D. Schauenburg[#], F. Zech[#], A. J. Heck, P. von Maltitz, M. Harms, S. Führer, **N. Alleva**, J. Münch, S. L. Kuan*, F. Kirchhoff*, T. Weil*; Bioconjugate Chemistry, 2023, 34, 9, 1645–1652; DOI: 10.1021/acs.bioconjchem.3c00314; Peptide Bispecifics Inhibiting HIV-1 Infection by an Orthogonal Chemical and Supramolecular Strategy

2023 **N. Alleva**, K. Eigen, D. Y. W. Ng*, T. Weil*; ACS Macro Letters, 2023, 12, 9, 1257-1263; DOI: 10.1021/acsmacrolett.3c00371; A Versatile and Efficient Method to Isolate DNA–Polymer Conjugates

2022 **N. Alleva**, P. Winterwerber, C. J. Whitfield, D. Y. W. Ng*, T. Weil*; J. Mater. Chem. B, 2022, 10, 7512-7517; DOI: 10.1039/D2TB00812B; Nanoscale patterning of polymers on DNA origami

CURRICULUM VITAE

PERSONAL DETAILS

Name:	Nico Alleva
Date of birth:	23.06.1994
Place of birth:	Itzehoe, Germany
Nationality:	German

ACADEMIC EDUCATION

01/2021– since today	Start the doctorate at the Max-Planck-Institute for Polymer Research under Prof. Dr. Tanja Weils supervision
04/2018 – 12/2020	Master of Science Biomedical Chemistry, Johannes-Gutenberg University, Mainz
09/2018 – 03/2020	Semester abroad at the Polymer Science and Engineering Department in Amherst
10/2013 – 03/2018	Bachelor of Science Biomedical Chemistry, Johannes-Gutenberg University, Mainz

CONFERENCE CONTRIBUTIONS

2024	Macromolecular Colloquium Freiburg, MAKRO 2024, Poster Presentation: DNA-polymer conjugates on self-assembled origami architectures
2022	5th Functional DNA Nanotechnology, FDN2022, Poster Presentation: Nanoscale patterning of polymers on DNA-origami

AWARDS

2023	Poster Prize for Photosynthesis in Lipid Bilayers CataLight Spring School 2023 at Kloster Banz

MAN MERKT NIE, WAS SCHON GETAN WURDE, MAN SIEHT IMMER NUR, WAS NOCH ZU TUN BLEIBT.

MARIE CURIE